



HAL
open science

Synergie entre biologie du développement et techniques d'assistance médicale à la procréation pour l'étude de l'embryon humain préimplantatoire

Jenna Lammers

► To cite this version:

Jenna Lammers. Synergie entre biologie du développement et techniques d'assistance médicale à la procréation pour l'étude de l'embryon humain préimplantatoire. Médecine humaine et pathologie. Nantes Université, 2023. Français. NNT : 2023NANU1020 . tel-04336953

HAL Id: tel-04336953

<https://theses.hal.science/tel-04336953v1>

Submitted on 12 Dec 2023

HAL is a multi-disciplinary open access archive for the deposit and dissemination of scientific research documents, whether they are published or not. The documents may come from teaching and research institutions in France or abroad, or from public or private research centers.

L'archive ouverte pluridisciplinaire **HAL**, est destinée au dépôt et à la diffusion de documents scientifiques de niveau recherche, publiés ou non, émanant des établissements d'enseignement et de recherche français ou étrangers, des laboratoires publics ou privés.

THESE DE DOCTORAT

NANTES UNIVERSITE

ECOLE DOCTORALE N° 605

Biologie-Santé

Spécialité : Biologie Cellulaire, Biologie du Développement

Par

Jenna LAMMERS

Synergie entre biologie du développement et techniques d'assistance médicale à la procréation pour l'étude de l'embryon humain préimplantatoire.

Thèse présentée et soutenue à Nantes, le 11/09/2023

Unité de recherche : CHU de Nantes, Service de Biologie et Médecine de la Reproduction.

Inserm, Centre de Recherche en Transplantation et immunologie, Unité mixte de recherche 1064, Institut de Transplantation Urologie Néphrologie.

Rapporteurs avant soutenance :

Patricia FAUQUE Professeur des universités, UMR 1231
Fabrice GUERIF Professeur des universités, UMR Université-CNRS INRA 7247

Composition du Jury :

Président : Fabrice GUERIF Professeur des universités, UMR Université-CNRS INRA 7247

Examineurs : Sophie BROUILLET Maître de conférences des universités-praticien hospitalier, INSERM U1203
Patricia FAUQUE Professeur des universités, UMR 1231
Jean-Maxime GIRARD PharmD, MSc, Centre AMP Procréalis
Fabrice GUERIF Professeur des universités, UMR Université-CNRS INRA 7247
Corinne MIRAL Maître de conférences HDR, US2B

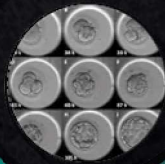
Dir. de thèse : Thomas FREOUR Professeur des universités, CRTI UMR 1064

Table des matières

INTRODUCTION	5
1) L'Assistance Médicale à la Procréation	5
a. Infertilité	5
b. Données d'Assistance Médicale à la Procréation	6
2) Le développement embryonnaire humain	9
a. Culture in-vitro	9
b. Evaluation de la morphologie	10
c. Observation en continu de développement = annexe A1	11
3) La recherche sur l'embryon humain	12
a. Réglementation française	12
b. Alternatives à l'utilisation d'embryons humains	13
PROJET	17
RÉSULTATS	20
1) Aspects cliniques du développement embryonnaire et time-lapse	20
a. Paramètres morphocinétiques des embryons 3PN = article 1	20
b. Influence de l'origine des spermatozoïdes sur la morphocinétique embryonnaire = article 2	25
c. Ploïdie embryonnaire et paramètres morphocinétiques : revue de la littérature et DPI pour translocation chromosomique = articles 3 et 4	35
d. Modification morphocinétique après biopsie embryonnaire au 3 ^{ème} jour de développement = article 5	54
2) Aspects fondamentaux du développement embryonnaire	63
a. La dérivation de cellules souches = annexe A2	65
b. L'annotation automatisée du développement embryonnaire = annexe A3	66
c. L'analyse transcriptomique de cellules uniques d'embryons humains = annexe A4	67
d. Le modèle blastoïde humain = annexe A5	69
3) Application des compétences techniques pour développer les connaissances fondamentales = article 6	71
DISCUSSION	82
CONCLUSION	90
ANNEXES	91
BIBLIOGRAPHIE	152

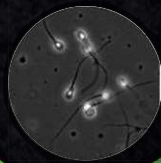
2012

L'observation en continu du développement embryonnaire en FIV (time lapse) à l'aide de l'Embryoscope. A1



2015

Does sperm origin affect embryo morphokinetic parameters? 2



2018

Can time-lapse predict embryo ploidy? A systematic review 3



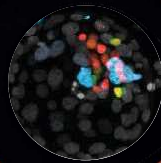
2020

Development of automated annotation software for human embryo morphokinetics. A3



2021

Integrated pseudotime analysis of human pre-implantation embryo single-cell transcriptomes reveals the dynamics of lineage specification. A4



2023

Developmental-stage specific single-cell Human embryo dissociation. 6



2014

Morphokinetic parameters of ICSI tri-pronucleated embryos observed using time lapse. 1



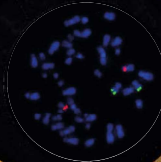
2018

Parallel derivation of isogenic primed and naïve induced pluripotent stem cells. A2



2019

Morphokinetic parameters in chromosomal translocation carriers undergoing preimplantation genetic testing. 4



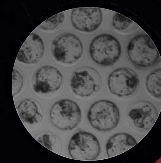
2021

Modification of late human embryo development after blastomere removal on day 3 for preimplantation genetic testing. 5



2022

Human blastoids model blastocyst development and implantation. A5



Abréviations

ABM : Agence de la Bio-Médecine

AMP : Assistance Médicale à la Procréation

DPI : Diagnostic Pré-Implantatoire

DPI-A : Diagnostic Pré-Implantatoire pour recherche d'Aneuploïdie

EPI : Epiblaste

ESHRE : European Society of Human Reproduction and Embryology (Société européenne de reproduction humaine et d'embryologie)

FLIM : Fluorescence Lifetime Imaging Microscopy (Microscopie d'imagerie à durée de vie par fluorescence)

hPSC : human Pluripotent Stem Cells (Cellules Souches Pluripotentes humaines)

hTSC : human Trophoblastic Stem Cells (Cellules Souches Trophoblastiques humaines)

hESC : human Embryonic Stem Cells (Cellules Souches Embryonnaires humaines)

hNPSC : human Naive Pluripotent Stem Cells (Cellules Souches Pluripotentes Naïves humaines)

IA : Intelligence Artificielle

ICSI : Intra Cytoplasmique Sperm Injection (Injection intracytoplasmique de spermatozoïde)

NGS : Next Generation Sequencing (Séquençage nouvelle génération)

PE : Primitive Endoderm (Endoderme primitif)

PN : ProNucléi

scRNAseq : single cell RNA sequencing (Séquençage de l'ARN en cellule unique)

TE : Trophectoderme

INTRODUCTION

1) L'Assistance Médicale à la Procréation

a. Infertilité

L'Organisation Mondiale de la Santé a défini l'infertilité comme une affection du système reproducteur rendant impossible l'aboutissement d'une grossesse après au moins 12 mois de rapports sexuels réguliers non protégés chez des personnes en âge de procréer. Dans le monde, ce sont 17,5% de la population adulte qui seraient concerné (OMS 2023).

Chez la femme, au niveau du système reproducteur, l'origine de l'infertilité peut être associée à des pathologies du système endocrinien impactant la régulation hormonale, des pathologies utérines impactant l'implantation et le développement embryonnaire, des pathologies ovariennes impactant la production ou la qualité des ovocytes ou des pathologies tubaires impactant la rencontre des gamètes au sein du tractus génital. Des causes génétiques peuvent également expliquer des anomalies gamétiques qui induiront des difficultés à concevoir (ovogenèse, implantation, développement de la grossesse).

Au niveau du système reproducteur masculin, l'infertilité peut être causée par des troubles hormonaux impactant la régulation, des pathologies testiculaires empêchant la production de spermatozoïdes, des anomalies de la fonction propre des spermatozoïdes, des dysfonctionnements de l'excrétion du liquide séminale par obstruction de l'appareil reproducteur impactant la rencontre des gamètes au sein du tractus génital. Certaines anomalies génétiques peuvent également être impliquées dans des troubles de la spermatogenèse qui causeront des difficultés à concevoir. L'infertilité masculine reste néanmoins idiopathique dans plus de 40% des cas (Ventimiglia et al. 2021).

La stratégie d'exploration de l'infertilité des patients est aujourd'hui codifiée et permet de proposer une prise en charge adaptée en assistance médicale à la procréation (AMP) aux patients (Szamatowicz et Szamatowicz 2020).

L'âge des femmes est un facteur d'infertilité connu depuis de nombreuses années (American College of Obstetricians and Gynecologists Committee on Gynecologic Practice and Practice Committee 2014). Même si cette données est moins étudiée en raison d'un déclin de la fertilité plus tardif, il en est de même chez les hommes (Auger et Jouannet 2005). Il a été établi qu'au-delà des difficultés à procréer, les patients d'âge avancé ou, autre contraire, des patients très jeunes, peuvent donner naissance à des enfants qui auront plus de risque d'être porteurs d'anomalies génétiques (Bellver et Donnez 2019).

Des facteurs environnementaux ou liés au mode de vie peuvent également impacter la fertilité des hommes et des femmes. Chez l'homme une addiction à des drogues dures, à l'alcool, à certains médicaments, au tabac et au café ont été étudiés dans une méta-analyse (Alghobary et Mostafa 2022). De façon générale, ces addictions ont toutes un effet négatif sur la fertilité masculine. Une association entre la pollution de l'air ambiant et l'altération de la fertilité des hommes et femmes exposés a aussi pu être mise en évidence (Checa Vizcaíno, González-Comadran, et Jacquemin 2016). Le mode de vie (nutrition, exposition à de fortes températures, radiations, stress, perturbateurs endocriniens), peut également altérer la fertilité des hommes (Leisegang et Dutta 2021). L'impact du tabac sur la fertilité de la femme a également été démontré (Budani et Tiboni 2017). Le poids des patients, hommes ou femmes, est un autre paramètres pouvant affecter leur fertilité dans les catégories extrêmes (Zhang et al. 2020).

En plus d'affecter la fertilité, certaines pathologies semblent avoir des conséquences sur la santé des enfants nés (Bellver et Donnez 2019).

b. Données d'Assistance Médicale à la Procréation

En France, d'après les rapports annuels d'activité publiés par l'Agence de la Biomédecine (ABM), entre 2008 et 2018, le nombre total de tentatives d'Assistance Médicale à la Procréation (AMP) est passé de 126 587 à 148 711. En 2020, les 20 223 enfants nés d'une AMP représentent 2,7% des naissances du pays. Un tel résultat conforte le travail publié par l'Ined en 2018 qui estimait qu'un enfant sur 30 était conçu à la suite d'une prise en charge en AMP (de La Rochebrochard 2018). Depuis 2021,

la révision des lois de bioéthique a permis d'élargir l'accès à l'AMP aux femmes non mariées et aux couples de femmes. Ce changement augmentera très probablement le nombre d'actes d'AMP réalisés dans le pays ainsi que les naissances.

Malgré la prise en charge de l'AMP par la sécurité sociale en France, les arrêts de prise en charge décidés par les patients sont fréquents et représentent 25 à 37% pour les 1^{ers} cycles et 39 à 49% pour les 3^{èmes} cycles (Troude et al. 2012). Ces arrêts de parcours semblent plus marqués dans les zones géographiques concurrentielles où plusieurs centres d'AMP peuvent proposer leur expertise aux patients. Parmi les couples qui interrompent définitivement leur parcours en AMP de leur plein gré ou suite à un refus de poursuite par l'équipe médicale, une proportion non négligeable pourra accomplir son projet parental. En effet, 71% des couples qui ont débuté une prise en charge en AMP finissent par fonder une famille soit à l'aide de l'AMP (48%), soit par la suite par une grossesse spontanée (12%) ou une adoption (11%) (Troude et al. 2016).

En se plaçant du point de vue européen, l'analyse des données d'AMP publiées en 2022 par l'ESHRE (European IVF Monitoring Consortium (EIM), for the European Society of Human Reproduction and Embryology (ESHRE) et al. 2022) reflète bien l'augmentation des prises en charge en AMP au cours des 20 dernières années. Les évolutions des protocoles de traitement et des techniques de laboratoire ont permis d'augmenter les taux de grossesse et d'accouchement par transfert tout en diminuant la proportion des grossesses multiples (Figures 1 et 2). Entre 1997 et 2018, en Europe, ce sont plus de 2 millions d'enfants qui sont nés suite à une AMP. En 2018, 39 pays européens réalisaient des tentatives d'AMP, l'activité française représente donc près de 15% des tentatives européennes.

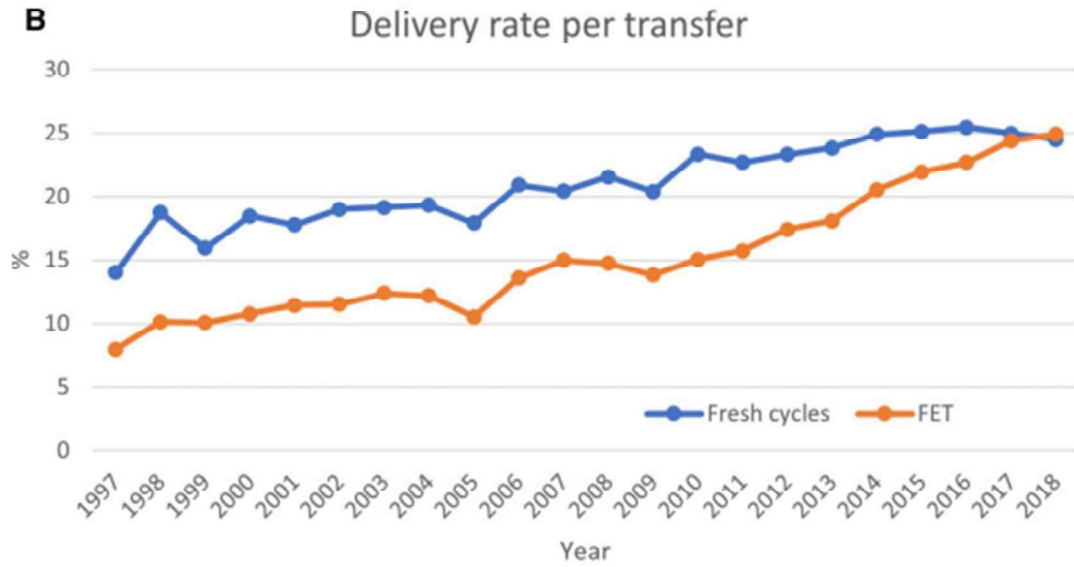


Figure 1: Taux d'accouchement annuel par transfert en Europe (données « ART in Europe, 2018: results generated from European registries by ESHRE »). En bleu, les taux d'accouchement par transfert d'embryon frais, en orange, les taux d'accouchement par transfert d'embryons congelés)

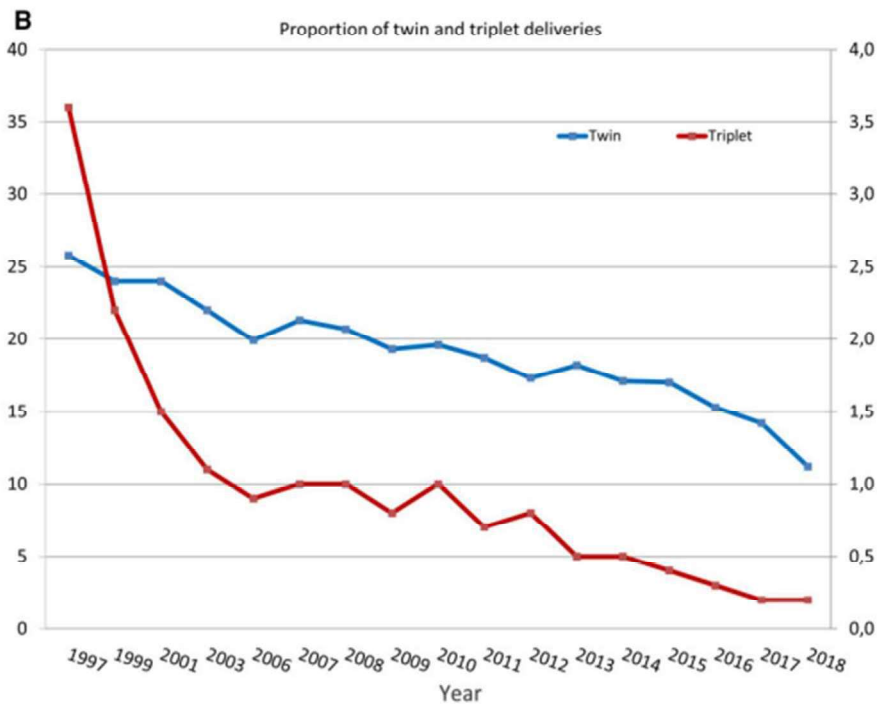


Figure 2 : Taux d'accouchement multiple annuel en Europe (données « ART in Europe, 2018: results generated from European registries by ESHRE »). En bleu, la proportion de naissance de jumeaux, en rouge, la proportion de naissance de triplets.

A titre de comparaison, aux Etats-Unis, le Center for Disease Control and Prevention recense les résultats d'AMP du territoire. Le premier rapport d'activité de 1995 déclarait 43 708 tentatives d'AMP et une moyenne de 4,07 embryons par transfert. Pour l'année 2018, ce sont 306 198 cycles d'AMP qui ont été réalisés dans 456 centres d'AMP et qui ont permis la naissance de 81 478 enfants ce qui représente 2% des enfants nés aux Etats-Unis (Sunderam et al. 2022). Le taux de transfert d'un embryon unique est monté à 74,1% chez les femmes de moins de 35 ans et 66,4% pour celles de plus de 37 ans. Malgré ces efforts, le nombre de grossesses multiples reste supérieur à 12% avec des disparités en fonction des états.

Ces différences entre continents s'expliquent par les importantes disparités concernant l'accès aux soins selon les différentes lois et prises en charge financières proposées par les pays.

2) Le développement embryonnaire humain

a. Culture *in-vitro*

L'ambition des embryologistes est de trouver les conditions de culture les plus adaptées au développement de l'embryon humain (Niederberger et al. 2018). Depuis les premiers travaux de Robert Edwards à la fin des années 60, au cours desquels il a démontré que la fécondation était possible *in-vitro* (Edwards, Bavister, et Steptoe 1969) les observations en laboratoire n'ont cessé d'améliorer les résultats des cultures. Les premiers blastocystes obtenus *in-vitro* chez l'humain l'ont été après une culture de 6 jours en atmosphère contrôlée à 37°C, 5% d'oxygène et 5% de dioxyde de carbone, dans des microgouttes de milieu au pH contrôlé à 7,3 sous huile (Steptoe, Edwards, et Purdy 1971). A cette époque le taux de blastulation publié était déjà de 56,8% (Fishel et al. 1985) alors que les bornes recommandées récemment par l'ESHRE sont de 44 à 80% à J5 (ESHRE Special Interest Group of Embryology et Alpha Scientists in Reproductive Medicine 2017).

Au début des années 2000, Gardner a publié un travail sur la physiologie et la culture des blastocystes dans lequel il explique les particularités de ce stade embryonnaire

tardif (David K. Gardner, Lane, et Schoolcraft 2002). L'utilisation de milieu de culture séquentiel ou global était déjà un sujet de discussion.

De nos jours, la majorité des laboratoires de biologie de la reproduction suivent les recommandations des experts pour la mise en place des techniques de culture *in-vitro* (ESHRE Group on good practice in IVF lab 2015).

De nombreuses études rassurantes sur la santé des enfants issus d'AMP ont été publiées (Berntsen et al. 2019; Hart et Wijs 2022). Néanmoins, certaines anomalies non chromosomiques semblent être plus représentées chez ces enfants sans que la cause ne puisse être clairement identifiée (technique d'AMP et/ou infertilité des patients) (Luke et al. 2021). De la même façon, les effets épigénétiques de la culture *in-vitro* des embryons posent encore question, la méthylation du gène à empreinte *SNRPN* est plus élevée chez les enfants conçus après ICSI et chez ceux nés après un long délai à concevoir (Whitelaw et al. 2014). Plus récemment, des changements de niveaux de méthylation des gènes à empreinte ont été retrouvés chez des enfants issus d'AMP par rapport à un groupe contrôle sans que des différences aient pu être retrouvées entre les sous-groupes dépendant du milieu de culture utilisé (Barberet et al. 2021). L'absence d'influence du milieu de culture semble être confirmée par l'analyse du méthylome d'enfants issus d'AMP (Koeck et al. 2022).

b. Evaluation de la morphologie

Une fois les embryons cultivés au laboratoire, il est nécessaire d'observer leur développement afin de définir ceux qui sont transférables. Pour cela des observations microscopiques ont été mises en place à des moments clés.

Dès les années 90, Steer et al. ont commencé à proposer des scores pour choisir les embryons offrant les plus grandes chances de grossesse (Steer et al. 1992). Le score proposé prenait en compte la régularité des cellules à J2 et leur nombre ainsi que la présence de fragments. Le score total étant une addition du score de chaque embryon transféré il avait pour objectif secondaire de réduire le nombre de grossesses multiples.

Au début des années 2000, plusieurs équipes se sont intéressées au clivage précoce des zygotes, c'est-à-dire à l'occurrence de la première division 25 à 27h après la mise en fécondation. Il a été montré que les zygotes qui atteignent le stade de 2 cellules de façon précoce, avait un meilleur potentiel de développement et d'implantation lors de transferts à J2 ou J3 (Lundin, Bergh, et Hardarson 2001). Le clivage précoce et le nombre de cellules à J2 semblent être de bon marqueur pour prédire le développement et la morphologie des blastocystes, néanmoins avec la morphologie des PN et le taux de fragmentation de l'embryon précoce, ces paramètres ne sont pas suffisants pour prédire la blastulation (Guerif et al. 2007). C'est l'apport du time-lapse, quelques années plus tard, qui permettra d'affiner les critères de sélection des embryons au meilleur potentiel de développement.

Les travaux de Gardner sur la morphologie des blastocystes publiés en 1999 servent toujours de référence aux embryologistes actuels (D. K. Gardner et Schoolcraft 1999). L'expansion de la cavité du blastocyste et la qualité des cellules du trophoctoderme et du bouton embryonnaire restent les critères cruciaux d'évaluation de ce stade tardif.

c. Observation en continu de développement = annexe A1

Début 2011, j'ai eu la chance de participer à la mise en place du 1^{er} Embryoscope français au laboratoire d'AMP du CHU de Nantes. Dès les premiers cycles intégrés à cet incubateur équipé d'un système-time lapse, nous avons passé de nombreuses heures à observer toutes ces étapes de développement jusqu'alors hors de notre vue.

En 2012, nous avons publié un retour d'expérience sur l'utilisation de ce nouvel incubateur et des acquisitions d'images qu'il fournit (Freour et al. 2012).

En 2019, après plusieurs années d'utilisation et la lecture de nombreuses publications dans ce domaine, l'équipe a publié un bilan de l'utilisation de cette technologie, « Le time-lapse bilan et perspectives » (Reignier et al. 2019), illustrant les limites existantes, les avantages cliniques et les autres perspectives pouvant être attendues.

L'utilisation du time-lapse en embryologie est un outil précieux pour une meilleure compréhension du développement de l'embryon humain et des données qui peuvent en être extraites pour faciliter la recherche.

3) La recherche sur l'embryon humain

Pour espérer améliorer les résultats de l'AMP et trouver les pistes qui permettraient de réduire l'infertilité, il est primordial d'améliorer la compréhension du développement embryonnaire préimplantatoire.

a. Réglementation française

Les premières lois de bioéthiques datent de 1994, la recherche sur l'embryon a fait l'objet d'évolution au cours des années. Elle est passée d'un régime d'interdiction avec dérogations depuis 2004 à un régime d'autorisation encadré en 2013. Les premières autorisations de recherches sur les cellules souches embryonnaires humaines et les embryons humains ont été délivrées en 2005. En 2020, l'Agence de la Biomédecine déclarait 9 projets de recherche en cours sur l'embryon humain et 19 publications dans des revues internationales.

La révision de la loi en 2021 (LOI n° 2021-1017 du 2 août 2021 relative à la bioéthique) a essentiellement séparé le cadre clinique du cadre de recherche en redéfinissant les critères d'acceptation des projets déposés. Elle a défini une durée de conservation maximale de 5 ans après le don à la recherche en cas de non utilisation de ces embryons. L'interdiction de mise en fécondation en vue de recherche et de création d'embryons chimères ont été confirmées. En revanche, l'édition du génome est désormais autorisée dans le cadre de la recherche, ainsi que la culture embryonnaire *in-vitro* jusqu'au 14^{ème} jour post-fécondation (Art. L. 2151-5.-I).

Les embryons qui peuvent être utilisés pour ces recherches, ne font plus l'objet d'un projet parental conçu dans le cadre d'une fécondation *in-vitro* que les patients choisissent de donner à la recherche. Chaque année, en France, près de 3000 embryons pourraient être donnés à la recherche par des patients qui n'ont plus de projet parental (Figure 3).

Tableau AMP78. Abandon du projet parental, quelle que soit l'année de congélation, pour les consentements signés dans l'année (2017 – 2020)

	2017		2018		2019		2020	
	Embryons	Couples	Embryons	Couples	Embryons	Couples	Embryons	Couples
Arrêt de conservation des embryons	8038	2723	9002	2985	8409	2938	12015	4242
Proposés à la recherche	2876	1037	3185	1196	2814	1070	3663	1498
Proposés à l'accueil	1654	582	1566	576	1516	549	1428	659

Figure 3: Nombre d'embryons proposés à la recherche par année (Rapport Annuel d'Activité - Agence de la Biomédecine).

Entre 2017 et 2020, ce sont ainsi 4801 couples qui ont souhaité ne pas poursuivre la conservation de leurs embryons et les proposer à la recherche. Cela représente 12538 embryons, soit 33.5% des embryons cryoconservés qui n'ont plus de projet parental. En raison de la nécessité d'obtenir la confirmation de ce choix par les patients, le nombre d'embryons réellement utilisables dans les protocoles de recherche est très certainement inférieur.

Avec l'évolution des techniques de culture embryonnaire et de congélation qui ont eu lieu au cours des dernières décennies (culture prolongée, vitrification), il est primordial de disposer d'embryons à différentes étapes de développement pour permettre d'étudier toutes les hypothèses scientifiques, quel que soit le stade embryonnaire.

b. Alternatives à l'utilisation d'embryons humains

- Modèles animaux

La première alternative à l'utilisation d'embryons humains en recherche est l'utilisation de modèles animaux. Historiquement, le modèle murin est l'un des plus utilisés en embryologie étant donné la courte période de gestation, l'efficacité de la reproduction, mais aussi le peu de place nécessaire à la mise en place d'une animalerie en comparaison à d'autres modèles de plus grande taille. D'autres espèces animales tels que les modèles ovins, bovins, porcins, les primates ou encore d'autres rongeurs sont fréquemment étudiés en biologie du développement ou pour les études de reprotoxicité.

Le modèle murin présente de nombreuses différences physiologiques avec l'espèce humaine qui sont connues depuis de nombreuses années. Par exemple, en 2012, il a

été démontré que la spécification de l'endoderme primitif chez l'humain ne dépend pas de la voie de signalisation FGF2 (Fibroblast Growth Factor 2) contrairement à ce qui était établi à partir du modèle murin (Roode et al. 2012). De la même façon, en 2013, CDX2 (Caudal type homeobox 2) connu pour être le premier marqueur du trophoctoderme apparaissant chez la souris au stade morula, n'apparaît qu'au stade blastocyste chez l'humain (Niakan et Eggan 2013). Enfin, le développement embryonnaire préimplantatoire est plus rapide chez la souris que chez l'Homme.

En 2013, pour la première fois, l'équipe de Yan et al. a publié des résultats de transcriptomes obtenus sur des cellules uniques d'embryons humains (Yan et al. 2013). Blakeley et al., à l'aide de techniques comparables, ont démontré en 2015, les différences qui existaient d'un point de vue transcriptomique entre les embryons murins et humains (Blakeley et al. 2015). Enfin, il a été mis en évidence, que l'embryon humain, contrairement au murin, induit la maturation du trophoctoderme du côté polaire (Aberkane et al. 2018). Pour compléter ces données transcriptomiques théoriques, des équipes ont étudié *in-vitro* l'effet de l'invalidation de gènes sur le développement embryonnaire (Fogarty et al. 2017).

Les modèles animaux restent donc de bons modèles lorsqu'il s'agit de réaliser des tests à grande échelle, en revanche, ils présentent parfois des limites puisque tous les résultats obtenus ne peuvent être transposés chez l'humain.

- Cellules souches embryonnaires

Les cellules souches sont cultivables indéfiniment en laboratoire, elles reflètent à des degrés variables les lignées embryonnaires présentes aux différents stades du développement pré, péri et post implantatoire. Elles peuvent être modifiées génétiquement, et permettre une étude mécanistique de la différenciation des lignées embryonnaires.

L'utilisation de cellules souches embryonnaires peut être une alternative intéressante pour étudier le développement péri-implantatoire. Ces cellules doivent être capables de proliférer et de se différencier dans tous les types cellulaires de l'embryon péri-implantatoire. Pour disposer de ces cellules au laboratoire il est possible d'isoler et de cultiver des cellules issues d'embryons (Figure 4).

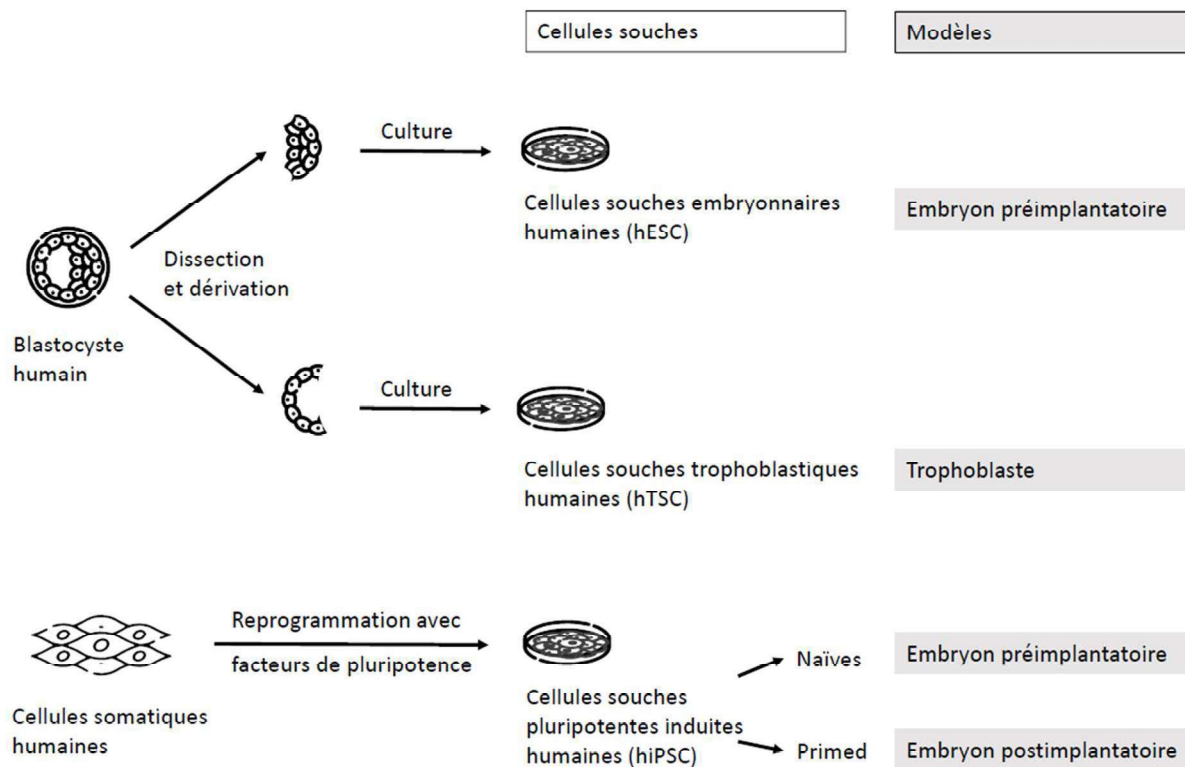


Figure 4 : Schéma des types de cellules souches utilisables en biologie du développement

Les cellules souches embryonnaires humaines (hESC) sont des cellules dérivées de l'épiblaste de la masse cellulaire interne de l'embryon. Ces cellules sont pluripotentes, c'est-à-dire capables de se différencier dans les trois feuillets embryonnaires (ectoderme, endoderme, mésoderme), et par extension en tout type cellulaire adulte, mais sans pouvoir former les annexes embryonnaires comme le placenta ou le sac vitellin. Des lignées de hESC ont été dérivées chez la souris en 1981 puis en 1998 à partir de blastocyste humains (Thomson et al. 1998). Il est également possible d'obtenir des cellules pluripotentes par reprogrammation de cellules somatiques par surexpression des facteurs de pluripotence (Takahashi et al. 2007) qui seront appelées cellules souches pluripotentes induites (hiPSC) et considérées comme des équivalents des hESC.

Cultivés isolés les uns des autres, les modèles cellulaires des lignées embryonnaires ne permettent pas d'étudier le développement de l'embryon dans son ensemble, et

notamment les mécanismes de communication entre les lignées, ou l'implantation de l'embryon dans l'utérus. En 2018, une équipe est parvenue à générer un modèle de blastocyste murin en agrégeant des cellules pluripotentes et trophoblastiques murines (Rivron et al. 2018). Ce modèle qui résulte d'un auto-assemblage de cellules souches embryonnaires avec des cellules souches trophoblastiques est appelé blastoïde. En 24h, une cavité apparaît et le blastoïde forme une structure sphérique creuse comportant un amas cellulaire interne ressemblant à un blastocyste. Quand ces blastoïdes de souris sont transférés dans un utérus de souris pseudo-gestante, ils sont capables d'initier une gestation. En revanche, le blastoïde transféré n'atteint pas le stade fœtal, il n'y a pas d'organisation tissulaire, et aucune naissance n'est possible.

Des blastoïdes ont pu être obtenus à partir de cellules souches embryonnaires humaines (Kagawa et al. 2022; Yu et al. 2021; Yanagida et al. 2021) et pourraient à l'avenir devenir un outil de validation technique avant l'application de protocole de recherche à des embryons humains et ainsi économiser cette ressource précieuse. Une autre alternative pour limiter l'utilisation d'embryons humains est l'utilisation de cellules souches pluripotentes induites (hiPSC) qui peuvent être considérées comme proches des hESC dans certains conditions (naïves). A partir de ces 2 modèles, de nombreuses hypothèses peuvent être testées avant qu'il ne soit nécessaire de manipuler des embryons humains pour la recherche.

PROJET

Ce doctorat, préparé sous un format de validation des acquis de l'expérience, s'appuie sur mon travail en biologie de la reproduction au cours des 10 dernières années (Livret validation des acquis de l'expérience).

Les compétences acquises en termes de techniques d'AMP, en recherche clinique et en recherche fondamentale ont comme dénominateur commun la technologie time-lapse pour l'observation embryonnaire et la micromanipulation embryonnaire pour réalisation de biopsie de blastomères (Figure 5).

Une partie de mes travaux publiés entre 2012 et 2023 (Figure 6), seront regroupés par thématique pour être présentés en 3 parties. Dans chaque partie, les travaux se lisent dans un ordre chronologique. L'évolution de l'état des connaissances depuis ces publications sera développée ensuite.

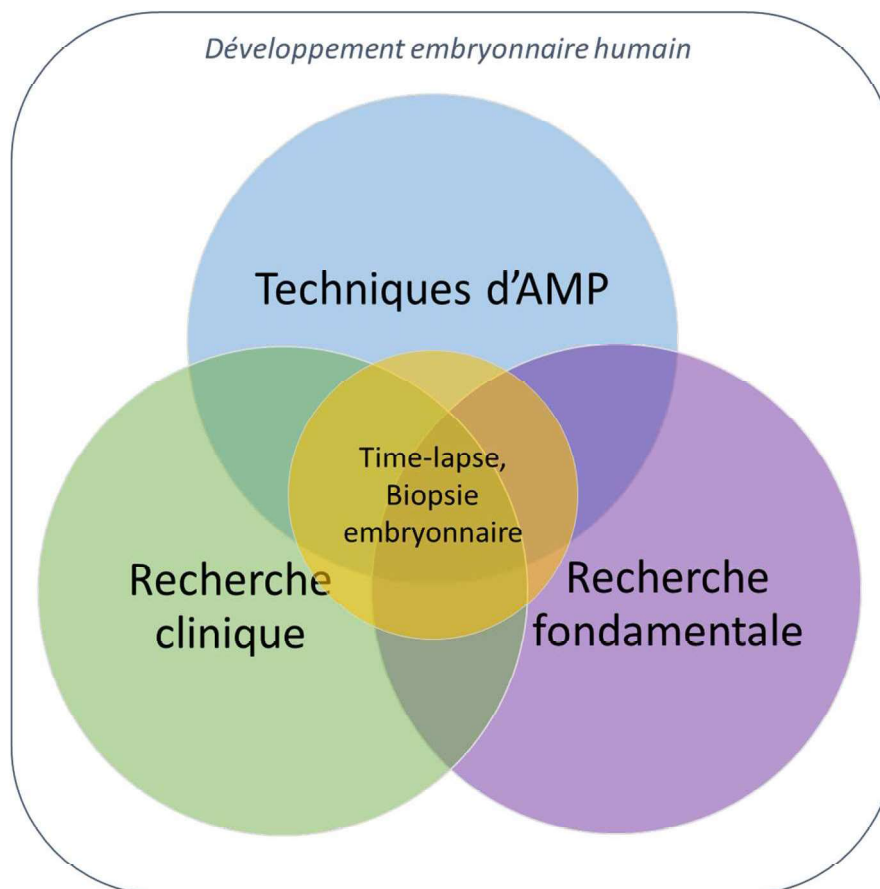


Figure 5: Schéma des thématiques présentées.

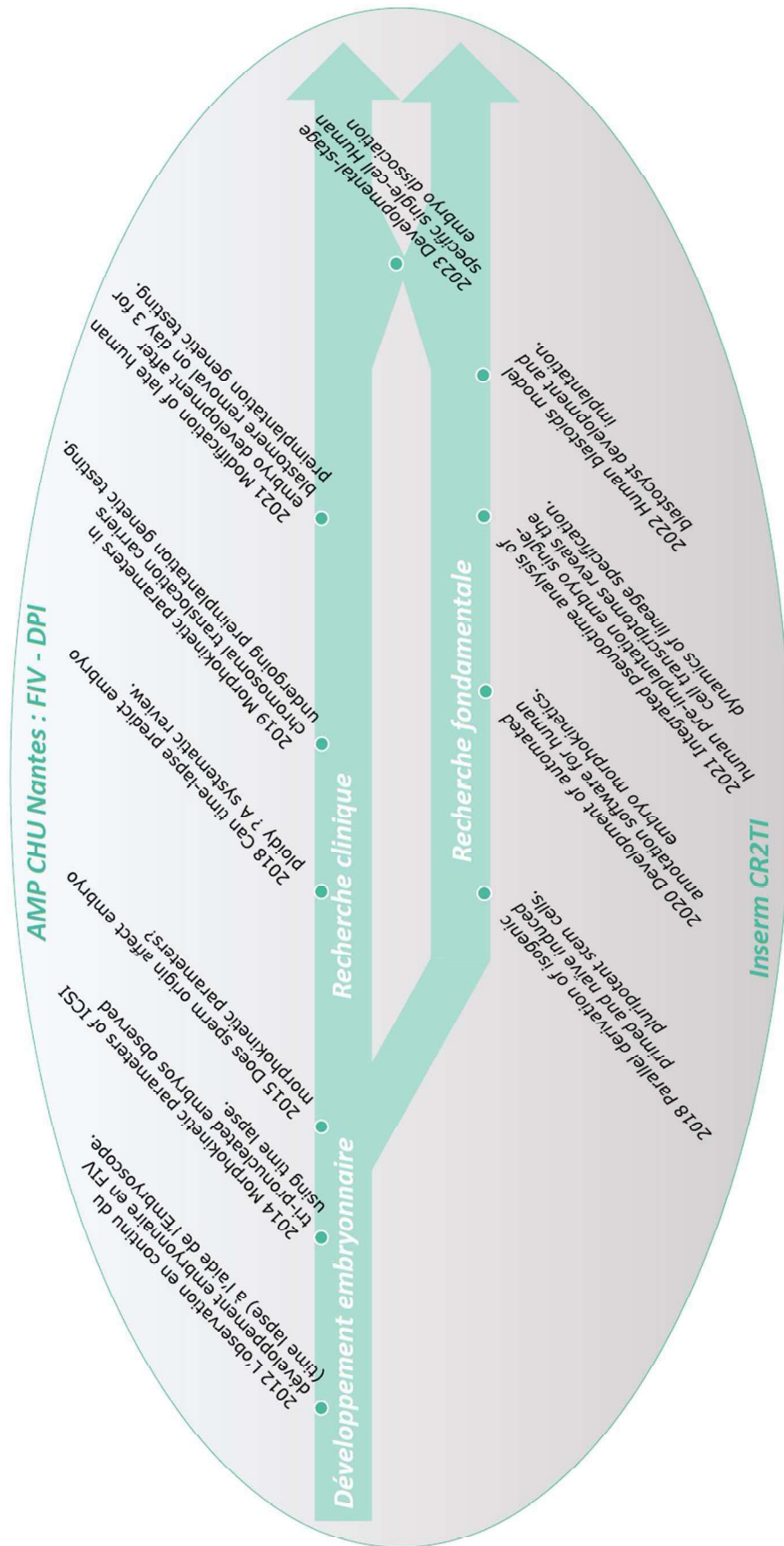


Figure 6: Chronologie des publications présentées

1/ Les aspects cliniques du développement embryonnaire et du time-lapse.

La mise en place et le développement du time-lapse nous ont permis d'observer de nombreux événements du développement embryonnaire jusqu'à lors invisibles lors des observations microscopiques ponctuelles. Depuis l'observation d'ovocytes anormalement fécondés, en passant par l'analyse du développement d'embryons issus de spermatozoïdes d'origines diverses, jusqu'à la recherche de l'effet de la biopsie de blastomères ou du contenu génétique de l'embryon sur son développement, les publications présentées illustrent nos interrogations et notre raisonnement en recherche clinique au cours des années.

2/ Les aspects fondamentaux du développement embryonnaire.

Le projet autorisé par l'ABM comprend l'étude des déterminants de la pluripotence lors du développement humain pré-gastrulation et l'étude du développement de l'embryon préimplantatoire et péri-implantatoire. Comprendre les mécanismes du développement préimplantatoire est primordial pour développer de nouvelles conditions de culture embryonnaire après une fécondation *in-vitro* et avant transfert des embryons dans la cavité intra-utérine. Les publications présentées sont le résultat des travaux de recherche fondamentale menés sur des embryons humains dans le cadre des projets autorisés.

3/ L'application des compétences techniques pour développer les connaissances fondamentales.

La publication présentée illustre la mise au point et l'application de nos compétences d'embryologie clinique pour développer les approches techniques et les protocoles indispensables à nos travaux de recherche sur l'embryon humain.

RÉSULTATS

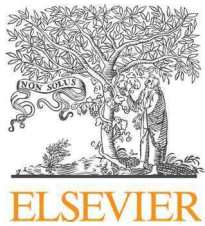
1) Aspects cliniques du développement embryonnaire et time-lapse

a. Paramètres morphocinétiques des embryons 3PN = article ①

Dès la mise en place d'un incubateur équipé de système time-lapse au sein du laboratoire de biologie de la reproduction du CHU de Nantes en 2011, nous avons cherché à mieux comprendre le développement embryonnaire qui était désormais observable en continu.

Les anomalies de fécondation que sont les zygotes tri-pronuclées étant facilement observables microscopiquement, je me suis intéressée à leur développement d'un point de vue morphocinétique. A partir des données des tentatives d'ICSI bénéficiant d'une culture embryonnaire en système time-lapse entre février 2011 et décembre 2012, nous avons observé de façon continue 126 embryons issus d'ovocytes fécondés à 3PN pour les comparer à 1482 obtenus suite à fécondation normale.

Pour cette publication je me suis chargée de réaliser une revue de la littérature pour définir les connaissances sur le sujet et identifier la question sur laquelle travailler. Je me suis chargée ensuite d'annoter les événements morphocinétiques des vidéos des embryons en culture time-lapse afin d'extraire une base de données du développement embryonnaire. J'ai pu réaliser les analyses statistiques pour comparer les données des 2 groupes une fois celles-ci extraites. Pour finir, je me suis chargée de la rédaction de la première version de l'article, de la soumission auprès d'une revue à comité de lecture et de répondre aux corrections posées par les relecteurs.



www.sciencedirect.com
www.rbmonline.com



SHORT COMMUNICATION

Morphokinetic parameters of ICSI tripronucleated embryos observed using time lapse




Jenna Lammers, Carole Spingart, Paul Barrière, Thomas Fréour *

Service de Médecine et biologie du développement et de la reproduction, CHU de Nantes, 38 boulevard Jean Monnet, 44093 Nantes, France

* Corresponding author. E-mail address: Thomas.freour@chu-nantes.fr (T Fréour).



Thomas Fréour studied at Nantes University, specializing in assisted reproduction technology. He started his career as a medical embryologist in the Department of Reproductive Medicine of Nantes University Hospital in 2008. He also holds a PhD from the University of Rennes, France. His main scientific fields of interest are ovarian reserve markers and innovation in the field of human reproductive biology, both in embryology and andrology.

Abstract Time-lapse analysis of tripronucleated zygotes obtained in ICSI cycles showed that 75.4% cleaved into embryos. These embryos subsequently demonstrated slower developmental kinetics than normally fertilized embryos. 

© 2014, Reproductive Healthcare Ltd. Published by Elsevier Ltd. All rights reserved.

KEYWORDS: embryos, fertilization, IVF, morphokinetic parameters, time lapse, tripronucleated zygotes

Introduction

Tripronucleated (3PN) zygotes can sometimes be observed in conventional IVF and intracytoplasmic sperm injection (ICSI) cycles. This chromosomal abnormality is one of the most common among embryos obtained in assisted reproduction cycles, and some authors have established that a high proportion of 3PN zygotes has poor prognosis for success rates in IVF cycles (Figueira et al., 2011). However, others demonstrated that self-correction of these 3PN zygotes is possible during embryo development (Grau

et al., 2011). Even if it has been well established that 3PN zygotes can develop and eventually become blastocysts (Escribá et al., 2006), very little is known on early development of these chromosomally abnormal embryos. Time-lapse analysis allows continuous and objective assessment of all in-vitro events and can thus be considered as a relevant strategy to study early embryo development (Herrero and Meseguer, 2013). The aim of this study was to study the morphokinetic parameters of 3PN zygotes obtained in ICSI cycles and to compare them with normally fertilized (2PN) embryos using the Embryoscope, a time-lapse monitoring system.

<http://dx.doi.org/10.1016/j.rbmo.2014.01.009>

1472-6483/© 2014, Reproductive Healthcare Ltd. Published by Elsevier Ltd. All rights reserved.

Materials and methods

This study retrospectively analysed the data of consecutive patients who had undergone IVF/ICSI cycles with oocyte and embryo cultures performed with the Embryoscope. These data had been collected and recorded in a registered database between February 2011 and December 2012.

Immediately after ICSI, oocytes were placed in individual microwells within a specific culture dish and loaded into the Embryoscope (Unisense Fertilitect, Aarhus, Denmark). Embryo culture was performed at 37°C, under a controlled atmosphere (5% O₂, 6% CO₂). Vitrolife sequential media (Gothenburg, Sweden) were used for embryo culture. Each embryo was investigated by detailed time-lapse analysis measuring the exact timing of all developmental events in hours after ICSI procedure. t_2 , t_3 , t_4 , t_5 and t_8 represent the exact timings of appearance of embryos with 2, 3, 4, 5 and 8 well-defined blastomeres, respectively. s_2 illustrates the synchrony of second cell cycle (i.e. the duration of the 3-cell stage). $cc2$ illustrates the duration of second cell cycle (i.e. the interval between t_3 and t_2). Pronuclei behaviour, size and score (based on nucleoli distribution and inspired from z-score) were also observed.

Statistical analysis was performed using Medcalc version 11.1.1.0. Student's t test and chi-squared test were used for mean and proportion comparison when appropriate. P -values ≤ 0.05 were considered significant.

Results

This study analysed 1609 zygotes originating from 455 ICSI cycles. A total of 126 zygotes were tripronucleated ($n = 113$ women), while 1483 were normally fertilized ($n = 452$ women). No couple had more than two 3PN embryos within the same cohort. Among the 126 tripronucleated zygotes, 16 (12.7%) first went through a normal 2PN stage before the third pronucleus appeared, potentially leading to a risk of inaccurate classification. Total asynchrony, with successive appearance of each of the three pronuclei, was observed only once. Asynchronous pronuclei fading was observed in three cases. Pronuclei surface was $357 \pm 94 \mu\text{m}^2$ on average, with a mean diameter of $21.1 \pm 3.4 \mu\text{m}$. The observation of nucleoli distribution showed that 6.4% of the 3PN zygotes had regular and aligned nucleoli in the three pronuclei (close to z1 pattern), 15.2% had all the nucleoli scattered (close to z2 pattern), 61.6% had at least one pronucleus with aligned nucleoli (close to z3 pattern) and 16.8% had uneven pronuclei (close to z4 pattern). Cleavage rate into 2-cell embryo was significantly lower in 3PN zygotes than in 2PN zygotes (75.4% versus 97.10%, $P < 0.001$). The proportion of zygotes reaching the 4-cell stage was also significantly lower in the 3PN group than in the 2PN group (63.5% versus 90.2%, $P < 0.001$). Time-lapse analysis from the zygote to the 8-cell embryo stage showed that pronuclei appearance and fading occurred significantly later in the 3PN group than in the 2PN group (both $P < 0.001$). Furthermore, 2-cell stage (t_2), t_3 , t_4 and t_8 occurred significantly later in 3PN embryos than in 2PN embryos ($P < 0.001$, $P < 0.05$, $P < 0.05$, $P < 0.01$ respectively; **Table 1**). In contrast, $cc2$ was significantly shorter in the 3PN group than in the 2PN group ($P < 0.01$;

Table 1 Time-lapse kinetic parameters of early embryo development after IVF/ICSI in normally fertilized and tripronucleated zygotes.

Time (h)	2PN (n = 1483)	3PN (n = 126)
PN appearance	10.72 ± 6.15 ^c	19.76 ± 15.19 ^c
PN fading	27.99 ± 6.53 ^c	31.79 ± 8.37 ^c
t_2	30.88 ± 7.33 ^c	34.65 ± 8.54 ^c
t_3	40.93 ± 8.57 ^a	42.78 ± 9.59 ^a
t_4	43.97 ± 10.14 ^a	46.10 ± 11.02 ^a
t_5	52.78 ± 11.30 ^a	52.27 ± 11.65 ^a
t_8	62.57 ± 12.94 ^b	65.97 ± 11.55 ^b
cc2	10.39 ± 6.48 ^b	8.64 ± 7.17 ^b

Values are mean ± standard deviation.

PN = pronuclei; t_2 = first cleavage (2-cell stage); t_3 = second cleavage (3-cell stage); t_4 = 4-cell stage; t_5 = 5-cell stage; t_8 = 8-cell stage; $cc2$ = second cell cycle duration (i.e. $t_3 - t_2$).

^a $P < 0.05$.

^b $P < 0.01$.

^c $P < 0.001$.

Table 1). Finally, the proportion of abnormal embryo divisions with direct cleavage from zygote to 3 cells or with very short 2-cell stage ($cc2 < 5$ h) was significantly higher in the 3PN group ($n = 18$, 14.3%) than in the 2PN group ($n = 120$, 8.1%) ($P = 0.03$).

A total of 25 3PN embryos were cultured for 6 days (the others being stopped on day 3). Among them, five (20%) developed to the blastocyst stage (two B1, one B3 and two top-quality B4 blastocysts on day 6), whereas four reached the morula stage but failed to cavitate.

Discussion

This work described the kinetic pattern of 3PN embryos obtained in ICSI cycles using a time-lapse device. It showed that 3PN embryos displayed a significantly different cleavage pattern from normally fertilized embryos, with all cellular events from the zygote to the 8-cell stage occurring significantly later in 3PN than in 2PN embryos. This could raise the question of a second assessment of fertilization a few hours after the usual assessment at 18–20 h post ICSI. Moreover, 12.7% of 3PN zygotes went through a 2PN stage before the appearance of the third pronuclei, thus highlighting the need for cautious interpretation of fertilization checking on day 1 after ICSI. Additionally, abnormal division was more frequent in the 3PN group than in the 2PN group.

In ICSI cycles, 3PN zygotes are digynic, this being caused by the nonextrusion of the second polar body. Dispermic triploidy is virtually absent in ICSI cycles because of the injection of a single spermatozoon into the oocyte. However, male infertility is frequently associated with sperm chromosomal abnormalities, and rarely with diploid spermatozoa, which can lead to the formation of tripronucleated zygotes (Figueira et al., 2011). The use of time-lapse analysis in IVF cycles has recently expanded. This technology allows accurate and objective monitoring of early embryo development. The relationship between ploidy and embryo developmental kinetics has been recently studied (Chavez et al., 2012). Time-lapse analysis associated with

karyotyping of individual blastomeres led to the conclusion that cell cycle and fragmentation parameters were prognostic of ploidy, thus opening a way for noninvasive prediction of embryo ploidy, among which would be 3PN embryos. The self-correction potential of ICSI 3PN embryos has been recently demonstrated and concerns half of them (Grau et al., 2011). Whether these self-corrected aneuploid embryos have a different cleavage pattern and developmental kinetics than those unable to restore euploidy remains to be studied. Moreover, these authors showed that neither parental inheritance nor ploidy determines the ability of ICSI 3PN embryos to reach the blastocyst stage (Grau et al., 2011). Because morphokinetic characteristics have been demonstrated to predict blastocyst formation in 2PN embryos (Herrero and Meseguer, 2013), the issue of predicting blastocyst formation in 3PN according to kinetic parameters could be addressed in further studies.

Microsurgical correction of 3PN embryos with removal of one pronucleus was evaluated and proposed to rescue these aneuploid embryos more than 25 years ago (reviewed in Rosenbusch, 2009). This strategy has allowed the formation of heteroparental blastocysts (Malter and Cohen, 1989; Rawlins et al., 1988). Some recent data demonstrated that the embryo kinetic pattern observed with a time-lapse device was related to its ploidy (Chavez et al., 2012), at least at early stages, so further studies based on time-lapse imaging could compare developmental aspects in 3PN and microsurgically corrected 3PN embryos.

This study describes the developmental timing of triprounuclear embryos in comparison with normal fertilized embryos (2PN) obtained by ICSI. Triprounuclear embryos showed slower development to the first sign of fertilization and through the cleavage stages.

References

- Chavez, S.L., Loewke, K.E., Han, J., Moussavi, F., Colls, P., Munne, S., Behr, B., Reijo Pera, R.A., 2012. Dynamic blastomere behaviour reflects human embryo ploidy by the four-cell stage. *Nat. Commun.* 3, 1251–1262.
- Escribá, M.J., Martín, J., Rubio, C., Valbuena, D., Remohí, J., Pellicer, A., Simón, C., 2006. Heteroparental blastocyst production from microsurgically corrected tripronucleated human embryos. *Fertil. Steril.* 86, 1601–1607.
- Figueira, R.C., Setti, A.S., Braga, D.P., Iaconelli Jr., A., Borges Jr., E., 2011. Prognostic value of triploid zygotes on intracytoplasmic sperm injection outcomes. *J. Assist. Reprod. Genet.* 28, 879–883.
- Grau, N., Escrich, L., Martín, J., Rubio, C., Pellicer, A., Escribá, M.J., 2011. Self-correction in tripronucleated human embryos. *Fertil. Steril.* 96, 951–956.
- Herrero, J., Meseguer, M., 2013. Selection of high potential embryos using time-lapse imaging: the era of morphokinetics. *Fertil. Steril.* 99, 1030–1034.
- Malter, H.E., Cohen, J., 1989. Embryonic development after microsurgical repair of polyspermic human zygotes. *Fertil. Steril.* 52, 373–380.
- Rawlins, R.G., Binor, Z., Radwanska, E., Dmowski, W.P., 1988. Microsurgical enucleation of tripronuclear human zygotes. *Fertil. Steril.* 50, 266–272.
- Rosenbusch, B.E., 2009. Selective microsurgical removal of a pronucleus from tripronuclear human oocytes to restore diploidy: disregarded but valuable? *Fertil. Steril.* 92, 897–903.

Declaration: The authors report no financial or commercial conflicts of interest.

Received 22 May 2013; refereed 23 January 2014; accepted 23 January 2014.

Ce travail, publié en 2014, nous a permis de constater de nombreux mouvements au sein des nucléoles, ainsi qu'une asynchronie d'apparition et de disparition des PN dans certains cas. Ces observations ont conduit à la remise en question de la classification des zygotes qui était alors bien répandue avant l'utilisation des systèmes time-lapse.

Concernant les embryons issus d'ovocytes fécondés 3PN, nous avons montré qu'ils présentaient de nombreux clivages anormaux, un développement plus lent et un taux de blastulation diminué. Peu de temps après notre publication, l'équipe de Grau et al. (Grau et al. 2015) s'est à nouveau intéressé aux embryons issus de 3PN et a confirmé que les premiers clivages de ces embryons apparaissaient plus tardivement que pour les embryons issus de 2PN. Ils ont complété ce travail par l'analyse de la ploïdie de ces embryons anormalement fécondés. Ceux qui étaient diploïdes montraient des paramètres morphocinétiques proches des embryons 2PN, le paramètre t5 (nombre d'heures pour atteindre le stade 5 cellules) semblait être un bon marqueur prédictif pour discriminer les embryons 3PN diploïdes et triploïdes.

En 2020, Mateo et al. (Mateo et al. 2020) ont étudié 149 embryons issus de zygotes 1PN qui montrent également une cinétique de division cellulaire ralenti. Seuls ceux ayant la capacité de se développer jusqu'au stade de blastocyste ont une cinétique similaire aux embryons issus d'ovocytes 2PN. Récemment, Ezoë et al. (Ezoë et al. 2022) ont confirmé que la survenue de clivages anormaux est plus fréquente chez les embryons issus d'ovocytes 1PN que ceux issus de 2PN et 3PN. La poursuite du développement est également affectée et illustrée par le taux de blastulation significativement réduit pour les 3PN et très faible pour les 1PN.

Ces différents résultats confirment ceux que nous avons publiés en 2014 et mettent en évidence une difficulté pour les embryons issus d'ovocytes 3PN à atteindre le stade de blastocyste. Néanmoins, certains embryons semblent être en capacité de corriger cette anomalie de fécondation et de se développer en un blastocyste euploïde. En revanche, l'analyse de la ploïdie embryonnaire n'étant pas autorisée actuellement en France, il n'est pas envisageable de conserver en culture ces ovocytes anormalement fécondés pour réaliser une analyse des blastocystes obtenus comme peuvent le faire d'autres pays ayant des réglementations différentes.

b. Influence de l'origine des spermatozoïdes sur la morphocinétique embryonnaire = article ②

A la suite de notre étude rétrospective d'embryons 3PN issus d'ICSI, nous nous sommes intéressés à l'influence de l'origine des spermatozoïdes sur le développement embryonnaire. L'utilisation de la technique d'ICSI pour la mise en fécondation des ovocytes permet l'utilisation de spermatozoïdes d'origine chirurgicale chez des patients aux paramètres spermatiques très altérés. Malgré des taux de grossesse satisfaisants dans cette population, j'ai souhaité évaluer l'influence de l'origine de ces spermatozoïdes en comparant les paramètres morphocinétiques des embryons obtenus avec des spermatozoïdes éjaculés ou chirurgicaux.

Pour cela, nous avons observé les embryons obtenus par ICSI pour indication masculine et bénéficiant d'une culture dans un système time-lapse entre février 2011 et octobre 2013. Cela représentait 1735 embryons issus de spermatozoïdes éjaculés de patients souffrant d'oligo-asthéo-tératozoospermie et 114 issus de spermatozoïdes chirurgicaux de patients souffrant d'azoospermie (67 prélèvements de pulpes testiculaires et 47 prélèvements de épididymaires).

Pour cette publication je me suis chargée de réaliser une revue de la littérature pour définir les connaissances sur le sujet et identifier la question sur laquelle travailler. Je me suis chargée d'annoter les événements morphocinétiques des vidéos des embryons en culture time-lapse afin d'extraire une base de données du développement embryonnaire. En parallèle j'ai extrait les données nécessaires à la création de la base de données des patients correspondants aux embryons étudiés. J'ai pu réaliser les analyses statistiques pour comparer les données des 2 groupes une fois celles-ci extraites. Pour finir, je me suis chargée de la rédaction de la première version de l'article, de la soumission auprès d'une revue à comité de lecture et de répondre aux corrections posées par les relecteurs.

Does sperm origin affect embryo morphokinetic parameters?

Jenna Lammers^{1,2,6} · Arnaud Reignier^{1,2,5,6} · Carole Spingart^{1,2,6} · Aurore Catteau¹ · Laurent David^{2,3,4,5,6} · Paul Barriere^{1,2,5,6} · Thomas Freour^{1,2,5,6,7}

Received: 11 March 2015 / Accepted: 15 June 2015 / Published online: 25 June 2015
© Springer Science+Business Media New York 2015

Abstract

Purpose The purpose of our study was to use time-lapse in order to evaluate the impact of sperm origin (fresh ejaculate or surgically retrieved) on embryo morphokinetic parameters and clinical outcome in intracytoplasmic sperm injection (ICSI) cycles.

Methods This retrospective monocentric study was conducted in 485 unselected couples undergoing 604 ICSI cycles with embryo culture in the Embryoscope®. Among them, 445 couples underwent ICSI cycle with fresh ejaculated sperm and 40 with surgically retrieved sperm (26 with testicular sperm and 14 with epididymal sperm). Embryo morphokinetic parameters and clinical cycle outcome were compared between fresh ejaculated sperm and surgically retrieved sperm. A subgroup analysis was also conducted between testicular and epididymal sperm ICSI cycles.

Results Clinical outcome was comparable between groups according to sperm origin. Although most early morphokinetic parameters were comparable between ejaculated and surgical sperm groups, a few parameters were significantly different between both groups, but with a considerable overlap in their distribution. Late cellular events occurred significantly later in the surgical sperm group than in the ejaculated sperm group.

Conclusions Morphokinetic analysis did not allow us to identify clinically relevant differences between fresh ejaculate and surgically retrieved sperm groups. Further studies are needed, especially concerning the relationship between sperm origin and late morphokinetic parameters, such as blastocyst development.

Keywords Time-lapse · Morphokinetic · ICSI · Azoospermia · Surgically retrieved sperm

Capsule Time-lapse parameters do not significantly differ according to sperm origin

✉ Thomas Freour
thomas.freour@chu-nantes.fr

- ¹ Service de Médecine et Biologie de la Reproduction, CHU de Nantes, Nantes 44093, France
- ² INSERM UMR 1064, ITERT, Nantes, France
- ³ INSERM UMS 016, SFR Santé, iPSC Core Facility, Nantes, France
- ⁴ CNRS UMS 3556, SFR Santé, iPS Core Facility, Nantes, France
- ⁵ UFR Médecine, Université de Nantes, Nantes, France
- ⁶ ITUN, CHU Nantes, Nantes, France
- ⁷ Clínica EUGIN, 08029 Barcelona, Spain

Introduction

The first technical revolution in terms of assisted reproductive technology (ART) after the first IVF cycle was pioneered in the late 1970s [1] consisted of intracytoplasmic sperm injection (ICSI) in the 1990s, allowing the numerous couples suffering from male infertility to seek IVF at last. Thanks to the implementation of ICSI, embryologists have progressively been able to treat patients with severe oligospermia or even azoospermia when surgical sperm retrieval could be attempted with success. Indeed, microepididymal sperm aspiration (MESA) can be attempted in cases of obstructive azoospermia (OA) with very high success rates (>90 %), and testicular sperm extraction (TESE) can be attempted in non-obstructive azoospermia (NOA) cases, albeit with lower success rates [2].

Although many studies have reported acceptable pregnancy rates in ICSI cycles with surgically retrieved sperm [3], very few data are available on the influence of sperm origin, i.e., ejaculated or surgically retrieved sperm, on early embryo development [4–6]. Moreover, all data are based on conventional embryo quality assessment with morphology, this technique being known to suffer from moderate sensitivity, moderate specificity [7], and inter/intra-observer variability [8]. The recent introduction of time-lapse monitoring (TLM) systems, providing stable incubation conditions and continuous follow-up of embryo development with exact measurement of all cleavage timings, has begun a new era in the field of embryology, allowing the implementation of a more accurate and reproducible embryo quality assessment method based on morphokinetics [9, 10]. TLM can thus be used to compare embryo development in ICSI cycles in terms of sperm origin more accurately than conventional morphology. As clinical implementation of TLM is based on the use of precise kinetic parameters combined into algorithms, it is important to identify any clinical or demographic factors that might significantly impact on morphokinetic parameters, in order to take them into account and control them.

The aim of our study was therefore to compare the morphokinetic aspects of early embryo development in ICSI cycles according to sperm origin, i.e., fresh ejaculated (FES) or surgically retrieved sperm (SRS).

Material and methods

We retrospectively analyzed the data of consecutive patients who had undergone IVF-ICSI with oocyte and embryo cultures performed with the Embryoscope®. These data were collected and recorded in a registered authorized database between February 2011 and October 2013 in our IVF unit. All the patients gave written informed consent to the procedures and to the digital recording and anonymous use of the data related to their history (IRB-approved procedure). Only ICSI cycles were included to determine as precisely as possible the timing of fertilization. All information on implantation, viable pregnancy occurrence, delivery, and early postnatal complications was available at the time of analysis.

A male factor was identified in all cycles, i.e., abnormal sperm analysis was performed strictly in accordance with WHO criteria (5th edition) [11]. When live sperm were present in the ejaculate, sperm preparation was performed on silica gradient (two layers, 90 and 50 %, Suprasperm®, Origio®). Azoospermia was diagnosed when no spermatozoa could be observed after centrifugation of two consecutive sperm analyses. NOA or OA diagnosis was based on medical history, physical examination, hormonal status, genetic workup, and testicular volume. In NOA cases, TESE

was performed with the open biopsy procedure. Testicular tissue was gently crushed in order to extract living spermatozoa. The cellular suspension was loaded onto 40 % silica suspension (Suprasperm®, Origio, France) and centrifuged at 2000 rpm for 15 min. Live spermatozoa found in the pellet (testicular sperm (TS)) within the silica layer and/or in the supernatant were resuspended in Universal IVF medium® (Origio®) and frozen in liquid nitrogen according to the standard slow freezing method until thawing, when the IVF-ICSI cycle could be performed. In OA cases, MESA was performed under general anesthesia, the urologist aspirating epididymal fluid with fine needles. Spermatozoa extracted from the epididymis (epididymal sperm (ES)) were then frozen, as in TESE. Thawing was performed immediately before ICSI, straws being incubated at 37 °C for 5 min and sperm suspension was gently mixed in 2 ml of pre-equilibrated sperm-washing medium (Universal IVF medium®, Origio). After a single washing step (5 min centrifugation in washing medium), the pellet was resuspended in a few drops of washing medium and evaluated under an inverted microscope in preparation for ICSI. No synchronous surgical retrieval was attempted. Only patients with successful surgical retrieval were included in the study (the usual success rate for TESE is 40 % in our local experience).

Before stimulation, all women had complete ovarian reserve exploration, with anti-Müllerian hormone (AMH) (Beckman Coulter Immunotech) measurement and antral follicle count (AFC) performed on day 2 or 3 of one of the three spontaneous cycles preceding the IVF cycle. AFC grouped all follicles with a mean diameter ranging from 2 to 9 mm.

All patients underwent ICSI and embryo transfer (ET) according to standard protocols. Women underwent controlled ovarian stimulation by an antagonist protocol with estrogen pretreatment [12]. Recombinant human chorionic gonadotropin (hCG) was administered when three or more follicles were >17 mm in diameter with the lead follicle ≥18 mm. Oocyte retrieval was performed 34 to 36 h later. Insemination was then achieved by intracytoplasmic sperm injection (ICSI), including mature metaphase II (MII) and immature metaphase I (MI) oocytes 38 to 40 h postovulation triggering. Immature MI oocytes could eventually be kept in culture for a few additional hours before being injected in order to observe the extrusion of the first polar body. As sperm finding can be tricky and last longer in SRS cycles than in FES cycles, oocytes were placed in groups of four in an injection dish in order to minimize the duration of exposure to suboptimal environmental conditions in SRS cycles. The average time of injection for the four oocytes was considered as t_0 in subsequent kinetic analysis. Injected oocytes were then immediately placed in individual microwells within a specific culture dish (Embryoslide®, Unisense Fertilitech®, Aarhus, Denmark) and loaded into the Embryoscope® (Unisense Fertilitech®, Aarhus, Denmark), a tri-gas incubator with a

built-in microscope allowing time-lapse monitoring of early embryo development. Embryo culture was performed at 37 °C under a controlled atmosphere with low oxygen pressure (5 % O₂, 6 % CO₂). Vitrolife® sequential media (Gothenburg, Sweden) were used for embryo culture, with embryos being cultured in G1plus® medium from day 0 to day 3 and then transferred to a new pre-equilibrated slide containing G2plus® medium and cultured from day 3 onwards. Each embryo was observed by detailed time-lapse analysis measuring the exact timing of the early developmental events in hours after ICSI procedure as described by Ciray and colleagues [13]. The terms t₂, t₃, t₄, t₅, t₆, t₇, and t₈ were respectively used for exact timings of appearance of embryos with 2, 3, 4, 5, 6, 7, and 8 well-defined blastomeres. The term t_{SC} refers to the timing of morula compaction onset, t_M to the timing when morula is fully compacted, t_{SB} to the timing of blastulation onset, and t_B to the timing of full blastulation. The duration of the cellular cycle between each cleavage was also considered. The term s₂ was used to illustrate the synchrony of the second cell cycle, i.e., transition from a three-cell to a four-cell embryo (t₄-t₃). The term CC₂ was used to illustrate the duration of the two-cell stage, i.e., transition from a two-cell embryo to a three-cell embryo (t₃-t₂). In order to minimize the operator-dependent variation, especially in blastocyst annotation, two embryologists were specifically trained and performed the annotation together according to the published guidelines [13].

Cleavage-stage embryo(s) or single blastocyst transfer was chosen depending on medical history, previous IVF attempts, and early embryo development. Younger women (under 32 years of age) undergoing their first or second IVF cycle were generally counseled to undergo single blastocyst transfer. In the case of cleavage-stage embryo transfer (day 3), single or double embryo transfer was decided conjointly by medical staff and the couple. A pregnancy test was carried out 12 days after embryo transfer, and, if it was positive, clinical pregnancy was confirmed ultrasonographically 5 weeks later by detection of gestational sac and fetal heart activity. Delivery term, newborn birth weight, and congenital malformation occurrence were also recorded.

Statistics

The main readout was the timing of developmental events in the hours after ICSI, as measured by time-lapse analysis. Cycle outcome was also compared between groups according to the sperm origin. As no data exist up to now on the potential impact of sperm origin on embryo development, we assume that it is not feasible to draw a relevant hypothesis on the sample size required for an adequate assessment of the treatment effect.

For basic comparisons, Student's or Wilcoxon's tests were used for continuous variables and χ^2 or Fischer's tests for qualitative variables.

Statistical analysis was performed with Medcalc® (version 11.1.1.0). *P* values ≤ 0.05 were considered to denote a significant difference.

Results

A total of 604 ICSI cycles performed in 485 couples were included in the analysis, corresponding to 3959 oocytes injected in ICSI. Among these 604 cycles, 556 were performed with fresh ejaculated semen (FES) (445 couples, 3662 oocytes injected), and 48 with frozen surgically retrieved sperm (SRS) (40 couples, 297 oocytes). Among these SRS cycles, 32 were performed with testicular spermatozoa (TS subgroup) (26 couples with the man suffering from NOA, 194 oocytes injected) and 16 with epididymal spermatozoa (ES subgroup) (14 couples with the man suffering from OA, 103 oocytes injected). Among these 14 OA patients, 13 had congenital bilateral absence of the vas deferens and one was postvasectomy. Patients' demographic characteristics in the FES and SRS groups and in the TS and ES subgroups are presented in Tables 1 and 2. No statistical difference was found between the FES and SRS groups. Ovarian reserve parameters were also comparable between both groups. When comparing the ES and TS subgroups, we found that infertility duration, male BMI, and female age were significantly lower in the ES subgroup than in the TS subgroup. Morphokinetic parameters are presented in Tables 3 and 4. When early embryo development was compared between the FES and SRS groups, only CC₂ and t₈ were found to be significantly higher in the FES group than in the SRS group (Table 3). These results remained the same when this analysis was conducted in first ICSI cycles only (data not shown). Concerning morula and blastocyst development, all cellular events occurred significantly later in the SRS group than in the FES group (Table 3). When the ES and TS subgroups were compared, we found that s₂ was significantly longer and t₃ and t₈ significantly shorter in the ES group than in the TS group (Table 4). ICSI cycle characteristics and outcomes are presented in Tables 5 and 6. All the parameters were comparable between the FES and SRS groups (Table 5), and between the ES and TS subgroups. The cycle outcome was comparable in the FES and SRS groups whatever the day of embryo transfer was (data not shown). We also recorded children's health at birth. No major congenital malformation was found in any group.

Discussion

In this study, we showed that ICSI cycles with frozen surgically retrieved sperm provide comparable outcomes to those with fresh ejaculated sperm. Morphokinetic analysis did not show any major differences between the groups, except for

Table 1 Patients' demographic characteristics

		FES group	SRS group	<i>P</i> value
Patients		445	40	
Cycles		556	48	
Infertility duration (years)		4.00 (2.04)	3.68 (2.68)	>0.05
Primary infertility of the couple (%)		62.59	64.58	>0.05
Male characteristics	Age (years)	34.90 (5.40)	35.38 (6.17)	>0.05
	BMI (kg/m ²)	23.30 (3.66)	23.71 (4.43)	>0.05
	Active smokers (%)	30.5	37.5	>0.05
Female characteristics	Age (years)	32.16 (4.32)	31.42 (3.85)	>0.05
	BMI (kg/m ²)	23.64 (3.66)	23.29 (3.89)	>0.05
	Smokers (%)	13.67	18.75	>0.05
	Serum AMH (μg/L)	4.75 (3.26)	5.27 (4.16)	>0.05
	Antral follicle count	20.02 (9.40)	20.90 (9.20)	>0.05

Results are presented as proportion or mean (standard deviation) when appropriate

three parameters. We also performed a subgroup analysis among surgically retrieved sperm cycles, comparing testicular and epididymal sperm cycles. This analysis did not show any significant differences in terms of cycle outcome and morphokinetic analysis, except for t3, t8, and s2. These kinetic parameters were different from the two found in the main analysis. In our opinion, this absence of a major morphokinetic pattern difference between fresh ejaculated sperm and surgically retrieved sperm cycles is of importance, as it demonstrates that TLM predictive models developed for clinical use in ICSI cycles do not need to be controlled for sperm origin.

To our knowledge, only one study comparing morphokinetic analysis according to sperm origin has been reported up to now. It was presented as an oral communication in an international congress and is only available as an abstract so far [14]. In this study, 192 embryos derived from frozen surgically retrieved sperm were compared with 156 embryos derived from fresh ejaculated sperm. Unfortunately, the authors did not reveal which kind of surgically retrieved sperm was used in their study, i.e.,

testicular or epididymal sperm. Embryos derived from SRS reached the two-cell stage significantly earlier, whereas morula formation and blastocyst hatching occurred significantly later than in embryos derived from FES. The authors concluded that these data suggest that the sperm source contributes to embryo morphokinetics and specifically impact first cleavage and embryo development after embryonic genome activation. However, the lack of information in this abstract regarding patient and sperm characteristics and cycle outcome prevents us from drawing any firm conclusion. Although annotating embryo development up to the blastocyst stage with TLM devices has been shown to be feasible with a fair reproducibility by trained operators [10], evaluating morula and the blastocyst stages remains a challenging issue. In order to minimize the operator-dependent variation in blastocyst annotation, two trained embryologists performed this analysis. Although we did not find the same trend in faster first cleavage (i.e., t2) in SRS cycles, we found the same delayed morula and blastocyst formation in SRS cycles in our database. However, whether this delay in late

Table 2 Patients' demographic characteristics

		TS subgroup	ES subgroup	<i>P</i> value
Patients		26	14	
Cycles		32	16	
Infertility duration (years)		4.13 (2.93)	2.13 (1.36)	0.02
Primary infertility (%)		62.50	68.75	>0.05
Male characteristics	Age (years)	35.78 (6.18)	34.56 (6.26)	>0.05
	BMI (kg/m ²)	24.59 (4.59)	21.50 (2.76)	0.03
	Active smokers (%)	46	21.4	>0.05
Female characteristics	Age (years)	32.31 (4.00)	29.63 (2.85)	0.04
	BMI (kg/m ²)	23.27 (4.00)	23.32 (3.80)	>0.05
	Active smokers (%)	18.75	18.75	>0.05
	Serum AMH (μg/L)	4.79 (3.86)	6.26 (4.72)	>0.05
	Antral follicle count	20.86 (9.01)	21.00 (9.78)	>0.05

Results are presented as proportion or mean (standard deviation) when appropriate

Table 3 Timings and intervals of cellular cleavages in hours

	FES group	SRS group	<i>P</i> value
Embryos with full annotation up to day 3	1735	114	
tPNa (hours)	10.57 (5.78)	9.58 (3.91)	>0.05
tPNf (hours)	27.96 (7.28)	27.93 (8.87)	>0.05
t2 (hours)	32.26 (10.16)	33.02 (10.81)	>0.05
t3 (hours)	41.50 (10.02)	40.86 (11.28)	>0.05
t4 (hours)	44.46 (11.17)	43.78 (11.00)	>0.05
t5 (hours)	53.10 (12.08)	50.84 (12.24)	>0.05
t6 (hours)	56.90 (12.08)	55.24 (12.15)	>0.05
t8 (hours)	61.34 (10.8)	55.79 (10.13)	<0.001
CC2 (t3-t2) (hours)	9.84 (6.82)	7.98 (6.54)	0.005
s2 (t4-t3) (hours)	3.49 (6.70)	3.32 (5.56)	>0.05
tSC	88.68 (11.60)	100.39 (12.48)	<0.001
tM	97.81 (11.52)	108.40 (12.43)	<0.001
tSB	107.79 (11.94)	115.03 (13.37)	<0.001
tB	115.19 (12.80)	124.06 (7.63)	<0.001

Results are presented as mean (standard deviation)

tPNa appearance of pronuclei, *tPNf* time of pronuclei disappearance, *t2* to *t8* timing of 2 to 8 cell-stages, *CC2* duration of cellular cycle 2, *s2* synchronicity of the two blastomeres' divisions within the second cell cycle, *tSC* timing of compaction onset, *tM* timing of full compaction, *tSB* timing of blastulation onset, *tB* timing of full blastulation

embryo development could be related with lower implantation potential was not confirmed in our study and has not been demonstrated yet to our knowledge. Actually, the blastulation rate and the pregnancy rate remained comparable in both groups in our study, whatever the day of embryo transfer was. In order to go further into this analysis of a sperm origin-mediated impact on embryo morphokinetics, a study including a sufficient number of single blastocyst transfer cycles and comparing both blastocyst kinetics and morphology grading in FES and SRS cycles should be specifically designed.

The issue of sperm freezing impact on embryo development could eventually be raised. As we do not perform synchronous TESE or MESA, we could not compare fresh versus frozen-thawed surgically retrieved sperm cycles. Concerning frozen ejaculated sperm, our population was too small (*n*=19 cycles) and too heterogeneous (absence, sperm cryopreservation before cancer treatment, difficulties to provide sperm sample) in our opinion to be analyzed. However, there is no evidence in the literature on an eventual detrimental effect of frozen-thawed ejaculated

Table 4 Timings and intervals of cellular cleavages in hours

	TS subgroup	ES subgroup	<i>P</i> value
Embryos with full annotation up to day 3	67	47	
tPNa (hours)	9.60 (4.56)	9.54 (2.78)	>0.05
tPNf (hours)	29.12 (10.49)	26.94 (4.77)	>0.05
t2 (hours)	34.36 (12.73)	30.75 (5.83)	>0.05
t3 (hours)	42.15 (13.14)	36.69 (6.68)	0.01
t4 (hours)	43.93 (12.11)	43.54 (8.82)	>0.05
t5 (hours)	50.54 (12.61)	51.35 (11.72)	>0.05
t6 (hours)	52.63 (10.34)	56.77 (14.30)	>0.05
t8 (hours)	57.64 (10.33)	52.82 (10.16)	0.02
CC2 (t3-t2) (hours)	7.67 (7.06)	8.50 (5.59)	>0.05
s2 (t4-t3) (hours)	2.38 (4.36)	4.98 (6.95)	0.02

Results are presented as mean (standard deviation)

tPNa appearance of pronuclei, *tPNf* time of pronuclei disappearance, *t2* to *t8* timing of 2 to 8 cell-stages, *CC2* duration of cellular cycle 2, *s2* synchronicity of the two blastomeres' divisions within the second cell cycle

Table 5 ICSI cycles characteristics and outcomes

	FES group	SRS group	<i>P</i> value
IVF cycle rank	1.95 (1.14)	1.94 (1.07)	>0.05
Oocytes retrieved	10.03 (4.20)	10.08 (3.43)	>0.05
Total dose of FSH injected (IU)	2162.65 (766.82)	2091.15 (847.15)	>0.05
Oocytes injected	3662	297	NA
Zygote (2PN)	2235	144	NA
Fertilization rate (%)	61.0 %	48.48 %	>0.05
Extended culture cycles (<i>n</i> , %)	281, 50.54 %	18, 37.5 %	>0.05
Blastulation rate (% of extended culture embryos)	52.52 %	59.07 %	>0.05
Cycles with embryo transfer (%)	70.3	56.3	>0.05
Embryos transferred	1.34 (0.48)	1.30 (0.47)	>0.05
Pregnancy rate per cycle (%)	28.8	22.9	>0.05
Clinical pregnancy rate per cycle (%)	23.4	18.8	>0.05
Live birth rate per cycle (%)	18.7	16.7	>0.05
Twin delivery rate (%)	9.7	14.3	>0.05
Preterm deliveries (<37 SA) (<i>n</i>)	7	1	NA
Average birth weight (kg)	3.48 (1.06)	2.77 (0.84)	>0.05

Results are presented as mean (standard deviation), proportion (%) or numbers when appropriate. No statistical difference was found
NA not applicable

sperm on embryo development and morphokinetics. This point would deserve attention in further studies.

Various morphokinetic parameters have been identified as prognostic markers of embryo implantation [15, 16]. Among them, *t8*, *s2*, and *cc2* have been reported to be correlated with implantation by some authors [17, 18], whereas others did not identify them as significant predictors [15]. Specifically, none of these parameters showed predictive power when

considered individually. Moreover, we recently reported in an external validation study that *cc2* could lower the performance of TLM-based prediction model [19]. Although the differences between these groups were statistically different for *t8*, *s2*, and *cc2* in our database, the huge overlap between the confidence intervals of these variables prevented us from using them as clinically relevant prognostic tools.

Table 6 ICSI cycles characteristics and outcomes in TS and ES subgroups

	TS subgroup	ES subgroup	<i>P</i> value
IVF cycle rank	2.00 (1.03)	1.81 (1.17)	>0.05
Oocytes retrieved	9.94 (3.44)	10.38 (3.50)	>0.05
Total dose of FSH injected (IU)	2160.53 (892.15)	1952.38 (756.95)	>0.05
Oocytes injected	194	103	NA
Zygote (2PN)	87	57	NA
Fertilization rate (%)	44.8	55.3	>0.05
Extended culture cycles (<i>n</i> , %)	11, 34.4 %	7, 43.7 %	>0.05
Blastulation rate (% of extended culture embryos)	53.6	67.6	>0.05
Cycles with embryo transfer (%)	50	68.8	>0.05
Embryos transferred	1.31 (0.48)	1.27 (0.47)	>0.05
Pregnancy rate per cycle (%)	18.8	31.3	>0.05
Clinical pregnancy rate per cycle (%)	15.6	25	>0.05
Live birth rate per cycle (%)	12.5	25	>0.05
Twin delivery rate (%)	33.3	0	>0.05
Preterm deliveries (<37 SA) (<i>n</i>)	1	0	NA
Average birth weight (kg)	2.28 (0.67)	3.44 (0.56)	NA

Results are presented as mean (standard deviation), proportion (%), or numbers when appropriate
NA not applicable

However, we acknowledge that evaluating embryo development after embryo genomic activation (EGA) could be of interest in evaluating the potential impact of sperm origin on embryo development. In any case, it is interesting that recent publications have questioned the relevance of azoospermia and testicular sperm use as an indication of blastocyst stage transfer in ICSI cycles [20, 21].

The use of TLM systems allowed us to optimize embryo quality assessment compared with conventional embryo morphology assessment. Indeed, morphokinetics has been shown to be more reproducible [10] and more accurate in predicting embryo quality and subsequent implantation than morphology alone [22], which suffers from limited performance. As the few other studies comparing embryo development according to sperm origin have been based on conventional morphology assessment, their conclusions should be treated with caution. In a recent study, Ben-Ami et al. [3] compared ICSI outcome in patients with cryptozoospermia after use of either ejaculated or testicular sperm. Epididymal sperm was not included in this work. Only 17 patients were included, but a total of 116 ICSI cycles (68 with ejaculated sperm and 48 with SRS) were analyzed. Despite a significantly lower cleavage rate when ejaculated sperm cells were used compared with TESE cycles, there were no statistically significant differences between the two subgroups in the mean morphology scores of day 2 and day 3 embryos. However, clinical outcome in this study was significantly higher with surgical sperm than with ejaculated sperm, although embryo quality was almost comparable, leading the authors to recommend TESE in patients with cryptozoospermia who fail to conceive by ICSI with ejaculated spermatozoa. This surprising difference in terms of clinical outcome between surgical sperm and ejaculated sperm was not found in three other recent studies [6, 23, 24]. Although embryo quality was unfortunately not described in one of them [22], the others reported comparable embryo quality regardless of the sperm origin [6, 24]. Interestingly, this last study also included MESA cycles in the analysis, showing no significant difference from TESE cycles [24].

Another quite similar study aimed at assessing the putative effectiveness of sperm origin, ejaculated or testicular, in cryptozoospermia treatment [25]. Embryo quality was compared in two independent groups, and did not show significant differences between the two groups, except for grade A embryos (but with low significance). This is in keeping with previous comparable studies [26]. However, as clinical outcome was not reported in this study, the authors' recommendation to use ejaculated sperm rather than testicular sperm in patients with cryptozoospermia was not supported by the data.

Unfortunately, our study did not include child follow-up after birth. Neonatal outcomes for children conceived with testicular or epididymal sperm have been studied in more than 400 children, singletons, and twins [27]. Neonatal outcome and total malformation rates were similar between testicular

and epididymal sperm groups, and between ICSI and IVF with ejaculated sperm groups. The authors concluded that these treatments were equally safe.

In our study, mean AFC appeared to be high, suggesting a high PCOS prevalence in the study population. This could be related to the routine practice of AFC in our center, where very small follicles are included in AFC, leading to a slightly overestimated AFC compared with numbers usually seen in the literature. This high mean AFC is consistent with relatively high serum AMH levels, and may also be correlated with the relatively young age of the patients included in this study. However, it should be noted that PCOS prevalence was far from negligible in this study, although we cannot provide precise numbers, as the Rotterdam criteria were not systematically explored and noted in the database.

One possible limitation of this study is its monocentric design. However, in our opinion, the relatively large number of cycle/embryos included in the analysis is sufficient to provide a relevant answer to our study question. Moreover, we used the most generally accepted nomenclature for embryo annotation with TLM systems, limiting the inter-observer variability and theoretically allowing our results to be generalized to other users of such systems. Finally, the absence of data and consensus on sample size required for an adequate assessment of the treatment effect compared with the control group prevented us from providing absolutely rigorous statistical analysis as requested by the guidelines and standards in clinical studies. However, this limitation is frequently observed in pilot retrospective studies, and we chose to include as many embryos as possible in both treatment and control groups to try to overcome it in our own retrospective study. Another limitation could be that not only first ICSI cycles were included in our study. Actually, we chose to include as many cycles as possible in our analysis, in order to study an unselected population reflecting routine daily activity. However, the statistical comparison between the FES and SRS groups yielded comparable results when performed in first ICSI cycles only, thus apparently ruling out this potential source of bias.

Conclusion

In conclusion, this study comparing morphokinetics according to sperm origin showed that few kinetic variables differed. However, these variables were not considered individual predictive markers in the literature, and there was a considerable overlap in their distribution between groups. Finally, no significant difference in terms of clinical outcome was found according to sperm origin. This study does not support the concept of an impact of sperm origin, i.e., fresh ejaculated or surgically retrieved, on embryo quality. Further studies could include embryo monitoring and annotation up to the blastocyst stage and should

be multicentric in order to increase the number of cycles performed with surgically retrieved sperm.

Funding None

References

- Stephens PC, Edwards RG. Birth after the reimplantation of a human embryo. *Lancet*. 1978;2:366.
- Bromage SJ, Falconer DA, Lieberman BA, Sangar V, Payne SR. Sperm retrieval rates in subgroups of primary azoospermic males. *Eur Urol*. 2007;51:534–9.
- Ben-Ami I, Razieli A, Strassburger D, Komarovskiy D, Ron-El R, Friedler S. Intracytoplasmic sperm injection outcome of ejaculated versus extracted testicular spermatozoa in cryptozoospermic men. *Fertil Steril*. 2013;99:1867–71.
- Desai N, AbdelHafez F, Sabanegh E, Goldfarb J. Paternal effect on genomic activation, clinical pregnancy and live birth rate after ICSI with cryopreserved epididymal versus testicular spermatozoa. *Reprod Biol Endocrinol*. 2009;7:142.
- Ishikawa T, Shiotani M, Izumi Y, Hashimoto H, Kokeguchi S, Goto S, et al. Fertilization and pregnancy using cryopreserved testicular sperm for intracytoplasmic sperm injection with azoospermia. *Fertil Steril*. 2009;92:174–9.
- Tsai CC, Huang FJ, Wang LJ, Lin YJ, Kung FT, Hsieh CH, et al. Clinical outcomes and development of children born after intracytoplasmic sperm injection (ICSI) using extracted testicular sperm or ejaculated extreme severe oligo-astheno-teratozoospermia sperm: a comparative study. *Fertil Steril*. 2011;96:567–71.
- van Loendersloot L, van Wely M, van der Veen F, Bossuyt P, Repping S. Selection of embryos for transfer in IVF: ranking embryos based on their implantation potential using morphological scoring. *Reprod Biomed Online*. 2014;29:222–30.
- Paternot G, Wetzels AM, Thonon F, Vansteenbrugge A, Willems D, Devroey J, et al. Intra- and interobserver analysis in the morphological assessment of early stage embryos during an IVF procedure: a multicentre study. *Reprod Biol Endocrinol*. 2011;9:127.
- Herrero J, Meseguer M. Selection of high potential embryos using time lapse imaging: the era of morphokinetics. *Fertil Steril*. 2013;99:1030–4.
- Sundvall L, Ingerslev HJ, Breth Knudsen U, Kirkegaard K. Inter- and intra-observer variability of time-lapse annotations. *Hum Reprod*. 2013;28:3215–21.
- WHO. Laboratory manual for the examination and processing of human semen. Fifth ed. Geneva: World Health Organization; 2010.
- Cedrin-Dumerin I, Guivarc'h-Leveque A, Hugues JN. Pretreatment with estrogen does not affect IVF-ICSI cycle outcome compared with no pretreatment in GnRH antagonist protocol: a prospective randomized trial. *Fertil Steril*. 2012;97:1359–64.
- Ciray HN, Campbell A, Agerholm IE, Aguilar J, Chamayou S, Esbert M, et al. Proposed guidelines on the nomenclature and annotation of dynamic human embryo monitoring by a time-lapse user group. *Hum Reprod*. 2014;29:2650–60.
- Hickman C, Lennon J, Cook C, Perez MJ, Mania A, Lavery S. Factors affecting morphokinetics: sperm origin, maternal age and polyidy. *Fertil Steril*. 2013;100:S6–7.
- Chen AA, Tan L, Suraj V, Reijo Pera R, Shen S. Biomarkers identified with time-lapse imaging: discovery, validation, and practical application. *Fertil Steril*. 2013;99:1035–43.
- Kaser DJ, Racowsky C. Clinical outcomes following selection of human preimplantation embryos with time-lapse monitoring: a systematic review. *Hum Reprod Update*. 2014;20:617–31.
- Meseguer M, Herrero J, Tejera A, Hilligsøe KM, Ramsing NB, Remohi J. The use of morphokinetics as a predictor of embryo implantation. *Hum Reprod*. 2011;26:2658–71.
- Dal Canto M, Cotichio G, Mignini Renzini M, De Ponti E, Novara PV, Brambillasca F, et al. Cleavage kinetics analysis of human embryos predicts development to blastocyst and implantation. *Reprod Biomed Online*. 2012;25:474–80.
- Fréour T, Le Fleuter N, Lammers J, Spingart C, Reignier A, Barrière P. External validation of a time-lapse prediction model. *Fertil Steril*. 2015;103:917–22.
- Nilsson S, Waldenström U, Engström AB, Hellberg D. Single blastocyst transfer after ICSI from ejaculate spermatozoa, percutaneous epididymal sperm aspiration (PESA) or testicular sperm extraction (TESE). *J Assist Reprod Genet*. 2007;24:167–71.
- Braga DP, Setti AS, Vingris L, Figueira RC, Iaconelli A, Borges E. The male factor of infertility should not be an issue for the selection of patients for extended embryo culture programmes. *Andrology*. 2013;1:758–63.
- Meseguer M, Rubio I, Cruz M, Basile N, Marcos J, Requena A. Embryo incubation and selection in a time-lapse monitoring system improves pregnancy outcome compared with a standard incubator: a retrospective cohort study. *Fertil Steril*. 2012;98:1481–9.
- Oron G, Fisch B, Sapir O, Wertheimer A, Garor R, Feldberg D, et al. Pregnancy outcome after ICSI with thawed testicular sperm from men with non-obstructive azoospermia compared to ICSI with ejaculated sperm from men with severe oligoastheno-teratozoospermia and IVF with normal ejaculated sperm. *Gynecol Endocrinol*. 2014;30:103–6.
- Xie D, Qiu Z, Luo C, Chu Q, Quan S. Effect of spermatozoa from different sources on normal fertilization of oocytes and embryo quality and development in intracytoplasmic sperm injection cycles. *Nan Fang Yi Ke Da Xue Xue Bao*. 2014;34:857–61.
- Amirjannati N, Heidari-Vala H, Akhondi MA, Hosseini Jadda SH, Kamali K, Sadeghi MR. Comparison of intracytoplasmic sperm injection outcomes between spermatozoa retrieved from testicular biopsy and from ejaculation in cryptozoospermic men. *Andrologia*. 2012;44 Suppl 1:704–9.
- Bendikson KA, Neri QV, Takeuchi T, Toschi M, Schlegel PN, Rosenwaks Z, et al. The outcome of intracytoplasmic sperm injection using occasional spermatozoa in the ejaculate of men with spermatogenic failure. *J Urol*. 2008;180:1060–4.
- Fedder J, Loft A, Pamer ET, Rasmussen S, Pinborg A. Neonatal outcome and congenital malformations in children born after ICSI with testicular or epididymal sperm: a controlled national cohort study. *Hum Reprod*. 2013;28:230–40.

L'origine du sperme, éjaculé ou chirurgical, semble influencer les dernières étapes du développement embryonnaire. Les embryons issus de spermatozoïdes chirurgicaux ont un développement plus lent aux stades début de compaction, morula, début de blastulation et blastulation (tSC, tM, tSB et tB) mais ces résultats très dispersés ne semblent pas apporter de conclusion clinique. Dans ce travail de 2015, nous n'avons pas retrouvé de différence significative entre les sous-groupes chirurgicaux (pulpe testiculaire vs épидидyme).

En 2017, Eastick et al. (Eastick et al. 2017) ont comparé des embryons obtenus par ICSI avec des spermatozoïdes éjaculés frais à ceux obtenus à partir de spermatozoïdes congelés. En observant 172 embryons issus de spermatozoïdes frais et 62 de spermatozoïdes congelés, aucune différence significative n'a pu être retrouvée concernant les paramètres morphocinétiques. Dans un même temps, l'étude rétrospective de Scarselli et al. (Scarselli et al. 2018) comparant des embryons obtenus à partir de spermatozoïdes d'origine chirurgicale à des embryons obtenus à partir de spermatozoïdes congelés de donneurs a pu mettre en évidence que le t4 était plus précoce dans le groupe chirurgical et le t9 plus tardif. L'étude n'a porté que sur le développement précoce des embryons, jusqu'au 3^{ème} jour de culture, mais permet, elle aussi, de comparer deux populations d'embryons issus de spermatozoïdes congelés. Ces travaux suggèrent que ce n'est pas le paramètre de congélation qui a pu influencer les résultats que nous avons nous-mêmes observés à partir des spermatozoïdes chirurgicaux.

L'étude observationnelle de Desai et al. (Desai, Gill, et al. 2018) publiée en 2018 a comparé 385 embryons issus de spermatozoïdes obtenus chirurgicalement au niveau épидидymaire ou testiculaire avec 209 embryons obtenus à partir de spermatozoïdes éjaculés. Avec un effectif d'embryons obtenus à partir de spermatozoïdes chirurgicaux plus important que le nôtre, ils ont fait ressortir des différences entre les 2 sous-groupes : le passage à 2 cellules, 4 cellules, 8 cellules et le début de la compaction sont plus précoces dans le groupe épидидymaire. En revanche, les moyennes des paramètres morphocinétiques de ces 2 groupes se trouvant de part et d'autre des moyennes du groupe spermatozoïdes éjaculés, aucune différence avec celui-ci n'est retrouvée.

En 2019, Buran et al. (Buran et al. 2019) se sont également intéressés aux embryons obtenus avec des spermatozoïdes éjaculés ou chirurgicaux. La comparaison des données morphocinétiques de 148 embryons du groupe spermatozoïdes testiculaires, 107 embryons du groupe spermatozoïdes épидидymaires et 171 embryons du groupe spermatozoïdes éjaculés a montré que les stades t2, t4 et t6 surviennent plus tardivement chez les embryons issus de spermatozoïdes épидидymaires. En 2020, Karavani et al. (Karavani et al. 2021) ont mené une étude rétrospective sur 148 embryons obtenus avec des spermatozoïdes extraits chirurgicalement au niveau testiculaire et ceux obtenus à partir de spermatozoïdes éjaculés (190 embryons de patients normozoospermes et 419 oligo-astheno-tératozoospermes). Ils ont aussi démontré que les embryons issus de spermatozoïdes chirurgicaux avaient un développement plus lent.

Ces différents résultats confirment ceux que nous avons publiés en 2015. De façon globale, des différences significatives sont retrouvées pour les embryons issus de spermatozoïdes chirurgicaux qui semblent avoir un développement plus lent que ceux issus de spermatozoïdes éjaculés.

c. Ploïdie embryonnaire et paramètres morphocinétiques : revue de la littérature et DPI pour translocation chromosomique = articles

3 et 4

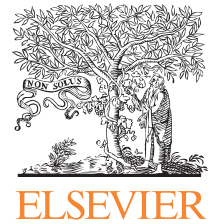
En 2013, j'ai eu l'opportunité de mettre en place l'activité de Diagnostic Préimplantatoire (DPI) au laboratoire de biologie de la reproduction du CHU de Nantes. A cette occasion, je me suis intéressée de plus près à l'analyse du statut génétique des embryons. La réglementation française ne permettant pas l'analyse du génome complet, je me suis intéressée aux paramètres morphocinétiques des embryons en DPI chromosomique afin d'évaluer si certains pouvaient permettre d'obtenir des informations sur le statut génétique de l'embryon.

De nombreux travaux existaient concernant la ploïdie embryonnaire et son impact sur le développement et sur les taux de réussite. Il nous a semblé intéressant d'étudier le lien entre le statut chromosomique des embryons et leur morphocinétique. Le travail bibliographique préliminaire à l'étude du contenu génétique des embryons dans notre population, nous a conduit à rédiger une revue de la littérature afin de faire un état des lieux des connaissances en 2018.

Etant donné la législation française, nous nous sommes intéressés aux embryons biopsiés dans le cadre de DPI pour lesquels étaient recherchées les anomalies chromosomiques portées par le couple demandeur. Nous avons comparé la morphocinétique des embryons équilibrés à celle des embryons porteurs du réarrangement chromosomique identifié chez les patients pris en charge. Il est important de conserver la notion que les embryons équilibrés peuvent également être porteurs d'autres réarrangements chromosomiques non identifiables lors du DPI. Cette étude a porté sur l'observation, entre mai 2013 et avril 2016, de 177 embryons équilibrés et 250 déséquilibrés.

Pour la revue de la littérature ③, je me suis chargée de rechercher les articles d'intérêts, d'une partie de la rédaction et de la relecture du manuscrit.

Pour la publication ④, je me suis chargée d'annoter les événements morphocinétiques des vidéos des embryons en culture time-lapse afin d'extraire une base de données du développement embryonnaire. En parallèle j'ai extrait les données nécessaires à la création de la base de données des patients correspondants aux embryons étudiées. J'ai pu réaliser les analyses statistiques pour comparer les données des 2 groupes une fois celles-ci extraites. Pour finir, je me suis chargée de la rédaction de la première version de l'article, de la soumission auprès d'une revue à comité de lecture et de répondre aux corrections posées par les relecteurs.



Review

Can time-lapse parameters predict embryo ploidy? A systematic review

Arnaud Reignier ^{a,b,c}, Jenna Lammers ^{a,b}, Paul Barriere ^{a,b,c},
Thomas Freour ^{a,b,c,*}

^a Service de Médecine et Biologie du Développement et de la Reproduction, CHU de Nantes, 38 boulevard Jean Monnet, Nantes, France

^b Centre de Recherche en Transplantation et Immunologie UMR 1064, INSERM, Université de Nantes, Nantes, France

^c Faculté de Médecine, Université de Nantes, Nantes, France



Thomas Freour, PharmD, PhD, is the head of the ART Center at the University Hospital of Nantes, France. He is also a member of the UMR1064 research team, co-leading the pluripotency and embryo development group. His main fields of interest are embryology, time-lapse, ovarian reserve, proteomics and sperm physiology.

KEY MESSAGE

Studies reporting an association between morphokinetic parameters and embryo ploidy status are controversial and do not support the predictive value of time-lapse analysis for embryo aneuploidy screening.

A B S T R A C T

Embryo morphology assessment performs relatively poorly in predicting implantation. Embryo aneuploidy screening (PGS) has recently improved, but its clinical value is still debated, and the development of a cheap non-invasive method for the assessment of embryo ploidy status is a highly desirable goal. The growing implementation of time-lapse devices led some teams to test the effectiveness of morphokinetic parameters as predictors of embryo ploidy, with conflicting results. The aim of this study was to conduct a comprehensive review of the literature on the predictive value of morphokinetic parameters for embryo ploidy status. A systematic search on PubMed was conducted using the following key words: time-lapse, morphokinetic, aneuploidy, IVF, preimplantation genetic screening, PGS, chromosomal status. A total of 13 studies were included in the analysis. They were heterogeneous in design, patients, day of embryo biopsy, statistical approach and outcome measures. No single or combined morphokinetic parameter was consistently identified as predictive of embryo ploidy status. In conclusion, the available studies are too heterogeneous for firm conclusions to be drawn on the predictive value of time-lapse analysis for embryo aneuploidy screening. Hence, morphokinetic parameters should not be used yet as a surrogate for PGS to determine embryo ploidy *in vitro*.

© 2018 Reproductive Healthcare Ltd. Published by Elsevier Ltd. All rights reserved.

* Corresponding author.

E-mail address: thomas.freour@chu-nantes.fr (T. Freour).

<https://doi.org/10.1016/j.rbmo.2018.01.001>

1472-6483/© 2018 Reproductive Healthcare Ltd. Published by Elsevier Ltd. All rights reserved.

Please cite this article in press as: Arnaud Reignier, Jenna Lammers, Paul Barriere, Thomas Freour, Can time-lapse parameters predict embryo ploidy? A systematic review, Reproductive BioMedicine Online (2018), doi: 10.1016/j.rbmo.2018.01.001

Introduction

The ultimate objective of assisted reproduction techniques is to offer patients the highest healthy live birth rate and the lowest multiple pregnancy rate. Morphology is the most common method used for evaluating embryo quality *in vitro*; however, it performs poorly in identifying the embryo with the highest implantation potential, even at the blastocyst stage (Gardner et al., 2015). This prevents many IVF teams implementing a largely single embryo transfer policy (Kushnir et al., 2017). Embryo morphology assessment has little predictive power for implantation because of its weak association with embryo ploidy status, which is the most critical factor for sustained implantation in IVF (Gardner et al., 2015). Embryo aneuploidy screening, also known as preimplantation genetic screening (PGS), allows the identification of embryo chromosomal status. Several technical improvements over the past decade have led to the identification of trophectoderm biopsy and array comparative genetic hybridization (aCGH) or next-generation sequencing as the technique of choice for PGS (Gardner et al., 2015). Although shown to be efficient and clinically relevant in some studies, this technique suffers from some limitations. Indeed, it raises regulatory issues in some countries (Harper et al., 2014), it can be considered invasive, it requires specific technical skills, it can take up to 24 h before obtaining the result according to the technique, and it still remains expensive (Gardner et al., 2015; Sermon et al., 2016). Therefore, the development of a non-invasive, rapid, and cheaper method for assessing embryo ploidy status would represent a breakthrough in the field of IVF (Gardner et al., 2015). The recent implementation of time-lapse devices in more IVF laboratories, allowing continuous embryo monitoring in stable culture conditions, has raised hopes among many embryologists. Although the clinical value of this strategy has been validated in some studies (Petersen et al., 2016; Rubio et al., 2014), literature reviews have provided various results (Armstrong et al., 2015; Chen et al., 2017), leading to ongoing debate on this topic (Harper et al., 2017). Among the numerous studies reported on time-lapse, some have evaluated the association between morphokinetic parameters and embryo ploidy to evaluate if time lapse could be the awaited non-invasive method for embryo aneuploidy screening. These studies provided discordant conclusions. They were conducted in various settings, with heterogeneous design, procedures and populations, ultimately failing to yield a firm conclusion.

Therefore, the aim of this study was to conduct a comprehensive review of the literature on the predictive value of morphokinetic parameters for embryo ploidy status.

Materials and methods

We conducted a systematic search on *Medline* of all articles related to time-lapse (or morphokinetic) analysis of human preimplantation embryo development and its association with aneuploidy evaluated with PGS technology published up to April 2017 using the *Pubmed* database with the following keywords: time-lapse, morphokinetic, aneuploidy, IVF, preimplantation genetic screening, PGS and chromosomal status.

This search was conducted according to Prisma guidelines (<http://www.prisma-statement.org/>), and only full-length articles in English dealing with clinical observations in humans were included. The principal summary measure was the predictive value of time-lapse

parameters for embryo ploidy. Comparison with a control group was not mandatory. No statistical tests were carried out with these data. All references were screened, and eligibility assessed by two independent reviewers (AR and JL). A third author (TF) checked the final list of references and made the final decision in case of disagreement.

The following data were extracted from the selected articles: study design, number of couples, clinical indication for PGS, number of embryos, embryo stage for biopsy, PGS technique, time-lapse device, embryo culture atmosphere, morphokinetic parameters studied, euploidy rate, clinical outcome measure, adjustment with patients' characteristics, relevant morphokinetic variables identified, statistical approach and main conclusion.

Results

A total of 161 studies were screened for eligibility. All records were screened, and 148 were excluded. A total of 15 full-text articles were assessed in detail for eligibility, among which two were excluded because they were conducted in preimplantation genetic diagnosis cycles rather than in PGS cycles, thus not allowing full information on embryo ploidy status to be obtained. Finally, 13 were selected for data collection on the predictive value of morphokinetic analysis for human embryo ploidy (Balakier et al., 2016; Basile et al., 2014; Campbell et al., 2013a, 2013b; Chavez et al., 2012; Chawla et al., 2015; Del Carmen Nogales et al., 2017; Kramer et al., 2014; Minasi et al., 2016; Mumusoglu et al., 2017; Patel et al., 2016; Rienzi et al., 2015; Yang et al., 2014) (Table 1).

Most studies were retrospective. Only two were prospective, with one conducted on embryos donated for research (Chavez et al., 2012) and the other one on clinical cycles (Yang et al., 2014). The number of couples and IVF-PGS cycles included in these studies varied significantly, ranging from 25 (Campbell et al., 2013a) to 444 (Minasi et al., 2016), and from 25 (Campbell et al., 2013a) to 530 (Minasi et al., 2016), respectively. Similarly, the number of embryos included in the analysis was heterogeneous in these studies, ranging from 53 (Chavez et al., 2012) to 928 (Minasi et al., 2016).

The clinical indication for PGS varied notably among these studies, even if most of them were conventional PGS cases, i.e. advanced maternal age, recurrent implantation failure and recurrent miscarriage. Only one study was conducted in PGS cycles for sex selection (Chawla et al., 2015) and one in couples with previous aneuploidy conceptions (Yang et al., 2014). Two studies included cases of PGS for severe male factor infertility in addition to conventional PGS indications (Balakier et al., 2016; Campbell et al., 2013a). Clinical indication for PGS could not be found in two studies (Campbell et al., 2013b; Minasi et al., 2016).

Embryo biopsy was carried out at cleavage stage in five studies (Basile et al., 2014; Chavez et al., 2012; Chawla et al., 2015; Del Carmen Nogales et al., 2017; Patel et al., 2016) and at the blastocyst stage in eight studies (Balakier et al., 2016; Campbell et al., 2013a, 2013b; Kramer et al., 2014; Minasi et al., 2016; Mumusoglu et al., 2017; Rienzi et al., 2015; Yang et al., 2014). When performed at the cleavage stage, no morphokinetic data were provided on subsequent embryo development, except in one study (Patel et al., 2016).

All studies but one (Chavez et al., 2012) were carried out with the Embryoscope® as time-lapse device. Although unlikely, whether the type of time-lapse device used could influence the eventual association of morphokinetic parameters with embryo ploidy status is not

Table 1 – Principal characteristics of the studies reporting on the value of morphokinetic parameters as predictors of embryo ploidy. Studies are listed in chronological order.

	Study design	Number of couple/ cycles	Clinical indication for PGS	Number of embryos	Embryo stage for biopsy	PGS technique	Time-lapse device	Atmosphere
Chavez et al. (2012)	Prospective on donated zygotes	45/NA	NA	53	Day 2	aCGH	custom-built miniature microscope system	6% CO ₂ , 5% O ₂
Campbell et al. (2013a)	Retrospective	25/25	AMA, RIF, recurrent miscarriage, severe male factor	98	Blastocyst	aCGH or SNP array	Embryoscope®	5.5% CO ₂ , 5% O ₂
Campbell et al. (2013b)	Retrospective/ validation study	69/69	Unknown	88	Blastocyst	aCGH or SNP array	Embryoscope®	5.5% CO ₂ , 5% O ₂
Basile et al. (2014)	Retrospective	87/125	RIF and recurrent miscarriage	504	Day 3	aCGH	Embryoscope®	Not described
Kramer et al. (2014)	Retrospective/ validation study	25/25	Recurrent miscarriage, AMA, others	149	Blastocyst	aCGH	Embryoscope®	6% CO ₂ , 5% O ₂
Yang et al. (2014)	Prospective	NA	RPL, RIF, PCA	285	Blastocyst	aCGH	Embryoscope®	6% CO ₂ , 5% O ₂
Chawla et al. (2015)	Retrospective	132/132	Sex selection	460	Day 3	aCGH	Embryoscope®	Not described
Rienzi et al. (2015)	Retrospective/ validation study	138/138	AMA, RIF, recurrent miscarriage	455	Blastocyst	aCGH	Embryoscope®	6% CO ₂ , 5% O ₂
Minasi et al. (2016)	Retrospective	444/530	Unknown	1730/928 cultured in time-lapse	Blastocyst	aCGH	Embryoscope®	6% CO ₂ , 5% O ₂
Balakier et al. (2016)	Retrospective	296 (113 with PGS)/296 (113)	AMA, PCOS, male factor and others	2441/607 with PGS	Blastocyst	aCGH	Embryoscope®	6% CO ₂ , 5% O ₂
Patel et al. (2016)	Retrospective	24/29	AMA, RIF, recurrent miscarriage	167	Day 3	aCGH	Embryoscope®	Not described
Mumusoglu et al. (2017)	Retrospective/ validation study	103/103	AMA, PGD	415	Blastocyst	aCGH	Embryoscope®	6.8% CO ₂ , 5% O ₂
Del Carmen Nogales et al. (2017)	Retrospective	112/112	AMA, RIF and recurrent miscarriage	485	Day 3	aCGH	Embryoscope®	Not described

(continued on next page)

Table 1 – (continued)

	Euploidy rate (%)	Clinical outcome measures	Morphokinetic parameters studied	Relevant morphokinetic variables	Adjusted with patients' characteristics	Statistical approach	Conclusion
Chavez et al. (2012)	24.5	NA	All up to day 2	cc2, s2	No	Mean comparison	Cell-cycle parameters could be diagnostic of ploidy and have clinical relevance.
Campbell et al. (2013a)	38.8	NA	All up to blastocyst stage	t5B, tB	No	Mean comparison; Fisher's test; decision-tree model	Late time-lapse parameters increase the probability of selecting euploid embryos.
Campbell et al. (2013b)	NA ^a	CPR and LBR	All up to blastocyst stage	t5B, tB	No	Decision-tree model	Late time-lapse parameters increase the probability of selecting euploid embryos.
Basile et al. (2014)	28.3	Implantation rate and CPR	All up to day 3	t5, t5-t2, cc3	No	Mean comparison; quartiles; logistic regression; ROC curve; decision tree	Time-lapse-based algorithm increases the probability of selecting euploid embryos.
Kramer et al. (2014)	43	NA	All up to blastocyst stage	None	No	Chi-squared ; ANOVA, ROC curve	Failure of Campbell's model. Time-lapse parameters cannot be used to select euploid blastocysts
Yang et al. (2014)	46	Implantation rate, OPR	All up to blastocyst stage	None	No	Mean and frequency comparison	Time-lapse increases the probability of non-invasively selecting normal embryos.
Chawla et al. (2015)	42.8	NA	All up to day 3	t5-t2, cc3	No	Mean and frequency comparison; Logistic regression; ROC curve	Time-lapse increases the probability of non-invasively selecting normal embryos.
Rienzi et al. (2015)	40.9	OPR and LBR	All up to blastocyst stage	None	Yes	Bivariate generalized mixed models, linear logistic model	Failure of Campbell and Basile's models. Time-lapse parameters Cannot be used to select euploid blastocysts.
Minasi et al. (2016)	34.9	CPR	All up to blastocyst stage	t5B, tB, tEB, tHB	Yes	Mixed logistic models; mixed linear regression	Late time-lapse parameters are different in euploid and aneuploidy embryos but do not improve clinical outcome.
Balakier et al. (2016)	49.8	Implantation rate, CPR and LBR	All up to blastocyst stage plus multinucleation at two- and four-cell stages	NA	Yes	Mean comparison, logistic regression	High implantation rate, even for embryos with multinucleation at the two-cell stage.
Patel et al. (2016)	24.5	NA	All up to blastocyst stage	t5-t2, cc3	No	Mean comparison; chi squared; quartiles; logistic regression; ROC curve	Time-lapse-based algorithm (Basile et al., 2014) increases the probability of selecting euploid embryos but should not replace PGS.
Mumusoglu et al. (2017)	41.7	NA	All up to blastocyst stage	t9, tM, t5B, tB, tEB	Yes	Clustered data analysis	Failure of most models and late time-lapse parameters to predict euploidy.
DeL Carmen Nogales et al. (2017)	38.1	NA	All up to day 3	t3, t5-t2	No	Mean comparison; chi squared; quartiles; logistic regression analysis	Time-lapse is useful to discard embryos with high risk of complex aneuploidies.

^a Validation study conducted in non-PGS cycles.

aCGH, array comparative genetic hybridization; AMA, advanced maternal age; ANOVA, analysis of variance; CPR, clinical pregnancy rate; LBR: live birth rate; NA, not applicable; OPR, ongoing pregnancy rate; PCA, previous aneuploidy conceptions; PCOS, polycystic ovary syndrome; PGD, preimplantation genetic diagnosis; PGS, preimplantation genetic screening; RIF, recurrent implantation failure; ROC, receiver operator characteristic; SNP, single nucleotide polymorphism.

known, as no comparative study has yet been conducted. Although embryo culture atmosphere was not reported in four studies (Basile et al., 2014; Chawla et al., 2015; Del Carmen Nogales et al., 2017; Patel et al., 2016), it was carried out under low oxygen tension in the nine remaining studies.

All studies on PGS technique were based on aCGH, allowing the evaluation of all chromosomes. Only two studies from the same group reported using both aCGH and single nucleotide polymorphism array (Campbell et al., 2013a, 2013b). Euploidy rate was reported in 12 studies (not applicable in Campbell et al., [2013b]), which was conducted in non-PGS cycles) and ranged from 24.5% (Chawla et al., 2015) to 49.8% (Balakier et al., 2016), with a trend towards higher euploidy rate when biopsy was carried out at the blastocyst stage than at the cleavage stage.

Six studies included clinical outcome measures after a PGS cycle (Balakier et al., 2016; Basile et al., 2014; Campbell et al., 2013b; Minasi et al., 2016; Rienzi et al., 2015; Yang et al., 2014). Most of them used clinical pregnancy rate; some also used implantation rate or live birth rate.

Concerning the morphokinetic parameters studied, all studies reported morphokinetic parameters up to embryo biopsy, including pronuclei appearance and fading, cellular cleavage timings and intervals, compaction and blastocyst formation and expansion. One study also reported multinucleation at the two-cell and four-cell stages (Balakier et al., 2016). Among the 13 selected studies, 11 aimed at identifying relevant morphokinetic variables, which could be significantly different between euploid and aneuploidy groups, and finally help in selecting euploid embryos for transfer, whereas two consisted of external validation of previously published models (Campbell et al., 2013b; Kramer et al., 2014). Studies conducted in early cleavage embryos mostly identified intervals between cleavages rather than cleavage timings as relevant for identifying euploid embryos (Basile et al., 2014; Chavez et al., 2012; Chawla et al., 2015; Del Carmen Nogales et al., 2017; Patel et al., 2016). Some studies conducted at the blastocyst stage identified late morphokinetic parameters, i.e. compaction or blastulation stages, but not early ones (cleavage stages) as relevant predictors of embryo ploidy (Campbell et al., 2013a; Minasi et al., 2016; Mumusoglu et al., 2017). Not all studies, however, conducted at the blastocyst stage reported significant morphokinetic differences between euploid and aneuploid embryos (Rienzi et al., 2015; Yang et al., 2014).

In addition to the studies aimed at identifying predictive morphokinetic markers, other investigators have conducted external validation of some previously published morphokinetic models. The model by Campbell et al. (2013a) was evaluated externally by Kramer et al. (2014) and by themselves in a separate cohort (Campbell et al., 2013b). Patel et al. (2016) tested the performance of the model by Basile et al. (2014). Rienzi et al. (2015) and Mumusoglu et al. (2017) tested the performance of both Campbell's and Basile's models, both concluding that the models failed to predict embryo euploidy.

Statistical approach varied greatly among these 13 studies, depending on the main outcome measure and study design. Most studies performed basic univariate analysis to compare morphokinetic parameters in euploid and aneuploid embryos. Most studies also carried out logistic regression analysis to identify some independent predictors of embryo ploidy, eventually integrated in a predictive model. The sensitivity and specificity of the model was then evaluated with receiver operator characteristic curve analysis when appropriate (Basile et al., 2014; Chawla et al., 2015; Kramer et al., 2014; Patel et al., 2016). Importantly, few authors emphasized the possible bias of considering

embryos as individuals in statistical analysis, as all embryos originating from the same patient are influenced by those patient-specific characteristics and are, therefore, not independent entities ('cohort effect'). Therefore, these investigators strongly recommended the adjustment of statistical analysis and its results with patient characteristics (Kirkegaard et al., 2016; Mumusoglu et al., 2017).

Finally, most, but not all, investigators reported significant differences in morphokinetic pattern between euploid and aneuploid embryos, but the clinical significance of these results was absent to modest (Table 1). Although the conclusions raised by investigators varied significantly, all concluded that time-lapse should not be considered as an appropriate non-invasive method for embryo ploidy assessment.

Discussion

This comprehensive review of the literature on the effectiveness of time-lapse as a predictor of embryo ploidy highlights the large heterogeneity of the studies published to date, concluding that neither a unique morphokinetic nor combined parameters could predict embryo ploidy with enough sensitivity, specificity, or both, to be used clinically for embryo selection.

First, most studies reviewed here were carried out retrospectively and within a single clinic, with different sample sizes. Although this does not necessarily lessen their value, there is a need for large multi-centre studies to enhance the overall quality of the evidence generated.

The second question raised in this review concerns the type of time-lapse device. Although this should theoretically not lead to a significant difference in measuring morphokinetic parameters, it should be noted that all studies, bar one, were conducted with the Embryoscope®, the first and most widely implemented time-lapse device to date, thus providing a certain inter-study homogeneity on technical aspects. Whether the use of different approaches, as well as devices and analytical methods, in the field of time-lapse could account for the conflicting findings found within the literature is hard to determine and quantify precisely. This should be explored in further studies. The issue of inter-operator variability in annotating morphokinetic parameters could eventually be raised, thus encouraging the development of automated annotation tools (Castello et al., 2016; Molder et al., 2015). Although this variability has been shown to be low (Sundvall et al., 2013), it is unclear how widely guidelines for annotation practice (Ciray et al., 2014) are followed and how consistent time-lapse users are in their operating procedures. Whether more recent time-lapse devices with automated detection of cell cleavages will provide different results and lead to different conclusions still needs to be tested.

Although the clinical indication for PGS varied notably among the studies, the main indications were advanced maternal age, recurrent implantation failure and recurrent miscarriage. It is, therefore, unlikely that differences in clinical indications would explain the discrepancy in conclusions of the studies cited here. Some patient characteristics, however, have been shown by some investigators to be critical for interpreting morphokinetic studies, as embryos from the same patient tend to cluster (Kirkegaard et al., 2016; Mumusoglu et al., 2017). This point will be discussed further in the discussion.

The most significant difference between the studies reviewed here was the stage at which embryo biopsy was carried out. Indeed, embryo biopsy was carried out at the cleavage stage in five studies (Basile

et al., 2014; Chavez et al., 2012; Chawla et al., 2015; Del Carmen Nogales et al., 2017; Patel et al., 2016), whereas embryo biopsy was carried out at the blastocyst stage in eight studies (Balakier et al., 2016; Campbell et al., 2013a, 2013b; Kramer et al., 2014; Minasi et al., 2016; Mumusoglu et al., 2017; Rienzi et al., 2015; Yang et al., 2014). The respective advantages and disadvantages of these two strategies have been debated in recent years (Scott et al., 2013; Sermon et al., 2016). Trophectoderm biopsy, however, has gained increasing interest, and is more widely used, as it is considered to optimize the whole procedure when fewer embryos are available, but with higher implantation potential than cleavage stage biopsy (Sermon et al., 2016). Moreover, it allows the biopsy of several cells and probably allows a better management of embryo mosaicism (Capalbo et al., 2013). Whether trophectoderm biopsy is more relevant than cleavage stage biopsy for PGS was not the topic of this review. Recent data, however, obtained in arrested embryos cultured in time-lapse device and extensively analysed by genome-wide SNP genotyping in both polar bodies and karyomapping of disaggregated embryonic cells, suggest that genomic imbalance and partial genome loss occurring during early cleavage affects embryonic gene expression and blocks the morula to blastocyst transition (Ottolini et al., 2017). This reinforces the value of trophectoderm biopsy compared with performing biopsy pre-zygote genome activation at the cleavage stages of development. The present comprehensive review of the literature could eventually be repeated and specifically focus on morphokinetic follow-up up to the blastocyst stage followed by trophectoderm biopsy when more studies are available.

Various technical approaches can be used for PGS. Here, all studies were based on aCGH, with two of them also using single nucleotide polymorphism array (Campbell et al., 2013a, 2013b). Whether the implementation of new technologies for embryo aneuploidy screening, such as next-generation sequencing, brings new insights into the association between morphokinetic parameters and embryo ploidy should be explored in further studies.

Embryo culture conditions could constitute a bias in assessing morphokinetics. Indeed, low oxygen tension has been shown to result in significantly different morphokinetic patterns (Kirkegaard et al., 2016) than atmospheric ones. Although this was not reported in four studies, most of them included in this review were conducted under low oxygen tension.

Six studies included clinical outcome measures after PGS cycle (Balakier et al., 2016; Basile et al., 2014; Campbell et al., 2013b; Minasi et al., 2016; Rienzi et al., 2015; Yang et al., 2014). Interpreting these data, however, remains hazardous, as none of them was specifically designed to determine the relevance of morphokinetic parameters in predicting clinical outcome after PGS cycle.

Concerning the type of morphokinetic parameters analysed, studies with trophectoderm biopsy obviously included additional data compared with those conducted in cleavage stage embryos. These studies mostly concluded that intervals between cellular cleavages were more relevant than cleavage timings for the selection of euploid embryos (Basile et al., 2014; Chavez et al., 2012; Chawla et al., 2015; Del Carmen Nogales et al., 2017; Patel et al., 2016). This value of cellular intervals was previously suggested in clinical studies conducted in IVF cycles aimed at identifying morphokinetic predictors of implantation (Meseguer et al., 2011). Not all studies carried out at the blastocyst stage reported significant morphokinetic differences between euploid and aneuploid embryos (Rienzi et al., 2015; Yang et al., 2014), but most did (Campbell et al., 2013a; Minasi et al., 2016; Mumusoglu et al., 2017). Interestingly, these studies did not confirm the value of these early

parameters as relevant predictors of embryo ploidy (Campbell et al., 2013a; Minasi et al., 2016; Mumusoglu et al., 2017). As genetic events, such as mitotic errors, genomic imbalance or genome loss, occur during late embryo development after embryo genomic activation (Capalbo et al., 2013; Ottolini et al., 2017), this might account for this apparent loss of predictive value of early morphokinetic parameters for embryo ploidy when evaluated at the blastocyst stage. This, however, remains to be confirmed in longitudinal studies with cleavage stage and blastocyst biopsy successively performed.

Finally, the recently raised issue of statistical approach and adjustment for patients' characteristics to take clustering effect into account in time-lapse studies (Kirkegaard et al., 2016) was also questioned in three studies included in this review (Minasi et al., 2016; Mumusoglu et al., 2017; Rienzi et al., 2015), and, particularly, in one of them (Mumusoglu et al., 2017). The concept of this approach is that embryos generated from one couple should not be considered individually. Instead, the statistical approach should consider intra-patient clustering effect to determine the extent to which the morphokinetic variation observed is independent of patient's clinical or cycle characteristics (Kirkegaard et al., 2016). In the study by Mumusoglu et al. (2017), 16–47% of the observed variation of morphokinetic parameters was found to be patient-related. Interestingly, the investigators concluded that considering embryos as individuals in statistical analysis could represent a major bias, leading to overestimated statistical associations and potentially incorrect conclusions, especially in heterogeneous populations. This was also highlighted in a commentary published in 2014 (Ottolini et al., 2014), in which the authors comment on the studies reported by Campbell et al. (2013a), Campbell et al. (2013b). The authors of this commentary particularly questioned the reported association between morphokinetic parameters and implantation, as no female age was provided, and insisted on the importance of confounding factors such as age in this non-age-controlled cohort. This was further debated by Campbell et al. (2014), who stated that age was not the likely causal factor of observed delays in blastulation.

Conclusion

This comprehensive review of the literature demonstrates that morphokinetic parameters should not yet be used as a surrogate for PGS to determine chromosomal status of the preimplantation embryo. More large-scale studies, conducted in homogeneous populations with standard culture and biopsy protocol, using relevant statistical approaches adjusted to patients' characteristics, are needed to gain insight into the putative association between embryo morphokinetic parameters and ploidy, ultimately improving IVF clinical outcome.

ARTICLE INFO

Article history:

Received 8 August 2017

Received in revised form 3 January 2018

Accepted 4 January 2018

Declaration: The authors report no financial or commercial conflicts of interest.

Keywords:

Time-lapse

Morphokinetic

Aneuploidy

Preimplantation genetic screening

REFERENCES

- Armstrong, S., Arroll, N., Cree, L.M., Jordan, V., Farquhar, C., 2015. Time-lapse systems for embryo incubation and assessment in assisted reproduction. *Cochrane Database Syst. Rev.* [27], CD011320.
- Balakier, H., Sojecki, A., Motamedi, G., Librach, C., 2016. Impact of multinucleated blastomeres on embryo developmental competence, morphokinetics, and aneuploidy. *Fertil. Steril.* 106, 608–614.
- Basile, N., Del Carmen Nogales, C., Bronet, F., Florensa, M., Riqueiros, M., Rodrigo, L., García-Velasco, J., Meseguer, M., 2014. Increasing the probability of selecting chromosomally normal embryos by time-lapse morphokinetics analysis. *Fertil. Steril.* 101, 699–704.
- Campbell, A., Fishel, S., Bowman, N., Duffy, S., Sedler, M., Hickman, C.F., 2013a. Modelling a risk classification of aneuploidy in human embryos using non-invasive morphokinetics. *Reprod. Biomed. Online* 26, 477–485.
- Campbell, A., Fishel, S., Bowman, N., Duffy, S., Sedler, M., Thornton, S., 2013b. Retrospective analysis of outcomes after IVF using an aneuploidy risk model derived from time-lapse imaging without PGS. *Reprod. Biomed. Online* 27, 140–146.
- Campbell, A., Fishel, S., Laegdsmand, M., 2014. Aneuploidy is a key causal factor of delays in blastulation: author response to 'A cautionary note against aneuploidy risk assessment using time-lapse imaging'. *Reprod. Biomed. Online* 28, 279–283.
- Capalbo, A., Bono, S., Spizzichino, L., Biricik, A., Baldi, M., Colamaria, S., Ubaldi, F.M., Rienzi, L., Fiorentino, F., 2013. Sequential comprehensive chromosome analysis on polar bodies, blastomeres and trophoblast: insights into female meiotic errors and chromosomal segregation in the preimplantation window of embryo development. *Hum. Reprod.* 28, 509–518.
- Castello, D., Motato, Y., Basile, N., Remohi, J., Espejo-Catena, M., Meseguer, M., 2016. How much have we learned from time-lapse in clinical IVF? *Mol. Hum. Reprod.* 22, 719–727.
- Chavez, S.L., Loewke, K.E., Han, J., Moussavi, F., Colls, P., Munne, S., Behr, B., Reijo Pera, R.A., 2012. Dynamic blastomere behaviour reflects human embryo ploidy by the four-cell stage. *Nat. Commun.* 3, 1251.
- Chawla, M., Fakhri, M., Shunnar, A., Bayram, A., Hellani, A., Perumal, V., Divakaran, J., Budak, E., 2015. Morphokinetic analysis of cleavage stage embryos and its relationship to aneuploidy in a retrospective time-lapse imaging study. *J. Assist. Reprod. Genet.* 32, 69–75.
- Chen, M., Wei, S., Hu, J., Yuan, J., Liu, F., 2017. Does time-lapse imaging have favorable results for embryo incubation and selection compared with conventional methods in clinical in vitro fertilization? A meta-analysis and systematic review of randomized controlled trials. *PLoS ONE* 12, e0178720.
- Ciray, H.N., Campbell, A., Agerholm, I.E., Aguilar, J., Chamayou, S., Esbert, M., Sayed, S., Time-Lapse User Group., 2014. Proposed guidelines on the nomenclature and annotation of dynamic human embryo monitoring by a time-lapse user group. *Hum. Reprod.* 29, 2650–2660.
- Del Carmen Nogales, M., Bronet, F., Basile, N., Martinez, E.M., Linan, A., Rodrigo, L., Meseguer, M., 2017. Type of chromosome abnormality affects embryo morphology dynamics. *Fertil. Steril.* 107, 229–235.
- Gardner, D.K., Meseguer, M., Rubio, C., Treff, N.R., 2015. Diagnosis of human preimplantation embryo viability. *Hum. Reprod. Update* 21, 727–747.
- Harper, J., Geraedts, J., Borry, P., Cornel, M.C., Dondorp, W.J., Gianaroli, L., Harton, G., Milachich, T., Kääriäinen, H., Liebaers, I., Morris, M., Sequeiros, J., Sermon, K., Shenfield, F., Skirton, H., Soini, S., Spits, C., Veiga, A., Vermeesch, J.R., Viville, S., de Wert, G., Macek, M., Jr., ESHG, ESHRE, EuroGenest2, 2014. Current issues in medically assisted reproduction and genetics in Europe: research, clinical practice, ethics, legal issues and policy. *Hum. Reprod.* 29, 1603–1609.
- Harper, J., Jackson, E., Sermon, K., Aitken, R.J., Harbottle, S., Mocanu, E., Hardarson, T., Mathur, R., Viville, S., Vail, A., Lundin, K., 2017. Adjuncts in the IVF laboratory: where is the evidence for 'add-on' interventions? *Hum. Reprod.* 32, 485–491.
- Kirkegaard, K., Sundvall, L., Erlandsen, M., Hindkjaer, J.J., Knudsen, U.B., Ingerslev, H.J., 2016. Timing of human preimplantation embryonic development is confounded by embryo origin. *Hum. Reprod.* 31, 324–331.
- Kramer, Y.G., Kofinas, J.D., Melzer, K., Noyes, N., McCaffrey, C., Buldo-Licciardi, J., McCulloh, D.H., Grifo, J.A., 2014. Assessing morphokinetic parameters via time lapse microscopy (TLM) to predict euploidy: are aneuploidy risk classification models universal? *J. Assist. Reprod. Genet.* 31, 1231–1242.
- Kushnir, V.A., Barad, D.H., Albertini, D.F., Darmon, S.K., Gleicher, N., 2017. Systematic review of worldwide trends in assisted reproductive technology 2004–2013. *Reprod. Biol. Endocrinol.* 15, 6–14.
- Meseguer, M., Herrero, J., Tejera, A., Hilligsoe, K.M., Ramsing, N.B., Remohi, J., 2011. The use of morphokinetics as a predictor of embryo implantation. *Hum. Reprod.* 26, 2658–2671.
- Minasi, M.G., Colasante, A., Riccio, T., Ruberti, A., Casciani, V., Scarselli, F., Spinella, F., Fiorentino, F., Varricchio, M.T., Greco, E., 2016. Correlation between aneuploidy, standard morphology evaluation and morphokinetic development in 1730 biopsied blastocysts: a consecutive case series study. *Hum. Reprod.* 31, 2245–2254.
- Molder, A., Drury, S., Costen, N., Hartshorne, G.M., Czanner, S., 2015. Semiautomated analysis of embryoscope images: using localized variance of image intensity to detect embryo developmental stages. *Cytometry A* 87, 119–128.
- Mumusoglu, S., Yarali, I., Bozdog, G., Ozdemir, P., Polat, M., Sokmensuer, L.K., Yarali, H., 2017. Time-lapse morphokinetic assessment has low to moderate ability to predict euploidy when patient- and ovarian stimulation-related factors are taken into account with the use of clustered data analysis. *Fertil. Steril.* 107, 413–421.
- Ottolini, C., Rienzi, L., Capalbo, A., 2014. A cautionary note against embryo aneuploidy risk assessment using time-lapse imaging. *Reprod. Biomed. Online* 28, 273–275.
- Ottolini, C.S., Kitchen, J., Xanthopoulou, L., Gordon, T., Summers, M.C., Handyside, A.H., 2017. Tripolar mitosis and partitioning of the genome arrests human preimplantation development in vitro. *Sci. Rep.* 7, 9744–9753.
- Patel, D.V., Shah, P.B., Kotdawala, A.P., Herrero, J., Rubio, I., Banker, M.R., 2016. Morphokinetic behavior of euploid and aneuploid embryos analyzed by time-lapse in embryoscope. *J. Hum. Reprod. Sci.* 9, 112–118.
- Petersen, B.M., Boel, M., Montag, M., Gardner, D.K., 2016. Development of a generally applicable morphokinetic algorithm capable of predicting the implantation potential of embryos transferred on Day 3. *Hum. Reprod.* 31, 2231–2244.
- Rienzi, L., Capalbo, A., Stoppa, M., Romano, S., Maggiulli, R., Albricci, L., Scarica, C., Farcomeni, A., Vajta, G., Ubaldi, F.M., 2015. No evidence of association between blastocyst aneuploidy and morphokinetic assessment in a selected population of poor-prognosis patients: a longitudinal cohort study. *Reprod. Biomed. Online* 30, 57–66.
- Rubio, I., Galan, A., Larreategui, Z., Ayerdi, F., Bellver, J., Herrero, J., Meseguer, M., 2014. Clinical validation of embryo culture and

- selection by morphokinetic analysis: a randomized, controlled trial of the EmbryoScope. *Fertil. Steril.* 102, 1287–1294.
- Scott, R.T., Jr., Upham, K.M., Forman, E.J., Zhao, T., Treff, N.R., 2013. Cleavage-stage biopsy significantly impairs human embryonic implantation potential while blastocyst biopsy does not: a randomized and paired clinical trial. *Fertil. Steril.* 100, 624–630.
- Sermon, K., Capalbo, A., Cohen, J., Coonen, E., De Rycke, M., De Vos, A., Delhanty, J., Fiorentino, F., Gleicher, N., Griesinger, G., Grifo, J., Handyside, A., Harper, J., Kokkali, G., Mastenbroek, S., Meldrum, D., Meseguer, M., Montag, M., Munné, S., Rienzi, L., Rubio, C., Scott, K., Scott, R., Simon, C., Swain, J., Treff, N., Ubaldi, F., Vassena, R., Vermeesch, J.R., Verpoest, W., Wells, D., Geraedts, J., 2016. The why, the how and the when of PGS 2.0: current practices and expert opinions of fertility specialists, molecular biologists, and embryologists. *Mol. Hum. Reprod.* 22, 845–857.
- Sundvall, L., Ingerslev, H.J., Breth Knudsen, U., Kirkegaard, K., 2013. Inter- and intra-observer variability of time-lapse annotations. *Hum. Reprod.* 28, 3215–3221.
- Yang, Z., Zhang, J., Salem, S.A., Liu, X., Kuang, Y., Salem, R.D., Liu, J., 2014. Selection of competent blastocysts for transfer by combining time-lapse monitoring and array CGH testing for patients undergoing preimplantation genetic screening: a prospective study with sibling oocytes. *BMC Med. Genomics* 7, 38.

ARTICLE



Morphokinetic parameters in chromosomal translocation carriers undergoing preimplantation genetic testing

**BIOGRAPHY**

Thomas Freour, PharmD, PhD, is the head of the ART Centre at the University Hospital of Nantes, France. He is also a member of the UMR1064 research team, co-leading the pluripotency and embryo development group. His main fields of interest are embryology, time-lapse, ovarian reserve, proteomics and sperm physiology.

Jenna Lammers^{1,2}, Arnaud Reignier^{1,2,3}, Carole Splingart^{1,2},
Kamran Moradkhani⁴, Paul Barrière^{1,2,3}, Thomas Fréour^{1,2,3,*}

KEY MESSAGE

Although significant morphokinetic differences exist between balanced and unbalanced embryos in translocation carriers undergoing preimplantation genetic testing for structural rearrangement cycle without aneuploidy screening, no relevant morphokinetic predictor of embryo chromosomal status could be found.

ABSTRACT

Research question: Can embryo morphokinetic parameters help identify unbalanced embryos in translocation carriers?

Design: This retrospective study was conducted in 67 translocation carriers undergoing 105 preimplantation genetic testing cycles for chromosomal structural rearrangements (PGT-SR) without aneuploidy screening (PGT-A). Using time-lapse imaging analysis, morphokinetic parameters of balanced and unbalanced embryos were compared, as well as the frequency of abnormal cellular events. The performance of a previously published prediction model of aneuploidy was also tested in this population.

Results: Significant differences were observed between balanced and unbalanced embryos for some morphokinetic parameters: t5 ($P = 0.0067$), t9+ ($P = 0.0077$), cc2 ($P = 0.0144$), s2 ($P = 0.0003$) and t5–t2 ($P = 0.0028$). Also, multinucleation at the two- or four-cell stages, abnormal division and cell exclusion at the morula stage were significantly (all $P < 0.05$) more frequent in unbalanced than in balanced embryos. None, however, could accurately predict embryo chromosomal status. A previously published morphokinetic prediction model for embryo aneuploidy did not adequately classify balanced and unbalanced embryos.

Conclusions: No significant morphokinetic predictor of chromosomal status could be found. Time-lapse should not be used as a diagnostic tool for chromosomal status in translocation carriers.

¹ Service de Médecine de la Reproduction, CHU Nantes, 38 boulevard Jean Monnet, Nantes Cedex 44093, France

² Centre de Recherche en Transplantation et Immunologie UMR 1064, INSERM, Université de Nantes, Nantes, France

³ Faculté de médecine, Université de Nantes, Nantes, France

⁴ Laboratoire de cytogénétique, Service de génétique médicale, CHU Nantes, Nantes, France

KEYWORDS

Aneuploidy
PGT
Prediction model
Time-lapse
Translocation

INTRODUCTION

Preimplantation genetic testing (PGT) is a procedure developed in the early 1990s for couples with a high risk of transmitting a genetic abnormality or with a high risk of miscarriage because of chromosomal structural rearrangement (*Harton et al., 2011*). Pre-implantation genetic testing for aneuploidy (PGT-A) consists of the evaluation of embryo ploidy, as reflected by the number of copies of each chromosome, and allows the selection of euploid embryos for transfer. Although the exact clinical benefit of PGT-A in subgroups of patients is still discussed and remains to be calculated, this approach is generally considered to result in a shorter time before pregnancy and higher pregnancy rate per transfer than conventional IVF and intracytoplasmic sperm injection (ICSI) (*Dahdouh et al., 2015*). Indeed, aneuploidy is commonly observed in human embryos obtained by IVF procedure, even in embryos developing to the blastocyst stage with good morphology, and accounts for the relatively limited implantation rate observed in human IVF cycles. The presence of chromosomal translocation in one or both partners in a couple is a situation with a particularly high risk of embryo aneuploidy. When authorized by regulation, the most recent techniques allow the simultaneous use of preimplantation genetic testing cycles for chromosomal structural rearrangements (PGT-SR) and PGT-A to optimize clinical efficiency and cost-effectiveness for couples with a genetic abnormality or chromosomal structural rearrangement (*Capalbo et al., 2016a; 2016b*). Both PGT-SR and PGT-A are based on the genetic analysis of embryonic blastomeres biopsied either at the cleavage stage (day 3) or at the blastocyst stage. Therefore, the success of PGT-SR and PGT-A greatly depends on the number and quality of the embryos available for biopsy.

Since the release of the first time-lapse system in 2009, several laboratories around the world have implemented this technology to improve embryo culture conditions and evaluate embryo quality according to various morphokinetic parameters and related algorithms (*Barrie et al., 2017*). Considering that embryo ploidy is a critical factor for implantation, but that PGT is an invasive and expensive technology, a number of authors

have raised the hypothesis that the morphokinetic pattern of embryos can indirectly reflect embryo ploidy and thus be used as a surrogate for PGT-A and PGT-SR. If true, this approach could be particularly relevant in countries in which PGT-SR, PGT-A, or both, are prohibited. These studies carried out in patients referred for PGT-A because of advanced maternal age, recurrent implantation failure or recurrent pregnancy loss yielded predictive models with either no or moderate sensitivity and specificity for the identification of aneuploid embryos up to now (reviewed in *Reignier et al., 2018*). As far as we know, such studies have not been specifically conducted in translocation carriers referred for PGT-SR until now. In France, PGT is allowed for specific inherited genetic abnormalities, such as translocations, whereas PGT-A is prohibited by regulation. As translocation carriers present great risks of having unbalanced embryos (*Tobler et al., 2014*), we wondered whether these embryos would display a specific morphokinetic pattern. Therefore, our first study aim was to compare the morphokinetic parameters of balanced and unbalanced embryos in couples referred for PGT-SR. We then performed an external validation study of a published prediction model of embryo ploidy based on PGT-A results (*Basile et al., 2014*) to evaluate its performance in our local PGT-SR population referred for chromosomal rearrangement.

MATERIALS AND METHODS

Patients

This monocentric retrospective cohort study was conducted in couples referred for PGT-SR because of a chromosomal rearrangement in one of the partners. We analysed the clinical and biological data of all consecutive patients who had undergone an ICSI-PGT-SR cycle with autologous oocyte and embryo culture performed using the Embryoscope® between May 2013 and April 2016 in our University Fertility Centre. All patients gave consent for the anonymous use of their data registered in this database. This protocol was approved by the local ethics committee on 12 July 2017.

Ovarian stimulation

Before stimulation, all women had complete ovarian reserve exploration, including FSH, LH, oestradiol, anti-Müllerian hormone and antral follicle count (AFC). All patients underwent

ovarian stimulation with the antagonist protocol. A gonadotrophin starting dose was chosen according to female age, ovarian reserve and previous IVF cycles, if they had been undertaken. Cycle monitoring consisted of hormonal assays and ultrasonography, and ovulation was triggered with recombinant HCG when at least three follicles reached 18 mm in diameter.

Oocyte retrieval and embryo culture for PGT

Oocyte retrieval was carried out 34–36 h later. After denudation with hyaluronidase (SynVibro® hyadase, Origio, Måløv, Denmark), all mature oocytes were microinjected and immediately placed in individual microwells within a specific culture dish (Embryoslide®, Vitrolife®, Stockholm, Sweden) before being loaded into the Embryoscope® (Vitrolife®). Embryo culture was carried out at 37°C under a controlled atmosphere with low oxygen pressure (5% O₂, 6% CO₂). Sequential media was used for embryo culture (G1plus® and G2plus®).

Time-lapse analysis

Each embryo was investigated by detailed time-lapse analysis measuring the exact timing of the developmental events in hours after ICSI procedure, as described by *Ciray et al. (2014)*. The terms t₂, t₃, t₄, t₅, t₆, t₇ and t₈ were used for the exact timings of appearance of embryos with 2, 3, 4, 5, 6, 7 and 8 well-defined blastomeres, respectively. The mean ± SD duration of cell cycle between each cleavage was also considered. The term s₂ is used to illustrate the synchrony of the second cell cycle, i.e. the transition from a two-cell to four-cell embryo. Also, cc₂ is defined as the time of the second cell cycle (t₃-t₂) and cc₃ as the time of third cell cycle (t₅-t₃). Abnormal division referred to chaotic cleavage, reverse cleavage or direct cleavage, all of which have been shown to lead to extremely low implantation rates (*Rubio et al., 2012; Zhan et al., 2016*).

The hierarchical model developed by *Basile et al. (2016)* was applied to all of the embryos biopsied on day 3. This model was based on the morphokinetic differences observed between euploid and aneuploid embryos and included the most relevant parameters identified in their database, i.e. t₅-t₂ and cc₃, to classify the embryos into four categories with a decreasing probability of euploid status (A to D).

Embryo biopsy, genetic analysis and embryo transfer

Embryo biopsy was carried out on day 3 for all embryos with at least six blastomeres, less than 25% fragmentation and fair evenness. Embryos were first briefly placed in Ca/Mg-free medium (G-PGD, Vitrolife®) for a few minutes, before laser-assisted zona pellucida hatching (ZilosTK, Hamilton Thorn®, Beverly, MA, USA). One or two cells were then gently aspirated for subsequent genetic analysis depending on the number of blastomeres (one cell in six- to seven-cell embryos, two cells in embryos with eight or more cells). On average, 1.81 cells were removed per embryo. Each biopsied blastomere was lysed and the nucleus spread on a separate poly-L-lysine-coated slide. Interphase fluorescence in-situ hybridization (FISH) analyses were carried out according to the following procedures. The bacterial artificial chromosome contig probes covering 1 Mb of the subtelomeric region of the chromosomes involved in translocations were used to make FISH probes. All probes were directly labelled by nick translation with SpectrumOrange, SpectrumGreen and Diethylaminocoumarin fluorophores. First, slides were pretreated with a 0.05% pepsin solution at 37°C for 3 min to remove any remaining cytoplasmic proteins, followed by washing with PBS and serial ethanol dehydration. A mix containing 60–80 pg of probes was applied to each slide and sealed with rubber cement. Denaturation was carried out at 73°C for 3 min and hybridization at 37°C overnight. After hybridization, slides were washed in 2 × SSC/1%NP40 at 72°C for 2 min. The slides were then air-dried and mounted in Vectarshield (Vector Laboratories, USA) anti-fade medium containing 1 ng/ml 40,6-diaminidino-2-phenylindole to counterstain the nuclei. Slides were analysed under the fluorescence microscope. The FISH signals were counted following the criteria described by *Wilton et al. (2009)*.

Balanced embryos were selected for transfer on day 4 according to post-biopsy development for practical and organizational reasons. Indeed, many patients live far away from our PGT centre and remain close to the centre after ovum retrieval up to the time of embryo transfer. Therefore, embryo transfer is generally carried out as soon as possible (day 4) to allow patients to

return home quickly. Moreover, day-4 embryo transfers have been shown to perform as well as day-5 transfers (*Feil et al., 2008*). Single or double embryo transfer was chosen by a joint decision between medical staff and the couple. A pregnancy test was carried out 11 or 12 days after embryo transfer, and, if positive, clinical pregnancy was confirmed ultrasonographically 4–5 weeks later by the detection of a gestational sac and fetal heart activity.

Statistics

Student's or Wilcoxon's tests were used for continuous variables and chi-squared or Fisher's tests for categorical variables. The non-parametric Mann–Whitney test was used for non-normally distributed variables. GraphPad Prism® software was used for statistical analysis. $P < 0.05$ were considered to denote significant differences.

RESULTS

Study group

A total of 67 couples undergoing 105 PGT-SR cycles for chromosomal translocation were included in the analysis. Among them, 42 couples (62.7%) undergoing 71 cycles were referred for paternal chromosomal translocation, whereas 25 (37.3%) undergoing 34 cycles were referred for maternal translocation. The mean \pm SD female and male ages were 32.0 ± 3.6 and 34.26 ± 4.87 years, respectively. The mean \pm SD female BMI was 24.3 ± 4.2 kg/m². The average \pm SD total FSH dose was 2511 ± 967 units. The average \pm SD number of mature oocytes collected was 11.7 ± 5.0 . A total of 1176 oocytes were microinjected and cultured in the Embryoscope®, with 749 being normally fertilized (63.7%).

Among the 480 embryos undergoing blastomere biopsy on day 3, 190 (39.6%) had nine cells or more, 196 (40.8%) had eight cells, 66 (13.8%) had seven cells and 28 (5.8%) were at the six-cell stage. A total of 427 embryos (89%) could be analysed by FISH, with 177 displaying a balanced chromosomal status (41.5%) and 250 (58.5%) being unbalanced with various chromosomal patterns. No results could be obtained in 53 embryos (11%), because of the absence of nuclei, dubious results or technical problems. Significant differences were observed between balanced and unbalanced embryos for t5 ($P = 0.0067$),

t9+ ($P = 0.0077$), cc2 ($P = 0.0144$), s2 ($P = 0.0003$) and t5–t2 ($P = 0.0028$) (TABLE 1), with t5 and t9 + occurring significantly earlier in unbalanced than in balanced embryos.

According to cell cycles and synchrony, cc2 and t5–t2 were significantly longer and s2 shorter in balanced than in unbalanced embryos. The classification of embryos inside or outside of the optimal range for each of these parameters (i.e. t5, t5–t2, cc2) based on quartiles (second and third quartiles represent the optimal range) did not allow us to identify relevant thresholds with acceptable sensitivity and specificity for the identification of balanced versus unbalanced embryos (Supplementary TABLE 1). Additionally, the frequency of multinucleation at the two- or four-cell stages (31.6% [$n = 79$]) versus 19.8% [$n = 35$]; $P < 0.05$), abnormal division (32.8% [$n = 82$] versus 11.3% [$n = 20$]; $P < 0.05$) and cell exclusion at the morula stage (36.4% [$n = 52$] versus 32.8% [$n = 40$]; $P < 0.05$) was significantly higher in unbalanced embryos than in balanced embryos. The repartition of balanced and unbalanced embryos according to conventional morphological criteria is presented in Supplementary TABLE 2.

Hierarchical classification of embryos according to Basile et al. (2014)

In the second phase, we tested the performance of the morphokinetic predictive model for embryo aneuploidy developed in a PGT-A population and published by *Basile et al. (2014)* in our PGT-SR population of couples with chromosomal rearrangements. The proportion of balanced embryos for the chromosomes involved in the translocation was not significantly different between the four groups (46.95%, 43.90%, 26.92% and 25.93%, respectively) (FIGURE 1A). As we observed a similar proportion of balanced embryos in groups A and B on the one hand and in groups C and D on the other, we tested the performance of a simplified model only, including the most significant morphokinetic variable in the original publication, i.e. the t5–t2 interval (FIGURE 1B). We found a significantly higher proportion of balanced embryos in the group [A + B] than in the group [C + D] (46.56% versus 26.17%, respectively) (FIGURE 1B). The performance of this simplified model, however, was low (sensitivity 47%,

TABLE 1 MORPHOKINETIC PARAMETERS ACCORDING TO THE ABSENCE OR PRESENCE OF CHROMOSOMAL STRUCTURAL REARRANGEMENTS

	Balanced embryos (n = 177)		Unbalanced embryos (n = 250)		Significant P-values
	n	Mean ± SEM	n	Mean ± SEM	
tPB2	177	3.690 ± 0.1053	250	3.958 ± 0.1393	
tPNa	177	7.820 ± 0.1671	250	7.987 ± 0.1582	
tPNf	177	25.25 ± 0.2495	250	25.44 ± 0.2438	
T2	177	27.76 ± 0.2519	250	28.07 ± 0.2554	
T3	177	38.92 ± 0.3258	250	37.90 ± 0.3560	
T4	177	40.12 ± 0.3322	250	40.24 ± 0.3076	
T5	177	51.01 ± 0.4792	250	49.45 ± 0.4687	0.0067
T6	177	53.44 ± 0.4099	250	53.02 ± 0.4312	
T7	175	55.24 ± 0.4453	232	56.15 ± 0.5668	
T8	165	59.17 ± 0.8216	192	58.29 ± 0.7001	
T9+	144	73.99 ± 1.013	179	70.61 ± 1.011	0.0077
tPGT	177	69.87 ± 0.1207	250	70.01 ± 0.2372	
tSC	153	89.01 ± 0.7485	176	89.70 ± 0.7083	
tM	122	94.93 ± 0.8118	143	95.88 ± 0.8043	
tSB	93	103.6 ± 1.191	86	102.4 ± 1.099	
tB	56	111.0 ± 1.425	47	110.6 ± 1.447	
tEB	32	109.6 ± 1.916	25	112.0 ± 2.107	
T5-t2	177	23.25 ± 0.3989	250	21.38 ± 0.4203	0.0028
Cc2 (t3-t2)	177	11.16 ± 0.2155	250	9.829 ± 0.2768	0.0144
S2 (t4-t3)	177	1.195 ± 0.1934	250	2.343 ± 0.2488	0.0003

tB, timing of full blastocyst formation; tEB, timing of blastocyst expansion; tM, timing of fully compacted morula; tPB2, timing of extrusion of the second polar body; tPGT, timing of embryo biopsy for preimplantation genetic testing; tPNa, timing of appearance of pronuclei; tPNf, timing of pronuclei fading; tSB, timing of onset of blastocyst cavitation; tSC, timing of onset of compaction; t2 to t9+, timings of appearance of embryos with 2, 3, 4, 5, 6, 7, 8 and 9 or more well-defined blastomeres.

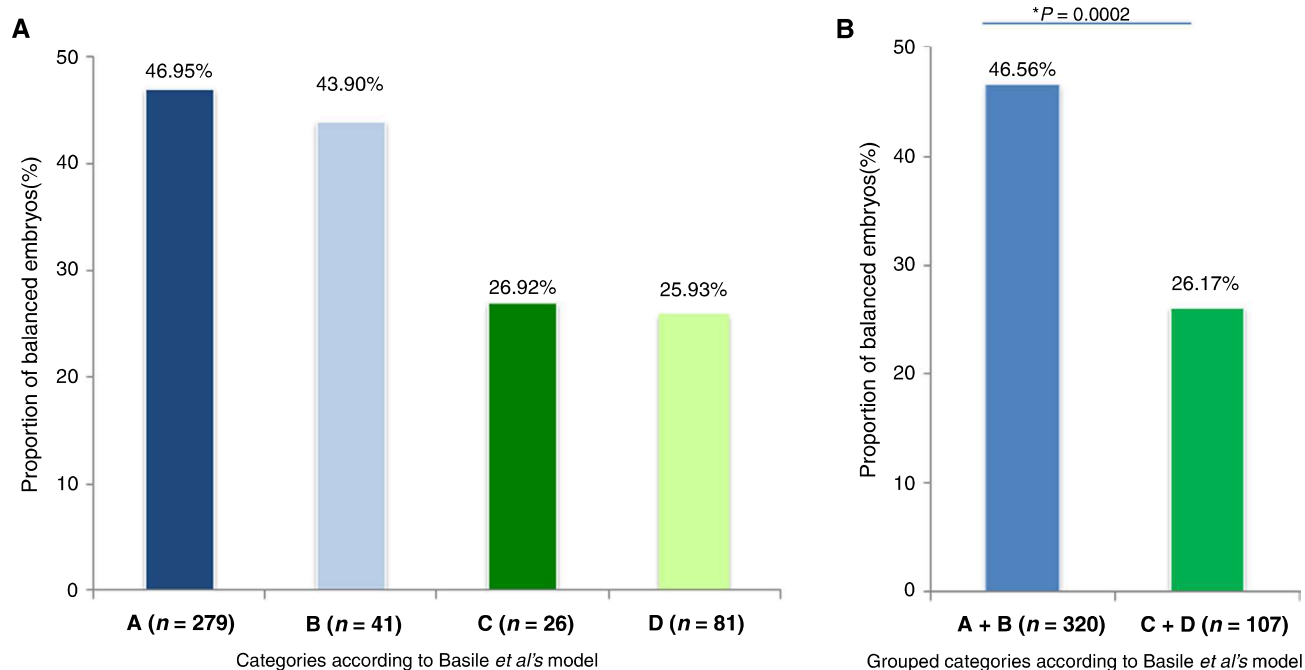


FIGURE 1 (A) Proportion of balanced embryos according to the four categories described in *Basile et al.'s model (2014)* and (B) after simplification into only two categories based on the most significant morphokinetic variable in the original publication, i.e. the t5-t2 interval.

specificity 73%, positive predictive value 84% and negative predictive value 32%).

DISCUSSION

In this study, we showed that significant morphokinetic differences exist between balanced and unbalanced embryos in translocation carriers. No significant predictor of embryo chromosomal status, however, could be identified.

Although we did not screen embryo aneuploidy but only chromosomes involved in translocation for regulatory reasons, these findings are consistent with other studies (*Campbell et al., 2013a; Mumusoglu et al., 2017*), where the association between morphokinetic parameters and embryo ploidy status using PGT-A was evaluated. Indeed, these studies demonstrated that some morphokinetic parameters were significantly different between euploid and aneuploid embryos, either in the early stages of embryo development or during the later stages (*Campbell et al., 2013a; Mumusoglu et al., 2017*). The relevance and clinical value of this strategy, however, was questioned (*Rienzi et al., 2015; Minasi et al., 2016; Reignier et al., 2018*).

As PGT-A is not allowed in France, we tested this approach in patients undergoing PGT-SR cycles for chromosomal translocation to evaluate its predictive value for chromosomal balance. We found that two cell cleavages (t5 and t9+) occurred significantly earlier in unbalanced than in balanced embryos, and that some cellular intervals (cc2, s2, t5-t2) were significantly different between unbalanced and balanced embryos. A considerable overlap, however, existed between the distribution of these variables in unbalanced and balanced embryos. Nevertheless, we used the same approach as other investigators (*Basile et al., 2014*) based on quartiles to try to build a prediction model. The classification of embryos according to their morphokinetic optimal range did not allow us to generate a relevant classification tree. We defined the optimal range as the interval between the 25th and 75th percentile, i.e. quartiles 2 and 3.

We also tested the performance of a previously published aneuploidy prediction model based on two morphokinetic parameters in our dataset of PGT-SR cycles (*Basile et al., 2014*).

We found that the original version of this model had a low clinical value for the classification of balanced versus unbalanced embryos. A simplified version of the model, however, performed slightly better and allowed embryos to be grouped into two categories with significantly different chances of being balanced. The main explanation of these slightly different results probably lies within the different populations being considered. Indeed, we specifically included couples undergoing PGT because of chromosomal rearrangements in one of the partners, whereas *Basile et al. (2014)* included patients undergoing PGT-A for recurrent miscarriage and repeated implantation. Moreover, we could only look at the chromosomes involved in the translocation, not others, for regulatory reasons. Although it has been largely reported that a significant proportion of embryos obtained from translocation carriers have chromosome imbalances unrelated to the rearrangement carried in the couple (*Alfarawati et al., 2011; Fiorentino et al., 2011*), we were prevented from extensively evaluating embryo chromosomal status, whereas *Basile et al. (2014)* carried out PGT-A analysis on all 46 chromosomes. Interestingly, in our previously published validation study aimed at evaluating the performance of a pregnancy prediction model based on morphokinetic parameters, we found that a simplified version of the model performed significantly better than the original one (*Fréour et al., 2015*). In both cases, the difference in atmosphere, i.e. low versus atmospheric oxygen pressure, could partly explain these slight discrepancies.

Among the several studies dealing with time-lapse in IVF, some advocated the value of this technique as a deselection tool used to discard embryos with very poor implantation potential rather than a selection tool for the embryos with a high probability of implantation (*Rubio et al., 2012; Liu et al., 2015; Zhan et al., 2016*). For instance, direct cleavage has been reported to be a strong predictor of implantation failure (*Rubio et al., 2012; Zhan et al., 2016*), depending on the cellular stage in which it occurred. Although this remains debated, multinucleation was also reported to be detrimental for implantation (*Aguilar et al., 2016; Desch et al., 2017*). In this study, we found that the frequency of multinucleation at the two- or four-

cell stage and abnormal division was significantly higher in unbalanced than in balanced embryos. Whether these abnormal events should be included in a hierarchical classification tree should be tested in further studies. We also observed that cell exclusion at the morula stage was slightly more frequent in unbalanced than in balanced embryos. A recent study of interest evaluated the chromosomal status of these excluded cells and demonstrated that they were more frequently aneuploid than the corresponding blastocysts, suggesting a possible cellular repair mechanism aiming at lowering the aneuploidy rate (*Lagalla et al., 2017*). These preliminary results, however, remain to be confirmed in further studies to determine whether the cell exclusion phenomenon and its pattern should be considered as an indicator of embryo ploidy.

Among the studies evaluating the value of time-lapse as a predictor of embryo ploidy, some were based on the day-3 embryo biopsy (*Basile et al., 2014; Chawla et al., 2015; Del Carmen Nogales et al., 2017*), whereas others used trophectoderm biopsy (*Campbell et al., 2013a; 2013b; Rienzi et al., 2015; Minasi et al., 2016; Mumusoglu et al., 2017*). The advantages of trophectoderm biopsy, such as the higher number of cells and amount of DNA required for analysis and increased euploidy rate in fewer embryos (*Scott et al., 2013*), account for the observed trend towards its increasing use in PGT centres, even though the advantages and pitfalls of embryo biopsy still remain to be deciphered (*Zacchini et al., 2017*). In parallel, some studies have advocated the value of late morphokinetic parameters at the blastocyst stage rather than early ones at the cleavage stage as predictors of embryo ploidy (*Campbell et al., 2013a; 2013b*). Although we recently implemented blastocyst biopsy for PGT-SR, the number of cycles at the time of this study was insufficient to compare with the day-3 biopsy strategy. Therefore, our study should be repeated in a large number of translocation carriers undergoing PGT-SR with trophectoderm biopsy to determine whether late morphokinetic parameters can help to identify balanced embryos and test the relevance of previously published models in this population.

The main limitation of our study is that we could only compare balanced

and unbalanced embryos for specific chromosome rearrangements because of French law. Any attempt to generalize the results to aneuploidy screening should be made with great care. Another limitation lies within the use of FISH for the assessment of chromosomal status. We acknowledge that this technique suffers from some limitations (Fiorentino *et al.*, 2011; Dahdouh *et al.*, 2015), exposing a risk of classification error and uninterpretable results (11% of biopsied embryos in this cohort had uninterpretable results). The most critical factors for FISH accuracy are quality of cell fixation, probe hybridization, signal overlap and subjective signal scoring. Our operators, however, were experienced, thus limiting this potential bias. Finally, the retrospective design of this study exposes a risk of bias and prevents the appropriate number of patients for proper statistical power to be calculated.

In conclusion, we found some significant morphokinetic differences between balanced and unbalanced embryos in couples undergoing PGT-SR for chromosomal translocation. The considerable overlap, however, between the variables did not allow the identification of relevant predictors of embryo chromosomal status, as reported previously. We have also shown that a previously published time-lapse model developed for embryo aneuploidy prediction was interesting but had a relatively low performance in our PGT-SR population. The exact clinical value of time-lapse in improving the selection of embryos with low probability of chromosomal abnormality remains to be confirmed.

SUPPLEMENTARY MATERIALS

Supplementary material associated with this article can be found, in the online version, at doi:10.1016/j.rbmo.2018.11.006.

REFERENCES

- Aguilar, J., Rubio, I., Muñoz, E., Pellicer, A., Meseguer, M. **Study of nucleation status in the second cell cycle of human embryo and its impact on implantation rate.** *Fertil. Steril* 2016; 106: 291–299.e2
- Alfarawati, S., Fragouli, E., Colls, P., Wells, D. **First births after preimplantation genetic diagnosis of structural chromosome abnormalities using comparative genomic hybridization and microarray analysis.** *Hum. Reprod.* 2011; 26: 1560–1574
- Barrie, A., Homburg, R., McDowell, G., Brown, J., Kingsland, C., Troup, S. **Examining the efficacy of six published time-lapse imaging embryo selection algorithms to predict implantation to demonstrate the need for the development of specific, in-house morphokinetic selection algorithms.** *Fertil. Steril* 2017; 107: 613–621
- Basile, N., Nogales, M., del, C., Bronet, F., Florensa, M., Riqueiros, M., Rodrigo, L., García-Velasco, J., Meseguer, M. **Increasing the probability of selecting chromosomally normal embryos by time-lapse morphokinetics analysis.** *Fertil. Steril* 2014; 101: 699–704
- Campbell, A., Fishel, S., Bowman, N., Duffy, S., Sedler, M., Hickman, C.F.L. **Modelling a risk classification of aneuploidy in human embryos using non-invasive morphokinetics.** *Reprod. Biomed. Online* 2013a; 26: 477–485
- Campbell, A., Fishel, S., Bowman, N., Duffy, S., Sedler, M., Thornton, S. **Retrospective analysis of outcomes after IVF using an aneuploidy risk model derived from time-lapse imaging without PGS.** *Reprod. Biomed. Online* 2013b; 27: 140–146
- Capalbo, A., Romanelli, V., Cimadomo, D., Girardi, L., Stoppa, M., Dovere, L., Dell'Edera, D., Ubaldi, F.M., Rienzi, L. **Implementing PGD/PGD-A in IVF clinics: considerations for the best laboratory approach and management.** *J. Assist. Reprod. Genet.* 2016a; 33: 1279–1286
- Capalbo, A., Rienzi, L., Ubaldi, F.M. **New approaches for multifactor preimplantation genetic diagnosis of monogenic diseases and aneuploidies from a single biopsy.** *Fertil. Steril* 2016b; 105: 297–298
- Chawla, M., Fakhri, M., Shunnar, A., Bayram, A., Hellani, A., Perumal, V., Divakaran, J., Budak, E. **Morphokinetic analysis of cleavage stage embryos and its relationship to aneuploidy in a retrospective time-lapse imaging study.** *J. Assist. Reprod. Genet.* 2015; 32: 69–75
- Ciray, H.N., Campbell, A., Agerholm, I.E., Aguilar, J., Chamayou, S., Esbert, M., Sayed, S., Time-Lapse User Group. **Proposed guidelines on the nomenclature and annotation of dynamic human embryo monitoring by a time-lapse user group.** *Hum. Reprod.* 2014; 29: 2650–2660
- Dahdouh, E.M., Balayla, J., García-Velasco, J.A. **Comprehensive chromosome screening improves embryo selection: a meta-analysis.** *Fertil. Steril* 2015; 104: 1503–1512
- Del Carmen Nogales, M., Bronet, F., Basile, N., Martínez, E.M., Liñán, A., Rodrigo, L., Meseguer, M. **Type of chromosome abnormality affects embryo morphology dynamics.** *Fertil. Steril* 2017; 107: 229–235.e2
- Desch, L., Bruno, C., Luu, M., Barberet, J., Choux, C., Lamotte, M., Schmutz, E., Sagot, P., Fauque, P. **Embryo multinucleation at the two-cell stage is an independent predictor of intracytoplasmic sperm injection outcomes.** *Fertil. Steril* 2017; 107: 97–103
- Feil, D., Henshaw, R.C., Lane, M. **Day 4 embryo selection is equal to Day 5 using a new embryo scoring system validated in single embryo transfers.** *Hum. Reprod.* 2008; 23: 1505–1510
- Fiorentino, F., Spizzichino, L., Bono, S., Biricik, A., Kokkali, G., Rienzi, L., Ubaldi, F.M., Iammarrone, E., Gordon, A., Pantos, K. **PGD for reciprocal and Robertsonian translocations using array comparative genomic hybridization.** *Hum. Reprod.* 2011; 26: 1925–1935
- Fréour, T., Le Fleuter, N., Lammers, J., Splingart, C., Reignier, A., Barrière, P. **External validation of a time-lapse prediction model.** *Fertil. Steril* 2015; 103: 917–922
- Harton, G.L., Harper, J.C., Coonen, E., Pehlivan, T., Vesela, K., Wilton, L., European Society for Human Reproduction and Embryology (ESHRE) PGD Consortium. **ESHRE PGD consortium best practice guidelines for fluorescence in situ hybridization-based PGD.** *Hum. Reprod.* 2011; 26: 25–32
- Lagalla, C., Tarozzi, N., Sciajno, R., Wells, D., Di Santo, M., Nadalini, M., Distratis, V., Borini, A. **Embryos with morphokinetic abnormalities may develop into euploid blastocysts.** *Reprod. Biomed. Online* 2017; 34: 137–146
- Liu, Y., Chapple, V., Feenan, K., Roberts, P., Matson, P. **Clinical significance of intercellular contact at the four-cell stage of human embryos, and the use of abnormal cleavage patterns to identify embryos with low implantation potential: a time-lapse study.** *Fertil. Steril* 2015; 103: 1485–1491.e1
- Minasi, M.G., Colasante, A., Riccio, T., Ruberti, A., Casciani, V., Scarselli, F., Spinella, F., Fiorentino, F., Varricchio, M.T., Greco, E. **Correlation between aneuploidy, standard morphology evaluation and morphokinetic development in 1730 biopsied blastocysts: a consecutive case series study.** *Hum. Reprod.* 2016; 31: 2245–2254
- Mumusoglu, S., Yarali, I., Bozdog, G., Ozdemir, P., Polat, M., Sokmensuer, L.K., Yarali, H. **Time-lapse morphokinetic assessment has low to moderate ability to predict euploidy when patient- and ovarian stimulation-related factors are taken into account with the use of clustered data analysis.** *Fertil. Steril* 2017; 107: 413–421.e4
- Reignier, A., Lammers, J., Barrière, P., Freour, T. **Can time-lapse parameters predict embryo ploidy? A systematic review.** *Reprod. Biomed. Online* 2018; 36: 380–387
- Rienzi, L., Capalbo, A., Stoppa, M., Romano, S., Maggiulli, R., Albricci, L., Scarica, C., Farcomeni, A., Vajta, G., Ubaldi, F.M. **No evidence of association between blastocyst aneuploidy and morphokinetic assessment in a selected population of poor-prognosis patients: a longitudinal cohort study.** *Reprod. Biomed. Online* 2015; 30: 57–66
- Rubio, I., Kuhlmann, R., Agerholm, I., Kirk, J., Herrero, J., Escrivá, M.-J., Bellver, J., Meseguer, M. **Limited implantation success of direct-cleaved human zygotes: a time-lapse study.** *Fertil. Steril* 2012; 98: 1458–1463
- Scott, R.T.Jr., Upham, K.M., Forman, E.J., Zhao, T., Treff, N.R. **Cleavage-stage biopsy significantly**

- impairs human embryonic implantation potential while blastocyst biopsy does not: a randomized and paired clinical trial.** *Fertil Steril* 2013; 100: 624–630
- Tobler, K.J., Brezina, P.R., Benner, A.T., Du, L., Xu, X., Kearns, W.G. **Two different microarray technologies for preimplantation genetic diagnosis and screening, due to reciprocal translocation imbalances, demonstrate equivalent euploidy and clinical pregnancy rates.** *J. Assist. Reprod. Genet.* 2014; 31: 843–850
- Wilton, L., Thornhill, A., Traeger-Synodinos, J., Sermon, K.D., Harper, J.C. **The causes of misdiagnosis and adverse outcomes in PGD.** *Hum. Reprod.* 2009; 24: 1221–1228
- Zacchini, F., Arena, R., Abramik, A., Ptak, G.E. **Embryo biopsy and development: the known and the unknown.** *Reproduction* 2017; 154: R143–R148
- Zhan, Q., Ye, Z., Clarke, R., Rosenwaks, Z., Zaninovic, N. **Direct Unequal Cleavages: Embryo Developmental Competence, Genetic Constitution and Clinical Outcome.** *PLoS One* 2016; 11:e0166398

Received 3 January 2018; received in revised form 8 November 2018; accepted 9 November 2018.

En menant cette revue de la littérature en 2018, il en ressortait, qu'à l'unanimité les auteurs ne recommandaient pas d'utiliser les outils time-lapse pour statuer sur la ploïdie embryonnaire.

Dans un même temps, Desai et al. (Desai, Goldberg, et al. 2018) ont analysé le développement de blastocystes biopsiés dont 41,6% étaient euploïdes. Ils ont pu mettre en évidence que le taux d'anomalies de développement telles que les fusions cellulaires, les clivages directs, ou la multinucléation de blastomères n'était pas significativement différent dans les deux groupes. La cinétique des évènements précoces du développement est également similaire, en revanche, une blastulation plus tardive est corrélée à l'aneuploïdie. En 2019, Huang et al. (Huang et al. 2019) ont mené une analyse rétrospective du développement de 188 blastocystes, à leur tour, ils ont mis en évidence que l'expansion du blastocyste semble corrélée à la ploïdie embryonnaire. En revanche, la même année, Kimelman et al. (Kimelman et al. 2019) ont montré qu'il n'y avait pas de différence en lien avec la ploïdie dans les données cinétiques de blastulation de 2292 embryons.

En 2020, c'est aux contractions des blastocystes que l'équipe de Gazzo et al. (Gazzo et al. 2020) se sont intéressées. Une différence significative a été retrouvée sur le taux d'aneuploïdie, les embryons qui se contractent se révèlent euploïdes dans 53,6% des cas, contre 58,3% des embryons qui ne se contractent pas. En regardant les étapes préliminaires, ils ont mis en évidence que les embryons qui se contractent mettent plus de temps à atteindre le stade de blastocyste. Cimadomo et al. (Cimadomo et al. 2022) ont analysé 2348 vidéos de blastocystes et ont également mis en évidence que ceux qui se contractent ont moins de chance d'être euploïdes. Début 2023, Hur et al. (Hur et al. 2023) ont publié une analyse rétrospective sur 200 blastocystes pour lesquels le stade de morula avait été gradé selon la compaction (complète ou partielle), une plus grande proportion de mosaïcisme est retrouvée chez les blastocystes issus de morulas partielles qui ont, de plus, une morphologie moins qualitative.

Récemment, les outils d'intelligence artificielle semblent pouvoir apporter une aide pour la recherche non invasive de la ploïdie. Grâce au développement de ces outils dans l'analyse d'image, un algorithme a été développé pour déterminer si un embryon

est euploïde à partir de photos de blastocystes et a été évalué sur 1 231 images. Dans près de 80% des cas, il classe en premier un embryon euploïde avec les meilleures chances d'implantation (Chavez-Badiola et al. 2020). Lee et al. (Lee et al. 2021) ont montré qu'un logiciel était capable de discriminer les embryons aneuploïdes des embryons euploïdes ou en mosaïque. En étudiant les vidéos de 690 embryons analysés en séquençage nouvelle génération (NGS), ils sont les premiers à associer cette technologie à la recherche d'aneuploïdie. La possibilité de prédire l'aneuploïdie embryonnaire à partir de l'analyse d'image time-lapse et d'outils d'intelligence artificielle a été confirmée en 2022 par Diakiw et al. (Diakiw et al. 2022).

Une nouvelle revue de la littérature a été publiée en 2022, en associant les analyses de morphologie et de morphocinétique à la ploïdie embryonnaire. Bamford et al. (Bamford et al. 2022) ont mis en avant que les temps t_8 , t_9 et t_{EB} pourraient être inclus dans de futur modèle prédictif pour prioriser les embryons à biopsier dans le cadre de la recherche d'aneuploïdie. Récemment, Zou et al. (Zou et al. 2022) ont mis au point un modèle prédictif à partir de 851 embryons testés pour une recherche d'aneuploïdie en combinant des données de time-lapse et des données cliniques. Ce modèle semble robuste mais ne permet pas de s'affranchir de la biopsie nécessaire à l'analyse génétique.

Dans le cadre des prises en charge en DPI réalisée au CHU de Nantes, les biopsies embryonnaires sont réalisées au stade précoce. En s'intéressant à notre population de DPI cytogénétique, nous avons mis en évidence des différences entre les embryons équilibrés et déséquilibrés pour les paramètres des premiers jours de développement sans pouvoir néanmoins trouver de paramètre morphocinétique discriminant. En 2019, l'équipe de Amir et al. (Amir et al. 2019) a publié un travail sur le même sujet avec une méthodologie similaire. Leur analyse a porté sur 270 embryons biopsiés à J3, les temps t_4 et t_{SB} étaient significativement retardés dans leur groupe d'embryons déséquilibrés (209) par rapport aux embryons équilibrés (61).

Le sujet est aujourd'hui toujours d'actualité et continue d'intéresser de nombreuses équipes qui cherchent à développer des alternatives à l'analyse invasive des embryons. Les outils de time-lapse actuels ne semblent pas apporter les solutions

attendues mais pourraient être assistés de logiciel d'intelligence artificielle pour améliorer la puissance des données prises en compte et permettre aux embryologistes de disposer d'un outil supplémentaire de discrimination des embryons.

d. Modification morphocinétique après biopsie embryonnaire au 3^{ème} jour de développement = article 5

Lors de la mise en place du DPI au CHU de Nantes en 2013 nous avons intégré la technique de biopsie embryonnaire à J3 au laboratoire. La littérature disponible discutait déjà de l'impact de la biopsie de blastomère à ce stade et de la biopsie de trophoctoderme au stade blastocyste (Kokkali et al. 2007; Brodie et al. 2012; K. Xu et Montag 2012). Il nous a paru intéressant d'observer de plus près, grâce au système time-lapse, la reprise de développement des embryons suite au prélèvement des blastomères réalisé au 3^{ème} jour de culture.

Nous avons comparé le développement des embryons issus de cycles de DPI, entre mai 2013 et août 2017, à ceux obtenus en cycles d'ICSI sur la même période. Cela représente 1691 embryons biopsiés à J3 et 2578 non biopsiés, tous en culture dans un système time-lapse.

Pour cette publication je me suis chargée de réaliser une revue de la littérature pour définir les connaissances sur le sujet et identifier la question sur laquelle travailler. Je me suis chargée d'annoter les événements morphocinétiques des vidéos des embryons en culture time-lapse afin d'extraire une base de données du développement embryonnaire. En parallèle j'ai extrait les données nécessaires à la création de la base de données des patients correspondants aux embryons étudiées. J'ai pu réaliser les analyses statistiques pour comparer les données des 2 groupes une fois celles-ci extraites. Pour finir, je me suis chargée de la rédaction de la première version de l'article, de la soumission auprès d'une revue à comité de lecture et de répondre aux corrections posées par les relecteurs.



Modification of late human embryo development after blastomere removal on day 3 for preimplantation genetic testing

Jenna Lammers^{a,b}, Arnaud Reignier^{a,b,c}, Sophie Loubersac^{a,b}, Sana Chtourou^d, Tiphaine Lefebvre^{a,c}, Paul Barrière^{a,b,c}, and Thomas Fréour^{a,b,c} 

^aService de Biologie et Médecine de la Reproduction, CHU Nantes, Nantes, France; ^bCentre de Recherche en Transplantation et Immunologie UMR 1064, INSERM, Université de Nantes, Nantes, France; ^cFaculté de Médecine, Université de Nantes, Nantes, France; ^dLaboratoire de Biologie de la Reproduction et de Cytogénétique, Hôpital Aziza Othmana, Tunis, Tunisia

ABSTRACT

The purpose of our study was to use a time-lapse monitoring (TLM) system to determine if day 3 blastomere biopsy for preimplantation genetic testing (PGT) had an impact on subsequent morphokinetic parameters at the morula and blastocyst stages. In this retrospective monocentric study conducted between May 2013 and August 2017, we compared late morphokinetic parameters in embryos undergoing day 3 blastomere biopsy for PGT and in control non-biopsied embryos obtained in intracytoplasmic sperm injection (ICSI) cycles for male infertility. All embryos in both groups were cultured in a TLM system. The biopsy group was composed of 1691 embryos (386 PGT cycles). The control group was composed of 2578 embryos (786 ICSI cycles). Early morphokinetic parameters up to day 3 were similar in both groups. Concerning late morphokinetic parameters, the onset of compaction (tSC), fully-compacted morula stage (tM), onset of cavitation/early blastulation (tSB), and blastocyst stages (tB and tEB) appeared significantly earlier in the biopsy group than in the control group. We found that late morphokinetic events at the morula and the blastocyst stages occurred significantly earlier in biopsied embryos than in control non-biopsied-embryos. The mechanisms underlying these modifications of embryo development after biopsy should be investigated in order to determine precisely, and this phenomenon could be associated with embryo, fetal, and offspring development.

Abbreviations: TLM: time-lapse monitoring; PGT: preimplantation genetic testing; ICSI: intracytoplasmic sperm injection; tSC: the onset of compaction; tM: fully-compacted morula stage; tSB: onset of cavitation/early blastulation; tB and tEB: blastocyst stages; OHSS: ovarian hyperstimulation syndrome

ARTICLE HISTORY

Received 15 July 2020
Revised 30 September 2020
Accepted 1 October 2020

KEYWORDS

IVF; blastocyst; biopsy; time-lapse; preimplantation genetic testing

Introduction

Pre-implantation genetic testing (PGT) is a procedure developed in the early 90s for couples with a high risk of transmitting a genetic abnormality or with a high risk of miscarriage because of chromosomal translocation (Harton et al. 2011a). Cleavage-stage blastomere biopsy has been the most commonly used method during many years. However, it is an invasive procedure in which a zona pellucida breaching, a cell adhesion disruption and an aspiration of one or 2 blastomeres are needed (Harton et al. 2011b). Trophectoderm biopsy has recently gained interest in PGT cycles. Indeed, this approach allows a better assessment of embryo quality and the analysis of more embryonic cells, leading to improved clinical outcome in PGT cycles (Scott et al. 2013). However, day 3 blastomere biopsy also has a few advantages, as it allows fresh embryo transfer and requires less time

and material for embryo culture. As such, day 3 embryo biopsy is used in a significant number of PGT centers.

Some studies have explored the potential impact of the day 3 biopsy procedure on subsequent embryo development. Most authors found that removing two cells on day 3 could reduce the blastulation rate and subsequently implantation rate as compared to one cell [2, 3]. However, few authors studied in detail the impact of day 3 embryo biopsy on subsequent embryo developmental stages, i.e., morula and blastocyst. Studies on human embryos evoked delayed compaction and blastulation as compared to non-biopsied embryos (Kirkegaard et al. 2012, Bar-El et al. 2016).

Since the release of the first commercial time-lapse monitoring (TLM) system in 2009, several laboratories around the world have implemented this technology in order to improve embryo culture conditions and embryo quality evaluation. As it allows continuous

monitoring of embryo development, this technology is a useful tool to observe embryo development after blastomere biopsy. The studies of Kirkegaard et al. 2012 and Bar-El et al. 2016, reported the use of TLM system to evaluate post-biopsy embryo development in PGT cycles. Both found that embryonic development was significantly delayed after blastomere biopsy on day 3, as compared to non-biopsied embryos. However, these studies were conducted in relatively limited population (109 and 751, respectively), thus highlighting the need for confirmation in larger studies. Therefore, this study aimed at evaluating the potential impact of blastomere biopsy on subsequent embryo development by comparing late morphokinetic parameters in embryos with or without blastomere biopsy on day 3.

Results

A total of 1691 embryos obtained in 386 PGT cycles and undergoing blastomere biopsy on day 3, were compared to 2578 non-biopsied embryos obtained in 786 control ICSI cycles.

Demographic and cycle characteristics are presented in Table 1. Control group and biopsy group were not different concerning female characteristics, except for serum AMH level and smoking status. The proportion of couples with secondary infertility and fertilization rate were significantly higher in the PGT group than in the control ICSI group. There was no significant difference in terms of mean number of day 3 embryos available for biopsy (or theoretically compatible with biopsy), i.e., good or medium quality embryos. As

expected in the context of PGT, the proportion of clinically usable embryos, i.e., transferred or frozen, was significantly lower in the biopsy group than in the control ICSI group.

Next, we compared embryo morphokinetic parameters between the two groups. Early morphokinetic events up to day 3 were similar in both groups (data not shown). Late embryo development events (day 4 onwards) were significantly different between the two groups. Indeed, the onset of compaction (tSC), fully-compacted morula stage (tM), onset of cavitation/early blastulation (tSB) and blastocyst stages (tB and tEB) occurred significantly earlier in the biopsy group than in the control group (Figure 1).

Discussion

In the present study, we found that late morphokinetic events at the morula and the blastocyst stages occurred significantly earlier in biopsied day 3 embryos than in non-biopsied control embryos, suggesting that blastomere biopsy on day 3 affects subsequent embryo development.

Apart from embryo development *in vitro*, the impact of day 3 embryo biopsy on implantation potential has already been reported. Scott et al. (2013) demonstrated that day 3 embryo biopsy-impaired embryo implantation compared to a control sibling embryo. Indeed, the transfer of two embryos on day 3, one biopsied and one sibling control, resulted in significantly higher live birth rate in control embryos as compared to the biopsied embryos (50% vs 30%, respectively).

Table 1. Patients' and IVF cycle characteristics: demographic, cycle, and embryologic characteristics in control and biopsy groups.

	Control group (n = 786 cycles)	Biopsy group (n = 386 cycles)	
<i>Demographic characteristics</i>			
Female age (years)	32.6 ± 4.4	32.4 ± 3.8	NS
Female BMI (kg/m ²)	24.0 ± 4.9	23.8 ± 4.4	NS
AFC	19.2 ± 8.9	16.6 ± 11.3	NS
AMH (µg/L)	3.97 ± 3.33	4.56 ± 3.99	*
Proportion of women currently smoking (%)	38.2%	27.0%	*
Secondary infertility (history of at least one clinical pregnancy)	41.6%	67.9%	*
Male age (years)	35.7 ± 6.1	35.0 ± 4.9	*
<i>Cycle characteristics</i>			
IVF cycle rank	1.7 ± 1.2	1.3 ± 0.6	*
Total dose of gonadotropins (FSH units)	2460 ± 1048	2434 ± 954	NS
Total number of oocytes retrieved	11.6 ± 4.9	14.2 ± 6.3	*
Mature oocytes	8.6 ± 3.7	11.0 ± 5.2	*
Fertilization rate	58.72%	62.62%	*
<i>Embryos characteristics</i>			
D3 embryos compatible with biopsy procedure (≥6 cells, <25% fragmentation, fair evenness)	2578	1691	NS
Proportion of embryos undergoing compaction at the morula stage	52.21%	51.08%	NS
	2039	1338	
	79.1%	79.1%	
Proportion of clinically usable embryos (Transferred or frozen embryos on day 4, 5 or 6)	1473	600	*
	57.16%	35.48%	

Results are presented as mean ± standard deviation or proportion when appropriate. * $p < 0.05$.

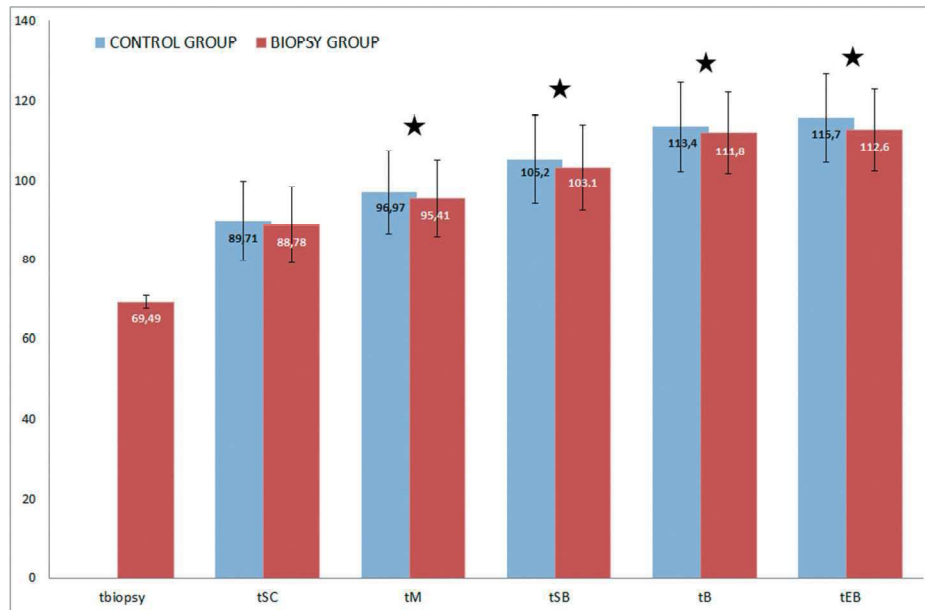


Figure 1. Average timing of late morphokinetic parameters in control and biopsy groups. Results are represented in blue for control group and red for biopsy group. Time is expressed in hours post injection, time when embryos are biopsied (tbiopsy), the 9-cell stage (t9+), the onset of compaction (tSC), the fully-compacted morula stage (tM), the onset of cavitation (tSB) and blastocyst stages (tB) were compared. Parameters with star are significantly different between the 2 groups ($*p < 0.05$). Late morphokinetic events at the morula and the blastocyst stages, tM, tSB, tB and tEB, occurred significantly earlier in biopsied embryos than in control non biopsied-embryos.

Our results are in contradiction with the only two previous studies performed with a quite similar method. In a series of 56 biopsied and 53 non-biopsied embryos cultured in a time-lapse system, Kirkegaard et al. (2012) reported that the duration of compaction, morula, and early blastocyst stages were identical in the two groups, while the duration of the expanded blastocyst stage was significantly shorter in the biopsied group than in the control group. In addition to the very limited number of embryos included in this study, it should be noted that embryo culture was performed under atmospheric O₂ pressure (20%) in this study, whereas we cultured embryos under low O₂ pressure (5%). This might account, at least in part, for these conflicting results, as oxygen concentration has been shown to influence embryo developmental rate (Kirkegaard et al. 2013). Although this remains speculative in the absence of specific trial, the different method used for blastomere biopsy (i.e., blastomere aspiration versus pressure/extrusion) might also account for these differences. Another similar recent study compared morphokinetic parameters in 366 biopsied embryos and 385 non-biopsied embryos (Bar-El et al. 2016). Unlike our study, the authors reported that post-biopsy morphokinetic parameters were significantly delayed in the biopsy group as compared to the control group. The main difference between this study

and ours lies within its design. Indeed, control embryos were not selected according to their morphology on day 3, but rather to their late developmental ability (blastulation).

An older study based on conventional static microscopy (without time-lapse) also evaluated the effect of blastomere biopsy on day 3 on subsequent embryo development (Tarin et al. 1992). Tarin et al. studied 129 human embryos randomized in the day 2 biopsy group on or non-biopsy group. Although the blastulation rate was similar in both groups, they observed a significantly higher proportion of embryos reaching the morula stage after day 4 in the biopsied-group as compared to the control group, suggesting acceleration to late embryo developmental stages in the biopsy group, in agreement with our findings.

In parallel to morphologic/morphokinetic events occurring after blastomere biopsy, the issue of genetic modifications potentially induced by the biopsy procedure is of utmost importance. All experiments conducted in mouse lead to reassuring conclusions, with no significant modification of the global gene expression pattern (Duncan et al. 2009) while maintaining the expression of a critical micro RNA and its target genes (Naseri et al. 2019) after blastomere biopsy.

Biophysical mechanisms and forces regulating actively participate in embryonic cell adhesion,

which in turn sets the stage for blastocyst formation and cell fate (Maître 2017); (White et al. 2018). In this context, it can be speculated that the use of calcium and magnesium-free medium followed by an invasive procedure such as blastomere biopsy on day 3 might disturb spatial organization and emerging cell-to-cell interactions, even though they are theoretically put in place slightly later at the morula stage (on day 4 in humans and on day 3 in mouse). However, the majority of the existing literature on cell fate and cell adhesion in embryos was obtained in mouse, thus questioning its generalizability in humans. Whether embryo biopsy procedure significantly impacts cell fate and embryo organization in human embryos is not known yet, and the need for research focused on blastomere biopsy has been recently highlighted in a review (Maître 2017). In any case, the increasing use of trophectoderm biopsy will probably soon make these concerns less relevant.

Although statistical power calculation could not be performed according to the retrospective design of this study, the large number of embryos included here might represent a significant strength over the existing literature. Time-lapse systems are objective and accurate tools to observe cell division kinetics. In this respect, this technology is relevant for the study of fine differences in embryo developmental speed after biopsy. However, our results should be interpreted with care, as the biopsy procedure was not strictly homogeneous in all cases, with either 1 or 2 blastomeres extracted. Moreover, this study was not designed to evaluate the impact of embryo biopsy on implantation, and the statistical differences identified might not be representative of altered implantation potential. The significant differences observed between the 2 groups in terms of ovarian reserve and smoking status might also be considered as potential confounding factors, as some studies reported an association between these factors and morphokinetic parameters (Salvarci et al. 2017) (Bourdon et al. 2020). In conclusion, the present study demonstrates that late morphokinetic events at the morula and the blastocyst stages occurred significantly earlier in biopsied embryos than in control non-biopsied-embryos. The mechanisms underlying these modifications of embryo development after biopsy should be investigated in order to determine precisely is this phenomenon could be associated with embryo, fetal and offspring development.

Materials and methods

Patients

This monocentric retrospective cohort study was conducted in couples referred for PGT because of a structural chromosomal rearrangement (PGT-SR) or for monogenic/single gene defect (PGT-M). PGT cycles for aneuploidy screening (PGT-A) are not allowed in our country. We analyzed the clinical and biological data of all consecutive patients who had undergone a PGT cycle with autologous oocyte and embryo culture performed using the Embryoscope® (Vitrolife®) between May 2013 and August 2017 in our University Fertility Center.

All morphokinetic parameters were compared in PGT cycles (pre- and post-biopsy) and in the control group. The control group consisted in intracytoplasmic sperm injection (ICSI) cycles performed in patients with male factor during the same time period and whose embryos (cultured in the Embryoscope® up to blastocyst stage) had medium to good morphology on day 3, i.e., theoretically compatible with embryo biopsy.

Ovarian stimulation

All patients underwent controlled ovarian stimulation with the antagonist protocol. Gonadotropin starting dose was chosen according to female age, ovarian reserve and previous PGT cycles, if any. Cycle monitoring consisted of regular hormonal assays and ultrasonography, and ovulation was triggered with recombinant hCG when at least three follicles reached 18 mm in diameter, or with GnRH agonist in case of ovarian hyperstimulation syndrome (OHSS).

Oocyte retrieval, ICSI and embryo culture

Oocyte retrieval was performed 34–36 h later. Control and biopsied embryos were treated exactly the same way for embryo culture. After denudation with hyaluronidase (SynVibro® hyadase, Origio), all mature oocytes were microinjected and immediately placed in individual microwells within a specific culture dish (Embryoslide®, Vitrolife®) before being loaded into the Embryoscope®. Embryo culture was performed at 37°C under a controlled atmosphere with low oxygen pressure (5% O₂, 6% CO₂). Sequential media were used for embryo culture, (G1plus® up to day 3 and G2plus® up to day 6, Vitrolife®).

Time lapse analysis

Each embryo was investigated by detailed time-lapse analysis measuring the exact timing of the developmental events in hours after ICSI procedure, as described by (Ciray et al. 2014). The terms t2, t3, t4, t5, t6, t7, and t8 were used for the exact timings of appearance of embryos with 2, 3, 4, 5, 6, 7, and 8 well-defined blastomeres, respectively. Concerning late embryonic events, the onset of compaction (tSC), the fully-compacted morula stage (tM), the early cavitation/onset of blastulation (tSB), the onset of expansion (tB) and the fully expanded stage (tEB) were recorded. The annotation of morphokinetic parameters was performed by two trained senior embryologists. Quality control where regularly processed in the laboratory to ensure the reproducibility and the precision of the results.

Embryo biopsy and embryo transfer

Embryo biopsy was performed on day 3 for all embryos with at least 6 blastomeres, <25% fragmentation and fair evenness. Briefly, embryos were first placed in Ca/Mg-free medium (G-PGD, Vitrolife®) for a few minutes, before laser-assisted zona pellucida hatching (ZilosTK, Hamilton Thorn®). One to 2 cells were then extracted for subsequent genetic analysis depending on the number of blastomeres (1 cell in 6 to 7-cell embryos, 2 cells in ≥8-cell embryos). Cell extrusion was obtained by gently pressing on the zona pellucida with the biopsy pipette close to the breach. In our experience, this allows faster procedure and less cell damage than with conventional blastomere aspiration.

Balanced or unaffected embryos were selected for transfer on day 4 or 5 according to post-biopsy development for practical and organizational reasons. Single or double embryo transfer was chosen jointly by medical staff and the couple. A pregnancy test was carried out 11 or 12 days after embryo transfer, and if positive, clinical pregnancy was confirmed ultrasonographically 4–5 weeks later by the detection of a gestational sac and fetal heart activity.

Statistics

Student's or Wilcoxon's tests were used for continuous variables and χ^2 or Fischer's tests for categorical variables. The non-parametric Mann-Whitney test was used for non-normally distributed variables. Statistical analysis was performed using GraphPad Prism® software. P values <0.05 were considered to denote a statistically significant difference.

Ethics approval

All patients gave consent for the anonymous use of their data registered in this database. This protocol was approved by the local ethics committee (GNEDS).

Disclosure statement

The authors have nothing to disclose.

Author contributions

Analyzed the data, wrote and revised the manuscript: JL, AR; expert knowledge, critically revised the manuscript: SL, SC, TL, PB; designed and supervised the study: TF.

ORCID

Thomas Fréour  <http://orcid.org/0000-0002-7243-7709>

References

- Bar-El L, Kalma Y, Malcov M, Schwartz T, Raviv S, Cohen T, Amir H, Cohen Y, Reches A, Amit A, et al. 2016. Blastomere biopsy for PGD delays embryo compaction and blastulation: a time-lapse microscopic analysis. *J Assist Reprod Genet.* 33(11):1449–1457. doi:10.1007/s10815-016-0813-2
- Bourdon M, Ferreux L, Maignien C, Patrat C, Marcellin L, Pocate-Cheriet K, Chapron C, Santulli P. 2020. Tobacco consumption is associated with slow-growing day-6 blastocysts. *F&S Rep.* 1(1):30–36. doi:10.1016/j.xfre.2020.04.006.
- Ciray HN, Campbell A, Agerholm IE, Aguilar J, Chamayou S, Esbert M, Sayed S. 2014. Proposed guidelines on the nomenclature and annotation of dynamic human embryo monitoring by a time-lapse user group. *Hum Reprod.* 29(12):2650–2660. doi:10.1093/humrep/deu278.
- Duncan FE, Stein P, Williams CJ, Schultz RM. 2009. The effect of blastomere biopsy on preimplantation mouse embryo development and global gene expression. *Fertil Steril.* 91(4):1462–1465. doi:10.1016/j.fertnstert.2008.07.1710.
- Harton GL, Harper JC, Coonen E, Pehlivan T, Vesela K, Wilton L. 2011a. ESHRE PGD consortium best practice guidelines for fluorescence in situ hybridization-based PGD. *Hum Reprod (Oxford, England).* 26(1):25–32. doi:10.1093/humrep/deq230.
- Harton GL, Magli MC, Lundin K, Montag M, Lemmen J, Harper JC. 2011b. ESHRE PGD consortium/embryology special interest group–best practice guidelines for polar body and embryo biopsy for preimplantation genetic diagnosis/screening (PGD/PGS). *Hum Reprod (Oxford, England).* 26(1):41–46.
- Kirkegaard K, Hindkjaer JJ, Ingerslev HJ. 2013. Effect of oxygen concentration on human embryo development evaluated by time-lapse monitoring. *Fertil Steril.* 99(3):738–744.e4. doi:10.1016/j.fertnstert.2012.11.028.

- Kirkegaard K, Juhl Hindkjaer J, Ingerslev HJ. 2012. Human embryonic development after blastomere removal: a time-lapse analysis. *Hum Reprod.* 27(1):97–105. doi:[10.1093/humrep/der382](https://doi.org/10.1093/humrep/der382).
- Maitre J-L. 2017. Mechanics of blastocyst morphogenesis: mechanics of blastocyst morphogenesis. *Biol Cell.* 109(9):323–338. doi:[10.1111/boc.201700029](https://doi.org/10.1111/boc.201700029).
- Naseri F, Hosseini S, Ghaffari Novin M, Hosseini A, Heidari MH, Salehi M. 2019. Does blastomere removal alter the expression level of MiR-Let7a and its target genes following mouse embryo biopsy? *J Cell Biochem.* 120(6):9430–9436. doi:[10.1002/jcb.28218](https://doi.org/10.1002/jcb.28218).
- Salvarci A, Gurbuz AS, Uzman S, Kaya M, Gorkemli H. 2017. Comparison of embryo morphokinetics following intracytoplasmic sperm injection in smoker and non-smoker couples: are the results different? *J Pak Med Assoc.* 67(10):6.
- Scott RT, Upham KM, Forman EJ, Zhao T, Treff NR. 2013. Cleavage-stage biopsy significantly impairs human embryonic implantation potential while blastocyst biopsy does not: a randomized and paired clinical trial. *Fertil Steril.* 100(3):624–630. doi:[10.1016/j.fertnstert.2013.04.039](https://doi.org/10.1016/j.fertnstert.2013.04.039).
- Tarin JJ, Conaghan J, Winston RM, Handyside AH. 1992. Human embryo biopsy on the 2nd day after insemination for preimplantation diagnosis: removal of a quarter of embryo retards cleavage. *Fertil Steril.* 58(5):970–976. doi:[10.1016/S0015-0282\(16\)55444-2](https://doi.org/10.1016/S0015-0282(16)55444-2).
- White MD, Zenker J, Bissiere S, Plachta N. 2018. Instructions for assembling the early mammalian embryo. *Dev Cell.* 45(6):667–679. doi:[10.1016/j.devcel.2018.05.013](https://doi.org/10.1016/j.devcel.2018.05.013).

La majorité des pays réalisant des diagnostics génétiques sur embryons utilisent des techniques génétiques plus efficaces que celles utilisées en France et privilégient ainsi la biopsie au stade de blastocyste avec des techniques de séquençage nouvelle génération (NGS). La publication de ce travail en 2021 nous a permis de montrer que les évènements morphocinétiques qui ont lieu après la biopsie réalisée au 3^{ème} jour de développement sont accélérés dans le groupe des embryons biopsiés.

L'équipe de Aghajani et al. (Aghajani et al. 2022) a étudié en 2022 les résultats de 443 embryons biopsiés à J3 pour lesquels une seule cellule a été prélevée. Sans données time-lapse, ils ont constaté que les résultats en termes de développement embryonnaire et de grossesse étaient plus faibles que ceux du groupe contrôle qui ne bénéficiait pas de biopsie. Ces résultats peuvent suggérer que la biopsie, même d'une seule cellule reste une technique invasive qui altère le développement embryonnaire. Cependant, l'absence de culture en système time-lapse peut également laisser penser que le choix des embryons éligibles à la biopsie peut être différent lorsque l'on dispose de données morphocinétiques.

En 2020, Cimadomo et al. (Cimadomo et al. 2020) ont publié un travail sur l'histoire de la biopsie embryonnaire de ses débuts dans les années 1980 aux perspectives à venir qui pourraient permettre de ne plus avoir à biopsier les embryons pour obtenir un résultat génétique. Cette publication permet de constater que les techniques de biopsie des cellules aux différents stades de développement existent depuis la fin des années 80 et que les évolutions techniques viennent surtout d'optimisation des outils utilisés tels que les milieux de biopsie ou l'usage de laser. Les technologies d'analyse génétique ont également beaucoup évolué pour permettre une rapidité et une fiabilité d'analyse croissante.

Une revue de la littérature a été publiée par Leaver et Wells (Leaver et Wells 2020) pour présenter les alternatives non invasives à la biopsie embryonnaire. Dans ce travail, ils détaillent les protocoles existants en analyse de fluide blastocoelique et de milieu de culture ainsi que leurs avantages et inconvénients. En comparant les résultats obtenus sur milieu de culture et biopsie de trophoctoderme à partir de 1 301

embryons humains, Rubio et al. (Rubio et al. 2020) ont démontré, que ces techniques étaient comparables.

Une des limites de la biopsie embryonnaire au stade précoce est le taux d'embryons pour lesquels le résultat ne peut être rendu, ce qui peut conduire à la réalisation d'une nouvelle biopsie. En 2022, Carles et al. (Carles et al. 2022) ont étudié l'impact d'une seconde biopsie et ont montré qu'il était possible d'obtenir des résultats génétiques fiables ainsi que des grossesses cliniques avec les embryons biopsiés à deux reprises. Ces données permettent de relativiser l'impact négatif de la biopsie sur le potentiel implantatoire des embryons.

La revue de la littérature de Vlajkovic et al. (Vlajkovic et al. 2022) publiée dans la Cochrane Database en 2022, n'a pas su retrouver de différence significative en termes d'implantation ou de taux de grossesse selon le jour de biopsie embryonnaire à J3 ou J5.

Avec ces données récentes et rassurantes quant à l'impact de la biopsie et aux vues des données prometteuses des alternatives au prélèvement de cellules de l'embryon, il est raisonnable de penser que l'avenir de l'analyse des embryons humains sera un jour non invasive. En attendant, la biopsie embryonnaire reste une technique largement utilisée pour les diagnostics des embryons des patients pris en charge.

2) Aspects fondamentaux du développement embryonnaire

Notre expertise en culture embryonnaire et en morphocinétique ainsi que notre maîtrise des techniques de micro-manipulation des embryons nous a permis de développer des protocoles utiles aux projets de recherches menées avec le laboratoire Inserm CR2TI (Center for Research in Transplantation and Translational Immunology) (Figure 7).

La collaboration entre le laboratoire d'AMP du CHU de Nantes et celui du CR2TI a pu débuter en 2014 suite à l'obtention de l'autorisation de recherche sur embryons humains délivrée par l'Agence de la Biomédecine. Le projet comprend l'étude des déterminants de la pluripotence lors du développement humain pré-gastrulation et l'étude du développement de l'embryon préimplantatoire et péri-implantatoire.

Dans un premier temps, notre stratégie est d'étudier le profil d'expression génique des cellules d'embryons humains cultivées *in-vitro* puis d'en déduire un modèle de spécification des lignées trophoctoderme (TE), épiblaste (EPI) et endoderme primitif (PE) chez l'humain. Ensuite, nous travaillons à la formulation et à la validation d'hypothèses concernant les voies de signalisation impliquées dans le développement préimplantatoire humain pour enfin mettre en place un modèle d'implantation *in-vitro* qui a pour objectif d'évaluer l'impact de la modification du milieu de culture sur la fonctionnalité de l'embryon. Pour ce faire, nous avons l'opportunité de travailler à partir de cellules souches embryonnaires humaines mais aussi, à partir d'embryons humains cryoconservés à différents stades de développement.

Afin de faciliter la lecture globale du manuscrit, les travaux présentés dans cette partie sont disponibles en annexe.

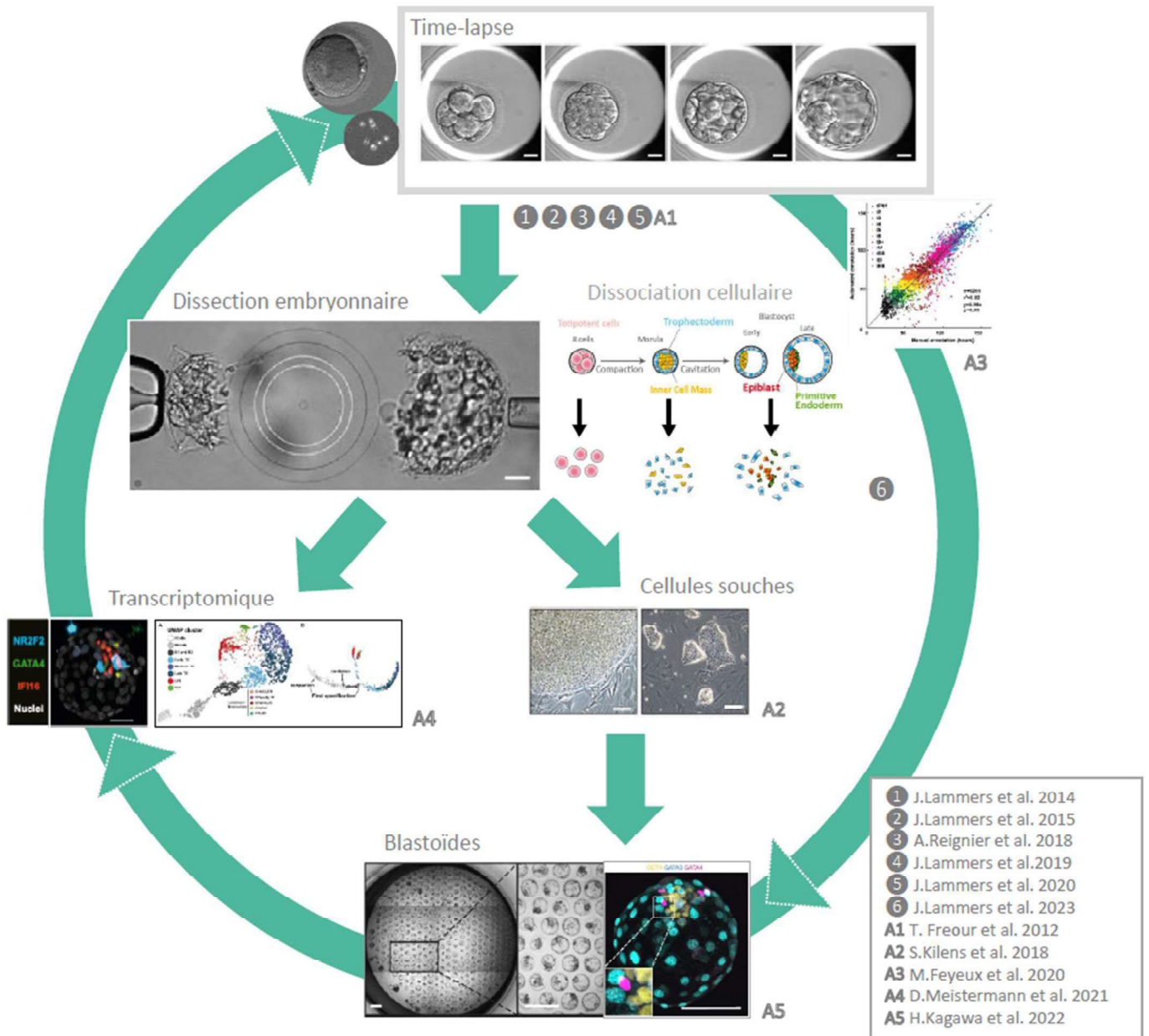


Figure 7 : Représentation schématique des liens existants entre les thématiques de recherche en biologie du développement

a. La dérivation de cellules souches = annexe A2

Les cellules souches embryonnaires humaines sont un premier outil qui peut permettre de mimer l'embryon. En disposant de modèles cellulaires capables de proliférer *in-vitro* qui ont le potentiel de se différencier dans tous les types cellulaires de l'embryon péri-implantatoire, il est possible de valider des hypothèses sans avoir à manipuler de nombreux embryons. Les cellules souches pluripotentes humaines (hPSC) ont le potentiel de participer à la formation du fœtus (épiblaste), de la vésicule vitelline (endoderme primitif) et du placenta (trophectoderme). Elles peuvent être obtenues à partir de cellules souches embryonnaires humaines (Thomson et al. 1998) (Okae et al. 2018).

En 2018 nous avons publié un article traitant de la dérivation de cellules semblables à des cellules souches embryonnaires humaines (Kilens et al. 2018). Pour son travail de thèse, l'objectif de Stéphanie Kilens était de reprogrammer des cellules somatiques en cellules souches pluripotentes induites (hiPSC) puis de les comparer avec des cellules embryonnaires humaines de l'épiblaste préimplantatoire (au niveau transcriptomique, métabolomique et épigénétique). Les cellules obtenues par dérivation ont pu être comparées aux résultats obtenus sur des embryons entiers mis en culture et fixés à des stades différents pour réalisation d'immunofluorescence mais aussi au niveau cellulaire par isolation de cellules uniques d'épiblaste. Ma contribution à ce travail concernait l'isolation des cellules et la fixation des embryons.

Pour cette publication, je me suis chargée de la gestion de la banque d'embryons humains destinés à la recherche et de sélectionner les stades adaptés à la question posée. J'ai réalisé la décongélation des échantillons et leur mise en culture en système time-lapse, et j'ai annoté les événements morphocinétiques des vidéos des embryons. J'ai ensuite réalisé les fixations des embryons aux stades voulu pour réalisation des immunofluorescences. J'ai également réalisée des isolations en cellules uniques aux différents stades embryonnaires. Pour finir, je me suis chargée de la rédaction du chapitre matériel et méthode concernant les manipulations réalisées et j'ai participé à la relecture du manuscrit.

Depuis cette publication, le protocole de reprogrammation a pu être utilisé pour d'autres travaux de l'équipe (Castel et al. 2020; Castel et David 2022; Onfray et al. 2022). Ainsi, il a par exemple été montré que l'obtention de cellules souches trophoblastiques humaines (hTSC) est possible par conversion de cellules souches pluripotentes naïves humaines (hNPSC) et cellules souches pluripotentes humaines (hPSC) ou par reprogrammation de cellules somatiques avec les facteurs de transcription.

De la même façon, d'autres laboratoires ont pu mettre en place et optimiser ce protocole de reprogrammation pour poursuivre leurs recherches sur la thématique des cellules souches pluripotentes induites (iPSC) (Kunitomi et al. 2022; Charlesworth et Nakauchi 2022).

***b. L'annotation automatisée du développement embryonnaire =
annexe A3***

L'annotation du développement embryonnaire permet d'obtenir les données morphocinétiques des embryons cultivés en système time-lapse. Cette étape d'observation et d'annotation des vidéos est chronophage et peut dépendre de l'opérateur, le développement d'approches automatisées est donc essentiel.

En 2020, nous avons publié un travail réalisé en collaboration avec la plateforme MicroPiCell traitant de l'annotation automatisée des événements du développement embryonnaire grâce à un outils d'analyse d'images basé sur l'évaluation des niveaux de gris.

Pour cette publication, je me suis chargée de l'annotation manuelle des événements morphocinétiques des vidéos des embryons et de l'extraction des données brutes et des vidéos. Pour finir, je me suis chargée de la rédaction du chapitre matériel et méthode concernant les manipulations réalisées et j'ai participé à la relecture du manuscrit.

L'étude a été réalisée à partir de 701 vidéos de développement embryonnaire de 584 patients pris en charge en AMP. L'outil d'annotation morphocinétique automatisé a été développé à partir de la détection de l'épaisseur de la zone pellucide et du coefficient

de variation de niveau de gris. La détection des évènements a été comparée à celle obtenues manuellement. Une concordance globale significative, de la fécondation jusqu'au stade de blastocyste, a été trouvée, bien que certaines différences étaient visibles en considérant individuellement certains embryons. Le développement de ces outils ouvrait la voie à une analyse à haut débit des bases de données morphocinétiques multicentriques fournissant de nouvelles informations sur la valeur clinique de ces données en tant que prédicteur de la qualité embryonnaire.

Depuis cette publication en 2020, les différents équipements time-lapse disponibles en embryologie ont évolué et proposent désormais des logiciels de détection des évènements morphocinétiques qui peuvent, à l'aide d'algorithmes et d'outils d'intelligence artificielle aider à la décision du devenir de l'embryon.

c. L'analyse transcriptomique de cellules uniques d'embryons humains = annexe A4

Une des ressources incontournables pour l'étude du développement embryonnaire humain est l'analyse de la base de données de Fredrik Lanner qui a publié en 2016 un jeu de données de séquençage ARN de plus de 1 500 cellules allant du stade 8 cellules jusqu'au stade blastocyste (Petropoulos et al. 2016).

Pour compléter ces éléments, notre objectif a été de réaliser à notre tour une analyse transcriptomique de cellules uniques à différents stades de développement de l'embryon à partir de données de séquençage issues d'embryons suivis par système time-lapse. Ce travail a été une association de compétences de bio-informatique et de culture embryonnaire pré et post-implantatoire. Les premières analyses séquençage de l'ARN en cellule unique (scRNAseq) ont débuté en 2014.

D'autres équipes intéressées par ce sujet ont publié des données d'embryons humains (Yan et al. 2013; Blakeley et al. 2015; Petropoulos et al. 2016) que nous avons pu comparer à nos données. Nos résultats obtenus sur les morulas étaient bien moins hétérogènes que les données de Petropoulos et al. concernant les résultats obtenus sur les blastocystes, ces données obtenues à J5 regroupaient des embryons avant et après la spécification des lignées.

Grâce à notre évaluation morphologique, nous étions sûrs du stade de développement des embryons que nous avons analysés par scRNAseq, notamment pour différencier les morulas des jeunes blastocystes B1-B2 entre J4 et J5. A J5, une grande variété de morphologies embryonnaires peut être observée, de la même façon, notre expertise en embryologie nous a permis de consolider la classification morphologique embryonnaire au stade blastocyste. L'annotation embryonnaire nous a permis d'affiner nos analyses en associant précisément un stade morphologique à un transcriptome, et de réannoter les jeux de données publiés précédemment.

L'objectif du travail de thèse de Dimitri Meistermann était de modéliser la dynamique d'expression du transcriptome embryonnaire entre J3 et J6. Ainsi nous avons publié une représentation transcriptomique et protéique du développement humain entre J3 et J7.

Pour cette publication, je me suis chargée de la gestion de la banque d'embryons humains destinés à la recherche et de sélectionner les stades adaptés à la question posée. J'ai réalisé la décongélation des échantillons et leur mise en culture en système time-lapse, ainsi que d'annoter les événements morphocinétiques des vidéos des embryons. J'ai ensuite réalisé les dépellucidation des embryons et la mise en culture post-implantatoire. J'ai également réalisé des isolations en cellules uniques aux différents stades embryonnaires. Pour finir, j'ai participé à la rédaction du chapitre matériel et méthode concernant les manipulations réalisées et à la relecture du manuscrit.

La publication de Meistermann et al. (Meistermann et al. 2021) présente le travail réalisé par l'équipe concernant l'analyse des transcriptomes pour créer des pseudo-temps et ainsi cartographier les événements moléculaires du développement préimplantatoire. Nous avons combiné des données morphologiques cliniques, bio-informatiques, et protéiques d'embryons humains afin de situer dans le temps et l'espace certains moments clés du développement. Ces données ont ensuite été validées par immunofluorescence. Ceci a notamment permis de caractériser l'émergence des lignées embryonnaires, ainsi que leur maturation péri-implantatoire.

La première étape a consisté en la validation de l'approche intégrée chez la souris, afin de s'assurer de la qualité de notre approche bioinformatique. Ensuite, pour résoudre la problématique de l'évaluation de la morphologie embryonnaire et apporter une évaluation précise du stade de développement des embryons analysés, l'utilisation de la classification et des annotations morphocinétiques utilisées en embryologie clinique a permis d'obtenir une base de données précise. Enfin, la dernière étape du projet consistait en l'application de l'approche de pseudo-temps à ces données.

Ce travail a pu servir de support à une étude plus récentes sur les cellules hiPSC qui a caractérisé 4 principaux types cellulaires avec des caractéristiques propres au sein de cette population (Moya-Jódar et al. 2023). Des cellules semblables à l'épiblaste du blastocyste tardif ont été retrouvées, mais aussi, des cellules semblables au trophoctoderme et au stade 8 cellules.

d. Le modèle blastoïde humain = annexe **A5**

Le blastoïde doit être composé des trois lignées cellulaires qui forment le blastocyste (trophoctoderme, épiblaste et endoderme primitif) qui se différencient selon la séquence spatio-temporelle embryonnaire physiologique. En plus, il est défini par sa similarité morphologique avec le stade B6 du blastocyste humain composé d'une cavité entourée d'une monocouche cellulaire d'un diamètre de 150 à 200µm qui comprend une masse cellulaire interne.

Depuis 2019, nous collaborons avec Nicolas Rivron, intéressé par nos travaux sur les cellules souches trophoblastiques, il prévoyait d'utiliser ces cellules comme analogues du trophoctoderme pour tenter de former des blastoïdes humains comme il l'avait déjà fait chez la souris (Rivron et al. 2018). Récemment, nous avons travaillé ensemble à la validation de son modèle.

Nous avons deux objectifs dans ce travail, montrer que les blastoïdes ressemblent bien aux embryons humains et proposer des hypothèses, issues de nos travaux sur l'embryon, à tester sur le modèle ainsi créé.

Pour cette publication, je me suis chargée de la gestion de la banque d'embryons humains destinés à la recherche et de sélectionner les stades adaptés à la question posée. J'ai réalisé la décongélation des échantillons et leur mise en culture en système time-lapse, et j'ai annoté les événements morphocinétiques des vidéos des embryons. Pour finir, j'ai participé à la relecture du manuscrit.

L'article illustre la comparaison entre les modèles blastoïdes produits à partir de cellules souches et les embryons obtenus en parcours d'AMP. Dans ces blastoïdes, nous avons retrouvé une répartition de cellules de trophoctoderme, d'épiblaste et d'endoderme primitif correspondant à celle des blastocystes humains. A nouveau, notre expertise en culture embryonnaire et en morphocinétique nous a permis de collaborer à ce travail afin de valider les blastoïdes comme structures cellulaires comparables aux blastocystes.

L'analyse transcriptomique et le profil d'expression des marqueurs moléculaires suggèrent que la formation du blastoïde est différente de celle d'un blastocyste qui se forme depuis une morula. Le blastoïde ne semble pas être adapté à l'étude de la première spécification, mais est un bon modèle d'étude du blastocyste à partir du stade B3 jusqu'en post implantation. Le blastoïde ressemble à l'embryon de par sa forme, sa taille et par le nombre de cellules qui le compose. De plus, au cours du développement, il cavite, s'expande, spécifie des lignées cellulaires différentes, et est capable de modéliser l'implantation *in-vitro*.

En France, la dernière révision de la loi de bioéthique autorise expressément la création de blastoïdes humains. Générer des milliers de blastoïdes par semaine est donc désormais possible. Cette avancée permet de trouver une alternative à l'utilisation d'embryons humains pour initier les projets de recherche. L'approfondissement des connaissances dans le domaine du développement du blastocyste et de son implantation pourrait permettre d'améliorer les taux de réussite des tentatives d'AMP mais aussi de comprendre les anomalies comme la pré-éclampsie, ou le placenta prævia. Le modèle de l'embryon humain reste cependant la référence indispensable pour valider les observations réalisées dans des modèles alternatifs.

3) Application des compétences techniques pour développer les connaissances fondamentales = article ⑥

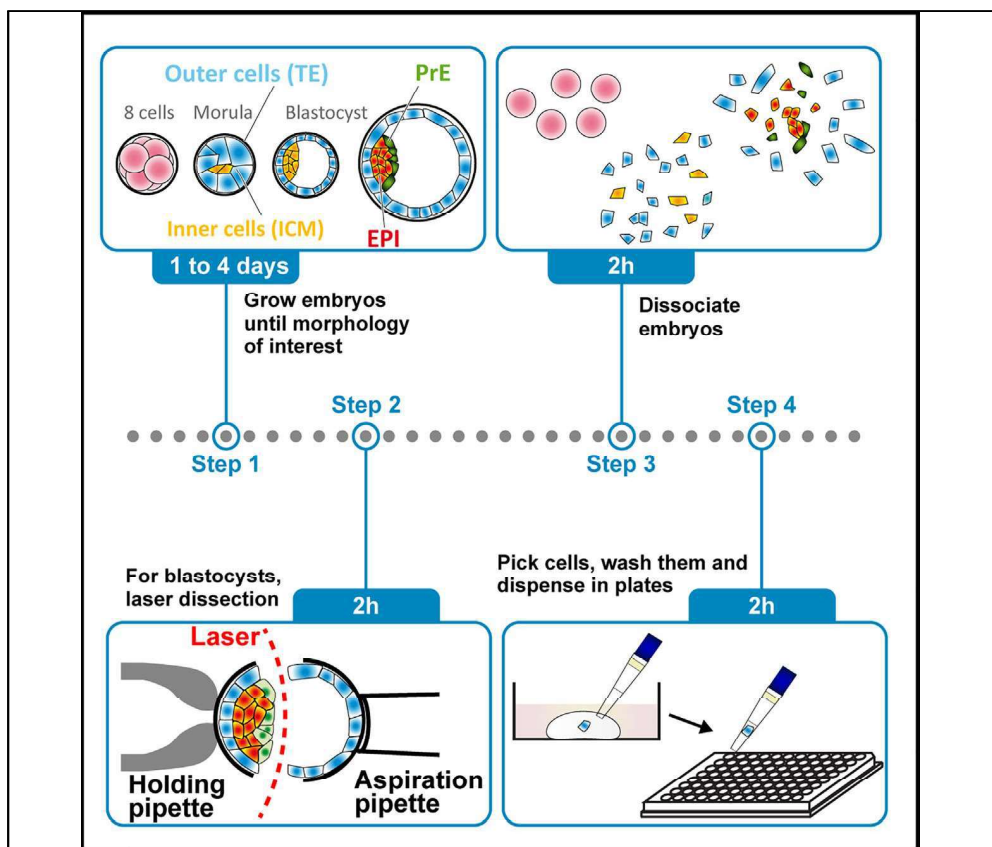
Les travaux, présentés précédemment, portant sur la culture ou l'analyse de cellules embryonnaires uniques ont été possibles grâce à la mise en place de protocoles d'isolation cellulaire.

Récemment, nous avons rédigé une publication récapitulant les techniques de dissociations cellulaires selon le stade embryonnaire que nous avons pu mettre au point à partir des compétences techniques acquises en AMP et ainsi permettre de développer les connaissances fondamentales en biologie du développement.

Pour cette publication je me suis chargée de réaliser une revue de la littérature pour définir les connaissances sur le sujet. J'ai mis au point les techniques de dissection embryonnaire aux différents stades à partir des embryons que j'avais pu intégrer à la banque d'échantillons disponibles pour la recherche. Pour finir, je me suis chargée de la rédaction de la première version de l'article, de la soumission auprès d'une revue à comité de lecture et de répondre aux corrections posées par les relecteurs.

Protocol

Developmental-stage specific single-cell human embryo dissociation



Isolation of individual cells ensures detailed analysis of human embryos and promotes our understanding of molecular mechanisms driving embryo development and cell specification. Here, we present a protocol for the processing of human embryos for single-cell analysis. We describe steps for growing embryos and individualizing cells from the polar and the mural parts of trophectoderm at the blastocyst stage using laser dissection. We then detail embryo dissociation followed by steps to pick, wash, and dispense cells in plates.

Publisher's note: Undertaking any experimental protocol requires adherence to local institutional guidelines for laboratory safety and ethics.

Jenna Lammers,
Sophie Loubersac,
Laurent David,
Thomas Freour,
Arnaud Reignier

arnaud.reignier@
chu-nantes.fr

Highlights
Technique to isolate
embryo cells by
mechanical
dissociation

Technique suitable
from cell stage to
blastocyst

Lammers et al., STAR
Protocols 4, 102363
September 15, 2023 © 2023
The Authors.
[https://doi.org/10.1016/
j.xpro.2023.102363](https://doi.org/10.1016/j.xpro.2023.102363)



Protocol

Developmental-stage specific single-cell human embryo dissociation

Jenna Lammers,^{1,2,3,4} Sophie Loubersac,^{1,2,3} Laurent David,^{1,2} Thomas Freour,^{1,2} and Arnaud Reignier^{1,2,5,*}

¹Université de Nantes, CHU Nantes, Inserm, Centre de Recherche en Transplantation et Immunologie, UMR 1064, ITUN, 44000 Nantes, France

²Service de Médecine et Biologie de la Reproduction, CHU de Nantes, Nantes, France

³These authors contributed equally

⁴Technical contact: jenna.lammers@chu-nantes.fr

⁵Lead contact

*Correspondence: arnaud.reignier@chu-nantes.fr
<https://doi.org/10.1016/j.xpro.2023.102363>

SUMMARY

Isolation of individual cells ensures detailed analysis of human embryos and promotes our understanding of molecular mechanisms driving embryo development and cell specification. Here, we present a protocol for the processing of human embryos for single-cell analysis. We describe steps for growing embryos and individualizing cells from the polar and the mural parts of trophoctoderm at the blastocyst stage using laser dissection. We then detail embryo dissociation followed by steps to pick, wash, and dispense cells in plates.

BEFORE YOU BEGIN

This protocol requires having access to a fully equipped *in vitro* fertilization (IVF) lab, in particular the micromanipulation workstation equipped with a laser. Operators must be specifically and properly trained for micromanipulation on those equipment.¹ Of note, local regulations concerning research on human embryos can vary and should always be followed.

In order to have precise staging of the embryos, culture in a time-lapse incubator is definitely a plus, as it provides dynamic and continuous monitoring of embryo development in an undisturbed environment. Either fresh or frozen-thawed embryos can be used. Freezing/thawing procedures are not presented here but must be performed according to manufacturer's instructions. Embryo culture should be performed according to the European Society of Human Reproduction (ESHRE) Guidelines (1). As our procedures for single-cell isolation is not affected by the protocol and medium used for embryo culture, we will not detail these aspects. Specific detailed procedure for *in vitro* embryo culture is available from the manufacturers. For example, we use Vitrolife® G-TL® medium in our setting (<https://www.vitrolife.com/products/ivf-media-oil/g-tl/>). Embryo morphology assessment should be performed according the Istanbul Alpha – ESHRE consensus workshop on embryo assessment.²

Dissociation of human embryos into single cells depends of their developmental stage (Figure 1A). At 8-cell stage (Figure 1B) and morula stage (Figure 1C), the zona pellucida is laser-opened (step-by-step method details 1), and cells simply dissociated by gently pipetting the morula into Mg-Ca free decompaction medium (G-PGD®) buffer (step-by-step method details 4). At the early blastocyst stage (Figure 1D), the zona pellucida is laser-opened (step-by-step method details 1), and embryo dissociated with the use of Accutase®, a cell detachment solution of proteolytic and collagenolytic



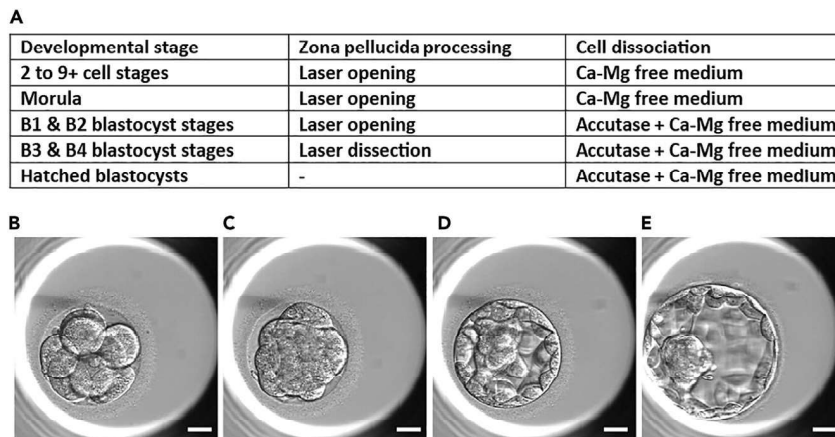


Figure 1. Typical embryonic morphologies (scale bar 30 μm)

(A) Detail of steps necessary for each developmental stage.

(B–E) Typical embryos morphology are shown for a 8-cell stage embryo B (cultured at 68h), a morula C (“MC” cultured 92h), a blastocyst D (“B2” cultured 108h), and an expanded blastocyst E (“B4” cultured 116 h).

enzymes ([step-by-step method details 5 to 7](#)). At the expanded blastocyst stage ([Figure 1E](#)), the embryos are laser-dissected to separate the mural from the polar side ([step-by-step method details 2, 3](#)). Cells are then dissociated with Accutase® ([step-by-step method details 5–7](#)). At the hatched blastocyst stage, the cells are dissociated with Accutase® ([step-by-step method details 5–7](#)).

Mg-Ca free decompaction medium supplementation with HSA

⌚ Timing: 5 min

1. Add 10 μL of HSA in 190 μL of G-PGD® (Mg-Ca free decompaction medium following manufacturer’s instructions).

Biopsy medium warming

⌚ Timing: 1 h

2. Place bottle of mineral oil, G-PGD® and Accutase® at 37°C for 1 h.

Micromanipulation workstation set up

⌚ Timing: 5 min

3. Install properly holding and biopsy pipettes on micromanipulation workstation.

⚠ **CRITICAL:** Make sure the heating stage has reached 37°C.

Micromanipulation dish preparation

⌚ Timing: 5 min on heating stage at 37°C

4. For 1 blastocyst, deposit 2 \times 10 μL droplets of the mix (G-PGD + HSA) in the center of the dish, covered with warmed mineral oil. Add an additional droplet per additional blastocyst.
5. Put 1 blastocyst in 1 droplet with a 290 μm tips.

Single cell isolation dish preparation

⌚ Timing: 5 min at room temperature, when blastocyst dissection is done

6. 1 × 30 μL G-PGD® + HSA droplet.
7. 3 × 30 μL Accutase® droplets.
8. 15 × 10 μL GTL® droplets.
9. All droplets covered with mineral oil.

⚠ **CRITICAL:** Prepare the dish, just before cell isolation, when blastocyst dissection is done; make sure the heating stage is off to work at room temperature.

KEY RESOURCES TABLE

REAGENT or RESOURCE	SOURCE	IDENTIFIER
Biological samples		
Human embryos	N/A	N/A
Chemicals, peptides, and recombinant proteins		
Human serum albumin solution (100 mg/mL)	Vitrolife	10064
G-PGD®	Vitrolife	10074
Accutase®	STEMCELL Technologies	07920
Ovoil®	Vitrolife	10029
G-TL®	Vitrolife	10145
Other		
Inverted microscope	Leica	AM6000
Micromanipulation station	Eppendorf	Cell Tram
Incubator	Panasonic	MCO-5M
Objective 40x with laser	Hamilton Thorne	Zilos-TK laser desktop
Heating stage	Leica	MATS Type I2
Stereo microscope	Leica	M125
ICSI dish	Vitrolife	16006
290 μm tips	Origio - Cooper Surgical	7-72-2290/5
170 μm tips	Origio - Cooper Surgical	7-72-2170/5
135 μm tips	Origio - Cooper Surgical	7-72-2135/5
75 μm tips	Origio - Cooper Surgical	7-72-2075/5
Stripper	Origio - Cooper Surgical	MXL3-STR
100 μL tips	Thermo Scientific	10287524
P100 pipet	BIOHIT Proline	NA
Pasteur pipet	Dominique Dutscher	043262S
Holding micropipet	Origio - Cooper Surgical	MPH-MED-30
Biopsy micropipet	Origio - Cooper Surgical	MBB-FP-SM-30
60 × 15 mm Dish	Starlab	CC7672-3359

STEP-BY-STEP METHOD DETAILS

Zona pellucida removal (for cleaved embryos, morula, early blastocyst stages (B1/B2 according to Gardner's classification))

⌚ Timing: 5–15 min

The goal is to retrieve the embryo from the zona pellucida.

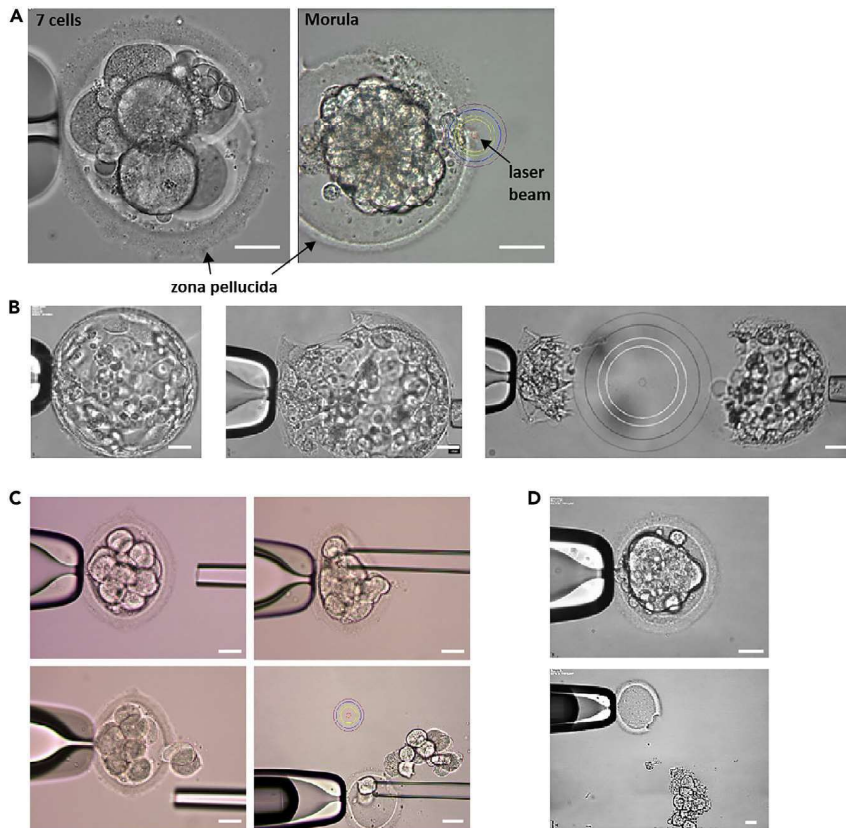


Figure 2. Single-cell picking at each developmental stage (scale bar 30 μm)

(A) Sample images of laser opening of zona pellucida at indicated developmental stages.
 (B) Snapshots showing an expanded blastocyst before, during and after laser dissection.
 (C) Snapshots showing a 10-cell embryo before, during and after biopsy.
 (D) Snapshots showing a morula before and after biopsy.

This step is only performed if processing cleavage stage, morula stage and early blastocyst stage embryos (B1/B2). The operator performs brief laser impulses (around 9) to open the zona pellucida.

1. In the GPGD/HSA droplet hold and immobilize the embryo with the holding micropipet.
2. Use the laser to perform the hole, shoot the zona pellucida as far as possible of cells to open a hole large as $1.5\times$ the biopsy micropipet (with a ZILOS-tk Hamilton-Thorne we use a laser power at 100% for 300 μs). A hole is visible in the zona pellucida (Figure 2A and Methods video S1: Zona pellucida removal for cleaved embryos).

Mural / polar laser dissection

⌚ Timing: 5–15 min

This step is specifically for expanded blastocysts (B3/B4 according to Gardner's classification³). At this stage, dissociating polar vs. mural is critical, either to focus the analysis on the polar side, that contains the 3 main cell types of interest: epiblast (EPI), primitive endoderm (PrE) and trophectoderm (TE), or to capture differential-maturation events between mural and polar TE.

The operator starts by performing brief laser impulses to separate the polar TE and Inner cell mass (ICM) from the mural TE of the blastocyst (Figure 2B and Methods video S2: Mural / polar laser dissection).

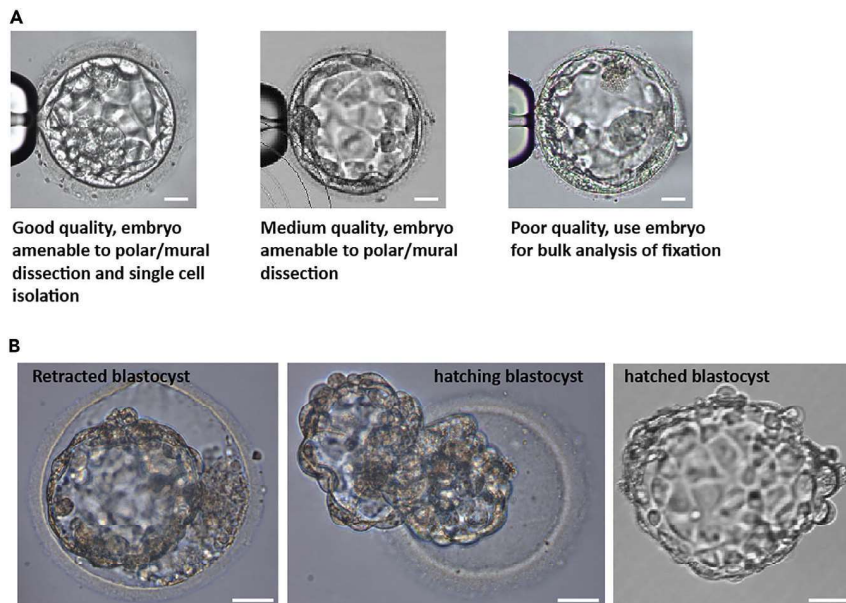


Figure 3. Trouble shooting examples (scale bar 30 μm)

(A) Embryo morphology associated with recommended processing.
(B) Examples of retracted, hatching and hatched blastocysts.

3. In the droplet, with the help of micropipettes, rotate the embryo in order to have the polar side close to the holding micropipet.
 - a. Hold and immobilize the blastocyst to strongly maintain the polar side in front of the holding micropipet.
 - b. Place the biopsy micropipet as close as possible to the mural trophectoderm, at the complete opposite side and apply a gentle suction pressure.
4. Use the laser to perform the dissection.
 - a. Shoot the zona pellucida and the trophectoderm as close as possible to the ICM, in each visible cell junction from one side to the other (up and down on the screen, 3 times, with a ZILOS-tk Hamilton-Thorne we use a laser power at 100% for 700 μs).
 - b. Simultaneously separate the 2 parts progressively by pulling each micropipet apart.
 - c. Use the laser until the 2 parts (mural and polar) are fully separated.

△ CRITICAL: Aspiration / holding setup should be equilibrated. Embryo should be placed at the bottom of the dish to ensure stability and homogeneous laser power.

Single cell dissociation at cleavage stage and morula stage

⌚ Timing: 5–20 min

Once extruded or aspirated through the zona pellucida hole, cells should be gently pipetted in and out with 135 μm tips in G-PGD/HAS solution at 37°C to be individualized (Figure 2C and Methods video S3 Single cell dissociation at morula stage).

5. Perform the cell dissociation:
 - a. Triturate with gentle pipette flush under stereo microscope. G-PGD-HAS solution allows very easy dissociation of the cells.
 - b. Single cell can be isolated by aspiration and flushing.

Note: It is important to respect tips size to avoid breaking cell membrane.

- c. Washing may be necessary depend on the analysis performed. Three washing steps in individual droplets of appropriate medium (often PBS) is recommended.
- d. Replace cell isolated in the adapted container for your analysis.

Single cell dissociation at B1/B2 stage, B3/B4 or B5/B6 hatched blastocysts

⌚ **Timing:** 15–60 min

Embryos or embryo sections were incubated in G-PGD/HSA and transferred in Accutase. Embryos were gently pipetted in and out under stereo microscope. Single-cells/clumps were washed in GTL and gently pipetted in and out again if necessary. Single-cells were picked one by one upon dissociation (Figure 2D).

6. The mural or polar section, or the entire blastocyst, is incubated in the GPGD droplet for 10 min at 37°C with a 170 µm tips.

Note: Repeated aspirations and flush helps homogeneous diffusion of the media.

7. Place the section or the entire blastocyst in the accutase droplet for 3–4 min at room temperature with a 135 µm tips.
 - a. Pipet in and out around thirty to fifty times the cell cluster in the droplet with gentle pipette flush under stereo microscope.
 - b. During pipetting, to avoid, bubbles formation or cell lost, use the three droplets.
 - c. Single cell can be picked as soon as they individualize (Methods video S4 Isolation of single cells after accutase treatment of blastocysts).
8. Place the single cell or the clumps in the first GTL droplet at room temperature with a 75 µm tips.
 - a. Triturate with gentle pipette flush under stereo microscope.
 - b. Single cell can be isolated by aspiration and flushing.
 - c. Washing may be necessary depend on the analysis performed. Three washing steps in individual droplets of appropriate medium (often PBS) is recommended
 - d. Replace cell isolated in the container adapted for your downstream analysis.

⚠ **CRITICAL:** Steps 1 to 6 are performed at 37°C; steps 7 to 8 - with accutase - were performed at room temperature.

EXPECTED OUTCOMES

Upon laser opening of the zona pellucida, single cell / blastomeres dissociation at the cleavage or at the morula stage should be easily feasible. For example, out of 10 morula, we retrieved 85% of the cells for subsequent analysis (Methods video S5: Single cell dissociation at morula stage).

Upon dissection of B3/B4 blastocysts, you should first obtain a polar side and a mural side. Then, single cells can be dissociated. For example, out of 8 blastocysts, we retrieved 9 to 47 cells for subsequent analysis (average 18 cells per blastocyst).

The clumps that cannot be individualized after 30 min are processed as clumps.

LIMITATIONS

Embryo culture setup should be appropriate in order to avoid poor embryo development, both in terms of developmental rate and morphology. When using frozen-thawed embryos for research, the thawing procedure needs to be perfectly tuned, strictly following manufacturer's instructions,

in order to maximize embryo survival rate and subsequent development. Please refer to IVF Guidelines (1) to get guidance towards high-standard human embryology practice.

Operator needs to be experienced with the use of microscope and micromanipulators in order to perform precise, stable and extremely careful manipulation of the embryos and isolated cells. Any suboptimal setup of the workstation, inadvertent movement or brutal manipulation will result in poor single cell recovery rate, or even embryo or cell lysis.

Of note, it is almost impossible to dissociate and collect all cells from each embryo. Part of cells can eventually be lysed during laser assisted-zona opening or lost during washing or enzymatic treatment steps.

TROUBLESHOOTING

Problem 1

Poor quality blastocysts (Figure 3A)

In the case of poor-quality blastocysts (grade C for ICM or trophoctoderm), single cell picking can become particularly difficult and time-consuming.

Potential solution

Operators need to train with human embryos and become experts in embryo morphology classification to be able to identify good, medium and poor quality embryos. The use of Morphological atlas, reference morphological classifications and participation in external quality control program is strongly recommended (2,3).

Problem 2

Retracted/hatched blastocysts (Figure 3B)

If expanded blastocysts are retracted/collapsed, it may become difficult to locate the ICM and therefore to separate accurately polar TE and ICM from mural TE. Similar issues can occur with hatching/hatched blastocysts which have a spontaneous tendency to collapse and retract during micromanipulation and laser shootings. As retracted blastocysts do not expand when zona pellucida is removed, it is important to avoid this situation and prefer (whenever possible) the use of expanded blastocyst when attempting to dissect mural and polar sides.

Potential solution

If the embryo is not or insufficiently expanded, it is advised to postpone experiment and prolong embryo culture for a few hours until proper expansion.

If the blastocyst is hatching (or has already hatched) or does not re-expand, it is however possible to perform laser dissection. After complete removing of the ZP with laser, the suspected polar side of the embryo (where ICM is located) should be aspirated in the biopsy pipette, while the rest of the blastocyst remains floating out of the pipette. The end of the biopsy pipette should then be put into direct contact with the end of the holding pipette and both should then be rubbed against each other, resulting in the mechanical dissection of the polar TE contained in the biopsy pipette on one side and mural TE released in the medium on the other side. This method is referred to as flicking technique and frequently used for trophoctoderm biopsy in PGT-A program.

Problem 3

Cell loss

Single cell handling requires isotonic medium in order to protect cells membrane integrity. This is often possible with the use of media containing HSA. Of note, HSA obviously interferes with single

cell proteomics, requiring multiple washing steps in ultrapure water to remove protein contaminants. However, cell handling in ultrapure water involves tricky and lengthy manipulation time and can result in an increased risk of cell loss.

Potential solution

The addition of Polyvinylpyrrolidone (PVP 7%) to ultrapure water could enable more comfortable manipulation and limit cell loss.

If cells are sticking to each other, it could also be due to poor Accutase quality. We recommend to aliquot Accutase medium and avoid multiple freeze / thaw cycles. Additional washes can also help to isolate cells.

RESOURCE AVAILABILITY

Lead contact

Further information and requests for resources and reagents should be directed to and will be fulfilled by the lead contact, Arnaud Reignier, arnaud.reignier@chu-nantes.fr.

Materials availability

No materials have been specifically designed for this protocol.

Data and code availability

Our original datasets and codes are available in our resource paper in *Cell Stem Cell*.⁴

SUPPLEMENTAL INFORMATION

Supplemental information can be found online at <https://doi.org/10.1016/j.xpro.2023.102363>.

ACKNOWLEDGMENTS

We thank Gedeon Richter, Theramex, Ferring, IBSA-Genévrier, MSD, Merck Serono for funding this work through donations to Nantes Université's Foundation. We thank the staff of the IVF unit of the CHU de Nantes for help and support.

AUTHOR CONTRIBUTIONS

Methodology, validation, investigation, writing, J.L., S.L.; supervision, review, editing, project administration, L.D., T.F.; methodology, validation, investigation, writing, project administration, A.R.

DECLARATION OF INTERESTS

The authors declare no competing interests.

REFERENCES

1. ESHRE Guideline Group on Good Practice in IVF Labs, De los Santos, M.J., Apter, S., Coticchio, G., Debrock, S., Lundin, K., Plancha, C.E., Prados, F., Rienzi, L., Verheyen, G., et al. (2016). Revised guidelines for good practice in IVF laboratories (2015). *Hum. Reprod.* *31*, 685–686.
2. Alpha Scientists in Reproductive Medicine and ESHRE Special Interest Group of Embryology in Reproductive Medicine and ESHRE Special Interest Group of Embryology (2011). The Istanbul consensus workshop on embryo assessment: proceedings of an expert meeting. *Hum. Reprod.* *26*, 1270–1283.
3. Gardner, D.K., and Schoolcraft, W.B. (1999). Culture and transfer of human blastocysts. *Curr. Opin. Obstet. Gynecol.* *11*, 307–311.
4. Meistermann, D., Bruneau, A., Loubersac, S., Reignier, A., Firmin, J., François-Campion, V., Kilens, S., Lelièvre, Y., Lammers, J., Feyeux, M., et al. (2021). Integrated pseudotime analysis of human pre-implantation embryo single-cell transcriptomes reveals the dynamics of lineage specification. *Cell Stem Cell* *28*, 1625–1640.e6.

Pour les stades précoces, nous avons choisi de réaliser la dissociation des cellules embryonnaires humaines comme cela est effectué lors des prélèvements de blastomères dans le cadre de prise en charge en DPI. Pour le stade de blastocyste, pour lequel les cellules du trophoctoderme doivent être isolées d'un côté et les cellules du bouton embryonnaire d'un autre, les méthodes publiées par Capalbo (Capalbo et al. 2013) et Xu (J. Xu et al. 2014) nous ont permis de tester des protocoles de dissection et de mettre au point celui actuellement utilisé dans notre laboratoire.

Les analyses embryonnaires en cellules uniques sont de plus en plus répandues. Pour être interprétés et comparés, les résultats obtenus doivent tenir compte du stade de l'embryon mais aussi de la technique de dissociation, en particulier au stade de blastocyste où les changements morphologiques sont rapides et où la dissociation peut être imprécise. Il est primordial de maîtriser ces techniques pour pouvoir analyser de façon pertinente les cellules issues d'embryons humains.

A partir de ces cellules uniques embryonnaires à différents stades il est possible d'étudier leur devenir par différents types d'analyses. Des analyses métabolomiques par séquençage d'ARN de cellule unique, comme nous avons réalisés dans le travail de l'équipe publié en 2021 (Meistermann et al. 2021) peuvent être menées afin de mieux comprendre les étapes de différenciation des cellules au cours du développement de l'embryon. Des analyses protéomiques de ces cellules uniques par spectrométrie de masse sont également réalisables et permettent d'étudier le contenu protéique au cours du développement embryonnaire.

DISCUSSION

Mes publications présentées dans cette thèse, reflètent en partie l'évolution des connaissances dans les domaines de l'AMP et de la recherche fondamentale en biologie du développement au cours des dernières années, et illustrent les synergies possibles entre embryologie clinique et fondamentale.

Au cours de cette dernière décennie, la technologie de time-lapse appliquée à l'embryologie clinique a permis de faire progresser les prises en charge proposées aux patients en optimisant les conditions de culture et l'évaluation de la qualité embryonnaire grâce aux données morphocinétiques. Au cours de cette période, ce sont aussi les technologies « Omics » qui sont devenues plus performantes et donc mieux adaptées à des projets d'analyse de cellules embryonnaires isolées. Les nouvelles techniques d'analyses bio-informatiques, les protocoles de culture embryonnaire pré et post-implantatoire ainsi que la création de modèles blastoïdes ont donné de nouvelles possibilités aux projets de recherche existant dans le domaine de la biologie du développement humain.

Plus de 10 ans après son apparition sur le marché et dans les laboratoires d'AMP, l'intérêt clinique de la culture embryonnaire en système time-lapse est encore discuté. Récemment, une étude randomisée, multicentrique en double aveugle a été menée pour comparer les résultats obtenus en termes de taux cumulés de grossesses pour trois groupes de prises en charge : culture embryonnaire ininterrompue en système time-lapse avec utilisation des critères morphocinétiques, culture ininterrompue en système time-lapse avec utilisation des critères de morphologie statique et un groupe contrôle avec une culture embryonnaire en incubateur standard et utilisation des critères de morphologie statique (Kieslinger et al. 2023). Ce travail de Kieslinger et al. (2023) mené chez 1731 couples a démontré que les résultats en termes de grossesses évolutives ne sont pas significativement différents entre les trois groupes. Ni les données morphocinétiques, ni les conditions de culture ininterrompues ne semblent

apporter de bénéfices en termes de résultats pour les patients pris en charge. Pour compléter ce travail, la population a été divisée en sous-groupes afin de rechercher un éventuel bénéfice chez une population ciblée. Il semble que pour les patientes de 39 ans et plus, les chances de grossesse seraient augmentées grâce à la culture ininterrompue et aux critères morphocinétiques. Néanmoins cette étude a porté sur un système time-lapse précis qui s'utilise dans des incubateurs classiques, et les transferts embryonnaires étaient réalisés à J3. La généralisation de ces résultats non concluants aux systèmes time-lapse complets et aux transferts au stade blastocyste doit être prudente et confirmée par des études spécifiques.

Actuellement, bien que très répandue, la culture embryonnaire en système time-lapse n'a pas encore démontré sa supériorité clinique face à la culture conventionnelle en incubateur standard en termes de taux d'implantation, même si les études actuelles ne permettent pas d'écarter un bénéfice en termes de taux cumulé ou de délai d'obtention de la grossesse. Néanmoins la stabilité des conditions de culture, la souplesse d'observation et le bénéfice pour la formation en font un outil utile. L'apport de technologies informatiques dans l'aide à l'analyse d'images et de combinaisons de paramètres en feront peut-être un équipement incontournable des laboratoires d'AMP à l'avenir.

Afin de disposer de méthodes robustes d'évaluation de la qualité embryonnaire, l'intelligence artificielle (IA) a récemment fait son apparition dans le domaine de l'embryologie. A l'aide d'un système informatique basé sur le principe du réseau de neurones, développé pour être capable de mimer un raisonnement intellectuel humain, l'intelligence artificielle analyse de grande base de données pour déterminer des tendances, des liens et réaliser des prédictions à partir d'algorithmes. La mise en place de cette technologie nécessite une phase d'entraînement sur base de données puis une phase de test et enfin, une phase de validation sur une nouvelle base de données. L'application en AMP a pour objectif d'augmenter les chances de grossesse et de raccourcir la durée des prises en charge. Les IA sont capables d'étudier objectivement et très rapidement de nombreuses données et de repérer des événements

indétectables à l'œil humain. Ainsi, elles peuvent servir à évaluer la morphologie embryonnaire de façon automatisée comme cela a été démontré par le travail de Chen et al. (Chen et al. 2019). Sur une cohorte de 16 000 embryons, le modèle était fiable dans plus de 75% des cas et faisait ainsi gagner du temps au laboratoire. Les IA peuvent également servir à prédire les chances de grossesse à partir d'images de blastocystes obtenus au microscope (VerMilyea et al. 2020). Certains travaux semblent laisser penser que des facteurs prédictifs peuvent être obtenus à partir des données cliniques des patients avant même de débiter la prise en charge (Hassan et al. 2020). La majorité de ces IA ne permettent pas d'avoir un regard critique sur le résultat rendu étant donné la complexité des algorithmes et l'accès à leur paramétrage souvent limité. Bien que les systèmes d'annotations automatisées proposés par les fournisseurs d'équipements time-lapse apportent des avantages notables en terme de temps d'analyse des images, les paramètres prédictifs des algorithmes d'aide à la décision doivent encore faire leurs preuves.

Comme lors de l'arrivée du time-lapse dans les laboratoires d'AMP, l'apport des IA va nécessiter d'être mieux évalué et mieux compris afin d'envisager une maîtrise de ces outils qui pourront ensuite progressivement modifier les pratiques.

L'identification de biomarqueurs permettant de prédire les chances d'implantation semble réalisable grâce à l'essor des outils « Omics » tels que la génomique, l'épigénomique, la transcriptomique, la protéomique ou la métabolomique. Ces technologies sont des sources précieuses de données pour l'analyse d'embryons humains mais aussi pour étudier la réceptivité endométriale et les interactions embryon-endomètre (Hernández-Vargas, Muñoz, et Domínguez 2020).

L'analyse du contenu génétique de l'embryon est une pratique réalisée en France dans le cadre du diagnostic préimplantatoire (DPI) lorsqu'une anomalie génétique portée par l'un des patients est identifiée, pathologique et incurable. Dans un grand nombre de pays, le diagnostic préimplantatoire d'aneuploïdie (DPI-A) est autorisé et proposé aux patients. En effet, une des causes majeures d'échec d'AMP connue est le haut niveau d'aneuploïdie chromosomique au sein des gamètes et des embryons humains.

La majorité de ces aneuploïdies est causée par des anomalies de la méiose maternelle qui augmente avec l'âge de la femme (Webster et Schuh 2017). A partir de ces observations, la recherche d'aneuploïdie embryonnaire a été développée pour les patients pris en charge en AMP afin de ne transférer que des embryons diagnostiqués comme euploïdes après biopsie embryonnaire et ainsi espérer améliorer les délais nécessaires à l'obtention d'une grossesse. Une étude randomisée publiée en 2019 n'a pas mis en évidence d'avantage à réaliser un DPI-A chez des femmes de moins de 40 ans (Munné et al. 2019). La méta-analyse de Simopoulou et al. en 2021 a révélé que le DPI-A améliore les taux de naissance vivante par transfert lorsque l'analyse est réalisée après biopsie au stade de blastocyste pour des femmes de plus de 35 ans (Simopoulou et al. 2021).

La révision de la loi de bioéthique en 2021 n'a pas autorisé le recours au DPI-A en France, néanmoins un projet hospitalier de recherche clinique national est actuellement en cours pour évaluer son intérêt pour les patients (PHRC DEVIT). En parallèle, des approches non invasives d'évaluation du potentiel implantatoire de l'embryon se développent. Une revue de la littérature récente a mis en évidence que l'analyse des milieux de culture dans lesquels les embryons ont été cultivés individuellement était une source d'ADN permettant l'analyse de leur contenu génétique (Brouillet et al. 2020). L'analyse de cet ADN libre est une approche non invasive qui permet l'obtention de résultats à tous les stades de développement bien que le stade embryonnaire et la durée de culture semblent être des facteurs influençant l'obtention et la fiabilité des résultats. Cette approche non invasive est une alternative séduisante à la biopsie embryonnaire qui nécessite encore des études avant de pouvoir être proposée aux patients pris en charge en DPI.

La protéomique permet l'étude de la fonction biologique par le biais de l'analyse de l'ensemble des protéines d'une cellule, d'un tissu ou d'un organisme. En biologie de la reproduction, cela concerne donc l'analyse des gamètes, des cellules souches, des embryons entiers ou de certaines de leurs cellules mais aussi des milieux de culture dans lesquels ils sont cultivés. Ainsi, il est possible d'étudier le sécrétome

embryonnaire dans le milieu de culture en recherchant une protéine en particulier ou en analysant un large spectre d'intérêt. L'amélioration des techniques, avec notamment la spectrométrie de masse, a permis l'obtention de nombreuses données prometteuses. Grâce à la technique d'analyse des profils protéiques de milieux de culture par puce il a déjà été mis en évidence des différences de profils entre des blastocystes s'étant implantés et d'autres ayant échoués (Domínguez et al. 2008). De la même façon, il a été montré que les profils protéiques des embryons arrêtés sont différents de ceux atteignant le stade de blastocyste et que la morphologie des blastocystes peut être corrélée à ces profils (Lindgren et al. 2018). En analysant des données morphocinétiques obtenues par time-lapse et des résultats de protéomique, Dominguez et al. (Dominguez et al. 2015) ont mis en évidence que la présence de l'interleukine 6 (IL6) couplée à une durée du second cycle cellulaire (cc2) comprise entre 5 et 12h étaient des facteurs pronostics de meilleur taux d'implantation. De cette façon, un modèle décisionnel hiérarchique a pu être établi pour coupler ces 2 données. Malgré les résultats intéressants obtenus, la limitation majeure à la mise en place de ces technologies de protéomique en routine en AMP est liée aux milieux de culture. En effet, les embryons sont cultivés dans de très faibles volumes de milieux complexes aux compositions souvent inconnues ce qui entraîne des difficultés techniques majeures pour l'identification des protéines.

Actuellement, notre équipe travaille à l'analyse différentielle par spectrométrie de masse des milieux de culture usagés de blastocyste et de morula dans le but d'obtenir le sécrétome théorique de ces deux stades et donc des biomarqueurs intéressants. Par la suite, les milieux de culture des patients pris en charge pourront être analysés et comparés selon le résultat de la tentative. En parallèle, l'équipe collabore avec celle de Nikolai Slavov afin d'étudier l'expression protéique des cellules uniques de morula. La comparaison entre le blastocyste et le modèle blastoïde est envisagée pour le futur.

La métabolomique concerne l'étude des métabolites issus du fonctionnement cellulaire. Comme la précédente, cette technologie souffre des mêmes limitations en termes d'efficacité en raison des milieux de culture utilisés en AMP. Le métabolisme

des glucides est l'un des premiers à avoir été corrélé au développement jusqu'au stade de blastocyste, mais n'est néanmoins pas utilisable cliniquement pour la sélection embryonnaire (Uyar et Seli 2014). Le mécanisme du transport des cations Na^+ et K^+ par la pompe à sodium a également été étudié, mais de la même façon, l'application clinique ne semble pas adaptée en raison du coût des technologies utilisées (Hernández-Vargas, Muñoz, et Domínguez 2020). Un profil métabolique corrélé au taux de grossesse a été publié par Seli et al. à partir de milieux de culture embryonnaire (Seli et al. 2007). Une revue de la littérature publiée en 2017 n'a pas mis en évidence une amélioration des résultats pour les patients à partir des données métaboliques étudiées (Bracewell-Milnes et al. 2017). Ces difficultés s'expliquent très probablement par la grande hétérogénéité des milieux de culture utilisés, des conditions de culture appliquées et des techniques d'analyse. Récemment, un travail de revue de la technique de microscopie d'imagerie à durée de vie par fluorescence (FLIM) semble mettre en évidence un intérêt de cette technologie pour l'embryologie, sans pour le moment avoir démontré son innocuité pour les embryons humains (Venturas et al. 2023).

L'épigénomique quant à elle, s'intéresse à l'ensemble des modifications épigénétiques d'une cellule. Plusieurs études se sont concentrées sur le méthylome des gamètes et embryons précoces humains et ont mis en évidence que la principale vague de déméthylation du génome se déroule entre la fécondation et le stade 2 ou 8 cellules. De plus, il a été démontré que le génome paternel est rapidement et globalement déméthylé dans le blastocyste alors que le génome maternel conserve la méthylation sur des régions spécifiques à l'ovocyte pendant le développement préimplantatoire (Guo et al. 2014; Li et al. 2018). Une autre approche est l'analyse des ARN non codants en tant que régulateurs de l'expression des gènes qui semblent être des indicateurs précoces du potentiel développemental embryonnaire (Hernández-Vargas, Muñoz, et Domínguez 2020).

Notre équipe mène actuellement une étude qui a pour objectif d'explorer la contribution de la programmation épigénétique du spermatozoïde à l'expression génique au cours

de l'embryogenèse précoce (Teperek et al. 2016). Le protocole de recherche comporte une caractérisation des marques épigénétiques associées aux histones et de leur stabilité inter-cellule et inter-individuelle. Notre hypothèse est que ces marques épigénétiques conservées régulent l'expression génique dans l'embryon. Nous cherchons également à caractériser l'expression du génome paternel dans des embryons, aux stades morula et blastocyste, issus de spermatozoïdes épigénétiquement caractérisés.

Malgré les résultats encourageants obtenus grâce aux technologies « Omics » au cours des dernières années, des études prospectives de grande ampleur sont encore nécessaires avant d'envisager une application en routine pour les prises en charge des patients en AMP.

Les modèles post-implantatoires permettent d'étudier l'effet des conditions de culture sur le développement embryonnaire sans nécessiter de transfert *in-utero* non applicable au modèle humain.

Afin de mieux comprendre les mécanismes de l'implantation de l'embryon, la culture post-implantatoire est, depuis la révision des lois de bioéthique en 2021, autorisée en France jusqu'au 14^{ème} jour post fécondation. Les premières équipes qui ont réussi à cultiver des embryons in-vitro jusqu'au 13^{ème} jour post fécondation y sont parvenues en 2016 (Shahbazi et al. 2016; Deglincerti et al. 2016). Ils ont ainsi pu observer la maturation du trophoctoderme en cellules trophoblastiques mais aussi constaté que les embryons adhérents ne restaient pas sphériques et s'affaissaient au cours du développement. La culture non adhérente d'embryons a permis par la suite d'observer des structures comme l'épiblaste polarisé et la cavité amniotique, mais aussi de pouvoir observer pour la première fois l'ébauche de la lignée primitive (Xiang et al. 2020).

Avec le développement récent du modèle blastoïde humain, l'étude du développement embryonnaire semble pouvoir se faire aujourd'hui à grande échelle et sans dilemme

éthique. A partir de ces cellules souches pluripotentes naïves humaines (hNPSC) il est possible d'obtenir en quelques semaines des centaines de blastoïdes qui peuvent servir à tester des hypothèses de modifications du génome. Dans le travail de Kagawa et al. nous avons pu montrer que les blastoïdes étaient capables de s'attacher à des organoïdes qui mimaient les cellules endométriales (Kagawa et al. 2022).

Ces 10 dernières années, la recherche sur l'embryon humain autorisée en France pour sa finalité médicale s'est vu bousculée par les technologies de séquençage de plus en plus performantes, la génération de modèles cellulaires mimant les lignées embryonnaire, la culture *in-vitro* d'embryons humains post-implantatoires et l'apport de nouvelles techniques d'analyse bioinformatique. L'étude d'embryons humains reste néanmoins indispensable pour ce qui concerne l'étude des stades précoces du développement embryonnaire humain qui ne peuvent pour le moment pas être mimés par des modèles synthétiques et qui n'est pas toujours le reflet des découvertes faites chez des modèles animaux comme la souris.

L'optimisation des milieux de culture embryonnaire pour améliorer les résultats en AMP tout en évitant l'utilisation excessive d'embryons humains dans les protocoles de recherche semble désormais envisageable mais nécessite encore de nombreux travaux de grande ampleur. Les connaissances concernant le transcriptome et l'outil blastoïde semblent être une matière intéressante à l'élaboration de nouveaux milieux de culture.

CONCLUSION

Au fil de ces années de travail au sein d'une équipe composée de nombreux chercheurs aux profils très divers, les projets s'enrichissent des connaissances et compétences de chacun et les perspectives s'étoffent.

La maîtrise des techniques utilisées en assistance médicale à la procréation est un réel atout pour mener des projets de recherche de grande ampleur sur l'embryon humain. L'expertise des embryologistes, habitués à cultiver et à observer les embryons dans les laboratoires de FIV, associée à celle des chercheurs en biologie cellulaire, moléculaire, bio-informatique ... maîtrisant les technologies de pointe dans leurs domaines permettra certainement de créer une combinaison de marqueurs qui aideront à mieux comprendre le développement embryonnaire mais aussi à améliorer les prises en charge des patients en désir d'enfant.

ANNEXES

A1 : L'observation en continu du développement embryonnaire en FIV (time lapse) à l'aide de l'Embryoscope. T. Freour, J. Lammers, C. Springart, M. Jean, P. Barrière. Ref Gynecol Obstet. 2012

A2 : Parallel derivation of isogenic primed and naïve induced pluripotent stem cells. S. Kilens, D. Meistermann, D. Moreno, C. Chariou, A. Gaignerie, A. Reignier, Y. Lelièvre, M. Casanova, C. Vallot, S. Nedellec, L. Flippe, J. Firmin, J. Song, E. Charpentier, J. Lammers, A. Donnart, N. Marec, W. Deb, A. Bihouée, C. Le Caignec, C. Pecqueur, R. Redon, P. Barrière, J. Bourdon, V. Pasque, M. Soumillon, T. Mikkelsen, C. Rougeulle, T. Fréour, L. David. Nature Communication. 2018

A3 : Development of automated annotation software for human embryo morphokinetics. M. Feyeux, A. Reignier, M. Mocaer, J. Lammers, D. Meistermann, P. Barrière, P. Paul-Gilloteaux, L. David, T. Fréour. Human Reproduction. 2020

A4 : Integrated pseudotime analysis of human pre-implantation embryo single-cell transcriptomes reveals the dynamics of lineage specification. Meistermann D, Bruneau A, Loubersac S, Reignier A, Firmin J, François-Campion V, Kilens S, Lelièvre Y, Lammers J, Feyeux M, Hulin P, Nedellec S, Bretin B, Castel G, Allègre N, Covin S, Bihouée A, Soumillon M, Mikkelsen T, Barrière P, Chazaud C, Chappell J, Pasque V, Bourdon J, Fréour T, David L. Cell Stem Cell. 2021

A5 : Human blastoids model blastocyst development and implantation. H. Kagawa, A. Javali, H. Heidari Khoei, TM. Sommer, G. Sestini, M. Novatchkova, Y. Scholte op Reimer, G. Castel, A. Bruneau, N. Maenhoudt, J. Lammers, S. Loubersac, T. Freour, H. Vankelecom, L. David, N. Rivron. Nature. 2022

ARTICLE ORIGINAL/ORIGINAL ARTICLE

L'observation en continu du développement embryonnaire en FIV (time lapse) à l'aide de l'Embryoscope® : un an d'expérience au CHU de Nantes

T. Freour, J. Lammers, C. Spingart, M. Jean, P. Barrière

Service de Médecine et Biologie de la Reproduction, Hôpital Mère et Enfant, CHU de Nantes, 38 boulevard Jean-Monnet, 44093 Nantes cedex 1

RÉSUMÉ : Parmi les pistes explorées en vue d'augmenter les chances de succès en fécondation *in vitro*, l'optimisation des conditions de culture embryonnaire ainsi que l'amélioration des méthodes d'évaluation de la qualité embryonnaire sont prioritaires. L'immense majorité des équipes utilisent les incubateurs conventionnels d'une part et l'évaluation morphologique de la qualité embryonnaire d'autre part, mais cette stratégie présente des limites certaines. Le développe-

ment récent de systèmes associant conditions de culture optimales et observation en continu du développement embryonnaire permet d'envisager une amélioration globale des aspects embryologiques de la FIV. Parmi les systèmes disponibles, l'Embryoscope est le plus abouti et performant pour une utilisation en pratique quotidienne. Le CHU de Nantes a été le premier centre français équipé de ce système en 2011. Dans notre expérience, le temps nécessaire à la

maîtrise de l'outil reste relativement court, et les avantages sont nombreux en terme de flexibilité, d'évaluation de la qualité embryonnaire, d'observation d'événements anormaux, et de formation continue, aboutissant à une amélioration globale des taux de succès.

Mots-clés : Embryoscope – Fécondation *in vitro* – Culture embryonnaire

Time lapse as a routine technique in the IVF laboratory: a French experience with the Embryoscope®

ABSTRACT: Among all the strategies available in order to improve success rates in IVF cycles, a lot of work has been done on embryo culture conditions and embryo quality evaluation. Most IVF centres use conventional incubators and select embryo according to punctual morphological evaluation, but this strategy has several limitations. Recently developed commercial devices associating more stable culture conditions and time lapse

observation of embryo development provide new insights into early embryo development in IVF cycles. Among them, the Embryoscope appears to be the most user-friendly, performing and suited for routine daily practice. The first Embryoscope for France was installed in the University Hospital of Nantes in 2011. In our experience, it takes relatively short time to get used to this system. Moreover, its integration in routine process yielded se-

veral advantages, such as better embryo selection according to kinetic parameters and observation of abnormal cleavage events, continuing education and training, quality control and flexibility. This led to an overall increase in success rates in IVF cycles.

Keywords: Embryoscope – *In Vitro* Fertilization – Embryo culture – Time lapse

Introduction

Depuis la naissance du premier « bébé éprouvette » en 1978, on estime aujourd'hui à près de 5 % le nombre d'enfants nés de cette technique dans le monde. En effet, près de 15 % des couples en âge de procréer sont ou seront un jour confrontés à des difficultés à concevoir. Depuis ses débuts, l'AMP a bien sûr largement évolué, avec une augmentation sensible des chances de succès, afin de répondre au mieux aux attentes des couples sollicitant la médecine pour obtenir la grossesse tant désirée. Plusieurs techniques peuvent être

proposées aux couples infertiles ; l'insémination intra-utérine (IIU), la fécondation *in vitro* (FIV) ou encore la fécondation *in vitro* avec micro-injection (ICSI). Néanmoins, depuis la révolution de l'ICSI dans les années 90, les résultats ont relativement peu augmenté, et peu d'innovations majeures ont vu le jour sur le versant biologique. On constate notamment que le développement embryonnaire préimplantatoire *in vitro* reste largement méconnu, en partie en lien avec d'évidentes limites éthiques et réglementaires, aboutissant le plus souvent à un choix de l'embryon à transférer basé sur des critères morphologiques ponctuels

malheureusement imparfaits. Ainsi, afin d'améliorer significativement les chances de succès en FIV, avec d'une part une augmentation des taux d'implantation et d'autre part une diminution des taux de grossesse multiple, il apparaît fondamental pour les équipes de biologie de la reproduction d'apporter les meilleures conditions de culture possibles à l'embryon, tout en développant de nouvelles méthodes d'évaluation de la qualité embryonnaire. Parmi les stratégies envisageables actuellement, l'observation en continu du développement embryonnaire en FIV à l'aide de l'Embryoscope® est considérée comme

prometteuse. Nous proposons ici de rappeler le principe de cette technique, de discuter rapidement ses principaux avantages et limites, avant de présenter notre expérience après un an d'utilisation de ce système en pratique quotidienne.

I – L'évaluation morphologique de la qualité embryonnaire

L'immense majorité des équipes basent au quotidien leur choix de l'embryon à transférer sur les critères morphologiques observés ponctuellement. Cette procédure facile à mettre en place et peu coûteuse a été largement validée dans la littérature internationale (Baczkowski *et al.*, 2004), et des recommandations et consensus existent afin de tenter de standardiser les pratiques (Alpha and Eshre, 2011). En pratique, les principales étapes de cette évaluation morphologique sont les suivantes : morphologie du complexe cumulo-ovocytaire, de l'ovocyte décoronisé et du globule polaire le jour de la ponction, observation des 2 globules polaires et des pronucléi environ 18 heures après l'injection, observation d'un éventuel premier clivage au bout 25 heures, puis observation quotidienne du nombre, de la régularité des blastomères, avec détection d'éventuels fragments cytoplasmiques. La valeur prédictive de la morphologie embryonnaire pour les chances d'implantation a été largement validée depuis de nombreuses années, même si elle reste modérée. Néanmoins, cette évaluation morphologique présente un certain nombre de limites. Cette évaluation morphologique est opérateur-dépendante et peut manquer de reproductibilité (Arce *et al.*, 2006). Même si l'expérience permet de limiter dans une certaine mesure cette subjectivité, il est difficile de mettre en place des systèmes efficaces de formation continue et de contrôle qualité (Patnot *et al.*, 2011). De plus, l'observation morphologique impose de sortir les embryons des incubateurs pendant au moins une dizaine de secondes, voire beaucoup plus dans certains cas. Ceci entraîne leur exposition à la lumière, et à des variations de température et d'atmosphère importantes et non contrôlées. En outre, chaque ouverture de la porte d'un incubateur afin

d'observer une boîte de culture perturbe également les conditions de température des autres embryons qui resteront à l'intérieur de l'incubateur, pendant de longues minutes jusqu'au retour à des conditions de température et de gaz stables et optimales. Enfin, le développement embryonnaire préimplantatoire étant bien sûr un processus complexe et dynamique, l'observation ponctuelle quotidienne des embryons ne donne qu'un aperçu très fugace des nombreux événements pouvant se produire, qu'ils soient de bon ou de mauvais pronostic pour les chances d'implantation. Par ailleurs, il est désormais admis que la morphologie embryonnaire n'est pas un bon facteur prédictif de blastulation (Guérif *et al.*, 2010). Au final, l'évaluation de la qualité embryonnaire selon les critères morphologiques habituels reste intéressante en pratique quotidienne mais cette stratégie présente une performance limitée.

II – Le time lapse, l'Embryoscope®

Depuis la première publication en 1997 de travaux sur le suivi en continu du développement embryonnaire précoce *in vitro* chez l'homme (Payne *et al.*, 1997), plusieurs équipes ont cherché à développer des systèmes permettant d'observer les embryons tout au long de leur développement *in vitro*. Après des premiers essais « artisanaux » mais néanmoins prometteurs (Kirkegaard *et al.*, 2012), quelques systèmes commerciaux ont récemment vu le jour, avec pour but d'allier stabilité des conditions de culture et observation en continu. L'objectif est double : observer le développement embryonnaire en continu (Fig. 1), au-delà des intervalles habituels d'évaluation morphologique, et garantir une meilleure stabilité des conditions de culture puisqu'il n'est plus nécessaire de

sortir la boîte de culture de l'incubateur. Une fois atteint, ce double objectif devrait logiquement permettre d'améliorer les chances de succès pour les patients. Parmi les systèmes actuellement sur le marché et autorisés pour l'usage en FIV chez l'homme, l'Embryoscope®, commercialisé par la société danoise Unisense Fertilitech®, présente un certain nombre de spécificités en faisant sans aucun doute le produit le plus abouti disponible à ce jour (Fig. 2). Cet appareil est schématiquement constitué d'un incubateur au sein duquel est directement intégré un système optique haute définition relié à une station informatique. En pratique, les ovocytes/embryons sont déposés dans des micropuits individuels au sein d'une boîte de culture spécifique. Le faible volume de la chambre d'incubation ainsi que le débit réglable des gaz permet tout d'abord un retour à des conditions de culture optimales en un temps extrêmement court (moins de 3 minutes, à comparer aux 15 à 30 minutes nécessaires dans les gros incubateurs conventionnels). Le grand nombre de points de mesure de la température et de l'atmosphère permet de plus un suivi en continu des conditions de culture et une adaptation permanente en cas de dérive. Le bras motorisé sur lequel sont déposées les boîtes de culture amène celles-ci sur le système optique à intervalle régulier (généralement toutes les 15 minutes). Chaque embryon est alors photographié individuellement selon 7 à 9 plans focaux (Fig. 3) afin de permettre une évaluation de l'embryon sur l'ensemble de son volume, comme en microscopie optique. Tout ceci est réalisé sans intervention extérieure ni modification des conditions de culture. Ces données sont ensuite transmises au système informatique qui les sauvegarde et crée des vidéos alimentées en temps réel par les nouvelles images. L'avantage théorique de l'utilisation de

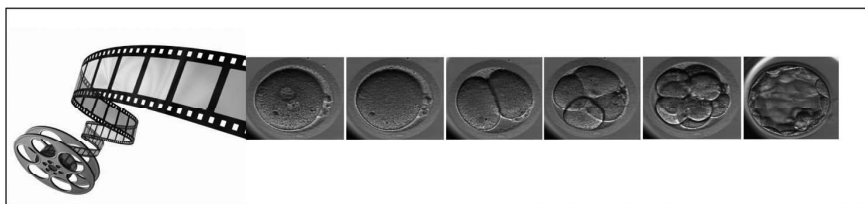


Fig. 1. Représentation schématique du suivi en continu du développement embryonnaire *in vitro*

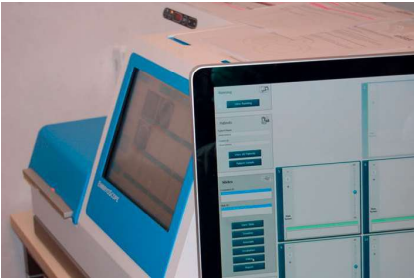
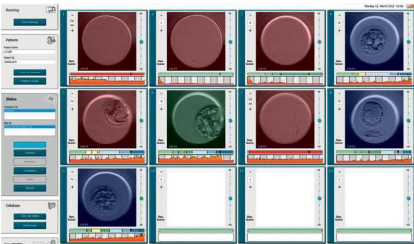


Fig. 2. Un aperçu de l'Embryoscope® en situation au laboratoire

Fig. 3. Capture d'écran du tableau de suivi d'un cycle (5^e jour de développement embryonnaire). Neuf ovocytes ont été cultivés pour ce couple. Les puits en rouge correspondent à des embryons non retenus (échec de fécondation, développement anormal, critères morphologiques défavorables...), celui en vert correspond à l'embryon transféré, et ceux en bleus aux embryons vitrifiés

cet appareil est double. Tout d'abord, il permet de travailler sans sortir les boîtes contenant les embryons (excepté pour le transfert, la congélation ou le changement de milieu séquentiel), limitant ainsi leur exposition à des conditions de culture non optimales, mais aussi aux risques de contamination ou d'accident. Le faible volume de la chambre d'incubation garantit de plus un retour très rapide aux conditions de culture optimales lors d'une ouverture de la porte. Ceci aboutit donc à l'amélioration des conditions de culture embryonnaire. D'autre part, le monitoring en continu du développement embryonnaire permet de détecter des événements anormaux se produisant en dehors des périodes habituelles d'observation, et permet également la mesure précise des temps de clivage, pour lesquels des valeurs de référence commencent à être publiées (Meseguer *et al.*, 2011). Ceci permet donc une meilleure évaluation de la qualité embryonnaire. Plusieurs publications récentes réalisées par des équipes utilisant l'Embryoscope® semblent confirmer les espoirs placés dans cette technologie (Meseguer *et al.*, 2011 ; Cruz *et al.*, 2012 ; Kirkegaard *et al.*, 2012).

III – L'expérience du CHU de Nantes

En Février 2011, le centre AMP du CHU de Nantes a été le premier centre français équipé d'un Embryoscope® et reste à ce jour le seul centre français équipé de ce système, alors même que plus de 120 sont installés à travers la grande majorité des pays européens. Après une courte période d'apprentissage de la préparation et de la manipulation des boîtes de culture et du système informatique (sans difficulté particulière), nous avons validé cette technique en réalisant un certain nombre de cycles partagés entre système d'incubation standard et Embryoscope®. Le développement embryonnaire étant strictement comparable dans les 2 groupes selon nos critères habituels (morphologie à J3, à J5, clivage précoce, etc.), il a été rapidement décidé de passer à une utilisation complète en pratique quotidienne. Afin d'éviter de favoriser (ou pénaliser) les couples bénéficiant de cette technique, il a été décidé par l'ensemble de l'équipe de ne pas sélectionner une population en particulier, mais au contraire d'intégrer dans l'Embryoscope® des cycles « tout venant ». En pratique, dès lors qu'une place est libre dans l'incubateur, le cycle suivant en bénéficie, quelles que soient les caractéristiques du cycle (age, nombre d'ovocytes, rang de tentative, etc.). Fin 2011, 300 cycles de fécondation *in vitro* avec ou sans micro injection ont été réalisés avec l'Embryoscope®, et l'appareil fait partie intégrante de l'activité du laboratoire. Au

cours de notre première année d'expérience, la mise en place de ce système a entraîné quelques modifications et remises en question dans notre organisation. Nous avons pu en effet observer en détail et de façon dynamique les événements successifs du développement embryonnaire précoce (fécondation, clivages, compaction, cavitation), et progressivement apprendre à évaluer leur impact ou leur importance pour la suite du développement, en particulier grâce aux études récemment publiées par d'autres utilisateurs (Meseguer *et al.*, 2011), même s'il est difficile d'utiliser au quotidien des valeurs de référence définies par d'autres équipes sur des populations et avec des procédures différentes. Nous avons par exemple rapidement remis en cause l'intérêt du score des pronuclei, puisque celui-ci évolue avec le temps. Nous avons assez régulièrement observé la présence fugace d'un troisième pronucleus, qui n'aurait pas été vu lors de l'évaluation morphologique à l'heure habituelle. Plus fréquemment, un clivage direct d'un blastomère en 3 cellules filles peut être mis en évidence, ce qui nous conduit le plus souvent à écarter ces embryons, même si la morphologie à J3 reste correcte (Fig. 4). De même, il est beaucoup plus aisé d'observer la multinucléation d'un ou plusieurs blastomères au stade 2 ou 4 cellules, avec la aussi un pronostic implantaire très défavorable. Concernant le clivage précoce, nous avons régulièrement observé que le seuil habituellement utilisé (25 h) est discutable et peut être élargi jusqu'à 28 h, et que certains embryons se

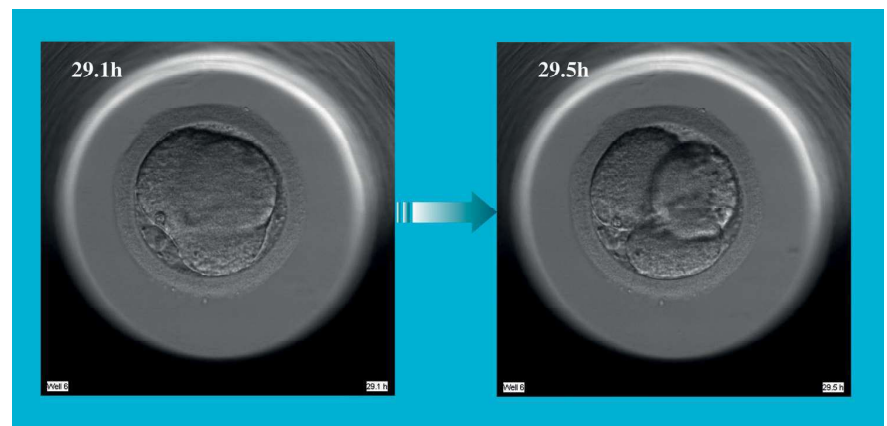


Fig. 4. Exemple de clivage direct anormal d'un zygote en 3 blastomères, sans passage par un stade à 2 cellules

clivent de façon trop précoce (avant 22 h). Nous avons confirmé que les fragments cytoplasmiques pouvaient apparaître mais aussi être réabsorbés.

Avantages

Nous avons rapidement pu intégrer les nouveaux critères cinétiques à notre stratégie de choix de l'embryon à transférer. En particulier, l'observation d'événements anormaux (clivage anormal, multinucléation) nous amène régulièrement à écarter des embryons présentant pourtant une morphologique correcte à J3. Il est parfois plus délicat d'intégrer les critères cinétiques dans la réflexion, mais les 2 principaux paramètres rapportés dans la littérature (fin du stade 2 cellules et fin du stade 4 cellules) sont relativement faciles à prendre en compte. Au final, cela s'est traduit par une tendance claire vers une augmentation des taux de grossesse évolutive par cycle et par transfert, même si l'absence de randomisation rend difficile l'exploitation de ces résultats. De plus, l'Embryoscope® est un excellent outil de formation continue et d'enseignement, facilitant l'homogénéisation des pratiques et l'intégration de nouveaux personnels dans le laboratoire. Les discussions en staff pluridisciplinaires sont également facilitées. Enfin, l'Embryoscope® sera certainement un atout en prévision des obligations à venir en terme d'assurance qualité. En effet, la traçabilité intégrale des conditions de culture (Fig. 5) et l'enregistrement complet du développement de chaque embryon en font un outil très performant pour la mise en place et le suivi de la politique qualité au laboratoire de FIV.

Limites

La principale limite actuelle de l'EmbryoScope® est liée à sa capacité relativement réduite. En effet, un appareil permet de suivre simultanément les cohortes de 6 patientes différentes, avec un maximum de 12 ovocytes par patiente. Un incubateur permet donc d'envisager environ 300 cycles par an. Il existe évidemment une période d'adaptation pour l'ensemble de l'équipe lors du début de l'utilisation de ce système. L'apprentissage technique est très court, et la manipulation sans difficulté.

Par contre, il peut être difficile au départ de gérer l'avalanche de données disponibles pour chaque embryon, de se repérer tout au long du développement embryonnaire alors que chacun est habitué à considérer un ou deux points quotidiens, et le biologiste peut facilement se sentir submergé ou perdu lors du choix de l'embryon à transférer. Cependant, les repères se prennent relativement rapidement, et l'outil informatique est adapté pour une progression rapide. La maîtrise s'acquiert en quelques semaines, mais il est important de savoir que l'utilisation ne sera optimale qu'au prix d'un investissement important de la part de l'ensemble de l'équipe. Enfin, l'aspect économique a bien évidemment son importance, mais l'investissement initial élevé doit être mis en balance avec l'amélioration espérée des taux de succès, la baisse de la consommation en gaz médicaux et en milieu de culture. De plus, le gain en flexibilité dans l'organisation de l'activité quotidienne ne se traduit pas directement en coûts économisés, mais permet dans une certaine mesure d'optimiser le temps des biologistes/techniciens, qu'ils pourront alors utiliser pour d'autres tâches habituellement délaissées et pouvant être valorisées, telle que la gestion des embryons congelés.

Conclusion

De nombreux progrès restent à faire pour améliorer les conditions de culture em-

bryonnaire et les critères de choix des embryons à transférer. Parmi les stratégies apparues récemment, le suivi en continu du développement embryonnaire précoce (time lapse) semble très prometteur. Dans ce cadre, l'Embryoscope® est à ce jour la solution technique la plus aboutie et la plus facile à mettre en œuvre. Seules des études prospectives randomisées pourront permettre de mesurer le bénéfice réel de ce système sur les chances de succès en FIV. Ces études sont en cours et devraient rapidement fournir les réponses attendues par beaucoup. Localement, l'ensemble de l'équipe est très satisfait de la mise en place de ce système, malgré le temps initial de formation, à la fois pour l'amélioration des taux de succès, mais aussi pour l'amélioration des connaissances et la remise en cause des repères habituels dont chacun avait conscience des limites. Cet outil nous semble être un très bon investissement, pour les patientes, mais aussi pour l'équipe biologique qui bénéficie d'une aide à la prise de décision. Enfin, les systèmes de « time lapse » ouvrent la voie à de très nombreux sujets de recherche appliquée non invasive dans le domaine de l'embryologie humaine.

Références

Arce JC, Ziebe S, Lundin K, Janssens R, Helmggaard L, Sørensen P (2006) Interobserver agreement and intraobserver reproducibility of embryo quality assessments. Hum Reprod 21: 2141-8

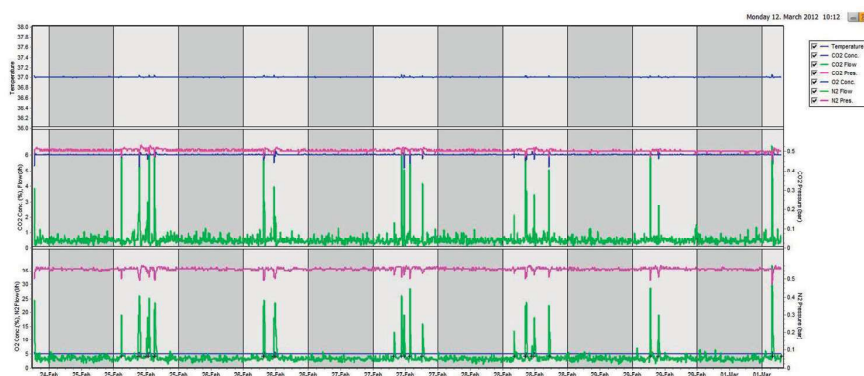


Fig. 5. Capture d'écran du tableau de suivi des conditions de culture. En abscisse apparaissent les dates, en ordonnée les différentes échelles correspondant au paramètre mesuré (température sur le graphique du haut, concentration et flux en CO2 sur le graphique du milieu, concentration en O2 et flux en N2 sur le graphique du bas). Chaque ouverture de la porte de la chambre d'incubation est symbolisée par une croix juste au-dessus de l'axe des abscisses. À noter que la température ne varie jamais au-delà de $37 \pm 0,05$ °C sur toute la période considérée

- ALPHA Scientists In Reproductive Medicine; ES-HRE Special Interest Group Embryology (2011) Istanbul consensus workshop on embryo assessment: proceedings of an expert meeting. *Reprod Biomed Online* 22: 632-46
- Baczowski T, Kurzawa R, Glabowski W (2004) Methods of embryo scoring in *in vitro* fertilization. *Reprod Biol* 4: 5-22
- Cruz M, Gadea B, Garrido N, Pedersen KS, Martínez M, Pérez-Cano I, Muñoz M, Meseguer M (2011) Embryo quality, blastocyst and ongoing pregnancy rates in oocyte donation patients whose embryos were monitored by time-lapse imaging. *J Assist Reprod Genet* 28: 569-73
- Guerif F, Lemseffer M, Leger J, Bidault R, Cadoret V, Chavez C, Gasnier O, Sausseureau MH, Royere D (2010) Does early morphology provide additional selection power to blastocyst selection for transfer? *Reprod Biomed Online* 21: 510-9
- Kirkegaard K, Agerholm IE, Ingerslev HJ (2012) Time-lapse monitoring as a tool for clinical embryo assessment. *Hum Reprod* 27 (5): 1277-85
- Meseguer M, Herrero J, Tejera A, Hilligsøe KM, Ramsing NB, Remohí J (2011) The use of morphokinetics as a predictor of embryo implantation. *Hum Reprod* 26: 2658-71
- Paternot G, Wetzels AM, Thonon F, Vansteenbrugge A, Willemen D, Devroe J, Debrock S, D'Hooghe TM, Spiessens C (2011) Intra- and interobserver analysis in the morphological assessment of early stage embryos during an IVF procedure: a multicentre study. *Reprod Biol Endocrinol* 15: 127
- Payne D, Flaherty SP, Barry MF, Matthews CD (1997) Preliminary observations on polar body extrusion and pronuclear formation in human oocytes using time-lapse video cinematography. *Hum Reprod* 12: 532-41

ARTICLE

DOI: 10.1038/s41467-017-02107-w

OPEN

Parallel derivation of isogenic human primed and naive induced pluripotent stem cells

Stéphanie Kilens et al.[#]

Induced pluripotent stem cells (iPSCs) have considerably impacted human developmental biology and regenerative medicine, notably because they circumvent the use of cells of embryonic origin and offer the potential to generate patient-specific pluripotent stem cells. However, conventional reprogramming protocols produce developmentally advanced, or primed, human iPSCs (hiPSCs), restricting their use to post-implantation human development modeling. Hence, there is a need for hiPSCs resembling preimplantation naive epiblast. Here, we develop a method to generate naive hiPSCs directly from somatic cells, using OKMS overexpression and specific culture conditions, further enabling parallel generation of their isogenic primed counterparts. We benchmark naive hiPSCs against human preimplantation epiblast and reveal remarkable concordance in their transcriptome, dependency on mitochondrial respiration and X-chromosome status. Collectively, our results are essential for the understanding of pluripotency regulation throughout preimplantation development and generate new opportunities for disease modeling and regenerative medicine.

Correspondence and requests for materials should be addressed to L.D. (email: Laurent.david@univ-nantes.fr).
[#]A full list of authors and their affiliations appears at the end of the paper

Pluripotent stem cells (PSCs) possess the unique ability to self-renew and differentiate into all cell types of a fully functional adult, making them invaluable tools to study human development, model diseases and design new regenerative medicine approaches. In mammals, pluripotency exists in at least two states: naive pluripotency that represents the ground state of pluripotency found in the preimplantation epiblast and primed pluripotency that corresponds to cells poised for differentiation found in the post-implantation epiblast^{1,2}. To date, the majority of human embryonic stem cell (hESC) lines have been derived and maintained in the primed state, and identifying culture conditions supporting human naive pluripotency has been a major goal for the past decade. Since 2013, several studies have yielded multiple, distinct conditions to induce and maintain naive pluripotency³⁻⁹. In parallel, significant progresses have been made to characterize the molecular signature of human pre-implantation epiblast cells¹⁰⁻¹⁵, establishing guidelines to assess human naive pluripotency¹⁶. Collectively, those studies showed that two media supported naive pluripotent stem cells converted from primed cells or derived directly from human embryos, demonstrating hallmarks of human epiblast cells: 5i/L/AF^{8,17,18} and T2iLGö^{7,15,19,20}. However, it remains unknown whether naive pluripotency can be induced from somatic cells directly without a primed intermediate, and if so, with sole expression of OKMS (Oct4, Klf4, cMyc and Sox2), like in mouse²¹⁻²³.

Here we present a protocol enabling the parallel derivation of isogenic human induced primed (hiPSCs) and naive (hiNPSCs) pluripotent stem cells. hiNPSCs are reprogrammed using T2iLGö^{7,19} or RSeT. hiNPSCs are benchmarked against the human preimplantation epiblast, the gold standard of human naive pluripotency, at the transcriptomic, metabolic and epigenetic levels. Overall, hiNPSCs derived in T2iLGö medium display remarkable similarities to preimplantation epiblast. Thus, direct somatic cell reprogramming to human naive pluripotency complements the array of assays enabling in-depth analysis of human pluripotency.

Results

Reprogramming somatic cells into naive hiPSCs. We aimed to develop a direct reprogramming method to simultaneously generate isogenic naive and primed human PSCs. We overexpressed *OCT4*, *KLF4*, *MYC* and *SOX2* in human fibroblasts from 5 healthy donors, using a non-integrative Sendai virus. At day 7, cells were split to 3 tissue culture dishes, enabling to induce multiple pluripotent states directly from the same parental cells. At day 9, we cultured emerging colonies in primed pluripotency medium (KSR+FGF2) and in media supporting human naive pluripotency (RSeT and T2iLGö) (Fig. 1a). Both media contain 2i, inhibitors of MEK and GSK3 β which are essential for mouse PSCs maintenance²⁴, and LIF. Besides 2i and LIF, T2iLGö medium contains a PKC inhibitor^{7,19,25}, while the RSeT is a medium derived from the NHSM⁵, composed of inhibitors of JNK and p38, FGF2 and TGF β 1, which supports interspecies chimeras. RSeT medium was chosen due to accessibility and apparent low genomic abnormality rate, and T2iLGö because it was reported to yield cells with more stable genome over 5i/L/AF^{7,8,17}. In order to broaden our analysis, we switched some KSR+FGF2 hiPSC lines to mTeSR1 feeder-free medium. In total, we generated 25 cell lines (Fig. 1b and Supplementary Table 1), of which cells grown in RSeT or T2iLGö formed dome-shaped colonies resembling mouse embryonic stem cells (mESCs). We controlled Sendai expression and confirmed transgene independence of hiNPSCs, but at higher passages than in hiPSCs (Supplementary Fig. 1 and Supplementary Table 1). hiPSCs and hiNPSCs display karyotype identical to the parental fibroblasts; however, hiNPSCs tend to acquire chromosomal abnormalities,

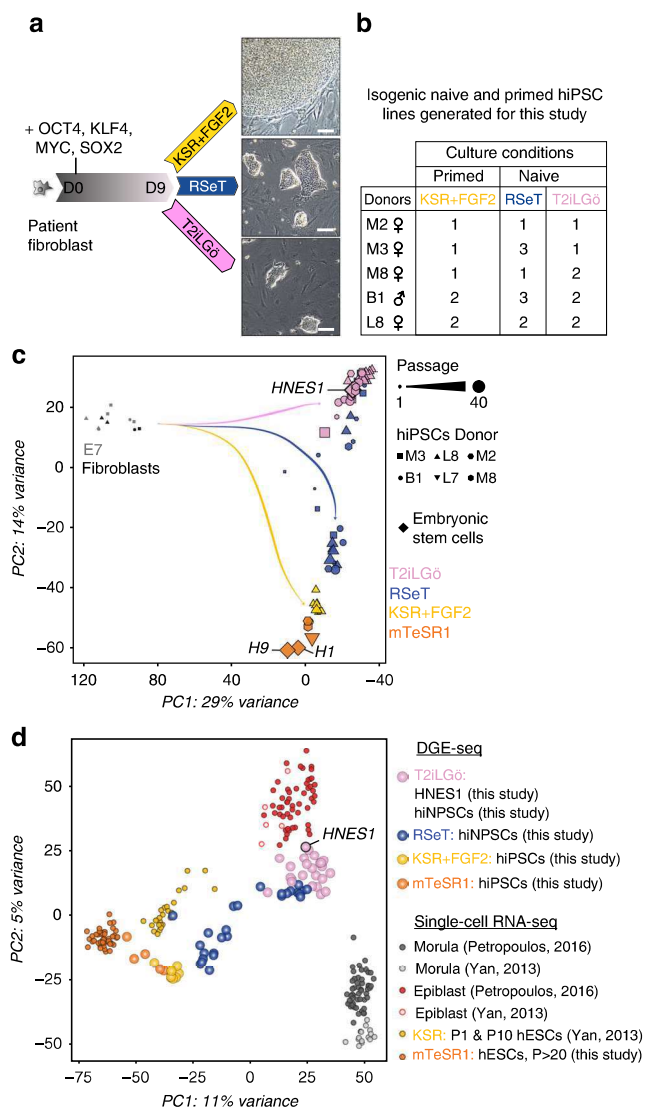


Fig. 1 Direct reprogramming of somatic cells into hiNPSCs. **a** Direct generation of isogenic naive and primed hiPSCs. Fibroblasts were transduced with 3 Sendai viruses expressing a polycistron KLF4/OCT4/SOX2, MYC and KLF4 at a ratio of 5:5:3, respectively. Cells were split on feeders at day 7, and placed in the indicated media at day 9. Scale bar = 100 μ m. **b** Summary of lines generated for this study in primed (KSR+FGF2, yellow) or naive culture media (RSeT, blue or T2iLGö, pink) originated from 5 different donors. **c** Different pluripotent states are induced depending on culture media. Transcriptomes of hiPSCs and hiNPSCs, control primed hESC lines H1 and H9 or the naive hESC line HNES1¹⁹ were analyzed by PCA. Symbols represent donor lines, and size of the symbols represents the passage. Arrows have been drawn to highlight the reprogramming trajectories. **d** T2iLGö hiNPSCs are the closest to human epiblast cells. PCA of single-cell RNA-seq data sets from preimplantation embryo samples^{11,12} compared to primed hPSCs from ref. ¹¹ and to primed/naive hiPSCs/hESCs from this study

as previously reported for human naive embryonic stem cells (hNESCs)^{8,17,19} (Supplementary Table 1). These genomic alterations have recently been associated with the inhibition of MEK through PD0325901, one major component of most media supporting human naive pluripotency²⁶. We limited the diploid/tetraploid ratio by reprogramming and growing cells under hypoxic conditions and constant rock inhibition (Y27632) (Supplementary Table 1), and by subcloning T2iLGö hiNPSCs.

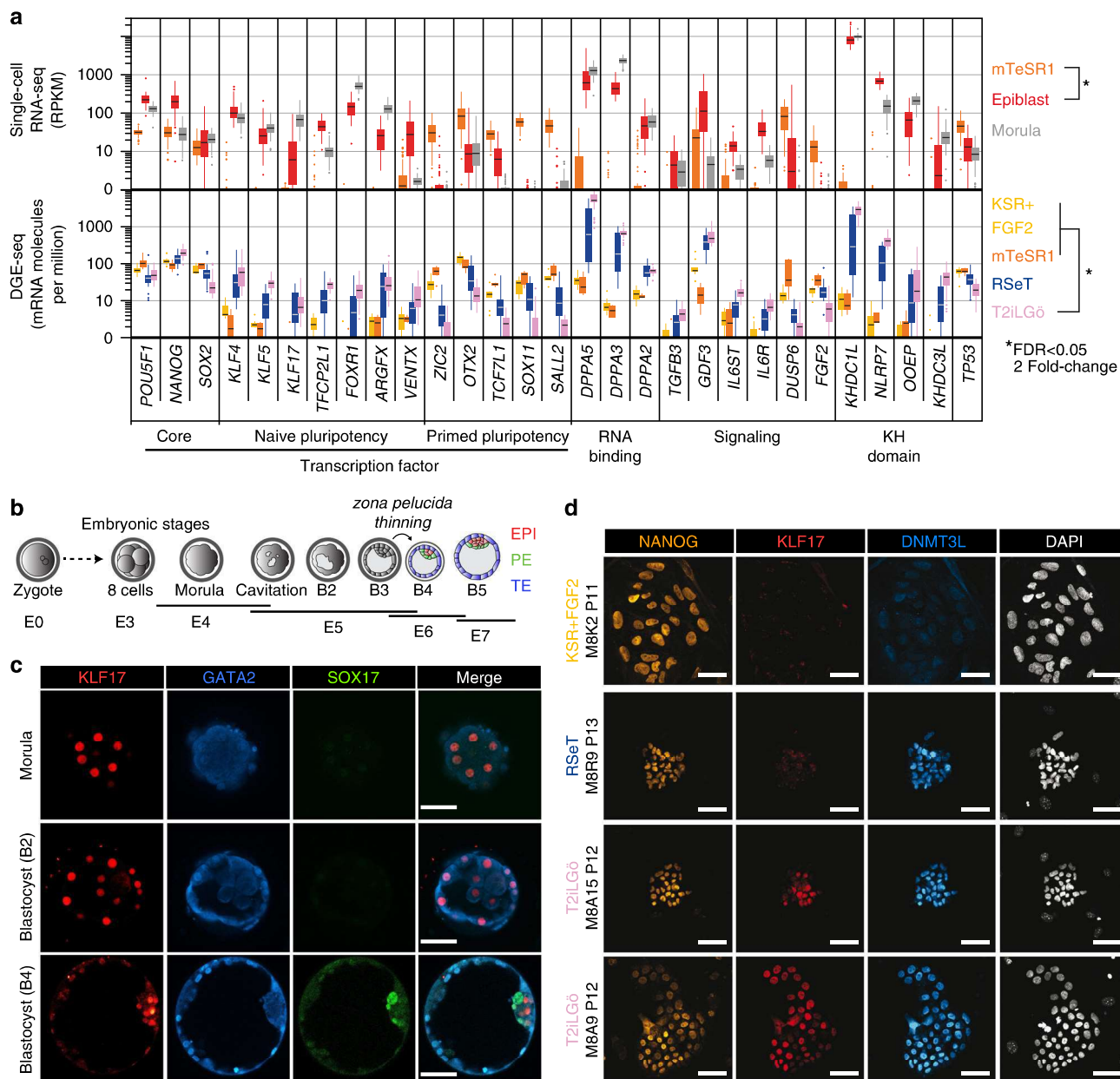


Fig. 2 hiNPSCs express markers specific to human epiblast cells. **a** Specific naive pluripotency markers display identical profiles in T2iLG6 hiNPSCs and preimplantation epiblast cells. Individual differentially expressed genes plotted as RPKM for single-cell RNA-seq or mRNA molecules per million of total mRNA molecules for DGE-seq. Upper panel: all genes are differentially expressed (Epi vs primed), except *SOX2*; lower panel: all genes are differentially expressed (T2iLG6 vs primed), except *POU5F1*(*OCT4*) and *NANOG*. Error bars are defined as s.e.m. Statistical tests used to compute differentially expressed genes are defined in the “Differential Expression profiling” section of the Methods. **b** Schematic representation of the human preimplantation development comparing clinical staging (Morula, B2, B3, B4 and B5) with corresponding embryonic days (E). EPI epiblast cells in red, PE primitive endoderm cells in green; TE trophectoderm cells in blue. **c** KLF17 protein is expressed in all morula cells before being restricted to epiblast cells in the blastocyst. Human embryos were cultivated in a time-lapse microscope and fixed at indicated stages (morula, B2 or B4 blastocysts). Immunofluorescence for KLF17 (red), GATA2 (blue) and SOX17 (green) was performed. For each indicated embryonic stage, immunofluorescence was performed on 3 biological replicates. Scale bar = 50 μ m. **d** KLF17 protein is specifically expressed in T2iLG6 hiNPSCs (pink) and not in isogenic lines cultivated in RSeT (blue) and KSR-FGF2 (yellow). Indicated cell lines were analyzed by immunofluorescence for NANOG (yellow), KLF17 (red) and DNMT3L (cyan). This figure is representative of 8 biological replicates. Scale bar = 50 μ m

We analyzed our hiNPSC and hiPSC lines, at different passages, by 3' digital gene expression RNA-sequencing (DGE-seq), a quantitative method based on molecular indexing of messenger RNA (mRNA) molecules^{27,28}. Controls used in this analysis are primed (H1 and H9) and naive (HNES1) hESC lines¹⁹. Principal component analysis (PCA) revealed two major components: the first discriminating between parental cells and

pluripotent stem cells, the second discriminating between H1 and H9 on one side and HNES1 on the other side (Fig. 1c). T2iLG6 and RSeT hiNPSC lines were separated along the second principal component. The majority of T2iLG6 hiNPSCs clustered with HNES1, regardless of passage number, while cells exposed to RSeT formed two intermediate clusters and tended to become more similar to primed human PSCs (hPSCs) at later passages

(trajectory drawn in Fig. 1c). To assess the development stage associated with hiNPSCs in different culture media, we compared them by PCA to the single-cell RNA-seq data sets of hESCs upon derivation (P1 and P10), high-passage hESCs, human epiblast cells and human morula cells^{11,12} (Fig. 1d). The first component classified samples from the morula cells, the cellular fate preceding pluripotency, to high-passage primed hESCs. Strikingly, T2iLGö hiNPSCs cluster together with epiblast cells while RSeT hiNPSCs sit between primed and naive PSCs. Altogether, these data reveal that our protocol can reprogram somatic cells directly to a state resembling the human epiblast, without an intermediate passage in primed media.

hiNPSCs express markers specific to human epiblast cells. To further characterize hiNPSCs, we compared in depth their transcriptomes (obtained by DGE-seq) to that of human preimplantation epiblast (generated by single-cell RNA-seq)^{11,12}. To reduce influence of sequencing protocols, we performed a two-step analysis. We first compared the human epiblast signatures¹² with those we obtained by performing single-cell RNA-seq from 52 H1 and H9 primed hESCs (Supplementary Fig. 2a). This yielded 6628 differentially expressed (DE) genes when a cutoff of twofold and false discovery rate (FDR) of <0.05 was applied. Second, we compared transcriptomes obtained by DGE-seq of primed hESCs and hiPSCs in KSR+FGF2 or mTeSR1 to T2iLGö hiNPSCs, as they clustered with HNES1 (Supplementary Fig. 2a). Using the same cutoff, we found 3003 DE genes between hiPSC and T2iLGö hiNPSC populations, among which 1980 are common DE genes between hESCs and epiblast cells. Among the top DE gene candidates overexpressed in epiblast and hiNPSCs, we found genes related to RNA binding, such as the *DPPA* family or the KH-domain proteins *KHDC1L*, *NLRP7*, *OOEP* and *KHDC3L* (Fig. 2a). Quantitative DGE-seq showed that those genes represent 1% of the transcriptome in T2iLGö hiNPSCs and HNES1, suggesting that mRNA processing regulated by those genes might play a prime role in naive pluripotency. Our analysis further identified transcription factors whose expression was specifically elevated in naive cells, such as *KLF4* and *KLF5*, and a cohort of specific naive pluripotency regulators: *KLF17*, *FOXRI*, *VENTX* and *ARGFX*; other transcription factors, such as *OTX2* and *SOX11*, were in contrast elevated in hiPSCs (Fig. 2a). Specific signaling pathways were also linked to pluripotency status. The transforming growth factor- β (TGFB) pathway ligands *TGFB3* and *GDF3* as well as the interleukin-6 (IL6) receptors *IL6R* and *IL6ST* were overexpressed in naive PSCs, while *FGF2* was distinctly overexpressed in primed PSCs.

Among the genes differentially expressed between naive and primed PSCs, we further investigated the extremely high expression of *DPPA5* in T2iLGö hiNPSCs (which represent around 0.2% of total mRNAs). We confirmed the expression of *DPPA5* at the protein level by western blot, only in T2iLGö hiNPSCs but not in the RSeT hiNPSCs or hiPSCs (Supplementary Fig. 3a). To our knowledge, it is the first time that *DPPA5* protein has been reported as a marker of human naive PSCs. We also investigated the expression of *KLF17* at the protein level, in hiPSCs, hiNPSCs and human embryos. During human preimplantation development, pluripotent cells emerge after the morula stage and are restricted to epiblast cells at the blastocyst stage²⁹ (Fig. 2b). Immunofluorescence (IF) analysis of human preimplantation embryos revealed that *KLF17* is strongly expressed in all cells of the morula (E4/E4.5). *KLF17* is also present at the B2 stages (E4.5/E5), and rapidly becomes restricted to the epiblast at the B4 blastocyst stage (E5.5/E6) (Fig. 2c). *KLF17* expression is distinct from that of *GATA2*, a marker of human trophoderm, expressed after B2 stage, and *SOX17*, a marker of primitive

endoderm, only expressed at the B4 stage. This supports an important role of *KLF17* during establishment of pluripotency in vivo, and is in line with single-cell RNA-seq analysis¹² (Supplementary Fig. 3b). IF analysis of *KLF17* and *NANOG* in primed and naive hiPSCs showed that while all PSCs expressed *NANOG*, only the T2iLGö hiNPSCs expressed *KLF17* (Fig. 2d and Supplementary Fig. 3c). This was further confirmed by flow imaging, highlighting a striking difference in signal intensity and in the number of *KLF17*-positive cells with nuclear localization between hiPSCs, RSeT and T2iLGö hiNPSCs (Supplementary Fig. 4). In particular, the intensity median of nuclear *KLF17* is 2.2 for the T2iLGö hiNPSCs, 1.08 for the RSeT hiNPSCs and 0.79 for the hiPSCs, confirming that the *KLF17* profile for RSeT hiNPSCs is closer to hiPSCs (Supplementary Fig. 4B). In contrast, *DNMT3L* is upregulated in both T2iLGö and RSeT hiNPSCs at the protein level, revealing the intermediate pluripotent state of RSeT hiNPSCs.

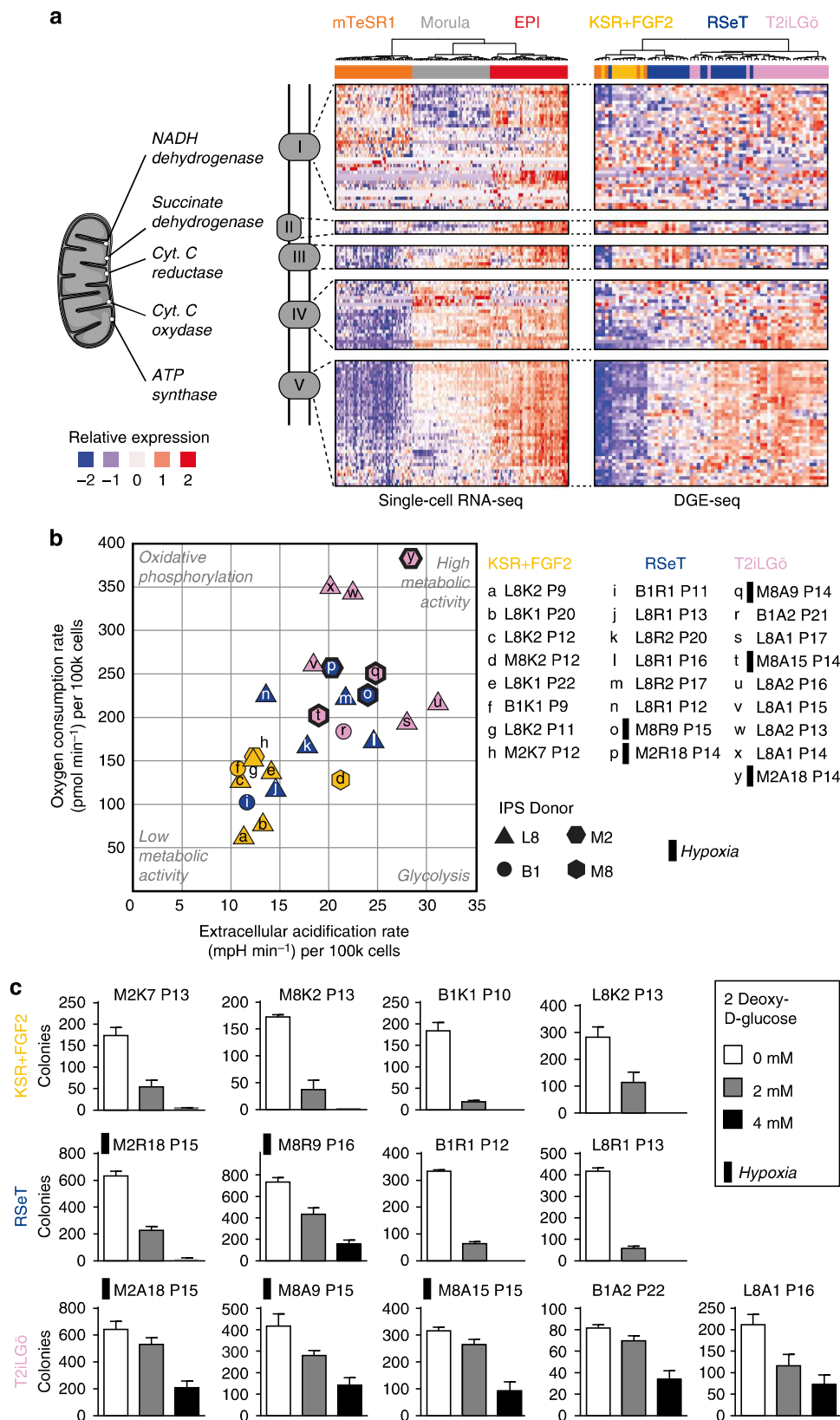
In addition to specific individual markers, we identified a strong correlation between naive pluripotency and pathways related to metabolism (Val-Iso-Leu degradation, purine and pyrimidine metabolism), cell cycle (p53 pathway, cell cycle, apoptosis) and cell junctions (adherent and tight junctions, focal adhesion) (Supplementary Fig. 2b). As those pathways are enriched in both epiblast cells and T2iLGö hiNPSCs, it suggests potential cross-talks between metabolic pathways and human naive pluripotency. Nonetheless, characterization of specific active pathways would be complementary to individual markers or to recently proposed transcriptome profile³⁰ to assess the naive nature of human PSCs. We tested the discriminative power of metabolism, cell cycle or cell junction pathways signatures to classify hiNPSCs, and observed that the result was depending on the pathway (Supplementary Fig. 2b). To improve the predictive power of our pathway-based approach, we performed PCA for each pathway and combined the first components to create a three-dimension space, in which we projected our samples. We observed that all the samples were aligned along a common axis, delimited by primed hESCs on one end and naive preimplantation epiblast cells on the other end. Suitably, each sample is clearly classified along this axis, including the RSeT hiNPSCs which have only partially gained expression of components of those pathways and are sitting between primed hiPSCs (in KSR +FGF2 or mTeSR1) and T2iLGö hiNPSCs (Supplementary Fig. 2c).

Altogether, our thorough analysis highlighted specific markers and pathways that characterize naive pluripotency. Moreover, we uncovered a hierarchy of markers distinguishing between T2iLGö hiNPSCs and intermediate RSeT PSCs.

Metabolic activity of hiNPSCs. To further characterize naive pluripotency, we analyzed enriched signaling pathways in naive pluripotent cells compared to primed pluripotent cells, based on Gene Ontology (GO) terms and the KEGG (Kyoto Encyclopedia of Genes and Genomes) database³¹, with FDR <0.01. The top enriched GO terms in hiNPSCs are related to the mitochondrial electron transport chain (Supplementary Data 2) and transcriptomic analysis of genes involved in oxidative phosphorylation shows an overall upregulation in human epiblast cells and hiNPSCs (Fig. 3a). To functionally validate the importance of enriched pathways, we tested the mitochondrial activity by measuring the oxygen consumption rate and the extracellular acidification rates in hiPSCs and hiNPSCs. This showed an increased metabolic activity in naive compared to primed cells, with a combined increase of glycolysis, recently reported in hNESCs³², and oxidative phosphorylation (Fig. 3b). Interestingly, the metabolic activity was proportional to the level of naive

pluripotency predicted by transcriptomic and pathway analysis: the RSeT hiNPSCs, with a mildly increased expression of electron transport chain genes, had a modest increase in metabolic activity. Moreover, analysis of oxidative phosphorylation capacity showed that hiNPSCs derived in T2iLGö have a higher

respiratory capacity than RSeT hiNPSCs or hiPSCs, in line with the analysis of HNES1 cells¹⁹ (Supplementary Fig. 5). Clonal assays in culture conditions supplemented with 4 mM 2-deoxy-D-glucose, a competitive inhibitor of glycolysis, confirmed the ability of T2iLGö hiNPSCs to mobilize oxidative phosphorylation



to proliferate. In contrast, RSeT hiNPSCs and primed hiPSCs did not grow under these culture conditions (Fig. 3c). Therefore, metabolic activity is an important discriminant of hiNPSCs, and could be used to select for naive PSCs.

Hypomethylation and X-chromosome reactivation in hiNPSCs. Naive pluripotency is characterized by DNA hypomethylation in human naive PSCs^{7,17} and preimplantation epiblast^{13,14}. Quantitation of 5-methyl-cytosine (5mC) by mass spectrometry showed that naive cells in T2iLGö had the lowest mC content of all tested lines, under 3% in average, while primed cells were all above 5%, in accordance with the previously published analysis of hNESc lines^{17,19} (Fig. 4a). Comparison of DNA methylation regulators expression between T2iLGö hiNPSCs and hiPSCs show that *DNMT3L* is dramatically increased (up to 0.1% of the transcriptome) in the former, while *DNMT3B* is decreased. The *TET* family has also been recently associated with human naive pluripotency, as *TET1* overexpression could transiently induce expression of naive markers³³. Quantitative DGE-seq shows a gain of *TET2* expression in T2iLGö hiNPSCs, whereas *TET1* expression level remains stable and *TET3* is poorly expressed in all samples (Fig. 4b). On another hand, RSeT hiNPSCs had intermediate levels of *DNMT3L*, *DNMT3B* and *TET2* and 5mC percentage between primed and T2iLGö hiNPSCs. Our results suggest mass spectrometry quantitation of 5mC as a convenient and accurate measurement to qualify hiNPSCs.

The presence of two active X chromosomes is considered a hallmark of human naive pluripotency^{12,18,34}. To assess the activity of the X chromosomes in primed and naive hiPSCs, we first analyzed by IF the distribution of H3K27me₃, a marker of the inactive X (Xi) chromosome. Xi-characteristic H3K27me₃ accumulation is seen in RSeT hiNPSCs and early-passage hiPSCs nuclei consistent with the presence of an Xi (Fig. 5a). In contrast, a low percentage of T2iLGö hiNPSCs and late-passage hiPSCs display H3K27me₃ foci, which could correspond either to the erosion of dosage compensation³⁵ that occurs spontaneously in primed hPSCs³⁶ or to the reactivation of the Xi, which has been observed in naive PSCs^{15,18,30}. To discriminate between the two hypotheses, we monitored by RNA fluorescent in situ hybridization (RNA-FISH) the activity status of the X chromosomes. We first focused on the expression of the protein-coding gene *ATRX*, which has been shown to resist erosion in most studied lines^{35,37}. Biallelic expression of *ATRX* is consistently observed in T2iLGö hiNPSC lines, with 36% to 100% naive T2iLGö hiNPSCs displaying only active X (Xa) (Fig. 5b). In contrast, biallelic expression of *ATRX* was rarely observed in RSeT, and never in KSR+FGF2 culture conditions. We next probed the expression of the lncRNAs *XIST* and *XACT*, as their relative patterns of expression clearly distinguish the various X-chromosome states. While early-passage hiPSCs have a characteristic post-inactivation staining, with the Xi coated by *XIST* and the Xa coated by *XACT*, we observed loss of *XIST* and biallelic accumulation of *XACT* in late-passage hiPSCs, further confirming

the erosion of X inactivation in these cells (Fig. 5c). In striking contrast, we observed co-accumulation of *XIST* and *XACT* on one active X chromosome in a significant proportion of T2iLGö and RSeT hiNPSCs, but we only observed co-accumulation of *XIST* and *XACT* on both X chromosomes in T2iLGö hiNPSCs, similar to previous findings¹⁵. Collectively, those results show that X-chromosome reactivation has occurred only in T2iLGö hiNPSCs. To ensure that X-chromosome reactivation was happening independently of chromosomal abnormalities, we subcloned the hiNPSCs M2A18, M8A9 and M8A15. Analysis of two subclones of each line by *ATRX*, *XACT* and *XIST* RNA-FISH demonstrated that X-chromosome reactivation occurs in diploid cells (Fig. 6).

Our FISH results stress out the importance of combining the analysis of *XACT*, *XIST* and *ATRX* expression, and not to rely only on *XIST* or H3K27me₃, in order to assess X-chromosome reactivation, a critical hallmark of naive pluripotency in humans¹⁵ (Fig. 5).

Discussion

We generated hiNPSCs directly from somatic cells by using OKMS overexpression and defined culture media. Our method enables parallel generation of naive and primed hiPSCs of the same genetic background, limiting tissue culture time and extended passaging compared to previously published strategies that require primed PSCs prior to their conversion into naive PSCs^{4–9}. Collectively, our results show that a human preimplantation-like state can be induced in somatic cells by directly shifting reprogramming cultures to naive conditions without the need for a primed intermediate. The resulting hiNPSCs in T2iLGö display all hallmarks of human naive pluripotency, while RSeT hiNPSCs display an intermediate naive phenotype. However, we recorded some genomic alterations in T2iLGö hiNPSCs and others showed aberrant imprinting^{17,25} of the cells. Thus, culture conditions are not yet ideal to maintain *in vitro*, the transient human naive pluripotent state.

Further analysis of the array of hiNPSCs that we generated could uncover hierarchy between molecular events necessary to achieve naive pluripotency (Fig. 7). Our data show that transcriptomics analysis is able to rank cells from morula, epiblast/T2iLGö hiNPSCs, RSeT hiNPSCs and primed hESCs/hiPSCs. This supports the concept of a “formative pluripotent state”, a state achieved during the transition from naive demethylated cells to cells primed for differentiation³⁸. Our protocol uses OKMS overexpression to achieve a state compatible with naive and primed pluripotency, in line with the first observation of a higher state of human pluripotency³⁹. One could envision to use factor-based reprogramming to capture the formative state using proper culture medium.

Besides representing a powerful model to study the differences between naive and primed pluripotency, the multiple metastable states of pluripotency could have significant biological properties. Indeed, one of the approach envisioned for regenerative medicine is to generate interspecies chimeras with human pluripotent stem

Fig. 3 T2iLGö hiNPSCs metabolic profile is closely related to preimplantation epiblast. **a** Genes coding proteins of the electron transport chain, located in the inner membrane of the mitochondria, are upregulated in human epiblast cells and T2iLGö hiNPSCs in comparison to their primed counterparts. Relative expression of genes related to oxidative phosphorylation pathway for hESC, morula and epiblast samples analyzed by single-cell RNA-seq (left), and analyzed by DGE-seq for primed or naive hPSCs (right). Genes were classified by mitochondrion complex and hierarchically clustered. **b** T2iLGö hiNPSCs have higher metabolic activity than their isogenic counterparts in RSeT and KSR+FGF2. A Seahorse apparatus was used to measure the oxygen consumption rate and the extracellular acidification rate of hiNPSC and hiPSC lines, maintained in indicated culture conditions. This figure presents six biological replicates. Each symbol in the panel is the average of a technical triplicate. **c** T2iLGö hiNPSCs have a higher resistance to inhibition of glycolysis. Quantification of colony numbers obtained after culture with the indicated concentrations of 2-deoxy-D-glucose. Primed cells were seeded in StemMACS™ iPS Brew XF, and naive cells were seeded in the indicated medium. Error bars indicate s.d. of three technical replicates. The presented experiment is representative of four independent experiments

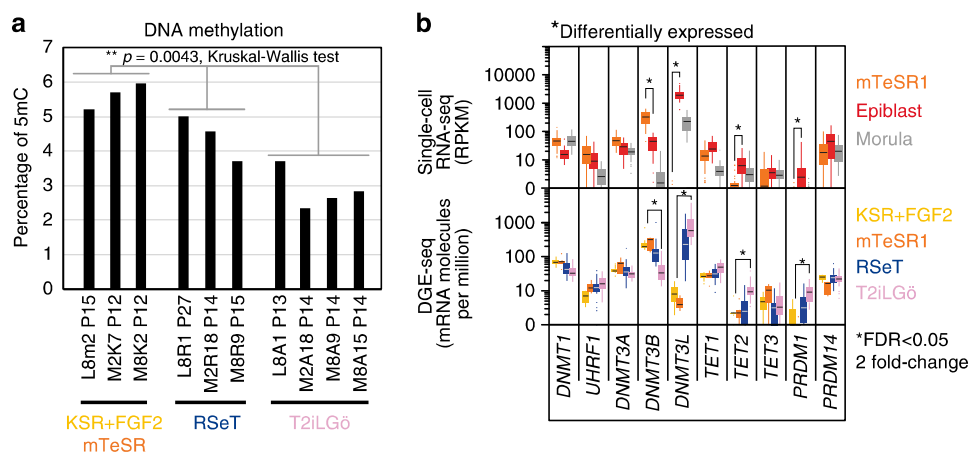


Fig. 4 T2iLGö hiNPCs are hypomethylated. **a** T2iLGö hiNPCs are hypomethylated in comparison to their RSeT and KSR+FGF2 counterparts. 5mC content is expressed as the percentage of 5mC in the total pool of cytosine for the indicated cell lines. Significance level was determined using Kruskal–Wallis test $**p < 0.01$. **b** Expression of indicated epigenetic-related genes is plotted as RPKM for single-cell RNA-seq or mRNA molecules per million of total mRNA molecules for DGE-seq. Error bars are defined as s.e.m. *Differentially expressed gene, as defined in Methods

cells. A recent report showed that specific pluripotent states might be needed depending on the recipient species, limiting the success of the chimeras⁴⁰. During the revision of our manuscript, Yang et al.⁴¹ described a specific medium allowing generation of pluripotent stem cells with extended potential to contribute to chimeras (EPS cells). However, further characterization is needed to show if those cells correspond to naive pluripotency or have specific features granting them superior chimerism capabilities. In that context, it will be interesting to see how EPS cells qualify using our proposed readouts (Fig. 7).

Altogether, direct reprogramming of somatic cells into hiNPCs will alleviate ethical issues linked with hESCs, therefore spreading the availability of this important cellular model. Indeed, naive PSCs are considered an alternative to human embryos to study regulation of human pluripotency, model preimplantation development and gonad diseases⁴². A concern for the clinical use of PSCs lies within their ability to keep a stable genome and epigenome, such as the X-chromosome dosage compensation in humans which is deregulated in primed hPSCs after long-term culture and is therefore a potential barrier for regenerative medicine³⁷. Combining knowledge obtained from both primed and naive hPSCs will contribute to a better understanding of molecular processes involved in human pluripotency like X-chromosome dynamics, facilitating the development of hPSC-based therapies.

Methods

Human preimplantation embryos. The use of human embryos donated to research was allowed by the French embryo research oversight committee: Agence de la Biomédecine, under approval number RE13-010. All human preimplantation embryos used in this study were obtained from and cultured at the Assisted Reproductive Technology unit of the University Hospital of Nantes, France, which are authorized to collect embryos for research under approval number AG11 0126AMP of the Agence de la Biomédecine. Embryos used were initially created in the context of an assisted reproductive cycle with a clear reproductive aim and then voluntarily donated for research once the patients have fulfilled their reproductive needs, or tested positive for the presence of monogenic diseases. All embryos used in this study were given to research after double consents from both parents. Donors did not receive any financial compensation. Molecular analysis of the embryos was performed in compliance with the embryo research oversight committee and The International Society for Stem Cell Research (ISSCR) guidelines⁴³.

Human preimplantation embryos culture. Day 3 cryopreserved embryos were thawed using Sydney IVF Thawing Kit (Cook Medical) and cultured in G2 Plus (Vitrolife), a specific medium for culture of embryos from day 3 to the blastocyst stage. Embryos were loaded into the Embryoscope® (Unisense Fertilitect®), a tri-gas incubator with a built-in microscope allowing time-lapse monitoring of early embryo development.

For embryos affected by a monogenic disease, insemination was achieved by intracytoplasmic sperm injection. Vitrolife® sequential media were used for embryo culture, with embryos being cultured in G1plus® medium from day 0 to day 3 and then transferred to a new pre-equilibrated slide containing G2plus® medium and cultured from day 3 onwards. Embryo biopsy of one or two blastomeres was performed at day 3 and the genetic results were obtained at day 4. Embryo culture was performed at 37 °C under a controlled atmosphere with low oxygen pressure (5% O₂, 5% CO₂). Embryos were fixed at the morula, B2 or B4 stages according to the grading system proposed by Gardner and Schoolcraft⁴⁴. Staging details of the embryos that are presented in Fig. 2b were as follows: the morula was fixed at 97 h post fertilization, and contained 24 cells; the B2 blastocyst passed through the morula stage at 59 h post thawing (8 cell stage), and was fixed at 76 h post thawing, it contained 33 cells; the B4 blastocyst passed through the morula stage at 95 h post fertilization, B2 stage at 111 h and was fixed at B4 stage at 118 h, it contained 135 cells, among which 8 PE cells (SOX17+) and 7 EPI cells (KLF17+).

Human cell lines. Three donor fibroblasts were used in this study, all of them being healthy donors: (1) B1 male fibroblasts are commercial BJ human neonatal fibroblasts extracted from normal human foreskin (Stemgent cat. no. 08-0027), (2) L8 female fibroblasts are normal human adult dermal fibroblasts extracted from a healthy woman aged 57 years, which are commercially available (Lonza cat. no. CC-2511 Lot 0000258580), (3) MIPS female fibroblasts are from three female patients from the Milieu Interieur Labex consortium, M2 and M3 are in their thirties while M8 is in the sixties. Human fibroblasts from the consortium were obtained after informed consent of patients, acknowledging the generation of hiPSC lines and use of those pluripotent lines for research. Primed hiPSCs from L7 human adult dermal fibroblasts extracted from a healthy male aged 51 years (Lonza cat. no. CC-2511 Lot 0000293971) were also used in this study. hESC lines H1 (WA01 Lot WB0111) and H9 (WA09 Lot WB0090) were obtained from the WiCell Research Institute, under authorization RE13-004 from the French embryo research oversight committee, Agence de la Biomédecine.

Tissue culture. Fibroblasts were cultured in fibroblast medium, composed of high glucose Dulbecco's modified Eagle's medium (DMEM) GlutamaxII (Life Technologies) supplemented with 10% fetal bovine serum (Hyclone), 1% sodium pyruvate (Life Technologies) and 1% non-essential amino acids (Life Technologies).

Mouse embryonic fibroblasts (MEFs) were prepared as previously described⁴⁵ and cultured in fibroblast medium supplemented with 0.5% of penicillin–streptomycin (Life Technologies). MEF isolation was performed in compliance with the French law and under supervision of the UTE animal core facility, University of Nantes. MEFs were mitotically inactivated using mitomycin C (Sigma) to be used as feeder cells.

Primed PSCs on feeder cells were cultured in DMEM/F-12 (Life Technologies) supplemented with 20% of Knockout™ serum replacement (Life Technologies), 1% non-essential amino acids (Life Technologies), 1% glutamax (Life Technologies), 50 μM 2-mercaptoethanol (Life Technologies) and 10 ng/ml fibroblast growth factor 2 (PeproTech). Primed PSCs were mechanically passaged by cutting colonies with a needle. Primed PSCs in feeder-free conditions were cultured on Matrigel (BD/Corning) in mTeSR1 media; cells were non-enzymatically dissociated with StemMACS passaging solution XF (Miltenyi Biotec) for passaging.

hiNPCs were cultured on feeder cells, either in RSeT™ medium (Stem Cell Technologies) or in T2iLGö medium^{7,19} which is composed of N2B27

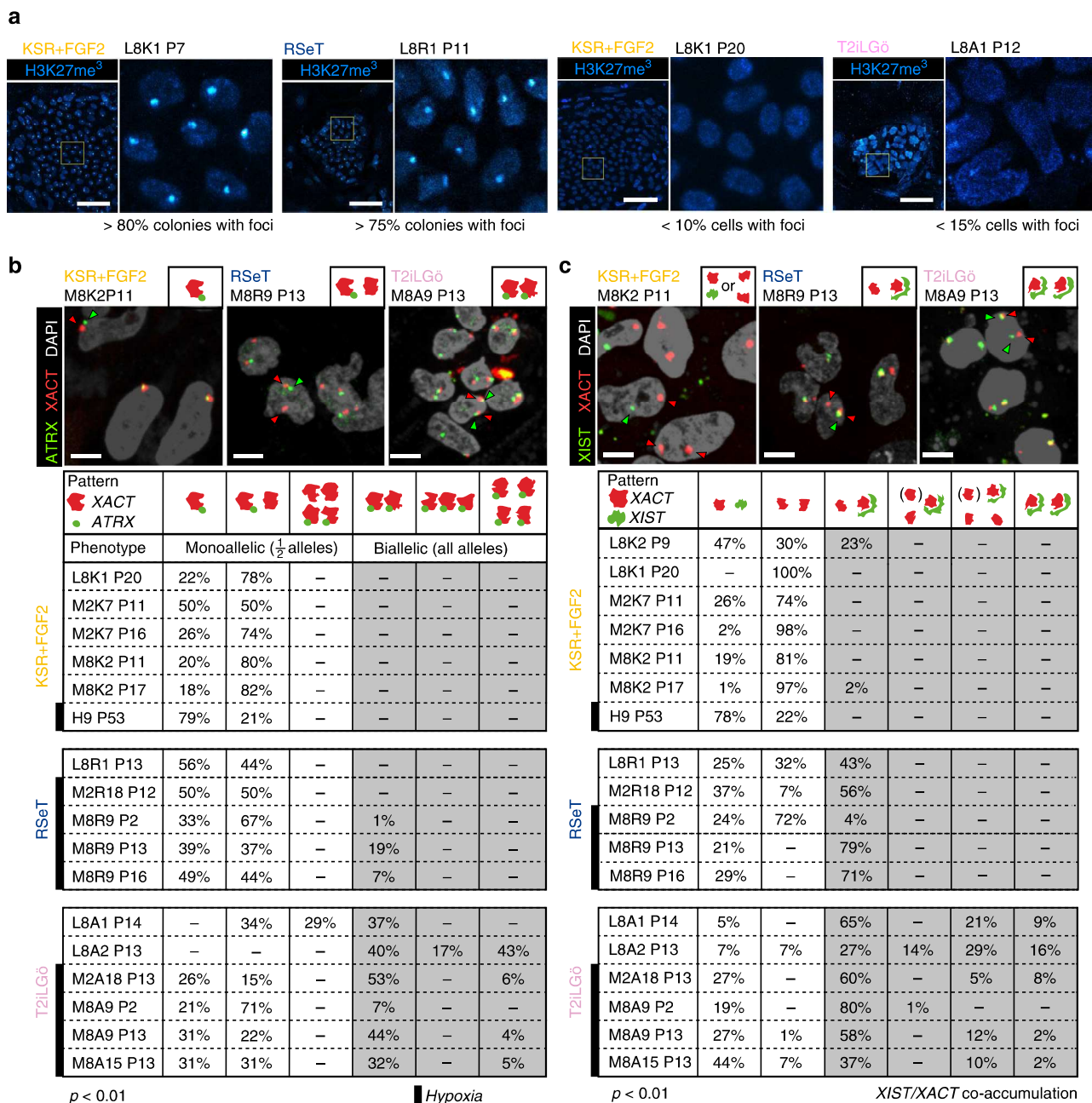


Fig. 5 T2iLGö hiNPCs have a X-chromosome status related to preimplantation epiblast. **a** T2iLGö hiNPCs or high-passage KSR-FGF2 do not display H3K27me3 foci. Indicated cell lines were analyzed by immunofluorescence for H3K27me3. This experiment is representative of three technical replicates performed at different passages of the cell lines. Scale bar = 50 µm. **b, c** T2iLGö hiNPCs show signs of X-chromosome reactivation. mRNA FISH analysis for **b** ATRX and XACT or **c** XIST and XACT. For each cell line represented, more than 100 cells were investigated for their nuclear expression of the indicated mRNA. Quantifications for each combination are indicated below pictures. For each table, samples distribution between FISH counting were found statistically different ($p < 0.01$) by a homogeneity χ^2 test. Scale bar = 20 µm

supplemented with 20 ng/ml LIF (Miltenyi Biotec), 1 µM of PD0325901 (Axon Medchem), 1 µM CHIR99021 (Axon Medchem) and 5 µM Gö6983 (TOCRIS). N2B27 medium is composed of DMEM/F-12 (Life Technologies) supplemented with 1% N2 (Life Technologies), 1% B27 (Life Technologies), 1% non-essential amino acids (Life Technologies), 1% glutamax (Life Technologies), 0.1 mM 2-mercaptoethanol (Life Technologies), 50 µg/ml bovine serum albumin (Sigma) and 0.5% penicillin-streptomycin (Life Technologies). hiNPCs were passaged using TrypLE (Life Technologies) for 5 min at 37 °C.

Naive and primed hPSCs were cultured at 37 °C under 20% O₂, 5% CO₂ and 10 µM Y27632 (TOCRIS) was added in the medium upon cell seeding. M2 and M8 naive hPSCs were cultured at 37 °C under 5% O₂, 5% CO₂ and 10 µM Y27632.

Somatic cell lines have been tested for mycoplasma presence using the MycoAlert kit (LONZA, LT07-318) before reprogramming. Only if the test was

negative, reprogramming was performed. Each iPSC line generated was tested for mycoplasma using the MycoAlert kit at various time points to ensure mycoplasma absence in both primed and naive hiPSCs.

Reprogramming of human somatic cells into iPSCs. Fibroblasts were reprogrammed using the CytoTune-iPS 2.0 Sendai reprogramming kit from Life Technologies. Two days before infection, 40,000 fibroblasts were seeded per well on a 12-well plate, coated with Matrigel. At day 0, cells were counted and infected with the three vectors: polycistronic Klf4-Oct4-Sox2, cMyc and Klf4 at a 5, 5 and 3 multiplicity of infection, respectively. At day 7 of infection, cells were dissociated using TrypLE and seeded on 3 × 35 mm dishes coated with mouse feeder cells. Cells were switched to naive pluripotency medium (RSeT or T2iLGö) or TeSR-E7 medium at day 9. For each of our reprogramming campaigns, we obtained more

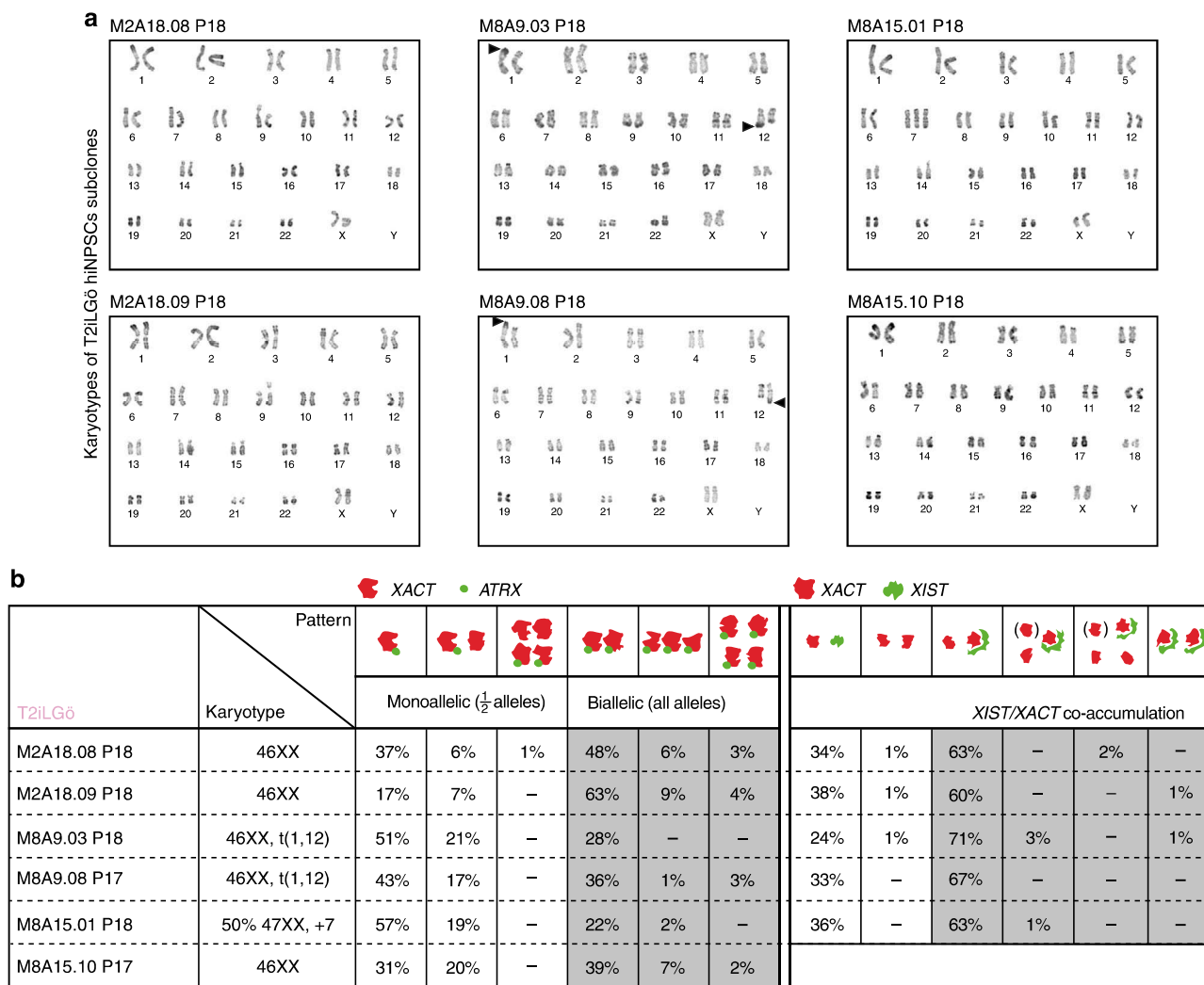


Fig. 6 Clonal analysis of X-chromosome reactivation in T2iLGö hiNPCs. **a** Representative karyotypes of T2iLGö subclones. **b** Karyotype and mRNA FISH analysis for *ATR*X and *XACT* (left) or *XIST* and *XACT* (right) of indicated subclones. For each subclone represented, more than 50 cells were investigated for their nuclear expression of the indicated mRNA. Quantifications for each combination are indicated below pictures

than 100 colonies in T2iLGö, TeSR-E7 and RSeT. RSeT and T2iLGö hiNPCs were trypsinized for passaging, primed hiPSCs were mechanically passaged to fresh feeder-coated tissue culture dishes, in KSR+FGF2, between day 16 and day 24.

SeaHorse analysis. Oxygen consumption rate and extracellular acidification rate were measured using an XF24 Analyser (SeaHorse Bioscience). At confluence, hiNPCs and hiPSCs were dissociated using TrypLE and cells were incubated on gelatin for 30 min at 37 °C to remove feeder cells. The SeaHorse plate was pre-treated with 2 µg/ml of Cell-Tak Cell and tissue adhesive (Corning). KSR, RSeTTM and T2iLGö cells were seeded at 200,000, 150,000 and 100,000 cells per well respectively prior to the experiment. Cells were incubated for 1 h at 37 °C and atmospheric CO₂ in DMEM (Sigma Aldrich) supplemented with 10 mM glucose, 2 mM glutamine, 2 mM pyruvate and the pH was adjusted to 7.4 using NaOH. During the mito stress kit experiment, Oligomycin (2 µM), CCCP (0.75 µM), Antimycin-A (2 µM) and Rotenone (1 µM) were injected at indicated time points.

Colony formation assay in 2-deoxy-D-glucose. hiNPCs or hiPSCs were seeded at 3000 cells per well in a 12-well plate, coated with feeder cells, in their respective media in addition to 10 µM Y27632. Of note, KSR cells were seeded and cultured in iPS Brew to boost clonogenicity of the cells. From day 1 after seeding onwards, 2 mM or 4 mM of 2-deoxy-D-glucose were supplemented in the culture medium. Cells were fixed between day 4 and day 6 post seeding and stained for alkaline phosphatase using the SIGMA FASTTM BCIP[®]/NBT kit (Sigma). Images were acquired using the Cellomics ArrayscanVTI (Thermo Fisher) at a 5× magnification. Colonies were counted manually. Presented results are from a representative experiment performed in triplicate.

Karyotype analysis. Karyotyping based on RTG-banding was performed at Cytogenetic Laboratory (CHU Nantes) using standard methods with minor modifications. Briefly, hiPSCs and hiNPCs were plated on Lab-Tek chamber slide. At 70% confluence, PSCs were submitted to hypotonic shock (20% fetal bovine serum in water), fixed in methanol/glacial acetic acid 3:1, then stained in Giemsa stain. Metaphase spreads for each sample were analyzed. A total of 30 pictures per slides were automatically acquired, chromosomes counted and at least 10 karyotypes for each cell line were classified. The commercial L8 fibroblast line contains a translocation from the chromosome 10 to 7 that is found in all derived iPSC lines. The B1 and M3 fibroblasts had normal karyotypes.

Immunofluorescence. For IF analysis, cells and embryos were fixed at room temperature using 4% paraformaldehyde for 15 min and 30 min (on a rotating shaker for embryos), respectively. Samples were then permeabilized and blocked in IF buffer (IF buffer: phosphate-buffered saline (PBS)–0.2% Triton, 10% fetal bovine serum) for 60 min at room temperature. Samples were incubated with primary antibodies overnight at 4 °C. Incubation with secondary antibodies was performed for 2 h at room temperature along with 4',6-diamidino-2-phenylindole (DAPI) counterstaining. Primary and secondary antibodies with dilutions used in this study are listed in Supplementary Table 2.

Imaging flow cytometry. Cells were stained with the Zombie NIRTM viability kit (BioLegend cat. no. 423105) for 20 min on ice. Potential nonspecific binding sites were blocked by incubation with human serum (obtained from healthy donor at the French blood establishment EFS) diluted to 1:20 in PBS for 30 min. Before performing intracellular staining, cells were fixed and permeabilized for 30 min on ice, using the Fixation/Permeabilization concentrate (eBioscience cat. no. 00-5123)

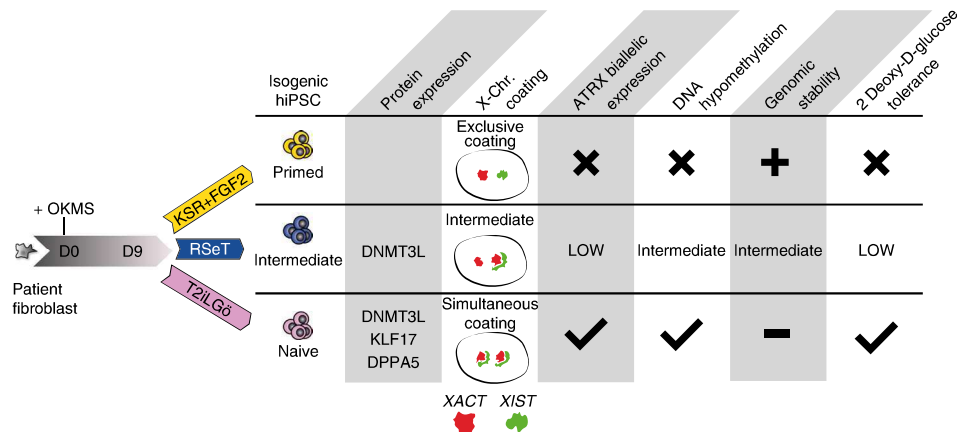


Fig. 7 hiNPCs in T2iLG6 achieve the most naive pluripotency hallmarks. The presented reprogramming method enables to simultaneously generate isogenic hiPSCs in KSR+FGF2, RSeT and T2iLG6 media. The naive pluripotency level of the generated cell lines can be assessed with specific markers, X-chromosome activity status, DNA methylation level and capacity to tolerate glycolysis inhibition

diluted in Fixation/Permeabilization Diluent (eBioscience cat. no. 00-5223) and in the Permeabilization buffer (eBioscience cat. no. 00-8333). Cells were incubated with the primary antibody (anti-KLF17, 1:100) for 45 min at room temperature. Further incubation with the secondary antibody (goat anti-rabbit, 1:500) was performed for 30 min on ice. Before imaging, DAPI was added to stain nuclei of the cells. References of antibodies with dilutions used in this study are listed in Supplementary Table 2.

Analyses were performed using an ImageStreamX Mark II Imaging Flow Cytometer (Amnis Corporation, Seattle, WA) equipped with the INSPIRE software.

A 40× magnification was used for all samples. Data analysis was performed using the IDEAS software (Amnis Corporation). The Zombie NIR[®] was excited with a 642 nm laser (power 50 mW) and the fluorescence signal was collected on channel 12 (745–800 nm). The DAPI was excited with a 405 nm laser (power 60 mW) and the fluorescence signal was collected on channel 7 (430–505 nm). KLF17 coupled to an Alexa 488 was excited with a 488 nm laser (power 80 mW) and the fluorescence signal was collected on channel 2 (480–560 nm). Intensity-adjusted brightfield images were collected on channel 1 (430–480 nm). The gating strategy for analysis involved the selection of focused, single and living cells on viability marker, then on DAPI and KLF17 fluorescence.

DNA methylation. For mass spectrometry analysis of DNA methylation, 1 µg of genomic DNA was analyzed using liquid chromatography triple-quadrupole mass spectrometry (KU Leuven Metabolomics Core). The concentration (µM) of Cytosine (unmodified), 5mC and 5-hydroxymethyl-cytosine (5hmC) were obtained using standard curves of known C, 5mC and 5hmC amounts. The percentage of 5mC or 5hmC in DNA was obtained by calculating the ratio of 5mC or 5hmC to the total pool of C.

RNA-FISH. RNA-FISH was performed as previously described³⁵. Briefly, cells were fixed between 36 h and 50 h post seeding in 3% paraformaldehyde for 10 min at room temperature. Cells were permeabilized in CSK buffer supplemented with 1 mM EGTA, 0.5% Triton and RNaseOUT inhibitor (20 U/ml) for 5 min on ice. After 3 washes in 70% EtOH, cells were dehydrated in 90% and 100% EtOH and incubated overnight with probes at 37 °C. After three 50% formaldehyde/2× SSC washes and three 2× SSC washes at 42 °C for 4 min, coverslips were mounted in Vectashield plus DAPI. SpectrumGreen or SpectrumRed-labeled probes (Vysis) were generated by nick translation for human *XIST*, *XACT* (RP11-35D3, BAC-PAC) and *ATRX* (RP11-42M11, BACPAC Resource). Images were acquired on an inverted Nikon A1 confocal microscope, according to the Shannon–Nyquist sampling rate. mRNA expression of *XIST*, *XACT* and *ATRX* are manually counted in more than 100 cells per cell line.

Western blot. Cells were lysed in 100 µl of TNTE buffer supplemented with protease inhibitor cocktail (Sigma) and phosphatase inhibitor cocktail (Sigma). TNTE buffer were composed of 50 mM Tris-HCl pH 7.4, 150 mM NaCl, 1 mM EDTA and 0.5% Triton X-100. Then, 20 µg of proteins samples were denatured using NuPAGE sample reducing agent and LDS sample buffer (Invitrogen) for 5 min at 98 °C. Next, 6 µl of spectra[™] multicolor broad-range protein ladder (Invitrogen) or 20 µg of denatured protein samples were loaded on a 4–15% mini-PROTEAN[®] TGX stain-free[™] precast gels (BioRad), transferred on trans-blot[®] turbo[™] RTA midi nitrocellulose transfer kit membranes (BioRad). The membranes were blocked for 1 h in tris-buffered saline with Tween-20/5% milk, incubated overnight with primary antibodies and incubated 1 h with secondary antibodies. Signal was revealed with Super signal west femto maximum sensitivity substrate (Thermo scientific) for DPPA5 or clarity[™] ECL western blotting

substrate (BioRad) for glyceraldehyde 3-phosphate dehydrogenase (GAPDH) and imaged on a Chemidoc[™] MP system (BioRad). Primary and secondary antibodies are listed in Supplementary Table 2. The stain-free blot image and the uncropped blot images can be found in Supplementary Fig. 6.

RNA extraction and quantitative real-time PCR. Total RNA was extracted using RNeasy[®] columns and DNase-treated using RNase-free DNase (Qiagen). For quantitative PCR, first-strand complementary DNAs (cDNAs) were generated using 500 ng of RNA, M-MLV reverse transcriptase (Invitrogen), 25 µg/ml polydT and 9.6 µg/ml random primers (Invitrogen).

To quantitate transcripts, absolute quantitative PCR was performed on a Viia 7 (Applied Biosystems) using power SYBR green PCR master mix (Applied Biosystems), for genes listed in the primers table (Supplementary Table 3). For each sample, the ratio of specific mRNA level relative to GAPDH levels was calculated. Experimental results are shown as levels of mRNA relative to the highest value.

All quantitative real-time PCR primers have a hybridization temperature of 60 °C and their sequences are listed in Supplementary Table 3. All amplicons span two adjacent exons. SeV primers are from Life Technologies (cytotune 2.0 kit).

Expression profiling by single-cell RNA-seq and DGE-seq. For single-cell RNA-seq, H1 and H9 cells were sorted on a FACS Aria in 5 µl lysis buffer (1:500 Phusion buffer, NEB; 1:20 RNASE out, Life Technologies), and frozen at –80 °C. The SmartSeq2 libraries were prepared according to the SmartSeq2 protocol^{16,47} with some modifications⁴⁸. Briefly, total RNA was purified using RNA-SPRI beads. Poly (A)+mRNA was converted to cDNA which was then amplified. cDNA was subject to transposon-based fragmentation that used dual indexing to barcode each fragment of each converted transcript with a combination of barcodes specific to each sample. In the case of single-cell sequencing, each cell was given its own combination of barcodes. Barcoded cDNA fragments were then pooled prior to sequencing. Sequencing was carried out as paired end 2 × 25 bp with an additional 8 cycles for each index.

The FASTQ files were mapped with Tophat2⁴⁹ on GRCH37.75.gtf genome version with Bowtie2⁵⁰ (human_g1k_v37). Of note, FASTQ from¹² were generated by single-end RNA-seq and in our data set in paired-end RNA-seq. HTSeq⁵¹ was used to generate raw counts tables from BAM files. For each sample, Q30 percentage was calculated with FASTQC, and samples with a score above 75% were kept. Additional filters were employed: samples with more than 5000 genes detected were kept, and a final gene filtering step was performed to keep genes with a sum of at least 10 counts across the 1976 samples. Samples with total quantity of count 2 s.d. away from mean total quantity of count were excluded.

Counts were normalized with scan⁵² and log₂ transformed for variance analysis (PCA and clustering on correlations matrix)

To obtain RPKM, BAM were computed to count using featureCount from Rsubread with GRCH37. Then, counts were normalized with calcNormFactors from edgeR⁵³ with default parameters, and RPKM were finally obtained using rpkm function from edgeR on normalized counts. RPKM were used for Figs. 2a and 4b.

For 3' DGE, RNA-sequencing protocol was performed according to ref. 28. Briefly, the libraries were prepared from 10 ng of total RNA. The mRNA poly(A) tails were tagged with universal adapters, well-specific barcodes and unique molecular identifiers (UMIs) during template-switching reverse transcriptase. Barcoded cDNAs from multiple samples were then pooled, amplified and tagmented using a transposon-fragmentation approach which enriches for 3' ends of cDNA. A library of 350–800 bp was run on an Illumina HiSeq 2500 using a HiSeq Rapid SBS Kit v2-50 cycles (ref FC-402-4022) and a HiSeq Rapid PE Cluster Kit v2 (ref PE-402-4002).

Read pairs used for analysis matched the following criteria: all 16 bases of the first read had quality scores of at least 10 and the first 6 bases correspond exactly to a designed well-specific barcode. The second reads were aligned to RefSeq human mRNA sequences (hg19) using bwa version 0.7.4 with non-default parameter “-l 24”. Reads mapping to several positions into the genome were filtered out from the analysis. DGE profiles were generated by counting for each sample the number of unique UMIs associated with each RefSeq genes. DGE-sequenced samples were acquired from three sequencing runs. Batch effects were corrected with the limma library function “removeBatchEffect”. All sequenced samples were retained for further analysis.

DESeq2 was used to normalize expression with the DESeq function⁵⁴. Normalized counts were transformed with vst (variance stabilized transformation) function from DESeq library. This log-like transformation was used for variance analysis.

Batch effects were corrected with the limma library function “removeBatchEffect”. All sequenced samples were retained for further analysis. This represents 78 samples cultured from passage 1 to 40 (Supplementary Table 1) in following media: 26 from T2iLG0, 26 RSet, 9 KSR+FGF2, 5 mTESR, 4 fibroblasts and 8 E7.

Samples assignment of single-cell RNA-seq data. Single-cell samples used in epiblast–hESC comparisons came from two data sets: the first was a subset of 52 hESCs from our own RNA-sequencing, the second was 104 cells from Petropoulos et al.¹². E4 samples were labeled as morula; epiblast cells were labeled from E5 and E6 blastocysts, after a filtering of cells expressing epiblast markers (Supplementary Table 4). Blastocysts from Yan et al.¹¹ were clustered by preimplantation lineage markers (Supplementary Table 4), and a cluster of 5 cells were selected and annotated as epiblast. Two outliers were removed from cells annotated as morula.

For the analysis of KLF17, GATA2 and SOX17 expression profile over development time, samples were stratified per embryonic days. Trophectoderm, and inner cell mass cells were segregated by unsupervised clustering using known lineage markers (Supplementary Table 4). A second clustering was applied on inner cell mass cells to segregate epiblast and primitive endoderm.

Differential expression profiling. For the DGE-seq data set, differential expressed *p*-values were processed with DESeq2 and FDRs were estimated with Benjamini–Hochberg procedure. For single-cell data set, *p*-values and FDR were computed with ROTS⁵⁵. Genes with FDR < 0.05 and a fold change < 0.5 or > 2 were qualified as differential expressed for both data sets. Two-sided Fisher’s exact test was computed to test dependency between single-cell differentially expressed genes and DGE-seq differentially expressed genes with the contingency table found in Supplementary Table 5.

Processing of principal component analysis. PCAs were computed with R princomp functions from centered data and plotted with R library ggplot2. PCA from Fig. 1d were computed from four data sets: Yan et al.¹¹, Petropoulos et al.¹² and this paper (single-cell and Bulk DGE-seq data). Each data set was transformed into transcripts per million, quantile normalized and *z*-scored by row separately. The data sets were reunified on the 15,315 genes in common for PCA computing.

To generate Supplementary Fig. 2c, a PCA was made for each of the three sets of pathways from Supplementary Fig. 2b (Supplementary Data 2 Tables 3–8). Each single-cell or DGE-seq sample was projected on the first component of the 3 PCA, and the first component coordinates were used to generate the three-dimension graph.

Processing of heatmaps. Heatmaps were drawn with the library complexHeatmap with *z*-score of expression. Cluster trees were computed with pvclust⁵⁶ with correlation method as distance calculation and Ward criteria as construction method.

For expression profile of KEGG pathways, genes were ordered per fold changes.

Functional enrichment. topGO⁵⁷ was used to identify enriched GO terms (Supplementary Data 2 Tables 9–10). Enrichment was performed by comparing GO terms present in differentially expressed genes vs. the whole transcriptome data set. Three annotation databases of GO terms were used (org.Hs.eg.db): Molecular Function (MF), Biological Process (BP) and Cellular Component (CC). According to the reference manual, *p*-values were computed with the “classic” and “elim” method algorithm parameter and “Fisher” as statistic parameter.

A gene set analysis method GAGE⁵⁸ was used with KEGG database to identify differentially regulated pathways. Pathways with FDR < 0.01 were retained for further analysis. Gage was used on unpaired mode with parameter “same dir” in false mode.

Quantification and statistical analysis. All data presented are representative of at least three independent experiments that yielded similar results. Statistical analyses were performed using the software Prism (Graphpad) or R.

DESeq2 was used for analysis considering RNA-seq data were following a negative binomial distribution. Other statistical tests were performed considering their specific assumption and hypothesis, notably for Pearson correlation’s test of

Supplementary Fig. 3c and homogeneity χ^2 tests of Fig. 5b, c. All graphical representations were chosen to accurately display variation within each group.

For each experiment, sampling was done to have comfortable group size that provide statistically robust results. For each figure and statistical analysis from RNA-seq data, size of each group is listed in the Supplementary Table 6.

Data and software availability. The authors declare that all data supporting the findings of this study are available within the article and its supplementary information files or from the corresponding author upon reasonable request.

The raw read sequence data and sample annotations generated for this paper are available at European Nucleotide Archive (ENA) with accession number PRJEB18663.

Received: 16 August 2017 Accepted: 27 October 2017

Published online: 24 January 2018

References

- Nichols, J. & Smith, A. Naive and primed pluripotent states. *Cell Stem Cell* **4**, 487–492 (2009).
- Weinberger, L., Ayyash, M., Novershtern, N. & Hanna, J. H. Dynamic stem cell states: naive to primed pluripotency in rodents and humans. *Nat. Rev. Mol. Cell Biol.* **17**, 155–169 (2016).
- Chen, H. et al. Reinforcement of STAT3 activity reprogrammes human embryonic stem cells to naive-like pluripotency. *Nat. Commun.* **6**, 7095 (2015).
- Chan, Y. S. et al. Induction of a human pluripotent state with distinct regulatory circuitry that resembles preimplantation epiblast. *Cell Stem Cell* **13**, 663–675 (2013).
- Gafni, O. et al. Derivation of novel human ground state naive pluripotent stem cells. *Nature* **504**, 282–286 (2013).
- Valamehr, B. et al. Platform for induction and maintenance of transgene-free hiPSCs resembling ground state pluripotent stem cells. *Stem Cell Rep.* **2**, 366–381 (2014).
- Takashima, Y. et al. Resetting transcription factor control circuitry toward ground-state pluripotency in human. *Cell* **158**, 1254–1269 (2014).
- Theunissen, T. W. et al. Systematic Identification of culture conditions for induction and maintenance of naive human pluripotency. *Cell Stem Cell* **15**, 471–487 (2014).
- Ware, C. B. et al. Derivation of naive human embryonic stem cells. *Proc. Natl. Acad. Sci. USA* **111**, 4484–4489 (2014).
- Blakeley, P. et al. Defining the three cell lineages of the human blastocyst by single-cell RNA-seq. *Development* **142**, 3151–3165 (2015).
- Yan, L. et al. Single-cell RNA-Seq profiling of human preimplantation embryos and embryonic stem cells. *Nat. Struct. Mol. Biol.* **20**, 1131–1139 (2013).
- Petropoulos, S. et al. Single-Cell RNA-Seq reveals lineage and X chromosome dynamics in human preimplantation embryos. *Cell* **165**, 1012–1026 (2016).
- Guo, H. et al. The DNA methylation landscape of human early embryos. *Nature* **511**, 606–610 (2014).
- Smith, Z. D. et al. DNA methylation dynamics of the human preimplantation embryo. *Nature* **511**, 611–615 (2014).
- Vallot, C. et al. XACT noncoding RNA competes with XIST in the control of X chromosome activity during human early development. *Cell Stem Cell* **20**, 102–111 (2017).
- De Los Angeles, A. et al. Hallmarks of pluripotency. *Nature* **525**, 469–478 (2015).
- Pastor, W. A. et al. Naive human pluripotent cells feature a methylation landscape devoid of blastocyst or germline memory. *Cell Stem Cell* **18**, 323–329 (2016).
- Sahakyan, A. et al. Human naive pluripotent stem cells model X chromosome dampening and X inactivation. *Cell Stem Cell* **20**, 87–101 (2016).
- Guo, G. et al. Naive pluripotent stem cells derived directly from isolated cells of the human inner cell mass. *Stem Cell Rep.* **6**, 437–446 (2016).
- Collier, A. J. et al. Comprehensive cell surface protein profiling identifies specific markers of human naive and primed pluripotent states. *Cell Stem Cell* **20**, 874–890 e877 (2017).
- Okita, K., Ichisaka, T. & Yamanaka, S. Generation of germline-competent induced pluripotent stem cells. *Nature* **448**, 313–317 (2007).
- Maherali, N. et al. Directly reprogrammed fibroblasts show global epigenetic remodeling and widespread tissue contribution. *Cell Stem Cell* **1**, 55–70 (2007).
- Wernig, M. et al. In vitro reprogramming of fibroblasts into a pluripotent ES-cell-like state. *Nature* **448**, 318–324 (2007).
- Ying, Q. L. et al. The ground state of embryonic stem cell self-renewal. *Nature* **453**, 519–523 (2008).
- Guo, G. et al. Epigenetic resetting of human pluripotency. *Development* **144**, 2748–2763 (2017).

26. Choi, J. et al. DUSP9 modulates DNA hypomethylation in female mouse pluripotent stem cells. *Cell Stem Cell* **20**, 706–719 e707 (2017).
27. Cacchiarelli, D. et al. Integrative analyses of human reprogramming reveal dynamic nature of induced pluripotency. *Cell* **162**, 412–424 (2015).
28. Soumillon, M., Cacchiarelli, D. & Semrau, S. Characterization of directed differentiation by high-throughput single-cell RNA-Seq. Preprint at *bioRxiv* <https://www.biorxiv.org/content/early/2014/03/05/003236> (2014)
29. Niakan, K. K., Han, J., Pedersen, R. A., Simon, C. & Pera, R. A. Human pre-implantation embryo development. *Development* **139**, 829–841 (2012).
30. Theunissen, T. W. et al. Molecular criteria for defining the naive human pluripotent state. *Cell Stem Cell* **19**, 502–515 (2016).
31. Ogata, H. et al. KEGG: Kyoto encyclopedia of genes and genomes. *Nucleic Acids Res.* **27**, 29–34 (1999).
32. Gu, W. et al. Glycolytic metabolism plays a functional role in regulating human pluripotent stem cell state. *Cell Stem Cell* **19**, 476–490 (2016).
33. Durruthy-Durruthy, J. et al. Spatiotemporal reconstruction of the human blastocyst by single-cell gene-expression analysis informs induction of naive pluripotency. *Dev. Cell* **38**, 100–115 (2016).
34. Okamoto, I. et al. Eutherian mammals use diverse strategies to initiate X-chromosome inactivation during development. *Nature* **472**, 370–374 (2011).
35. Vallot, C. et al. Erosion of X chromosome inactivation in human pluripotent cells initiates with XACT coating and depends on a specific heterochromatin landscape. *Cell Stem Cell* **16**, 533–546 (2015).
36. Mekhoubad, S. et al. Erosion of dosage compensation impacts human iPSC disease modeling. *Cell Stem Cell* **10**, 595–609 (2012).
37. Patel, S. et al. Human embryonic stem cells do not change their X inactivation status during differentiation. *Cell Rep.* **18**, 54–67 (2017).
38. Smith, A. Formative pluripotency: the executive phase in a developmental continuum. *Development* **144**, 365–373 (2017).
39. Buecker, C. et al. A murine ESC-like state facilitates transgenesis and homologous recombination in human pluripotent stem cells. *Cell Stem Cell* **6**, 535–546 (2010).
40. Wu, J. et al. Interspecies chimerism with mammalian pluripotent stem cells. *Cell* **168**, 473–486 e415 (2017).
41. Yang, Y. et al. Derivation of pluripotent stem cells with in vivo embryonic and extraembryonic potency. *Cell* **169**, 243–257 e225 (2017).
42. von Meyenn, F. et al. Comparative principles of DNA methylation reprogramming during human and mouse in vitro primordial germ cell specification. *Dev. Cell* **39**, 104–115 (2016).
43. Daley, G. Q. et al. Setting global standards for stem cell research and clinical translation: the 2016 ISSCR guidelines. *Stem Cell Rep.* **6**, 787–797 (2016).
44. Alpha Scientists in Reproductive Medicine and ESHRE Special Interest Group of Embryology. The Istanbul consensus workshop on embryo assessment: proceedings of an expert meeting. *Hum. Reprod.* **26**, 1270–1283 (2011).
45. Samavarchi-Tehrani, P. et al. Functional genomics reveals a BMP-driven mesenchymal-to-epithelial transition in the initiation of somatic cell reprogramming. *Cell Stem Cell* **7**, 64–77 (2010).
46. Picelli, S. et al. Full-length RNA-seq from single cells using Smart-seq2. *Nat. Protoc.* **9**, 171–181 (2014).
47. Picelli, S. et al. Smart-seq2 for sensitive full-length transcriptome profiling in single cells. *Nat. Methods* **10**, 1096–1098 (2013).
48. Trombetta, J. J. et al. Preparation of single-cell RNA-Seq libraries for next generation sequencing. *Curr. Protoc. Mol. Biol.* **107**, 4 22 21–17 (2014).
49. Trapnell, C. et al. Differential gene and transcript expression analysis of RNA-seq experiments with TopHat and Cufflinks. *Nat. Protoc.* **7**, 562–578 (2012).
50. Langmead, B. & Salzberg, S. L. Fast gapped-read alignment with Bowtie 2. *Nat. Methods* **9**, 357–359 (2012).
51. Anders, S., Pyl, P. T. & Huber, W. HTSeq—a Python framework to work with high-throughput sequencing data. *Bioinformatics* **31**, 166–169 (2015).
52. Lun, A. T., McCarthy, D. J. & Marioni, J. C. A step-by-step workflow for low-level analysis of single-cell RNA-seq data with Bioconductor. *F1000Res* **5**, 2122 (2016).
53. Robinson, M. D., McCarthy, D. J. & Smyth, G. K. edgeR: a Bioconductor package for differential expression analysis of digital gene expression data. *Bioinformatics* **26**, 139–140 (2010).
54. Love, M. I., Huber, W. & Anders, S. Moderated estimation of fold change and dispersion for RNA-seq data with DESeq2. *Genome Biol.* **15**, 550 (2014).
55. Suomi, T., Seyednasrollah, F., Jaakkola, M. K., Faux, T. & Elo, L. L. ROTS: An R package for reproducibility-optimized statistical testing. *PLoS Comput. Biol.* **13**, e1005562 (2017).
56. Suzuki, R. & Shimodaira, H. Pvcust: an R package for assessing the uncertainty in hierarchical clustering. *Bioinformatics* **22**, 1540–1542 (2006).
57. Alexa, A., Rahnenfuhrer, J. & Lengauer, T. Improved scoring of functional groups from gene expression data by decorrelating GO graph structure. *Bioinformatics* **22**, 1600–1607 (2006).
58. Luo, W., Friedman, M. S., Shedden, K., Hankenson, K. D. & Woolf, P. J. GAGE: generally applicable gene set enrichment for pathway analysis. *BMC Bioinformatics* **10**, 161 (2009).

Acknowledgements

We thank S. Bézine (UMR1064) and the following core facilities for their support: GenoBIRD, Cytocell, Micropicell, the Center of Excellence Nikon Nantes and iPSC core facility. We thank the “service de génétique médicale” of CHU de Nantes for the help with the karyotypes. This work was supported by “Paris Scientifique region Pays de la Loire: HUMPLURI” and IHU CESTI. S.K. is recipient of fellowships from Progreffe and Fondation pour la Recherche Médicale (FDT20160435459). D.M. is supported by FINOX Biotech FORWARD initiative. M.C. is supported by the “Who Am I?” Laboratory of Excellence #ANR-11-LABX-0071 funded by the French Government through its “Investments for the Future” program operated by the ANR under grant #ANR-11-IDEX-0005-01. L.F. is supported by the “Paris Scientifique region Pays de la Loire: TIPS” and LabEx IGO project (no. ANR-11-LABX-0016-01) funded by the «Investissements d’Avenir» French Government program, managed by the French National Research Agency (ANR). Milieu Interieur is supported by the French government’s Invest in the Future Program (ANR, reference 10-LABX-69-01). Research in the Pasque lab is supported by The Research Foundation – Flanders (FWO) (Odysseus Return Grant G0F7716N) and KU Leuven Research Fund (BOFZAP starting grant StG/15/021BF, C1 grant C14/16/077 and project financing PF/10/019). We thank Pr A. Smith and Dr G. Guo (Wellcome Trust-MRC Stem Cell Institute, University of Cambridge, UK) for providing HNES1 mRNA and sharing their protocols. L.Q.-M. and M.L.A. are co-coordinators of the Milieu Intérieur consortium. We thank Dr C. Hirsh (University of Toronto, Canada) for critical review of the manuscript.

Author contributions

S.K. and L.D. designed the study, with input from T.M., T.F., V.P., C.L.C., C.P., M.S., R.R. and J.B. S.K., D.M., C.R. and L.D. wrote the manuscript with input from all authors. A.R. and J.L. manipulated human embryos. D.M., Y.L. and E.C. performed bioinformatics analysis. S.K., D.M., C.C., A.R., A.G., C.V., A.D., M.S., W.D., S.N., M.C., J.S. and L.D. performed experiments. T.F. and P.B. supervised human embryo donation. All authors approved the final version of the manuscript.

Additional information

Supplementary Information accompanies this paper at <https://doi.org/10.1038/s41467-017-02107-w>.

Competing interests: The authors declare no competing financial interests.

Reprints and permission information is available online at <http://npg.nature.com/reprintsandpermissions/>

Publisher’s note: Springer Nature remains neutral with regard to jurisdictional claims in published maps and institutional affiliations.



Open Access This article is licensed under a Creative Commons Attribution 4.0 International License, which permits use, sharing, adaptation, distribution and reproduction in any medium or format, as long as you give appropriate credit to the original author(s) and the source, provide a link to the Creative Commons license, and indicate if changes were made. The images or other third party material in this article are included in the article’s Creative Commons license, unless indicated otherwise in a credit line to the material. If material is not included in the article’s Creative Commons license and your intended use is not permitted by statutory regulation or exceeds the permitted use, you will need to obtain permission directly from the copyright holder. To view a copy of this license, visit <http://creativecommons.org/licenses/by/4.0/>.

© The Author(s) 2018

Stéphanie Kilens^{1,2,3}, Dimitri Meistermann^{1,2,3,4}, Diego Moreno^{1,2,3}, Caroline Chariou⁵, Anne Gaignerie⁵, Arnaud Reignier^{1,2,3,6}, Yohann Lelièvre⁴, Miguel Casanova⁷, Céline Vallot⁷, Steven Nedellec⁸, Léa Flippe^{1,2,3}

Julie Firmin^{1,2,3,6}, Juan Song⁹, Eric Charpentier¹⁰, Jenna Lammers^{1,2,3,6}, Audrey Donnart¹⁰, Nadège Marec¹¹, Wallid Deb¹², Audrey Bihouée¹⁰, The Milieu Intérieur Consortium, Cédric Le Caignec^{12,13}, Claire Pecqueur¹⁴, Richard Redon^{10,15}, Paul Barrière^{1,2,3,6}, Jérémie Bourdon⁴, Vincent Pasque⁹, Magali Soumillon^{16,17}, Tarjei S. Mikkelsen^{16,18}, Claire Rougeulle⁷, Thomas Fréour^{1,2,3,6} & Laurent David^{1,2,3,5}

¹Centre de Recherche en Transplantation et Immunologie UMR1064, INSERM, Université de Nantes, Nantes, France. ²Institut de Transplantation Urologie Néphrologie (ITUN), CHU Nantes, Nantes, France. ³LabEx IGO “Immunotherapy, Graft, Oncology”, Nantes, France. ⁴Laboratoire des Sciences du Numérique de Nantes, LS2N, UMR CNRS 6004, Université de Nantes, Nantes, France. ⁵INSERM UMS 016, SFR Francois Bonamy, iPSC Core Facility, Nantes, France; CNRS, UMS 3556, Nantes, France; Université de Nantes, Nantes, France; CHU Nantes, Nantes, France. ⁶CHU Nantes, Service de Biologie de la Reproduction, Nantes, France. ⁷Sorbonne Paris Cité, Epigenetics and Cell Fate, UMR 7216 CNRS, Université Paris Diderot, Paris, France. ⁸INSERM UMS 016, SFR Francois Bonamy, MicroPicell Core Facility, Nantes, France; CNRS, UMS 3556, Nantes, France; Université de Nantes, Nantes, France; CHU de Nantes, Nantes, France. ⁹KU Leuven—University of Leuven, Department of Development and Regeneration, Stem Cell Biology and Embryology Unit, Leuven Stem Cell Institute, Herestraat 49, B-3000 Leuven, Belgium. ¹⁰INSERM UMR1087, CNRS UMR6291 Université de Nantes l’institut du thorax, Nantes, France. ¹¹INSERM, UMS 016, SFR Francois Bonamy Cytocell Core Facility, Nantes, France; CNRS, UMS 3556, Nantes, France; Université de Nantes, Nantes, France; CHU Nantes, Nantes, France. ¹²CHU Nantes, Service de génétique médicale, Nantes, France. ¹³INSERM, UMR1238, Bone Sarcoma and Remodeling of Calcified Tissue, Nantes, France. ¹⁴CRCINA, INSERM, Université de Nantes, Nantes, France. ¹⁵CHU Nantes, l’institut du thorax, Nantes, France. ¹⁶Department of Stem Cell and Regenerative Biology, Harvard University, Cambridge, MA, 02138, USA; Broad Institute, Cambridge, MA 02142, USA.; Harvard Stem Cell Institute, Harvard University, Cambridge, MA 02138, USA. ¹⁷Present address: Berkeley Lights Inc., 5858 Horton Street, Emeryville, CA 94608, USA. ¹⁸Present address: 10x Genomics, 7068 Koll Center Pkwy #401, Pleasanton, CA 94566, USA. Stéphanie Kilens and Dimitri Meistermann contributed equally to this work. A full list of consortium members appears at the end of the paper.

The Milieu Intérieur Consortium

Laurent Abel¹⁹, Andres Alcover²⁰, Kalla Astrom²¹, Philippe Bousso²², Pierre Bruhns²³, Ana Cumano²⁴, Darragh Duffy²⁵, Caroline Demangel²⁶, Ludovic Deriano²⁷, James Di Santo²⁸, Françoise Dromer²⁹, Gérard Eberl³⁰, Jost Enninga³¹, Jacques Fellay³², Antonio Freitas³³, Odile Gelpi³⁴, Ivo Gomperts-Boneca³⁵, Serge Hercberg³⁶, Olivier Lantz³⁷, Claude Leclerc³⁸, Hugo Mouquet³⁹, Etienne Patin⁴⁰, Sandra Pellegrini⁴¹, Stanislas Pol⁴², Lars Rogge⁴³, Anavaj Sakuntabhai⁴⁴, Olivier Schwartz⁴⁵, Benno Schwikowski⁴⁰, Spencer Shorte⁴⁶, Vassili Soumelis⁴⁷, Frédéric Tangy⁴⁸, Eric Tartour⁴⁹, Antoine Toubert⁵⁰, Marie-Noëlle Ungeheuer⁵¹, Lluís Quintana-Murci⁵² & Matthew L. Albert²⁵

¹⁹Laboratory of Human Genetics of Infectious Diseases, Necker Branch, INSERM U1163, Paris, France. ²⁰Institut Pasteur, Department of Immunology, Lymphocyte Cell Biology Unit, Paris, France. ²¹Department of Clinical Pathology and Cytology, Karolinska University Hospital, Stockholm, Sweden. ²²Institut Pasteur, Dynamics of Immune Responses Unit, 75015 Paris, France. ²³Unit of Antibodies in Therapy and Pathology, Department of Immunology, Institut Pasteur, Paris, France. ²⁴Unit for Lymphopoiesis, Immunology Department, Pasteur Institute, Paris, France. ²⁵Laboratory of Dendritic Cell Immunobiology, Department of Immunology, Institut Pasteur, 75015, Paris, France; INSERM U1223, 75015 Paris, France; Center for Translational Research, Institut Pasteur, 75015 Paris, France. ²⁶Immunobiology of Infection Unit, Institut Pasteur, 75015 Paris, France. ²⁷Genome Integrity, Immunity and Cancer Unit, Department of Immunology, Paris, France; Department of Genomes and Genetics, Institut Pasteur, 75015 Paris, France. ²⁸Innate Immunity Unit, Institut Pasteur, INSERM, U1223 Paris, France. ²⁹Institut Pasteur, Department of Mycology, Molecular Mycology-CNRS URA3012, Paris, France. ³⁰Unité Microenvironnement and Immunity, Institut Pasteur, 75724 Paris, France. ³¹Department of Cell Biology and Infection, Institut Pasteur, Paris, France. ³²Global Health Institute, School of Life Sciences, École Polytechnique Fédérale de Lausanne, Lausanne, Switzerland. ³³Unité de Biologie des Populations Lymphocytaires, Department of Immunology Institut Pasteur, and Centre National pour la Recherche Scientifique, URA1961, 75724 Paris, France. ³⁴Center for Translational Research, Institut Pasteur, Paris, France. ³⁵Institut Pasteur, Unité Biologie et génétique de la paroi bactérienne, Dept. Microbiologie, Paris, France. ³⁶Université Paris 13, Sorbonne Paris Cité, Equipe de Recherche en Épidémiologie Nutritionnelle, Centre de Recherche en Épidémiologies et Biostatistiques, Inserm (U1153), Inra (U1125), Cnam, F-93017 Bobigny, France. ³⁷Laboratoire d’immunologie clinique, CIC-4218 et Unité INSERM 932, Institut Curie, Paris, France. ³⁸Institut Pasteur, Unité de Régulation Immunitaire et Vaccinologie, Paris, France. ³⁹Laboratory of Humoral Response to Pathogens, Department of Immunology, Institut Pasteur, INSERM U1222, 75015 Paris, France. ⁴⁰Center of Bioinformatics Biostatistics, and Integrative Biology, Institut Pasteur, 75015 Paris, France. ⁴¹Institut Pasteur, Unit of Cytokine Signaling, Paris, France. ⁴²Université Paris Descartes et Département d’hépatologie, Groupe Hospitalier Cochin Hôtel-Dieu, Paris, France. ⁴³Immunoregulation Unit, Institut Pasteur, 75724 Paris, France. ⁴⁴Functional Genetics of Infectious Diseases Unit, Department of Genomes and Genetics, Institut Pasteur, 75015 Paris, France. ⁴⁵Virus & Immunity Unit, Department of Virology, Institut Pasteur, Paris, France. ⁴⁶Institut Pasteur, Imagopole-CITech, 75015 Paris, France. ⁴⁷PSL Research University, INSERM U932, Institut Curie, Paris, France. ⁴⁸Unité de Génomique Virale et Vaccination, Institut Pasteur, CNRS UMR3569, Paris, France. ⁴⁹Department of Immunology, Hôpital Européen Georges Pompidou, Paris, France. ⁵⁰INSERM UMR1160, Université Paris Diderot, AP-HP, Hôpital St Louis, Paris, France. ⁵¹Center for Translational Research, ICAREB Platform, Center for Translational Research, Institut Pasteur, Paris, France. ⁵²Laboratory of Human Evolutionary Genetics, Department of Genomes and Genetics, Institut Pasteur, Paris, 75015, France; CNRS URA3012, Paris 75015, France

Development of automated annotation software for human embryo morphokinetics

M. Feyeux^{1,3,†}, A. Reignier^{1,2,†}, M. Mocaer¹, J. Lammers^{1,2},
D. Meistermann¹, P. Barrière^{1,2}, P. Paul-Gilloteaux^{3,§}, L. David^{1,3,§}, and
T. Fréour^{1,2,*,§}

¹Nantes Université, Inserm, Centre de Recherche en Transplantation et immunologie, Unité mixte de recherche 1064, Institut de Transplantation Urologie Néphrologie, F-44000 Nantes, France ²Service de Médecine et Biologie du Développement et de la Reproduction, CHU Nantes, Nantes Université, Nantes, France ³Université de Nantes, Centre Hospitalier Universitaire Nantes, Inserm, CNRS, Structure Fédérative de Recherche en Santé Santé, Inserm Unité Mixte de Service 016, CNRS UMS 3556, F-44000 Nantes, France

*Correspondence address. Service de Médecine et Biologie du Développement et de la Reproduction, CHU de Nantes, 38 Boulevard Jean Monnet, Nantes, France. Tel: +33-240083234; Fax: +33-240083228; E-mail: thomas.freour@chu-nantes.fr

Submitted on August 7, 2019; resubmitted on December 26, 2019; editorial decision on January 9, 2020

STUDY QUESTION: Is it possible to develop an automated annotation tool for human embryo development in time-lapse devices based on image analysis?

SUMMARY ANSWER: We developed and validated an automated software for the annotation of human embryo morphokinetic parameters, having a good concordance with expert manual annotation on 701 time-lapse videos.

WHAT IS KNOWN ALREADY: Morphokinetic parameters obtained with time-lapse devices are increasingly used for the assessment of human embryo quality. However, their annotation is time-consuming and can be slightly operator-dependent, highlighting the need to develop fully automated approaches.

STUDY DESIGN, SIZE, DURATION: This monocentric study was conducted on 701 videos originating from 584 couples undergoing IVF with embryo culture in a time-lapse device. The only selection criterion was that the duration of the video must be over 60 h.

PARTICIPANTS/MATERIALS, SETTING, METHODS: An automated morphokinetic annotation tool was developed based on gray level coefficient of variation and detection of the thickness of the zona pellucida. The detection of cellular events obtained with the automated tool was compared with those obtained manually by trained experts in clinical settings.

MAIN RESULTS AND THE ROLE OF CHANCE: Although some differences were found when embryos were considered individually, we found an overall concordance between automated and manual annotation of human embryo morphokinetics from fertilization to expanded blastocyst stage ($r^2 = 0.92$).

LIMITATIONS, REASONS FOR CAUTION: These results should undergo multicentric external evaluation in order to test the overall performance of the annotation tool. Getting access to the export of 3D videos would enhance the quality of the correlation with the same algorithm and its extension to the 3D regions of interest. A technical limitation of our work lies within the duration of the video. The more embryo stages the video contains, the more information the script has to identify them correctly.

WIDER IMPLICATIONS OF THE FINDINGS: Our system paves the way for high-throughput analysis of multicentric morphokinetic databases, providing new insights into the clinical value of morphokinetics as a predictor of embryo quality and implantation.

STUDY FUNDING/COMPETING INTEREST(S): This study was partly funded by Finox-Gedeon Richter Forward Grant 2016 and NeXT (ANR-16-IDEX-0007). We have no conflict of interests to declare.

TRIAL REGISTRATION NUMBER: N/A

Key words: IVF / time-lapse imaging / automation / morphokinetics / computer-assisted diagnosis / embryonic development / embryo culture techniques

[†]The authors consider that the first two authors should be regarded as joint first authors.

[§]The authors consider that the last three authors should be regarded as senior authors.

© The Author(s) 2020. Published by Oxford University Press on behalf of the European Society of Human Reproduction and Embryology. All rights reserved. For permissions, please e-mail: journals.permissions@oup.com

Introduction

IVF has greatly improved over the past two decades. However, success rates are still not optimal and often variable across centers and countries, with multiple pregnancies still being an issue (European IVF-monitoring Consortium *et al.*, 2017). This situation is partially explained by the current limitations of embryo quality assessment methods. In fact, morphological assessment remains the most common method to evaluate embryo implantation potential and still suffers from a lack of predictive power despite the implementation of well-defined consensus guidelines (Alpha Scientists in Reproductive Medicine and ESHRE Special Interest Group of Embryology, 2011). Although embryo morphology on the day of transfer has been shown to be correlated with the outcome of the IVF cycle (Rhenman *et al.*, 2015), it has also been demonstrated that this evaluation suffered from a lack of inter- and intra-observer reproducibility (Paternot *et al.*, 2009) and was not correlated to embryo ploidy (Capalbo *et al.*, 2014).

Promoting single embryo transfer implies the availability of accurate and relevant strategies to identify embryos with the best chance to implant (Kushnir *et al.*, 2017). Various technologies, either invasive or non-invasive, have been developed over the past decade in order to improve embryo quality assessment *in vitro*, such as preimplantation genetic testing (Gardner *et al.*, 2015) or metabolomics (Sanchez *et al.*, 2017) with encouraging results, but also with some limitations such as cost, regulatory constraints and lack of clinical validation.

Time-lapse monitoring (TLM) systems allow continuous and dynamic annotation of individual embryo development while maintaining optimal culture conditions (Basile *et al.*, 2015; Castelló *et al.*, 2016), bringing opportunities for personalized medicine approaches in IVF. The data generated are called morphokinetic parameters, as they combine morphological features and kinetic evaluation of embryo development. Since the first commercial devices became available in 2010, this technology has been implemented in many IVF laboratories for routine embryo culture and selection. It was recently reported that 17% of the US IVF laboratories possessed at least one TLM system in 2017 (Dolinko *et al.*, 2017). This promising technology aims at correlating morphological features and kinetic parameters, such as the timing of cellular cleavages or intervals, with embryo implantation potential (Ciray *et al.*, 2014). To date, eight randomized controlled trials have evaluated the relevance of using morphokinetic parameters to select the embryo with the best chance of achieving pregnancy, with various results, in line with heterogeneous design and outcomes (Armstrong *et al.*, 2018).

Most TLM systems allow the individual monitoring of embryo development and its manual annotation. Thus, trained operators have to regularly annotate morphokinetic parameters for each embryo in culture, which can be time-consuming, depending on the number of cultured embryos and on the number of morphokinetic parameters annotated for each embryo. Moreover, the manual annotation of embryo developmental events can be impacted by inter-operator and inter-laboratory variability (Chen *et al.*, 2013; Sundvall *et al.*, 2013; Martínez-Granados *et al.*, 2017), preventing robust and high-throughput, multicentric database analysis. However, embryo annotations through TLM systems continue to be performed manually and suffer from the same inter-operator variability as microscopic observation (Martínez-Granados *et al.*, 2017). In addition, the type of TLM system can contribute to increasing embryo annotation discrepancies. Automated

annotation of embryo morphokinetic parameters could theoretically tackle these two issues, leading to improved workflow, high-throughput analysis and lower subjectivity. To our knowledge, only one pilot study reported the setup of a semi-automated script based on image analysis annotating of embryo morphokinetic parameters in humans (Mölder *et al.*, 2015). This script was, however, tested on a very limited population (39 embryos) and was limited to a proof of concept. Here, we have improved the method and enhanced its robustness and detection power.

The purpose of this study was to test the performance of a new fully automated tool (called 'Kinetembryo') for the annotation of embryo morphokinetic parameters obtained with a commercially available time-lapse incubation device on human embryos.

Materials and Methods

Design

This monocentric study was conducted in a university-based fertility center with data from unselected couples referred for ICSI and whose embryos were cultured in the Embryoscope® (Vitrolife, Sweden) between 16 February 2011 and 01 January 2017. The videos of embryo development used in this study were randomly extracted from the database. The only selection criterion was the duration of the video that must be over 60 h. In order to evaluate the performance of our method and software, we compared the morphokinetic annotation performed manually, as detailed below, with the automatic output of Kinetembryo on the same videos. All patients gave their consent for anonymous use of their data registered in this database. This project was approved by the local Institutional Review Board (Groupe Nantais d'Ethique dans le Domaine de la Santé). All patients underwent controlled ovarian stimulation with an antagonist protocol, as described in a previous study (Fréour *et al.*, 2015).

Embryology procedures

ICSI and embryo culture were performed as described previously (Fréour *et al.*, 2015) at 37°C under controlled atmosphere with low oxygen pressure (5% O₂, 6% CO₂). Sequential media were used for embryo culture (G1plus® and G2plus®, Vitrolife). Images were captured on seven focal planes at 10 min intervals using a Hoffman modulation contrast optical setup (Hoffman, 1977) and a 635 nm LED as light source as provided in the Embryoscope®. The resolution of the camera is 1280 × 1024 pixels. Two embryologists, who had already performed most of the embryo annotations at this center, retrospectively re-annotated all database entries since 2011 strictly according to Ciray *et al.* (2014). In order to harmonize annotation, this re-annotation was performed by the two embryologists at the same time, agreeing between themselves for all the annotation points. They re-annotated hundreds of videos in duet before prospectively and separately annotating the new cycles. As an internal quality control process, both embryologists annotated the same 10 videos and compared their results every 3 months. In case of more than 20 minutes (two images) discrepancy in the results, the videos were watched again and discussed in detail in order to keep inter-operator variability as low as possible. The term tPNf was used to describe pronuclei fading. The terms t2, t3, t4, t5, t6, t7, t8 and t9⁺ were, respectively, used for

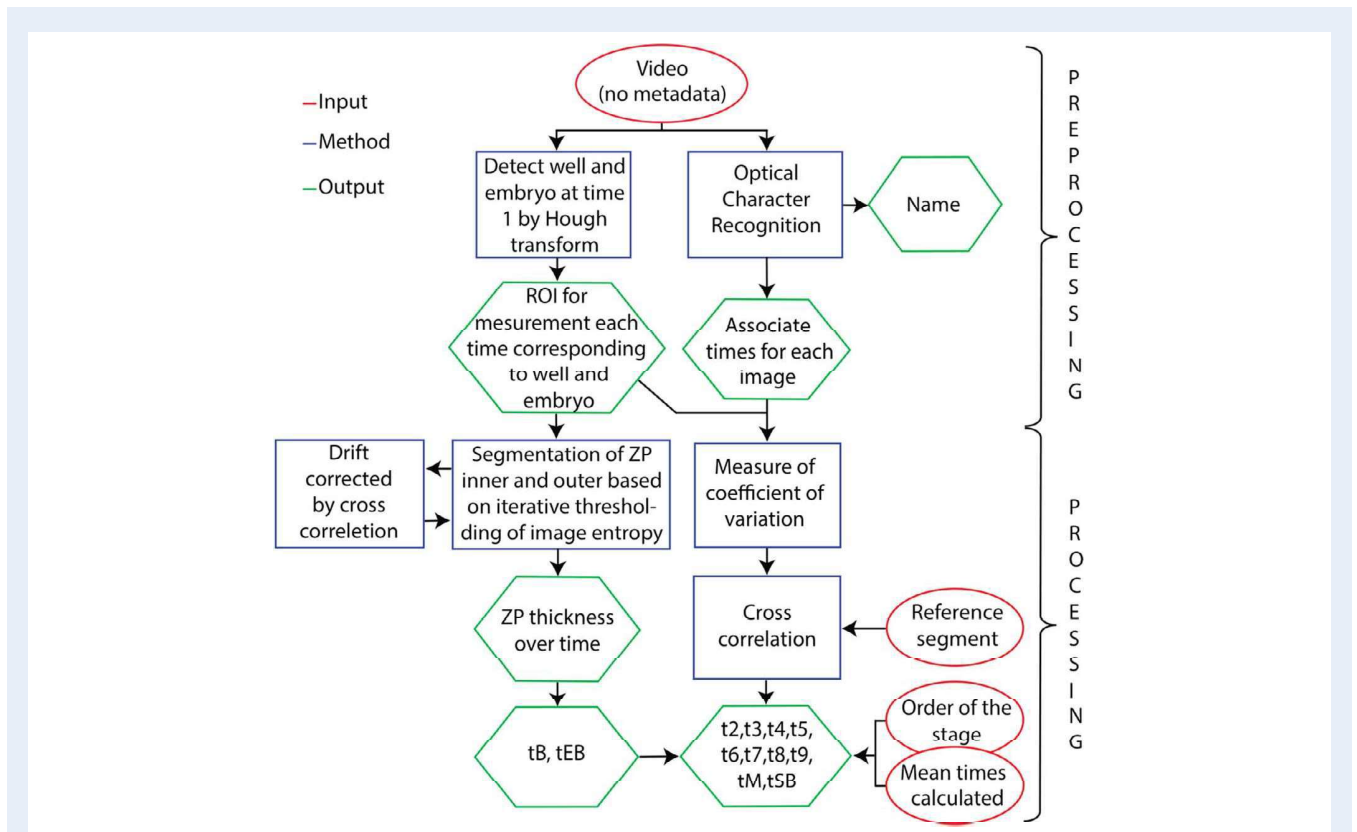


Figure 1 Schematic representation of the process used to develop the automated annotation tool. ROI: region of interest; ZP: zona pellucida; the terms t2, t3, t4, t5, t6, t7, t8 and t9+ refer to the exact timings of blastomere cleavage resulting in 2, 3, 4, 5, 6, 7, 8 and 9 well-defined blastomeres; tM refers to a fully compacted morula; tSB refers to the onset of a cavity formation; tB refers to full blastocyst (i.e. the last frame before ZP starts to thin); tEB refers to expanded blastocyst (i.e. when the ZP is 50% thinned).

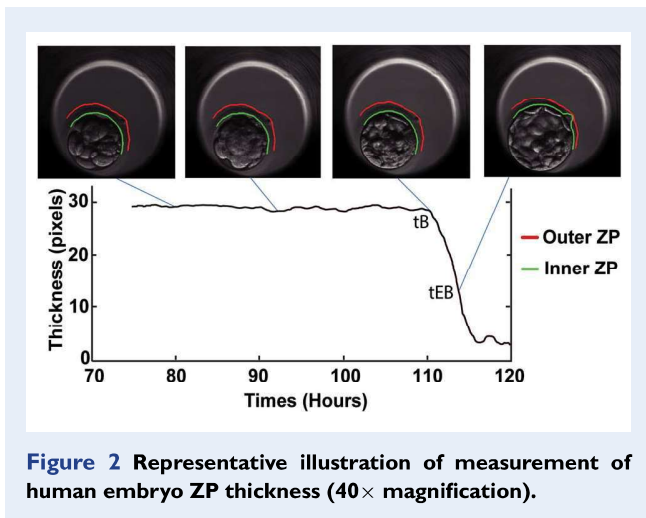
exact timings of blastomere cleavage resulting in 2, 3, 4, 5, 6, 7, 8 and 9 well-defined blastomeres. The term tM referred to a fully compacted morula. At the blastocyst stage, tSB was used to describe the onset of a cavity formation, tB was used for full blastocyst, i.e. the last frame before the zona pellucida (ZP) starts to thin and tEB for expanded blastocyst, i.e. when the ZP is 50% thinned.

Development of an automated annotation tool

The pipeline that we propose mainly consists of two steps: a preprocessing step and an automatic annotation (processing) step (Fig. 1). It was implemented as a stand-alone software written with Matlab®, the mathworks® (Natick, MA, USA), R2016a, with the image processing and the parallel toolboxes. The input of the pipeline is the videos generated by the TLM system, in our case the Embryoscope®, which are 2D videos taken in the optimal in-focus plane of acquisition. The preprocessing step consists of extracting metadata and region of interest (ROI). Note that the video reference name and acquisition times are directly printed on the videos. For this reason, Kinetembryo first propose an optical character recognition to extract the exact time of each frame of the video and the reference name of the video. The ROI for the measurement are then automatically extracted on the first frame: the well and the embryo cell are detected automatically by

Hough transform. The position of this ROI is then tracked over time by image cross correlation in order to correct for any drift.

The annotation step consisted of two main tasks. The first task allowed detection of tB and tEB. The ZP was segmented by an iterative automatic bi-thresholding method applied to the entropy image of each frame. This entropy-based segmentation allowed the operator to identify the inner and outer ZP, and consequently to track its thickness over time. Based on the expert definition (Ciray *et al.*, 2014) of tB and tEB, these two stage time points can then be automatically derived from the ZP thickness curve (Fig. 2). The second task consists of identifying earlier events, i.e. t1–t9, tM and tSB. The approach used for automated detection of cellular cleavages was inspired from a recent study that used the standard deviation of normalized gray levels of images as descriptors of embryo content (Mölder *et al.*, 2015). In our work, we measured the gray-level coefficient of variation (CV) of intensity into the tracked embryo ROI, giving a curve of variation over time (Fig. 3). The different key stages of embryo development are derived from this curve. First, we created a template curve of gray-level CV based on the mean of three curves obtained with reference videos, i.e. regular and ideal embryo development, no fragmentation, no variation of luminosity, no shift in embryo position. As the same template curve was used for the analysis of all videos and the algorithm has no stochastic aspect, the same code launched on the same data is always reproducible and gives the same result. Every stage of interest was then looked for

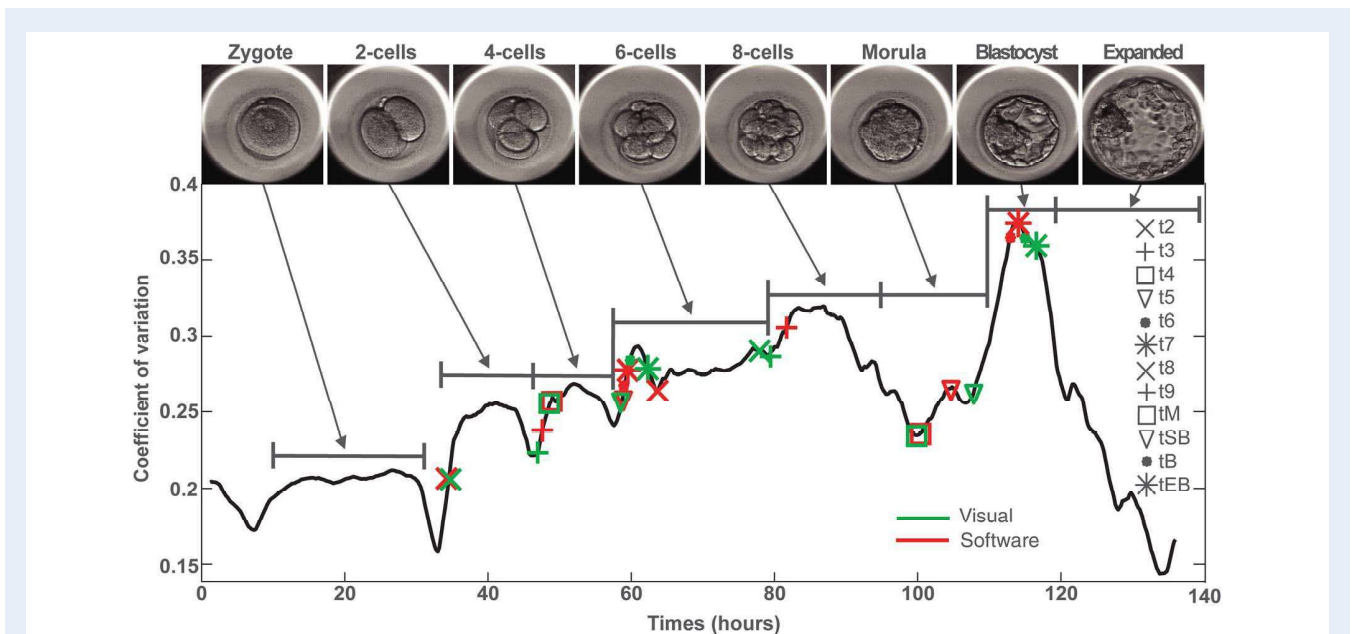


by cross-correlating the part of the template corresponding to the stage of interest within a search windows corresponding to average time ± 3 SD calculated for a database of measurements on 16 000 embryos annotated in our local database. For example, the search of t2 was constrained on a window centered at 30 hours post-fertilization ± 24 hours, since standard deviation was 8 hours. A global optimization of the cross correlation was then performed based on the knowledge of stage ordering and shape of the curve. The biological and mathematical rules used in the software are listed in the [Supplementary Data](#). A metric measure by statistical analysis was used to exclude very bad quality images, such as blurred images and the ones with insufficient brightness.

Validation of the automated annotation tool

In order to test the performance and the accuracy of this automated analysis process, we compared the results with the timings recorded by two users on a first set of 78 training videos before a validation step performed on a larger set of 701 individual videos (including the first 78 videos) extracted from the Embryoscope[®]. The video frames ranged from a minimum of zygote stage to a maximum of hatched blastocyst stage, including starting points at cleavage stage (thawed embryos) and chaotic developments. The normal distribution of the data was tested and rejected with the Shapiro–Wilk test. In order to evaluate concordance between software measures and expert measures and their reliability, the intra-class correlation coefficient (ICC) was calculated. The ICC form was chosen according to [Koo and Li \(2016\)](#). The ICC estimates and their 95% CI were calculated based on absolute agreement, using mixed effects and random effects models. [Fleiss \(1981\)](#) categorized the ICC values as follows: poor (<0.5), moderate (0.5–0.75), good (0.75–0.9) and excellent (>0.9) reliability. Bland–Altman curves with 95% concordance limits (mean difference ± 1.96 SD of the difference) were created for the measurement pairs in order to evaluate the agreement between the techniques ([Supplementary Fig. S1](#)). In order to evaluate the values of standard deviation that we observed between manual and automated annotations, they were compared with standard deviation values reported in a Spanish external quality control of time-lapse annotation program ([Martínez-Granados et al., 2017](#)). The same analysis was then performed on 600 videos with more typical embryo development, excluding chaotic development, videos starting at the cleavage stage and videos with a high degree of fragmentation.

All statistical analysis was performed with GraphPad Prism software (GraphPad Software Company, San Diego, CA, USA). A *P*-value below 0.05 was considered to be significant.



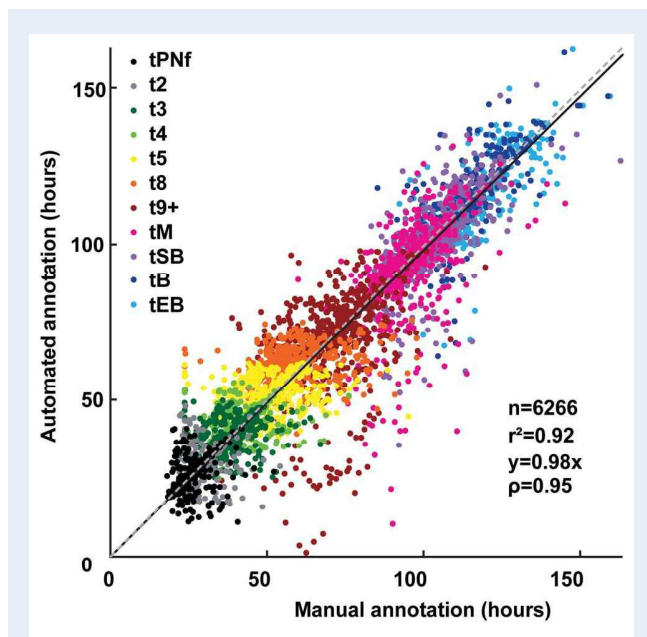


Figure 4 Performance test of the automated annotation tool, as reflected by correlation analysis between automated and expert manual morphokinetic annotation of the full development of 701 human embryos monitored with a time-lapse device.

Results

We tested the robustness of the software on 701 videos of embryos. For each video, the time associated with the beginning of a stage obtained by automated or manual annotation was used (Fig. 4). When comparing both annotation methods, an overall significant correlation with a R^2 value of 0.92 was found, supporting the high degree of sensitivity of the Kinetembryo tool. Time of processing on a personal computer was, on average, 20 minutes and did not require any external intervention, allowing batching all the videos together. Note that the code has been parallelized on the data, meaning that when run on several processors, several videos were processed in parallel, thus reducing the total processing time. The median timing, acceptable range of standard deviation according to Martínez-Granados *et al.* (2017) and ICC for each developmental stage are presented in Fig. 5. Pronuclei fading was correctly annotated according to the recently published acceptable values of standard deviation for manual morphokinetic annotation (Fig. 5) (Martínez-Granados *et al.*, 2017). The ICC showed a poor correlation (ICC = 0.445) overall between manual and automated annotations but a good correlation for this stage for the best 600 videos (ICC = 0.758). Kinetembryo was able to correctly annotate most of the first two mitotic divisions (2-cell to 4-cell stages) videos (Fig. 5). At the end, mean cleavage timings detected by automated annotation showed poor or moderate correlation with manual annotation (ICC < 0.75) (Fig. 5). The fully compacted morula stage was well detected by Kinetembryo in 82.6% of the samples. The following steps of blastulation (tSB, tB and tEB) were also accurately annotated by Kinetembryo. ICC showed a poor and fair correlation for tM

but fair and good correlations for the blastocyst stage (Fig. 5). No systematic automated annotation error was observed, as demonstrated by Bland–Altman plots (Supplementary Fig. S1). Examples of typical accurate (upper part) and inaccurate (lower part) annotations for human embryo development are provided (Supplementary Fig. S2).

No statistically significant difference was observed when videos with an image capture frequency of 10 minutes were compared with those using an image capture frequency of 20 minutes. This was further controlled by removing one image out of two before running the script. This did not significantly modify the results, demonstrating that the script is robustly identifying divisions.

Discussion

In this study, we showed that our automated software Kinetembryo based on image analysis and gray level variation offered a reliable tool for rapid annotation of human embryo morphokinetic parameters. Although some differences in the annotation were found when embryos were looked at individually, this tool could help set up high-throughput studies in large multicentric databases in a reproducible way. Altogether, these results suggest that Kinetembryo could move the field closer to better TLM standards, ultimately improving ART outcomes.

The TLM of embryo development applied to ART raises the hopes of better clinical outcomes for infertile couples, thanks to optimal embryo culture conditions and objective criteria for embryo selection in a single embryo transfer strategy. However, its clinical effectiveness over conventional morphology is still under discussion. In a recent meta-analysis, Chen *et al.* (2017) showed that clinical TLM may have the potential to improve outcomes but that more evidence was needed, while Pribenszky *et al.* (2017) concluded in another meta-analysis that there was an improvement of pregnancy rates and lower pregnancy losses when using TLM. The pros and cons were recently debated in a review on TLM (Paulson *et al.*, 2018). Overall, experts in both groups provided sound but opposing arguments and finally reached the conclusion that robust and appropriately designed clinical trials are needed to draw a firm conclusion on the clinical usefulness of TLM in ART. Such multicentric randomized trials (i.e. Randomized Controlled Trials) in large cohorts imply the analysis of huge databases originating from various settings. This means time-consuming manual annotation of embryo morphokinetic parameters in each participating center and large data management capacity. Moreover, the analysis of such results requires robust inter-centric embryo annotation, limiting as much as possible inter-operator variability (Sundvall *et al.*, 2013; Martínez-Granados *et al.*, 2017). Automated annotation of early embryo development probably represents the best way to reach such high standards. In this study, we have shown that our automated image analysis process was able to proceed to a full embryo annotation from first cleavage up to expanded blastocyst stage. Moreover, we observed improvable but quite good correlation with manual assessment validated on a large study population. Up to now, most of the published morphokinetic embryo selection algorithms were mainly based on early morphokinetic events (Rubio *et al.*, 2014; Petersen *et al.*, 2016). Following this strategy, Eeva[®], a semi-automated annotation tool for early embryo events detection, was developed with

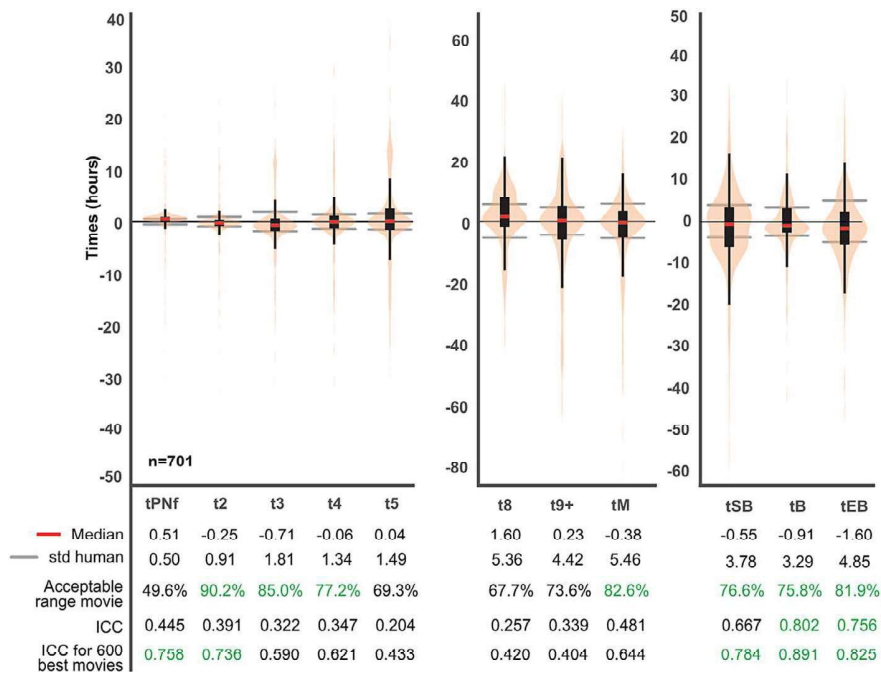


Figure 5 Performance test of the automated annotation tool. Performance is reflected by the graphical representation (boxplot in black and the median in red) and the density (violin plot: in beige) of the difference between manual annotation and automatic at each embryonic stage. On each box, the central mark indicates the median, and the bottom and top edges of the box indicate the 25th and 75th percentiles, respectively. The whiskers extend to the most extreme data points not considered as outliers. The intra-class correlation coefficient (ICC) calculation was also performed for 600 videos with more typical embryo development, excluding videos showing chaotic development, videos starting at the cleavage stage and videos with a high degree of fragmentation.

the aim of improving the selection of embryos with high developmental potential for early stages embryo transfer in addition to Day 3 morphology (Conaghan et al., 2013). The use of Eeva[®] in addition to standard morphology assessment has been compared with standard morphology assessment in a few RCTs with different conclusions. While Eeva[®] seemed to give objective information for helping embryologists with various levels of experience to choose the best embryo to transfer in a double-blinded multi-center study with 54 patients undergoing blastocyst transfer (Diamond et al., 2015), an observational prospective two-center study did not demonstrate any improvement in cycle outcome when using Eeva[®] (Kieslinger et al., 2016).

While providing promising preliminary results, the automated process described here should be further refined in order to improve its accuracy. The software did not have access to the 3D images but only one focal plane, while the manual annotations were realized on 3D images. We are confident in the fact that getting access to the export of 3D videos would enhance the quality of the correlation with the same algorithm and its extension to a 3D ROI. This 3D aspect is a current limitation of the data but not of the software that is expected to perform better on 3D data. One of the technical limitations of our work lies within the duration of the video. The more embryo stages the video contains, the more information the script has to identify them correctly. For example, automated tB annotation does not stand alone, as it is partly based on morula and early blastulation parameters.

The next step would be to undergo external validation in a multicentric design, regardless of the commercial TLM device used in the participating IVF centers. Once validated, this kind of automated process could help address the issues raised in most clinical studies on TLM, i.e. lack of robustness, objectivity and statistical power due to monocentric analysis (Armstrong et al., 2018). Indeed, predictive models have shown poorer performance when tested externally (Fréour et al., 2015; Barrie et al., 2017). Moreover, Storr et al. (2018) recently described discrepancies between published selection models and morphological assessment by trained embryologists.

Deep learning analysis and artificial intelligence are now tested or used in most medical fields. However, these approaches were tested in the field of embryology only recently (Curchoe and Bormann, 2019). Reported preliminary results are extremely encouraging and could be used to predict blastocyst quality (Khosravi et al., 2019). In another very exciting multicentric study, deep learning analysis was shown to predict fetal heart pregnancy from thousands of time-lapse images, with high performance (Tran et al., 2019). However, it should be kept in mind that artificial intelligence can suffer from biases that are not easily detectable (Osoba and Wesler, 2017) and that the implementation of new technologies for clinical decision making should always be done carefully, after proper validation and critical evaluation. In that sense, it would be beneficial to combine algorithmic image analysis with deep learning.

Conclusion

We developed an automated morphokinetic annotation process, which can easily be transferred to multiple platforms. Although this tool needs to be improved and externally validated, it could pave the way to a refined, deeper understanding of human preimplantation development and support further discovery of predictive tests to assist embryologists in embryo selection, ultimately improving ART success rates.

Supplementary data

Supplementary data are available at *Human Reproduction* online.

Acknowledgements

The authors wish to thank Pr Pierre-Antoine Gouraud and Abel Garnier (Clinique des données, CHU de Nantes) for their help with the statistics and the Cellular and Tissular Imaging Core Facility of Nantes University (MicroPICell).

Authors' roles

MF: drafted the manuscript, development of the automated annotation tool, analysis of the results. AR: drafted the manuscript, manual time-lapse annotation, analysis of the results. MM: development of the automated annotation tool. JL: manual time-lapse annotation. DM: expert knowledge in bioinformatics, critical revision of the manuscript. PB: critical revision of the manuscript. PPG: study design, supervision of the study, expert knowledge in image analysis. LD: study design, supervision of the study, critical revision of the manuscript. TF: study design, supervision of the study, critical revision of the manuscript, validated the final version of the manuscript.

Funding

Finox-Gedeon Richter Forward grant 2016 and NeXT (ANR-16-IDEX-0007).

Conflict of interest

We have no conflicts of interest to declare.

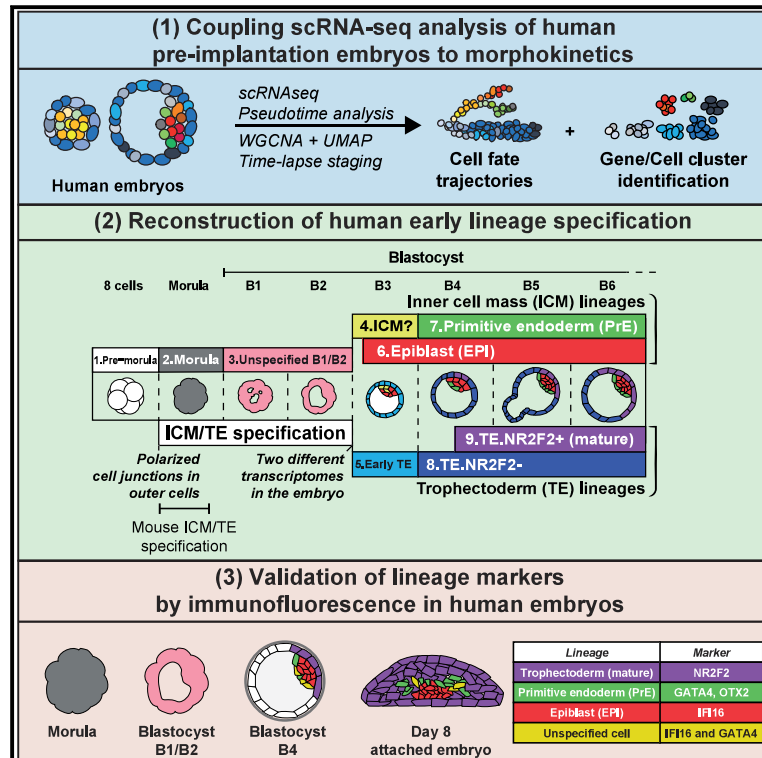
References

- Alpha Scientists in Reproductive Medicine and ESHRE Special Interest Group of Embryology. The Istanbul consensus workshop on embryo assessment: proceedings of an expert meeting. *Hum Reprod* 2011; **26**:1270–1283.
- Armstrong S, Bhide P, Jordan V, Pacey A, Farquhar C. Time-lapse systems for embryo incubation and assessment in assisted reproduction. *Cochrane Database Syst Rev* 2018; **5**:CD011320.
- Barrie A, Homburg R, McDowell G, Brown J, Kingsland C, Troup S. Examining the efficacy of six published time-lapse imaging embryo selection algorithms to predict implantation to demonstrate the need for the development of specific, in-house morphokinetic selection algorithms. *Fertil Steril* 2017; **107**:613–621.
- Basile N, Barrière P, Meseguer M, Fréour T. Time-lapse in the IVF lab: how should we assess potential benefit? *Hum Reprod* 2015; **30**:1276.
- Capalbo A, Rienzi L, Cimadomo D, Maggiulli R, Elliott T, Wright G, Nagy ZP, Ubaldi FM. Correlation between standard blastocyst morphology, euploidy and implantation: an observational study in two centers involving 956 screened blastocysts. *Hum Reprod* 2014; **29**:1173–1181.
- Castelló D, Motato Y, Basile N, Remohí J, Espejo-Catena M, Meseguer M. How much have we learned from time-lapse in clinical IVF? *Mol Hum Reprod* 2016; **22**:719–727.
- Chen AA, Tan L, Suraj V, Reijo Pera R, Shen S. Biomarkers identified with time-lapse imaging: discovery, validation, and practical application. *Fertil Steril* 2013; **99**:1035–1043.
- Chen M, Wei S, Hu J, Yuan J, Liu F. Does time-lapse imaging have favorable results for embryo incubation and selection compared with conventional methods in clinical *in vitro* fertilization? A meta-analysis and systematic review of randomized controlled trials. *PLoS One* 2017; **12**: e0178720.
- Ciray HN, Campbell A, Agerholm IE, Aguilar J, Chamayou S, Esbert M, Sayed S, Time-Lapse User Group. Proposed guidelines on the nomenclature and annotation of dynamic human embryo monitoring by a time-lapse user group. *Hum Reprod* 2014; **29**:2650–2660.
- Conaghan J, Chen AA, Willman SP, Ivani K, Chenette PE, Boostanfar R, Baker VL, Adamson GD, Abusief ME, Gvakharia M *et al*. Improving embryo selection using a computer-automated time-lapse image analysis test plus day 3 morphology: results from a prospective multicenter trial. *Fertil Steril* 2013; **100**:412–419.e5.
- Curchoe CL, Bormann CL. Artificial intelligence and machine learning for human reproduction and embryology presented at ASRM and ESHRE 2018. *J Assist Reprod Genet* 2019; **36**:591–600.
- Diamond MP, Suraj V, Behnke EJ, Yang X, Angle MJ, Lambe-Steinmiller JC, Watterson R, Athayde Wirka K, Chen AA, Shen S. Using the Eeva Test™ adjunctively to traditional day 3 morphology is informative for consistent embryo assessment within a panel of embryologists with diverse experience. *J Assist Reprod Genet* 2015; **32**:61–68.
- Dolinko AV, Farland LV, Kaser DJ, Missmer SA, Racowsky C. National survey on use of time-lapse imaging systems in IVF laboratories. *J Assist Reprod Genet* 2017; **34**:1167–1172.
- European IVF-monitoring Consortium, European Society of Human Reproduction and Embryology, Calhaz-Jorge C, De Geyter C, Kupka MS, de Mouzon J, Erb K, Mocanu E, Motrenko T, Scaravelli G *et al*. Assisted reproductive technology in Europe, 2013: results generated from European registers by ESHRE. *Hum Reprod* 2017; **32**:1957–1973.
- Fleiss J. *Statistical Methods for Rates and Proportions*. Hoboken, New Jersey, USA: John Wiley & Sons, 1981.
- Fréour T, Le Fleuter N, Lammers J, Splingart C, Reignier A, Barrière P. External validation of a time-lapse prediction model. *Fertil Steril* 2015; **103**:917–922.
- Gardner DK, Meseguer M, Rubio C, Treff NR. Diagnosis of human preimplantation embryo viability. *Hum Reprod Update* 2015; **21**:727–747.
- Hoffman R. The modulation contrast microscope: principles and performance. *J Microsc* 1977; **110**:205–222.

- Khosravi P, Kazemi E, Zhan Q, Malmsten JE, Toschi M, Zisimopoulos P, Sigaras A, Lavery S, Cooper LAD, Hickman C et al. Deep learning enables robust assessment and selection of human blastocysts after *in vitro* fertilization. *NPJ Digit Med* 2019;**2**:21.
- Kieslinger DC, De Gheselle S, Lambalk CB, De Sutter P, Kosteljik EH, Twisk JWR, van Rijswijk J, Van den Abbeel E, Vergouw CG. Embryo selection using time-lapse analysis (Early Embryo Viability Assessment) in conjunction with standard morphology: a prospective two-center pilot study. *Hum Reprod* 2016;**31**:2450–2457.
- Koo TK, Li MY. A guideline of selecting and reporting intraclass correlation coefficients for reliability research. *J Chiropr Med* 2016;**15**:155–163.
- Kushnir VA, Barad DH, Albertini DF, Darmon SK, Gleicher N. Systematic review of worldwide trends in assisted reproductive technology 2004–2013. *Reprod Biol Endocrinol* 2017;**15**:6.
- Martínez-Granados L, Serrano M, González-Utor A, Ortíz N, Badajoz V, Olaya E, Prados N, Boada M, Castilla JA, Special Interest Group in Quality of ASEBIR (Spanish Society for the Study of Reproductive Biology). Inter-laboratory agreement on embryo classification and clinical decision: conventional morphological assessment vs. time lapse. *PLoS One* 2017;**12**: e0183328.
- Mölder A, Drury S, Costen N, Hartshorne GM, Czanner S. Semiautomated analysis of embryoscope images: using localized variance of image intensity to detect embryo developmental stages. *Cytom Part J Int Soc Anal Cytol* 2015;**87**:119–128.
- Osoba OA, Welsch W IV. *An Intelligence in Our Image: the Risks of Bias and Errors in Artificial Intelligence*. Santa Monica, California, USA: Rand Corporation, 2017.
- Paternot G, Devroe J, Debrock S, D'Hooghe TM, Spiessens C. Intra- and inter-observer analysis in the morphological assessment of early-stage embryos. *Reprod Biol Endocrinol* 2009;**7**:105.
- Paulson RJ, Reichman DE, Zaninovic N, Goodman LR, Racowsky C. Time-lapse imaging: clearly useful to both laboratory personnel and patient outcomes versus just because we can doesn't mean we should. *Fertil Steril* 2018;**109**:584–591.
- Petersen BM, Boel M, Montag M, Gardner DK. Development of a generally applicable morphokinetic algorithm capable of predicting the implantation potential of embryos transferred on Day 3. *Hum Reprod* 2016;**31**:2231–2244.
- Pribenszky C, Nilselid AM, Montag M. Time-lapse culture with morphokinetic embryo selection improves pregnancy and live birth chances and reduces early pregnancy loss: a meta-analysis. *Reprod Biomed Online* 2017;**35**:511–520.
- Rhenman A, Berglund L, Brodin T, Olovsson M, Milton K, Hadziomanovic N, Holte J. Which set of embryo variables is most predictive for live birth? A prospective study in 6252 single embryo transfers to construct an embryo score for the ranking and selection of embryos. *Hum Reprod* 2015;**30**:28–36.
- Rubio I, Galán A, Larreategui Z, Ayerdi F, Bellver J, Herrero J, Meseguer M. Clinical validation of embryo culture and selection by morphokinetic analysis: a randomized, controlled trial of the EmbryoScope. *Fertil Steril* 2014;**102**:1287–1294.e5.
- Sanchez T, Seidler EA, Gardner DK, Needleman D, Sakkas D. Will noninvasive methods surpass invasive for assessing gametes and embryos? *Fertil Steril* 2017;**108**:730–737.
- Storr A, Venetis C, Cooke S, Kilani S, Ledger W. Time-lapse algorithms and morphological selection of day-5 embryos for transfer: a preclinical validation study. *Fertil Steril* 2018;**109**:276–283.e3.
- Sundvall L, Ingerslev HJ, Breth Knudsen U, Kirkegaard K. Inter- and intra-observer variability of time-lapse annotations. *Hum Reprod* 2013;**28**:3215–3221.
- Tran D, Cooke S, Illingworth PJ, Gardner DK. Deep learning as a predictive tool for fetal heart pregnancy following time-lapse incubation and blastocyst transfer. *Hum Reprod* 2019;**34**:1011–1018.

Integrated pseudotime analysis of human pre-implantation embryo single-cell transcriptomes reveals the dynamics of lineage specification

Graphical abstract



Authors

Dimitri Meistermann, Alexandre Bruneau, Sophie Loubersac, ..., Jérémie Bourdon, Thomas Fréour, Laurent David

Correspondence

thomas.freour@chu-nantes.fr (T.F.), laurent.david@univ-nantes.fr (L.D.)

In brief

Meistermann et al. use scRNA-seq, pseudotime analysis, and immunofluorescence validation to reconstruct the sequence of molecular events occurring in time-lapse-staged human preimplantation embryos. Their findings clarify specification, timing, and cell transcriptomes across early stages of human development.

Highlights

- Distinct trophectoderm/epiblast signatures arise at the B2–B3 blastocyst stages
- IFI16 is broadly expressed in the ICM and then restricted to epiblast after implantation
- NR2F2 arises from the polar TE in late blastocysts and then spreads to all TE cells
- Transcriptomics analysis suggests that PrE emerges from EPI in late blastocysts

Resource

Integrated pseudotime analysis of human pre-implantation embryo single-cell transcriptomes reveals the dynamics of lineage specification

Dimitri Meistermann,^{1,3,13} Alexandre Bruneau,^{1,13} Sophie Loubersac,^{1,2,13} Arnaud Reignier,^{1,2} Julie Firmin,^{1,2} Valentin François-Campion,¹ Stéphanie Kilens,¹ Yohann Lelièvre,³ Jenna Lammers,² Magalie Feyeux,^{1,4} Philippe Hulin,⁴ Steven Nedellec,⁴ Betty Bretin,¹ Gaël Castel,¹ Nicolas Allègre,⁹ Simon Covin,¹ Audrey Bihouée,^{4,5} Magali Soumillon,^{6,7,8,11} Tarjei Mikkelsen,^{6,7,8,12} Paul Barrière,^{1,2} Claire Chazaud,⁹ Joel Chappell,¹⁰ Vincent Pasque,¹⁰ Jérémie Bourdon,³ Thomas Fréour,^{1,2,*} and Laurent David^{1,4,14,*}

¹Université de Nantes, CHU Nantes, INSERM, Centre de Recherche en Transplantation et Immunologie, UMR 1064, ITUN, 44000 Nantes, France

²CHU Nantes, Université de Nantes, Service de Biologie de la Reproduction, 44000 Nantes, France

³LS2N, UNIV Nantes, CNRS, Nantes, France

⁴Université de Nantes, CHU Nantes, INSERM, CNRS, SFR Santé, FED 4203, INSERM UMS 016, CNRS UMS 3556, Nantes, France

⁵Institut du Thorax, UNIV Nantes, INSERM, CNRS, Nantes, France

⁶Department of Stem Cell and Regenerative Biology, Harvard University, Cambridge, MA 02138, USA

⁷Broad Institute, Cambridge, MA 02142, USA

⁸Harvard Stem Cell Institute, Harvard University, Cambridge, MA 02138, USA

⁹GReD Laboratory, Université Clermont Auvergne, CNRS, INSERM, Faculté de Médecine, CRBC, 63000 Clermont-Ferrand, France

¹⁰KU Leuven – University of Leuven, Department of Development and Regeneration, Institute for Single Cell Omics, Leuven Stem Cell Institute, Herestraat 49, 3000 Leuven, Belgium

¹¹Present address: Flexomics LLC, 38 Wareham Street, Fl 3, Boston, MA 02118, USA

¹²Present address: 10x Genomics, 7068 Koll Center Pkwy #401, Pleasanton, CA 94566, USA

¹³These authors contributed equally

¹⁴Lead contact

*Correspondence: thomas.freour@chu-nantes.fr (T.F.), laurent.david@univ-nantes.fr (L.D.)

<https://doi.org/10.1016/j.stem.2021.04.027>

SUMMARY

Understanding lineage specification during human pre-implantation development is a gateway to improving assisted reproductive technologies and stem cell research. Here we employ pseudotime analysis of single-cell RNA sequencing (scRNA-seq) data to reconstruct early mouse and human embryo development. Using time-lapse imaging of annotated embryos, we provide an integrated, ordered, and continuous analysis of transcriptomics changes throughout human development. We reveal that human trophectoderm/inner cell mass transcriptomes diverge at the transition from the B2 to the B3 blastocyst stage, just before blastocyst expansion. We explore the dynamics of the fate markers *IFI16* and *GATA4* and show that they gradually become mutually exclusive upon establishment of epiblast and primitive endoderm fates, respectively. We also provide evidence that *NR2F2* marks trophectoderm maturation, initiating from the polar side, and subsequently spreads to all cells after implantation. Our study pinpoints the precise timing of lineage specification events in the human embryo and identifies transcriptomics hallmarks and cell fate markers.

INTRODUCTION

A key question in biology is how cell fate specification takes place in the early human embryo. The main information we have from this period of development is the changes in morphology of the embryo. Concomitant with morphological changes and growth of the embryo, pluripotent epiblast and trophectoderm cells are established. Because human pluripotency is established during human preimplantation development, a better understanding of early human embryogenesis has a strong effect on research in the field of pluripotent stem cells.

Human preimplantation development is also important for fertility treatment and *in vitro* fertilization (IVF) in particular.

The main morphological events during pre-implantation development are compaction and cavitation. Compaction is characterized by the tight interactions that form between cells after the 8-cell stage. Cavitation is formation of a single cavity within the embryo through fluid pumping. Compaction and cavitation must be coordinated with lineage specification for normal development of the embryo. Indeed, work in mice has revealed that establishment of polarity in the outer cells of the morula, subsequent to compaction, is necessary for lineage specification

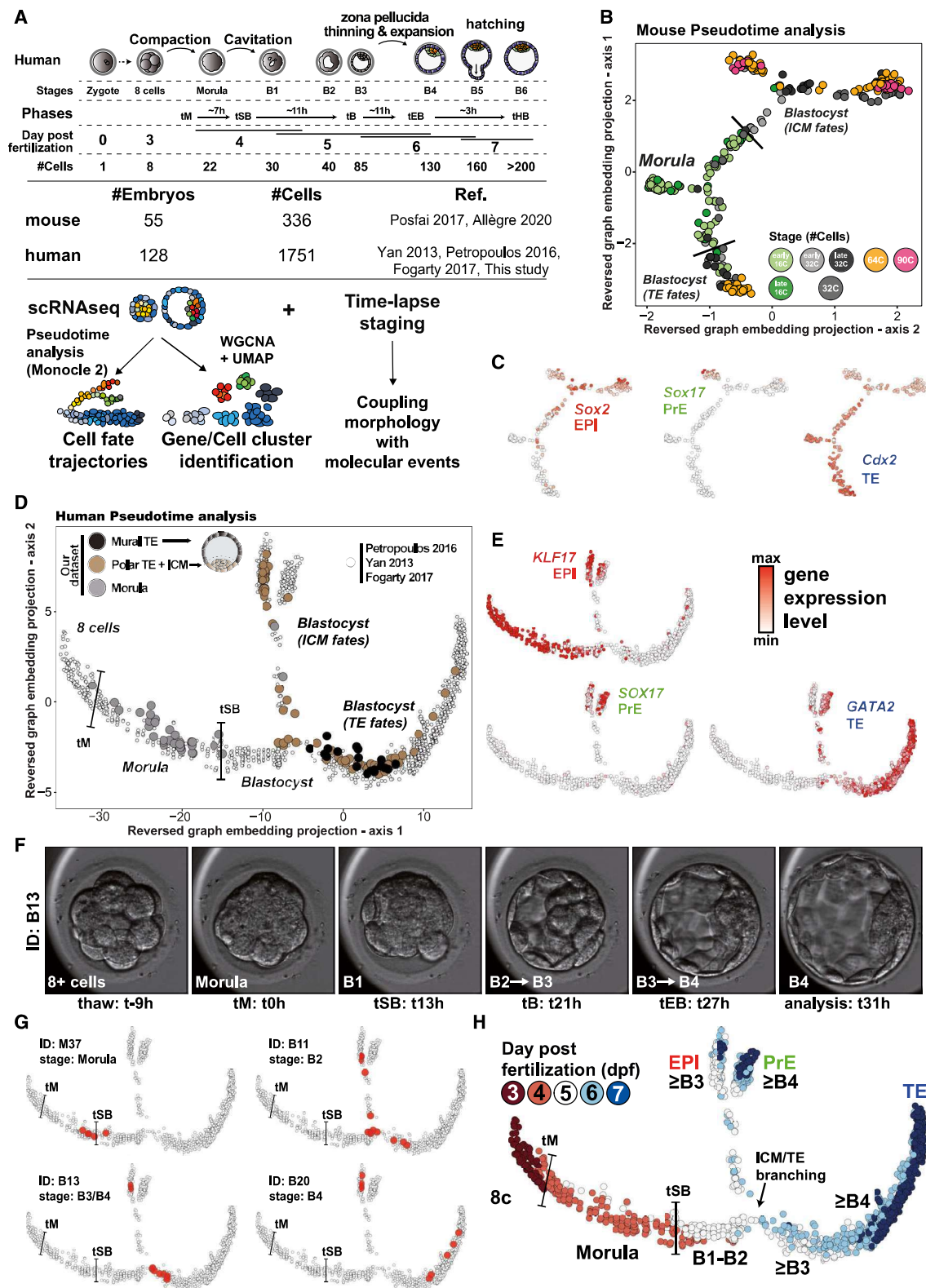


Figure 1. Pseudotime analysis of human and mouse pre-implantation embryo development

(A) Top: Schematic of human pre-implantation development, highlighting the link between developmental stages, morphological phases, dpf, and average number of cells observed. Center: summary of datasets used. Bottom: description of our experimental design. We used 2 mouse single-cell datasets and 4

(legend continued on next page)

(Hirate et al., 2013), and cavitation has been shown to be necessary for proper trophectoderm (TE) fate progression (Chan et al., 2019; Dumortier et al., 2019). Whether the regulation of morphogenesis is similar in human remains unclear.

Lineage specification in mice is considered to be driven by two sequential events. The first cell fate decision in the morula segregates the outer TE cells from inner cell mass (ICM) cells (White et al., 2018). Subsequently, in the blastocyst, ICM cells undergo a second cell fate decision to form the pluripotent epiblast (EPI) and primitive endoderm (PrE), precursors of the embryo proper and yolk sac, respectively (Chazaud et al., 2006). Whether this sequence is conserved in human embryos has been the subject of debate. On one hand, recent single-cell transcriptomics analysis of human pre-implantation embryos suggested simultaneous establishment of TE, EPI, and PrE lineages rather than a two-step model like in the mouse (Petropoulos et al., 2016). On the other hand, integrated analyses of several single-cell transcriptome studies of early human embryos supported the existence of an early human ICM molecular state, distinct from EPI and PrE, implying a two-step model, but could not definitively exclude the concurrent cell lineage specification model (Singh et al., 2019; Stirparo et al., 2018)

In the mouse, the first cell fate decision, segregating TE from ICM, occurs at the morula stage and is driven by a YAP/TEAD4/CDX2 axis (Chazaud and Yamanaka, 2016). Initially, outer cells are polarized and express aPKC and Amot, regulators of the Hippo pathway, at their apical membrane. In these outer polarized cells, the Hippo pathway permits Yap1 to translocate into the nucleus, where it binds to Tead4. The Yap/Tea4 complex activates TE fate drivers such as Cdx2, whereas non-polarized inner cells engage in an ICM fate.

A recent study showed that polarization/the Hippo pathway was involved in initiation of the TE fate in humans (Gerri et al., 2020). However, little is known regarding the progression of TE; CDX2 expression appears after cavitation in human embryos (Niakan and Eggan, 2013) and is therefore unlikely to be driving the TE fate as seen in the mouse. Only a few TE markers have been discovered in humans: GATA3, LAMA1, LAMA3, and KRT7 in hatched/post-implantation blastocysts; GATA2 in blastocysts after the B2/B3 stage, and CCR7 in polar TE cells (Aberkane et al., 2018; Deglincerti et al., 2016; Hannan et al., 2010; Kilens et al., 2018; Niakan and Eggan, 2013; Petropoulos et al., 2016; Shahbazi et al., 2016). Moreover, the molecular events that enable competent human blastocysts to interact with receptive luminal endometrium have remained largely elusive. An

important observation is that human blastocysts attach to the endometrial surface epithelium from the polar side (Aberkane et al., 2018; Grewal et al., 2008; Lindenberg, 1991). This suggests that specific molecular events occur on the polar TE side of the blastocyst; however, the molecular events and underlying mechanisms remain to be identified.

The second cell fate decision, separating ICM cells into EPI and PrE, occurs at the blastocyst stage in the mouse. This second lineage specification is driven by a Nanog/Fgf4/Gata6 axis (Chazaud and Yamanaka, 2016). In EPI cells, Nanog induces Fgf4 secretion; Fgf4 induces Gata6 expression, and, in turn, Gata6 inhibits Nanog in those cells, yielding PrE-fated cells. In human embryos, GATA6-specific expression in PrE occurs upon implantation, whereas it occurs at the 90-cell blastocyst stage in the mouse (Deglincerti et al., 2016). Additionally, fibroblast growth factor (FGF) signaling does not seem to regulate EPI/PrE specification in humans (Kuijk et al., 2012; Roode et al., 2012). These results demonstrate differences from the mouse model. Single-cell RNA sequencing (scRNA-seq) studies have provided atlases of gene expression during human pre-implantation development, but it is still not clear whether and when cell fate decisions take place (Blakeley et al., 2015; Petropoulos et al., 2016; Singh et al., 2019; Yan et al., 2013). How distinct molecular regulators relate to specification of TE, EPI, and PrE lineages in humans remains to be elucidated.

In this study, we define the precise kinetics of gene expression and cell fate decisions during mouse and human early embryo development. We coupled morphological staging with molecular events, highlighting differences and similarities of mouse and human embryos. Last, we identify proteins that mark EPI, TE, and PrE fate progression. This study is a resource to study cell fate decisions during early human development.

RESULTS

Designing an experimental approach coupling fine staging with scRNA-seq analysis

One of the main difficulties when comparing mouse and human development is the differences in timing of development and the specificity of each developmental stage in each species. In the mouse, embryonic days are accurately linked to morphology and molecular events (Figure S1A). In humans, however, *in vitro* culture of embryos shows discrepancies between the timing of culture and morphology. Therefore, for humans, reproductive biologists rely on morphology-based annotation with precise criteria (Figure 1A; Alpha Scientists in Reproductive

human single-cells datasets to identify cell fate trajectories, resulting in a continuous transcriptomic pseudotime. We also performed co-expressed gene module identification with WGCNA, and a UMAP was performed on the activation score of the WGCNA module (module eigengenes) to map cell identities during pre-implantation development. Human embryos used for this study were imaged using a time-lapse microscope.

(B) Projection from the mouse scRNA-seq and single-cell qPCR (scqPCR) samples (Allègre et al., 2019; Posfai et al., 2017) from the reversed graph embedding method (Monocle2). Developmental stages are indicated as number of cells in the embryo.

(C) Projection of lineage marker expression levels on the mouse pseudotime: Sox2 (EPI), Cdx2 (TE), and Sox17 (PrE).

(D) Projection of stage and positional information for the samples we analyzed for this study, on the pseudotime. Morula cells (gray) and blastocyst dissection origin of cells are indicated (mural TE, black; polar TE or ICM, brown). tM, morula compaction; tSB, blastulation.

(E) Projection of lineage marker expression levels on the human pseudotime: KLF17 (EPI), SOX17 (PrE), and GATA2 (TE).

(F) Frames from time-lapse microscopy for embryo B13. For each embryo sequenced in this study, its morphokinetics were acquired using time-lapse microscopy. Developmental events include tM, tSB leading to the B1 stage, full blastocyst (tB) at the B3 stage, and expanded blastocyst when the *zona pellucida* thickness is halved (tEB) at the B4 stage. tM is used as t0 to compare thawed embryos.

(G) Projection of cells from 4 embryos, including embryo B13 (F), on the pseudotime.

(H) Projection of developmental day (3–7 dpf) for all samples combined for this study and the result of our refined staging.

Medicine and ESHRE Special Interest Group of Embryology, 2011). The numerous morphological events during the fifth day post fertilization (dpf) illustrate this: at 5 dpf, human embryos progress from early blastocyst (B1 and B2) to blastocyst (B3) and expanded blastocyst (B4) (Figure 1A). Molecular analysis must be linked to morphological staging to better understand human pre-implantation development.

Pseudotime analysis of scRNA-seq data appeared to be a good approach to study lineage specification and hierarchize molecular events. We used Monocle2 to generate developmental cell fate trajectories and identify the most likely path that temporally orders transcriptomics signatures of single cells (Qiu et al., 2017; Figure 1A). To identify lineage signatures, an essential benchmark for stem cell models, we clustered cells based on their transcriptomes. Finally, because we used embryos donated for research, staged carefully using time-lapse monitoring and *zona pellucida* thickness measurements (Feyeux et al., 2020) and graded according to clinical criteria, we were able to link embryo morphology with molecular events.

Transcriptomic pseudotime analysis of mouse and human pre-implantation development

We first computed the pseudotime of mouse pre-implantation embryo development using two existing datasets spanning early 16-cell morula to 90-cell stage blastocysts (Allègre et al., 2019; Posfai et al., 2017). Pseudotime analysis identified a common pool of progenitor cells that subsequently separates into two branches (Figure 1B). The pseudotime value indicates the level of transcriptomic change from the root cell (Figure S2B). Projecting the developmental stage annotations onto the pseudotime identified that the initial unspecified branch is composed mostly of cells from early 16-cell morula. Late 16-cell morula cells occupy the bifurcation point where cells make their first fate decision. Future cells, from early 32- and late 32-cell morula, occupy one of the two branches toward the ICM and TE fates. Cells from 64- and 90-cell blastocysts are located at the tips of specified branches of the pseudotime (Figure 1B). Enrichment of *Sox2*, *Cdx2*, and *Sox17* expression allows identification of EPI, TE, and PrE branches, respectively (Frum et al., 2018; Figure 1C). Pseudotime analysis allowed us to reconstruct the developmental paths taken during early mouse embryo development, including the expected TE/ICM branchpoint as well as EPI/PrE bifurcation.

Having established the developmental pathways of early embryo cells in the mouse, we turned our focus to human embryos. We first generated scRNA-seq data of 25 human embryos from morula to B5 blastocysts (150 cells). We integrated our scRNA-seq dataset with available datasets (Fogarty et al., 2017; Petropoulos et al., 2016; Yan et al., 2013), resulting in an atlas of 1,751 cells from 128 embryos. Pseudotime analysis revealed 5 branches, with each branch containing samples from at least 2 datasets (Figure 1D; Figure S2A). Because our embryos were followed by time-lapse microscopy prior to scRNA-seq, we could univocally associate developmental stages for each embryo. Moreover, because blastocysts were laser dissected to physically separate the mural TE from the polar TE/ICM, we could also overlay positional information on the pseudotime (Figure 1D; Figures S1B–S1E). This revealed positioning of morula cells in the middle of the first branch of the pseudotime and the TE

branch as the longest branch extending on the right (Figure 1D). Projection of the expression levels of transcription factors suggested branches associated predominantly with EPI, PrE, and TE enriched for *KLF17* (EPI), *SOX17* (PrE), and *GATA2* (TE), respectively (Figure 1E; Blakeley et al., 2015; Kilens et al., 2018; Niakan and Eggan, 2013; Xiang et al., 2020).

To link developmental stage and molecular events, we performed a per-embryo analysis in which cells from the same embryo were analyzed together. We then regrouped embryos based on their position on the pseudotime (Figure S2C). Sample images are shown for blastocyst ID 13 (B4 stage upon scRNA-seq analysis) (Figure 1F). We projected all cells from our cohort of embryos on the pseudotime, linking embryo annotation to the pseudotime (Figure 1G; Figure S2C). Our precise annotation showed that, in humans, TE and ICM cells become transcriptionally distinct between the B2 and B3 stages, after the beginning of blastocyst cavitation (Figure 1H; Figure S2C). These results were in stark contrast to mouse embryos, where branching between ICM and TE fate occurred earlier, between the 16- and 32-cell morula stage (Figure 1B). Our results suggest that, in human embryos, ICM cells are transcriptionally distinct from TE cells shortly after formation of the blastocyst, unlike in the mouse, where this event takes place earlier.

Defining the hierarchy of gene expression and lineage signature during human pre-implantation development

The next step was to define lineages associated with each cell. Pseudotime analysis is particularly suited to studying pre-implantation development as a dynamic process. We used WGCNA (weighted gene co-expression network analysis) (Langfelder and Horvath, 2008) to identify gene expression signatures associated with distinct developmental stages and lineages. Gene module activation or repression can be summarized by a linear combination of gene expression values called module eigengenes. To produce precise mapping of transcriptome identity, we used module eigengenes from gene modules reduced in two dimensions by a UMAP (uniform manifold approximation and projection) approach (McInnes et al., 2018). Finally, we clustered cells based on their relative position on the UMAP (Ester et al., 1996). This featured 8 major clusters indicative of specific lineages and stages; we qualified cells located between clusters as undefined or “intermediates” (Figure 2A; Figure S3).

Module eigengenes classify EPI, PrE, and TE cells in an unsupervised manner. In contrast to Petropoulos et al. (2016), who used successive rounds of principal-component analysis (PCA) to identify different cell types and loadings to identify the associated markers, our method gives a more confined identification of PrE and a refined association of fates with developmental stages and also identifies cells that are undefined or intermediates, limiting the noise in the fate-associated signatures (Figure S4A). Stirparo et al. (2018) classified embryonic day 5 (E5) non-TE cells as ICM. The majority of the cells they identified as ICM are within our EPI cluster (Figure S4B). We did not identify a stringent population of unspecified cells that could be considered a proper ICM cluster. However, our analysis highlighted 3 clusters of unspecified cells and subdivided the TE cells into 3 subclusters based on their progression on the pseudotime (Figure 2B). Our unsupervised analysis therefore identified developmental molecular states during pre-implantation development and

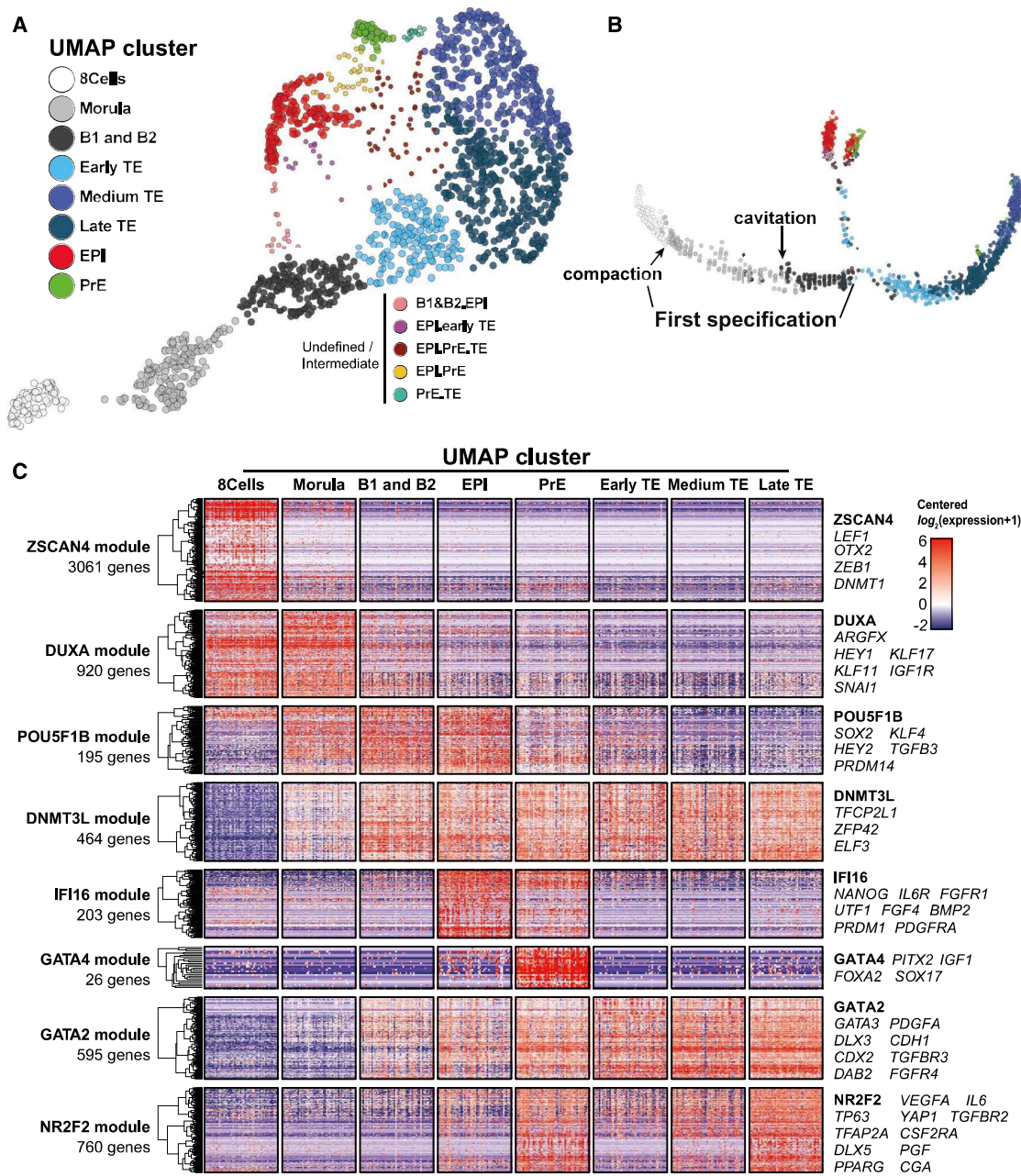


Figure 2. Gene modules define cell fate transcriptional signatures, and pseudotime indicates the hierarchy of events

(A) Dimension reduction (UMAP) of WGCNA module eigengenes, colored by density-based clusters. Small dots indicate a minor cluster composed of the intermediate transcriptome. Medium TE and late TE were segregated by additional k-means clustering based on NR2F2 and GATA2 module eigengenes.

(B) Projection of density-based clusters from (A) on the pseudotime.

(C) Expression heatmap of all genes related to WGCNA modules. Each row represents a WGCNA module, and each column is a set of 50 cells drawn from a UMAP cluster (A). The height of each row represents the number of genes in the corresponding WGCNA module following a log scale. For each module, a set of genes belonging to the module is indicated on the right side of the heatmap.

provides an alternative, refined cellular annotation of cell fate lineages in the early human embryo.

To further analyze the temporal dynamics of gene expression during human pre-implantation development, we matched gene module expression with each cluster of cells obtained with the UMAP (Figure 2C). This revealed unique behavior of 8 modules

of genes, named after a representative gene (Figure S3). The 3 clusters of unspecified cells are distinguished based on expression of (1) the ZSCAN4 module, exclusively within 8-cell stage embryos; (2) the DUXA module and onset of the POU5F1B and DNMT3L modules in morula cells; and (3) absence of the ZSCAN4 module, fading of the DUXA modules, and the presence

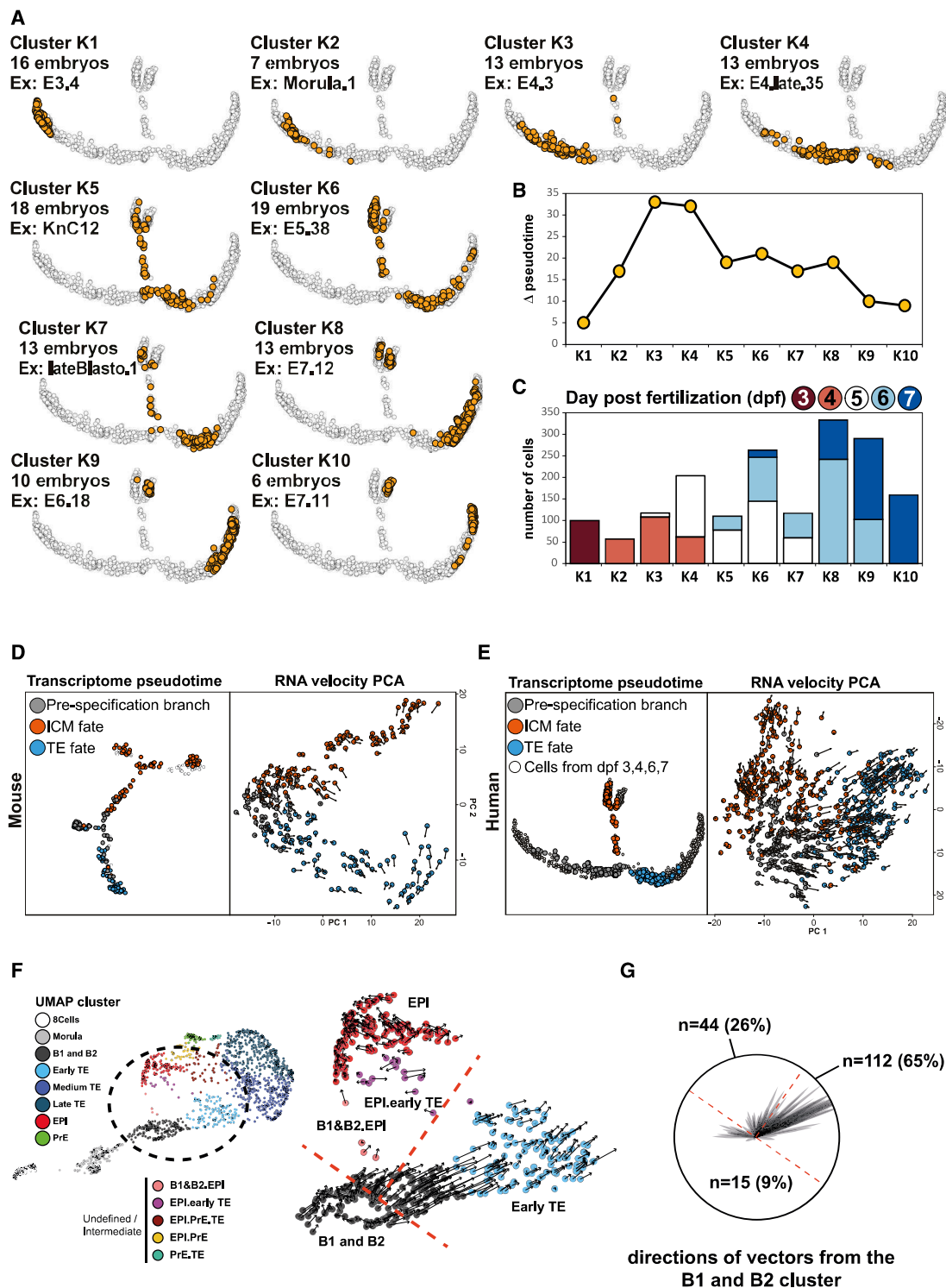


Figure 3. Early blastocysts contain a heterogeneous cell population that is preparing to specify despite having similar transcriptomes
 (A) Projection of each embryo cluster (k-means) according to the position of its cells on the pseudotime. For each embryo cluster, the corresponding number of embryos and a representative embryo are indicated. Clusters are ordered by their mean pseudotime.
 (B) Range of pseudotime values per embryo cluster.
 (C) Distribution of number of cells per embryo cluster subdivided by dpf.
 (D) Transcriptome pseudotime and RNA velocity comparison of cells before and after specification in the mouse.
 (E) Transcriptome pseudotime and RNA velocity comparison of cells before and after specification in humans.

(legend continued on next page)

of the POU5F1B/DNMT3L modules in early blastocysts (Figure 2C; Figure S4C). Regarding TE cells, 3 states emerge from the pseudotime analysis: (1) a cluster expressing the GATA2, POU5F1B, and DNMT3L modules that we called early TE; (2) a cluster expressing the GATA2 module but not POU5F1B; and (3) a cluster expressing the GATA2 and NR2F2 modules (Figure 2C; Figure S4C). These analyses defined distinct modules of genes whose dynamic expression characterizes early human embryo development.

The dynamic expression pattern of modules within clusters and pseudotime inform on the potential role of genes in each module. Some modules are not associated with fates but reflect overall changes in embryo development. For example, the ZSCAN4 and DUXA modules are associated with zygotic genome activation between the 8-cell and morula stages, whereas the DNMT3L module is emerging in all cells at the blastocyst stage and contains epigenetic regulators, in line with methylation dynamics in human pre-implantation development and metabolic pathways (Figure S4D; Greenberg and Bourc'his, 2019). On the other hand, some modules are associated with fates and are expressed sequentially. The POU5F1B module, containing pluripotency genes, is first detected in all cells of the morula and B1 and B2 blastocysts and is then maintained in the EPI but reduced in the PrE and TE. Consequently, the POU5F1B module is the first module that goes through a process of global to restricted lineage-specific expression in more developed embryos (Figure 2C). Other modules are related to specific lineages; for example, the IFI16 module for developed/stable EPI, the GATA4 module for PrE, the GATA2 module for early TE/medium TE/late TE, and the NR2F2 module for late TE. Expression of several genes within lineage-specific modules aligns with the current understanding of developmental expression dynamics. For example, the IFI16 module contains NANOG and overlaps with expression of the POU5F1B module in B4 blastocysts (Figure 2C). The GATA4 module contains the characterized regulators of PrE fate SOX17 and FOXA2. Our dual analysis by pseudotime and gene correlation allowed us to hierarchize states emerging during pre-implantation development, linking them with developmental stages (Figure S4C). This highlights how our analysis can be used to refine human pre-implantation studies by serving as a reference for developmental stages and progression of molecular signatures that lead to specification. All annotations and expression profiles can be found in a user-friendly online browser we generated to facilitate access to human and mouse pre-implantation datasets (Figure S4E).

Human morula and B1/B2 blastocyst cells show heterogeneity

Our pseudotime analysis, combined with time-lapse imaging of embryos, suggests that embryo cells are transcriptionally different after human cavitation. To refine this conclusion, we studied transcriptional heterogeneity within each embryo by clustering embryos based on their individual position on the

pseudotime. Cells belonging to each embryo can only belong to one cluster. We then measured the pseudotime spreading of each cluster because it reflects transcriptional variability, and reported annotations associated with embryos from each cluster. For example, cluster 1 spans a relatively short pseudotime distance and contains only 3-dpf embryos (Figure 3A). Clusters K3 and K4 have the highest pseudotime distance variation (Figure 3B). Interestingly, cluster K3 contains mostly 4-dpf embryos, suggesting that, within human morula, some cells develop faster (Figure 3C).

To test whether morula cells, located just prior to the first pseudotime bifurcation, have already initiated a transcriptional program biased toward a fate, we used RNA velocity, a measurement of non-spliced mRNA that infers cellular fate (La Manno et al., 2018). In the mouse, RNA velocity analysis of transcriptionally similar cells showed that cells had a velocity trending toward ICM or TE (Figure 3D). Thus, at the 16-cell stage, mouse cells are biased toward TE or ICM, but the transcriptomic (mRNA) differences are mostly visible at the 32-cell morula stage (Figure 3D; Jedrusik et al., 2008). Similarly, in humans, RNA velocity showed that, despite having similar mRNA profiles, unspecified cells localized on the pseudotime prior to branching are already biased toward ICM or TE fates, in agreement with mouse work (Graham and Zernicka-Goetz, 2016; Figure 3E). This can be observed when projecting the velocity vectors on the UMAP cluster B1/B2 (Figures 3F and 3G). Heterogeneity in human embryos seemed to be established at the morula stage, but inner and outer cells are not transcriptionally distinct until the B3 blastocyst stage.

Identification of markers of compaction and cavitation during human pre-implantation development

Compaction of cells at the morula stage requires establishment of apico-basal polarity. In the mouse, compaction is initiated or characterized by sequential establishment of adherent junctions, marked by CDH1, followed by establishment of tight junctions, marked by ZO1 (Barcroft et al., 1998, 2003; White et al., 2018). To refine our pseudotime, we investigated establishment of apico-basal polarity in human embryos. Immunostaining of ZO1 and CDH1 during human pre-implantation development showed basolateral expression of CDH1 from the morula stage, with subsequent apical recruitment of ZO1 (Figure 4A). This supports the theory that apico-basal polarity in human embryos is linked to molecular events, similar to other mammalian species (Gerri et al., 2020; Reijo Pera and Prezzoto, 2016).

After acquisition of apico-basal polarity and compaction, an important event in mammalian pre-implantation development is formation of a blastocoel cavity (White et al., 2018). This is mediated by expression of aquaporins at the morula/early blastocyst stage (Barcroft et al., 2003; Xiong et al., 2013). AQP3 is the main water channel expressed during human pre-implantation development and is one of the few genes that are initially expressed in all cells but then restricted to TE. Immunostaining

(F) RNA velocity vectors projected on the B1 and B2, B1&B2.EPI, EPI, EPI.early TE, and early TE clusters from the UMAP analysis. Cells are colored by cell clusters.

(G) Summary of the direction and magnitude of RNA velocity vector of the B1 and B2 cell cluster by a circular diagram. Each represented vector has an opacity of 20% to represent an estimation of vector density. 114 vectors of 171 are in a sector of 45° of the diagram that is facing the Early TE cluster, and 42 are facing the EPI cluster. The sectors are represented by a dashed orange line.

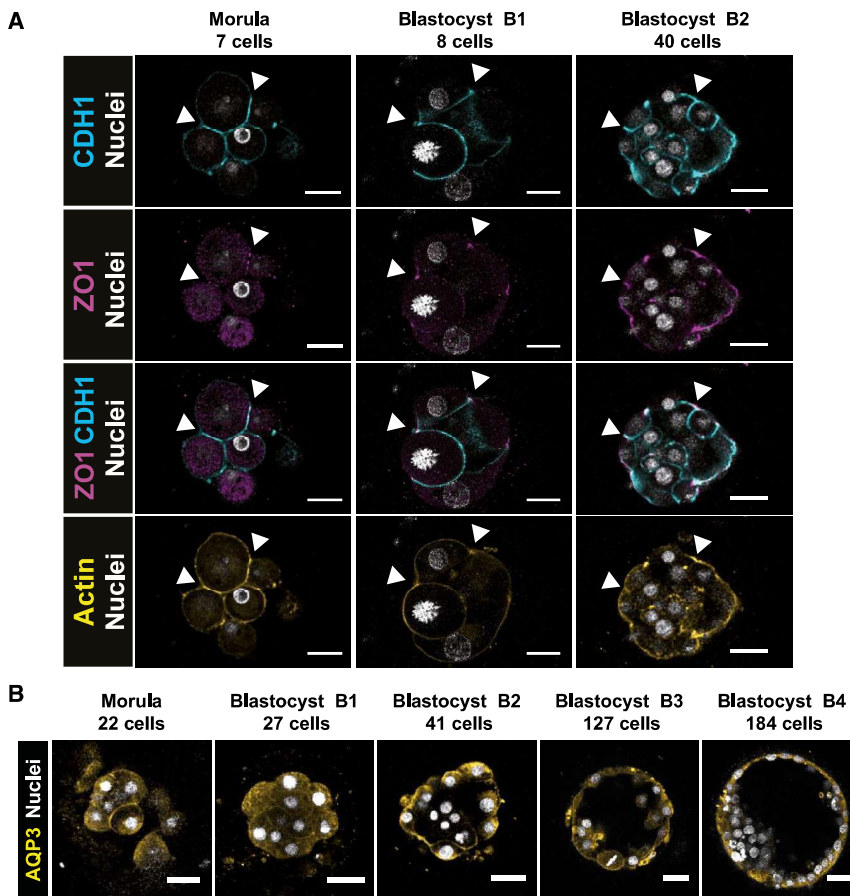


Figure 4. Polarization of outer cells of the morula precedes restriction of the TE marker AQP3

(A) IF of CDH1 (cyan), ZO1 (purple), Actin (yellow), and nuclear counterstaining (white) at the indicated stages. An arrowhead points to the apical part of the cell, with ZO1 staining next to CDH1 staining (n = 3).

(B) IF of AQP3 (yellow) and DAPI (white) as a nuclear counterstain at the indicated developmental stages (n = 6).

Scale bars, 47 μm .

To further understand IFI16 dynamics within the human ICM, we performed co-staining with NANOG and GATA4, which are mutually exclusive in expanded blastocysts (Figure 5C; Roode et al., 2012). In B4 and B5 embryos, IFI16 co-localized with NANOG (EPI)-positive cells or with GATA4 (PrE)-positive cells. To clarify whether IFI16 was restricted to EPI and/or PrE upon their maturation, we extended our analysis to later developmental time points. We used a recently established *in vitro* culture protocol to simulate implantation (Deglincerti et al., 2016; Shahbazi et al., 2016). Here B3 or B4 embryos were cultured for 72 h *in vitro*, which is considered equivalent to “day 8” human embryos. We observed NANOG-positive cells that clearly expressed IFI16, whereas GATA4-positive cells were IFI16 negative or expressed IFI16 weakly (Figure 5D). Quantification of immunofluorescence in pre-implantation embryos and B3 or B4 embryos cultured for 72 h *in vitro* suggests that, before implantation, ICM cells broadly express IFI16, whereas after implantation, cells expressing high levels of IFI16 are negative for GATA4 (Figures 5E and 5F).

for AQP3 revealed cytoplasmic membrane localization at the morula stage before being restricted apically at the B2 stage (Figure 4B). Loss of AQP3 in the ICM at the B2 blastocyst stage could therefore indicate onset of a program linked to the ICM, consistent with our pseudotime analysis.

These results allowed us to place the major morphogenesis events, compaction and cavitation, on the unspecified branch of the pseudotime (Figure 2D). CDH1, ZO1, and AQP3 can therefore be used as markers to identify molecular progression of human embryos.

IFI16 and GATA4 highlight progression of EPI and PrE specification

Currently, the number of markers used to study EPI/PrE lineage specification in human is limited. In particular, we need markers that allow us to track progression of cells within EPI or PrE fates. Using our integrated transcriptomics analysis, we sought to identify markers of developed EPI in B5 hatching blastocyst. Among transcription factors, we focused on IFI16 as a candidate for developed EPI. We analyzed protein expression of IFI16 in B5 embryos, which showed IFI16-positive staining restricted to ICM cells, in contrast to GATA2 expression in TE cells (Figure 5A). IFI16 was not detected before B2 and was robustly detected after B4 in ICM cells (Figure 5B). These results are consistent with previous transcriptional analyses suggesting a link between IFI16 and EPI (Boroviak et al., 2018).

We found that IFI16 is restricted to EPI post-implantation in human embryos. Loss of IFI16 might therefore indicate advancement toward the PrE fate. This observation raised an interesting hypothesis: PrE could be specified later than EPI in humans (EPI and PrE are linked differentially to dpf; linear regression, $p = 1.51 \times 10^{-12}$; Figure S5A). The difficulty to identify a distinct ICM molecular signature that would correspond to progenitors of EPI and PrE like in the mouse might indicate that EPI and ICM molecular fates in humans are highly similar or that PrE in humans differentiates from EPI. To better understand PrE fate, we analyzed a recent scRNA-seq dataset of human embryos cultured up to 120 h (day 5) and then switched to IVC medium for up to 216 h (day 14) (Zhou et al., 2019). We focused our analysis on day 5 + 24 h and day 5 + 72 h prolonged culture. UMAP showed that EPI and PrE cells were more related to each other (closer) at day 5 + 24 h than at day 5 + 72 h (Figures S5E and S5G). Interestingly, day 5 + 24 h embryos had cells co-expressing *IFI16* and *GATA4*, whereas this was not the case in day 5 + 72 h embryos (Figures S5F and S5H). We completed this analysis

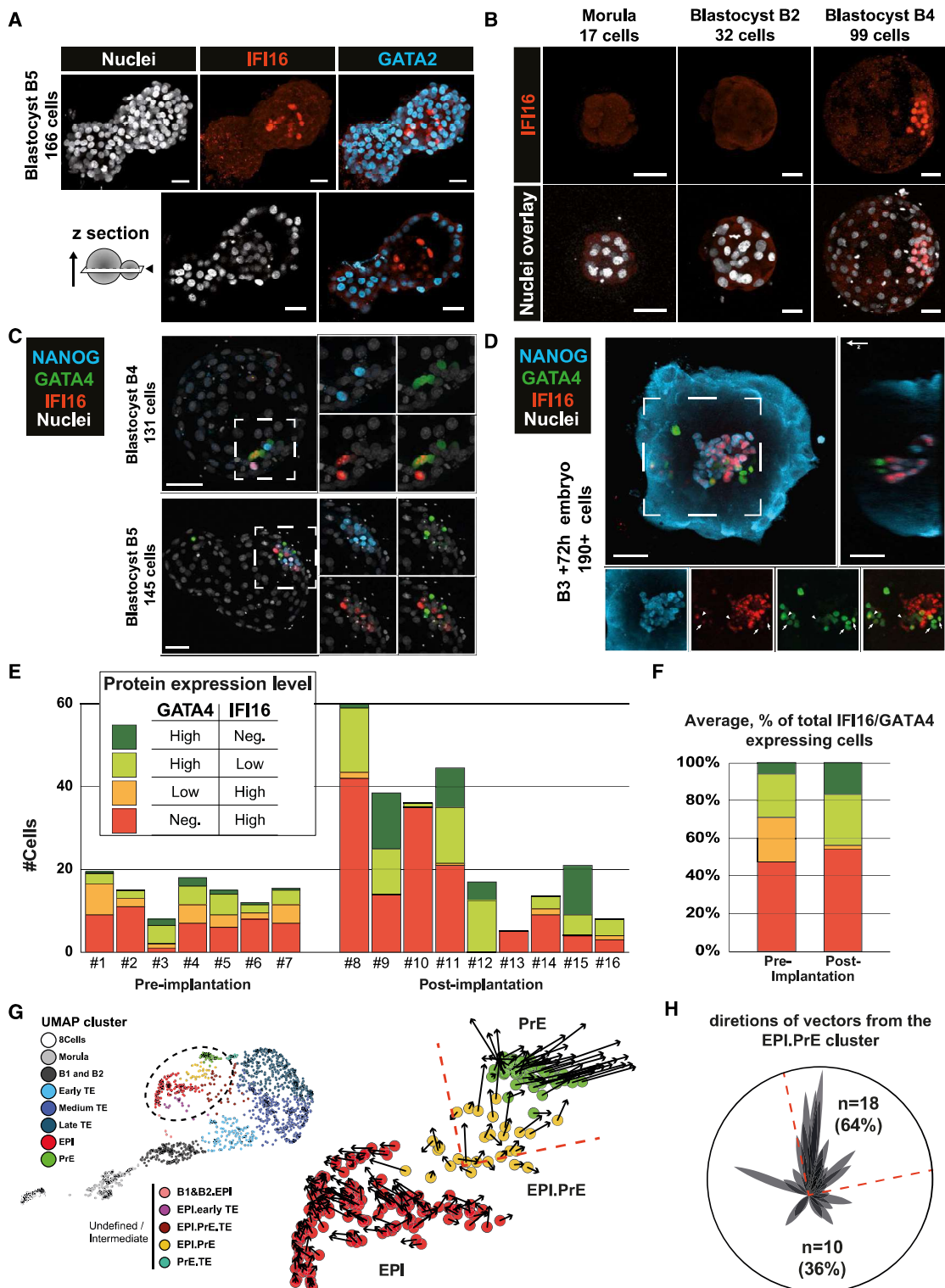


Figure 5. NANOG/IFI16/GATA4 dynamics highlight progression of EPI/PrE specification

(A) IF of IFI16 (red) and GATA2 (cyan) at the B5 blastocyst stage. The z section indicates a z cutting plane (n = 3).

(B) IF of IFI16 at the indicated stages. Nuclear counterstaining is white (n = 13).

(C) IF of NANOG (cyan), GATA4 (green), and IFI16 (red) at the indicated stages. Nuclear counterstaining is white (n = 3).

(D) IF of NANOG (cyan), GATA4 (green), and IFI16 (red) in a B3 + 72 h attached embryo. Arrow, GATA4⁺/IFI16⁺ cell. Arrowhead, GATA4⁺/IFI16⁻ cell (n = 4).

(legend continued on next page)

by projected velocity vectors on the UMAP from our dataset or the post-implantation dataset (Figures 5G and 5H; Figures S5E and S5F). The vectors show that, at late blastocyst stage, some EPI cells show a shift toward PrE gene expression. This further supports our hypothesis that PrE specification initiates at the B4 stage and that PrE might differentiate from cells that are transcriptionally close to EPI in humans. Further analysis is required at the B3 stage to identify the molecular states of cells that would eventually become PrE.

To further validate our observations, we investigated expression of another marker: OTX2. OTX2 is an EPI-associated lineage marker in mouse embryos (Acampora et al., 2016; Buecker et al., 2014; Shahbazi et al., 2017) but has been linked to PrE in humans (Boroviak et al., 2018; Zhou et al., 2019). In pre- and post-implantation embryos, we observed that OTX2 only co-localized with GATA4-positive cells and is not expressed in NANOG-positive cells (Figures S5B–S5D). Interestingly, in day 8 embryos, OTX2 was expressed in GATA4-positive cells closer to NANOG-positive cells (Figures S5B–S5D). It remains to be defined whether OTX2 indicates more advanced PrE development or a different subset of PrE.

Our transcriptomic analyses, validated by immunofluorescence (IF), support that EPI/PrE specification in humans occurs in B4 (late) blastocysts, which is different from the mouse, where EPI and PrE fates are established in 90-cell (early) blastocysts.

NR2F2 marks TE maturation at the polar side of human embryos

We next sought to decipher the maturation events in the TE branch. A transcription factor of interest was NR2F2 because of its expression in the later part of the TE branch, which corresponds to developmental stages of expanded/hatched blastocysts (B4 and thereafter; Figures S3A and S3B). In B5 blastocysts, IF showed that nuclear localization of NR2F2 was restricted to polar TE cells juxtaposed to EPI cells, expressing NANOG (Figure 6A). We then investigated NR2F2 expression in B4 blastocysts. Immunostaining revealed GATA3 and GATA2 expression throughout TE, whereas NR2F2 was only expressed in the subset of polar TE cells (Figure 6B). The pseudotime analysis indicates that NR2F2-expressing cells are the most mature because they are at the end of the trajectory. However, IF analysis showed expression of NR2F2 in B4 embryos, and B4 TE cells are generally localized in the middle of the TE branch of the pseudotime (Figure S2C). This suggests that maturation of TE is initiated on the polar side by an EPI-TE dialog.

To further characterize onset of NR2F2⁺ cells, we co-stained NR2F2 with markers of EPI (IFI16) and PrE specification (GATA4). This revealed that NR2F2 expression is concomitant with IFI16 and GATA4 expression (Figure 6C; Figure S6). Staining of NR2F2 in B3/B4 + 72 h *in vitro* cultured embryos confirmed

spreading of NR2F2 to all TE cells (Figure 6D). We therefore propose that maturation of TE is initiated by contact with EPI and then spreads upon implantation.

The observation that maturation of TE cells is initiated at the polar side is consistent with the observation that the majority of human blastocysts are attached to endometrial cells by the polar side with subsequent spreading of TE development to mural cells (Aberkane et al., 2018; Bentin-Ley et al., 2000; Grewal et al., 2008; Lindenberg, 1991). We grouped cells as NR2F2⁺ and NR2F2⁻ to highlight pathways specific to polar TE. This revealed pathways for which the receptor is on NR2F2⁺ polar TE cells (i.e., GM-CSFR), and the ligand is secreted by the endometrium (i.e., GM-CSF) (Giacomini et al., 1995; Ziebe et al., 2013). Analysis of the most enriched signaling pathways with tGSEA (Korotkevich et al., 2019) identified prime candidates potentially driving the molecular dialog from EPI toward TE, such as transforming growth factor β (TGF- β), insulin growth factor 1 (IGF1), BMP2, and FGF4, and from TE toward EPI, such as platelet-derived growth factor (PDGF), interleukin-6 (IL-6), and WNT (Figure S7; Figure 6E). This suggests that FGF4 might still have a role in pre-implantation development despite being ruled out from regulating PrE specification (Kuijk et al., 2012; Roode et al., 2012). BMP signaling has been shown recently to inhibit cavitation (De Paepe et al., 2019), but its function after the first lineage specification remains to be studied. The role of IL-6 has been studied recently in pigs; IL-6 knockout (KO) or inhibition of JAK signaling perturbed pre-implantation development, supporting the hypothesis that, in humans and pigs, in the absence of LIF, JAK/STAT signaling is triggered by IL-6 (Ramos-Ibeas et al., 2019). Polar TE-EPI interactions in humans is reminiscent of the ICM-polar TE molecular dialog observed in mouse blastoids (Rivron et al., 2018). Mouse blastoids showed that EPI is necessary for proper TE maturation. However, human-specific events might be involved because some genes critical for mouse TE maturation are not restricted to TE in humans, such as KLF6 (Rivron et al., 2018).

We found that NR2F2 marks mature TE in B4 expanded blastocyst and spreads to all TE cells. Identification of NR2F2⁺ cells will give rise to numerous hypothesis regarding the dual molecular dialog between polar TE and the EPI and endometrium.

DISCUSSION

We generated continuous mouse and human pre-implantation embryo transcriptome atlases by implementing lineage reconstruction approaches from scRNA-seq data. The pseudotime-ordered transcriptomic mouse trajectory corroborates existing functional experiments (Chazaud and Yamanaka, 2016; Posfai et al., 2017). For example, cells become transcriptionally distinct at the early 32-cell stage, immediately after differential Cdx2

(E) Manual counting of GATA4-high/IFI16⁻, GATA4-high/IFI16-low, GATA4-low/IFI16-high, and IFI16-high/GATA4⁻ cells in pre-implantation and post-implantation embryos.

(F) Average percentage of total IFI16/GATA4 expressing cells in pre- and post-implantation embryos. Scale bars, 47 μ m.

(G) RNA velocity vectors projected on the EPI, EPI.PrE, and PrE clusters from the UMAP analysis. Cells are colored by cell clusters.

(H) Summary of the direction and magnitude of RNA velocity vectors of the EPI.PrE cell cluster by a circular diagram. Each represented vector has an opacity of 45% to represent an estimation of vector density. 18 vectors of 28 are oriented within an angle of 45° in the direction of the PrE cluster ($p \approx 2.21 \cdot 10^{-6}$, obtained from the binomial distribution of parameter $p = 0.25$ and $n = 28$). The sectors are represented by dashed orange lines.

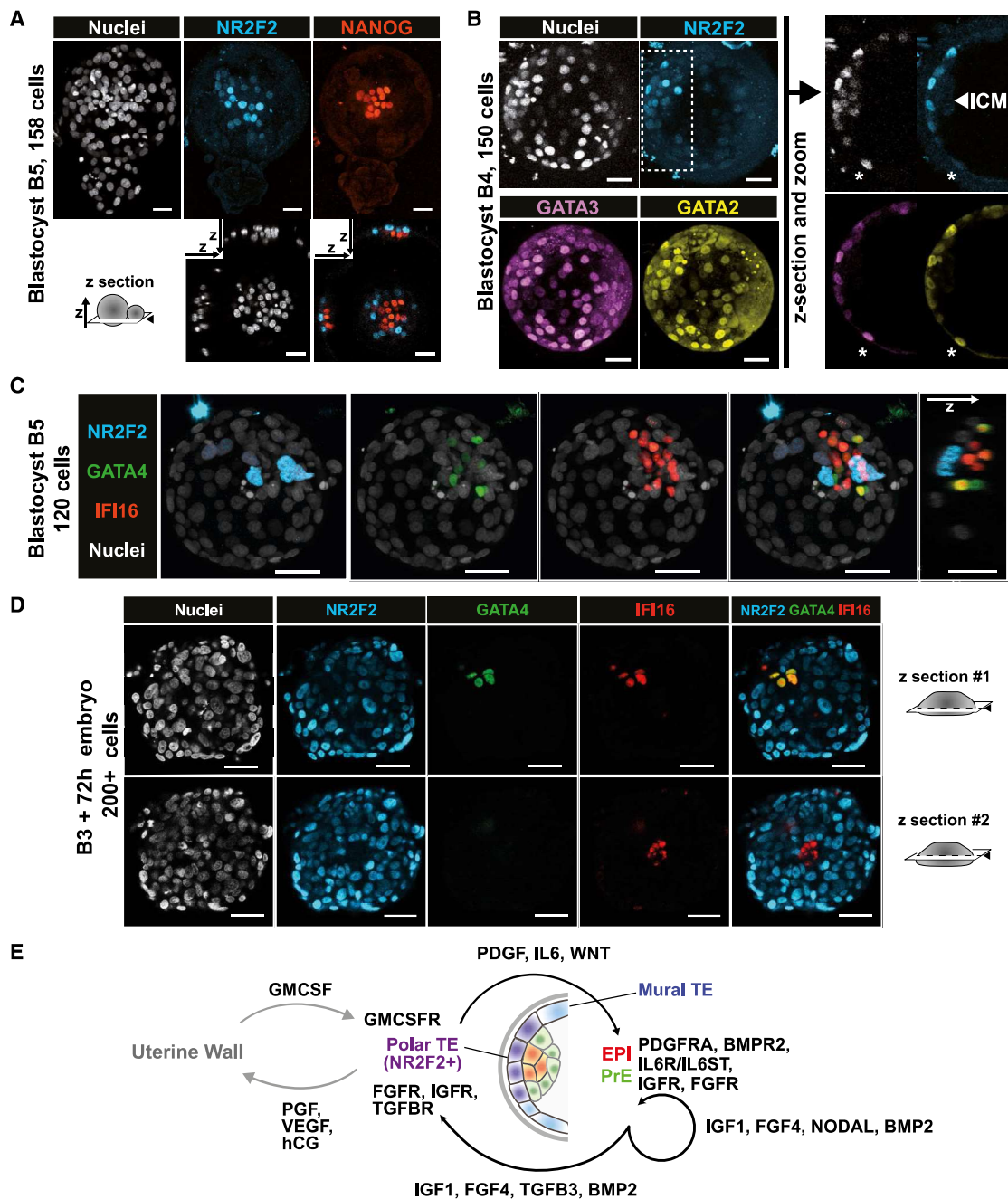


Figure 6. NR2F2 reveals differential maturation of polar and mural TE

(A and B) IF of NR2F2 (cyan) and NANOG (red) at the B5 stage (A) or with GATA2 (yellow) and GATA3 (purple) at the B4 stage (B). Asterisks mark cells that are negative for NR2F2 and positive for GATA3/GATA2 ($n = 3$).

(C) IF of NR2F2 (cyan), GATA4 (green), and IFI16 (red). Nuclear counterstaining (DAPI) is white ($n = 4$).

(D) IF of NR2F2 (cyan), GATA4 (green), and IFI16 (red) after 72 h of prolonged culture of a B3 blastocyst ($n = 3$). Scale bars, 47 μm .

(E) Schematic representing identified cytokine-receptor loops.

protein expression at the late 16-cell morula stage. Experimentally, mouse TE cells at the 32-cell stage are committed, whereas ICM cells may be specified but not yet committed (Grabarek et al., 2012; Handyside, 1978; Rossant and Lis, 1979). The human pseudotime analysis shows the precise timing of transcriptionally

distinct TE at the transition from the B2 to the B3 stage. Our embryo-per-embryo analysis strategy revealed that transcriptomic heterogeneity could be found in human morula prior to complete segregation of cells into either of the two lineages. Coupling pseudotime with gene correlation analysis revealed the dynamics of

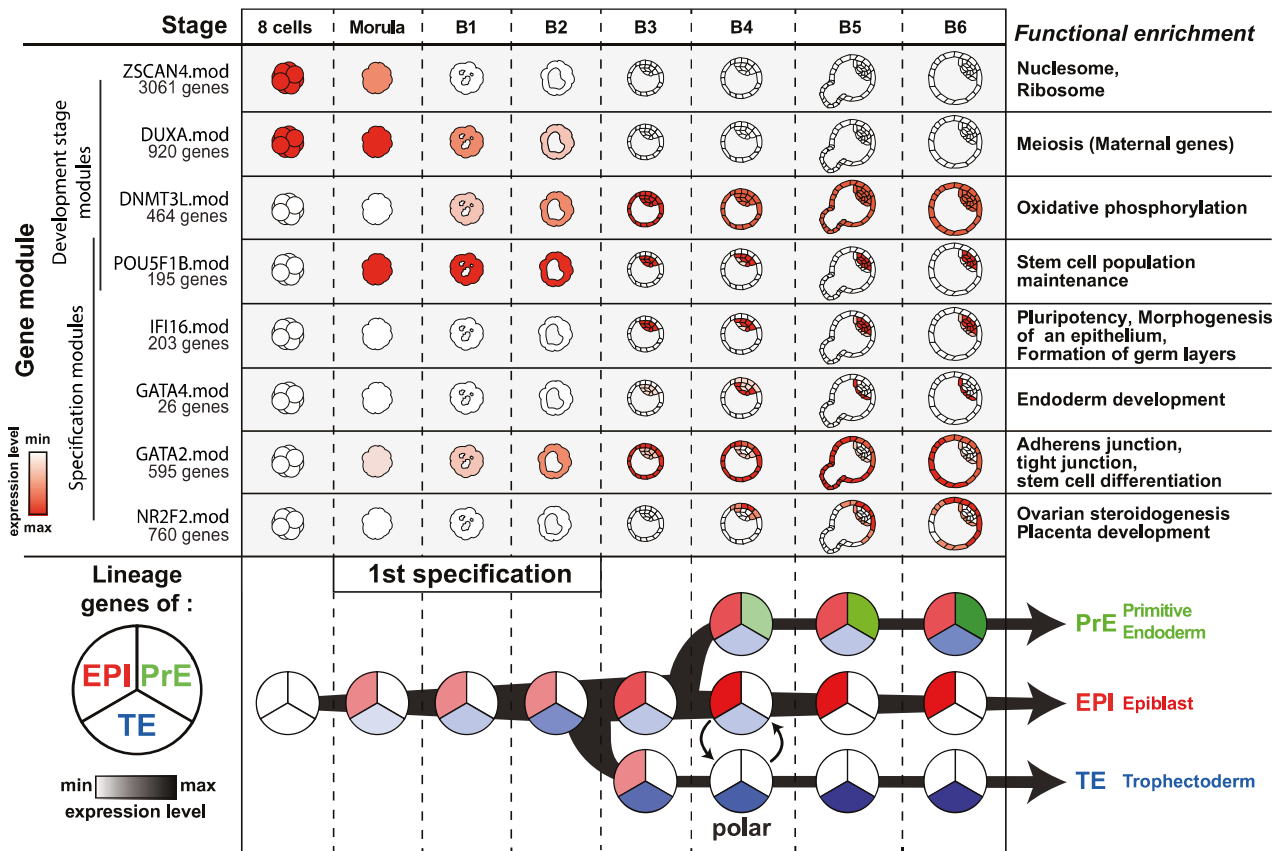


Figure 7. Human pre-implantation development model

Each annotation is represented according to morphology-based stages of human pre-implantation development. Top: schematic representation of gene module global expression. Terms highlighted by functional enrichment are presented on the right. Complete enrichment data are presented in [Figure S4D](#). Bottom: expression of lineage-specific stage per stage and per cell fate.

several gene modules that could be associated with specific states within each branch of the pseudotime. This led us to reveal, by IF, that IFI16 is expressed in a majority of ICM cells at the B4 stage, and progressively fades in the developing PrE cells. Moreover, we discovered that maturation of TE was initiated on the polar side, adjacent to the EPI, which yielded a molecular dialog. Our study improves our understanding of the molecular events occurring during human lineage specification and provides new markers of specific developmental steps ([Figure 7](#)).

Human *in vitro* pre-implantation development is highly heterogeneous from one embryo to another. The best way to annotate embryo stages to date is to record the development of human embryos with time-lapse devices ([Apter et al., 2020](#)). Combination of our scRNA-seq analysis of time-lapse annotated human embryos with previous datasets resolved annotation overlap between 4, 5, and 6 dpf, which previously limited translation of those datasets into a sequence of events, pacing human pre-implantation development. Indeed, binning embryos at 5 dpf results in averaging of transcriptome information from cavating B1 blastocysts to B4 expanded blastocysts. Because the TE, PrE, and EPI transcriptomes are emerging in that time frame, binning it all together creates a lot of noise in subsequent analyses. Our analysis, combining time-lapse annotation and

scRNA-seq, improves our ability to generate hypotheses regarding the molecular events regulating human pre-implantation development.

Two morphogenic events are particularly noticeable during mammalian pre-implantation development: compaction and cavitation. Compaction seems to involve rapid epithelialization in mouse and human ([White et al., 2018](#)). [Gerri et al. \(2020\)](#) showed that compaction coupled to the Hippo pathway triggers initiation of TE fate at the morula/B1 stage, which is characterized by expression of GATA3 in external cells. We found that transcriptional variability was increased greatly between cells from the morula but without achieving fate-associated transcriptomic signatures. The delay in the onset of distinct transcriptomic profiles of TE/ICM in humans compared with the mouse is rather surprising. This observation suggests that, in addition to compaction, other parameters are likely required to induce/complete lineage specification. One of these could be cell division. Human morulae compact at 10 cells and cavitate at 20 cells, resulting in a B1 stage that rapidly evolves to B2 stage blastocysts, generally composed of 40 cells. This suggests that two rounds of cellular division, after compaction, are required before cells can initiate/complete distinct transcriptomic programs relating to the ICM/TE. This occurs similarly but slightly earlier

in mouse development, where cell compaction takes place at the 8-cell stage and emergence of distinct cellular profiles is first seen at the 32-cell stage. Regarding cavitation, our analysis also revealed expression of AQP3, which was restricted to TE cells at the B2 stage. However, it remains to be demonstrated whether AQP3 expression depends on TE fate regulators or whether TE fate regulators depend on AQP3.

EPI/PrE specification is difficult to resolve in humans regardless of the approaches used (Blakeley et al., 2015; Petropoulos et al., 2016; Stirparo et al., 2018). Our analysis suggests that, within the ICM, the EPI fate is the first to be achieved. Computational modeling of the mouse raised similar conclusions: EPI cells need to secrete Fgf4 for PrE cells to specify (De Mot et al., 2016). Regarding PrE fate, we found that the PrE signature is defined better when analyses include embryos in prolonged culture; day 6 embryos cultured in IVC medium seem to have more developed PrE cells than day 6 embryos cultured in IVF medium (Petropoulos et al., 2016; Zhou et al., 2019). This could be because IVF media are not currently designed to support extended culture of embryos. It has been determined that day 7 blastocyst were less likely to implant (Shoukir et al., 1998) and are only transferred when no other embryos are available (Tiegs et al., 2019). Another possibility is that IVC medium favors rapid growth/development of human embryos. This observation shows how important it is to understand pre-implantation development in humans to improve embryo culture media.

We consider two main hypotheses for the EPI/PrE specification in humans: (1) early ICM cells are transcriptionally closer to EPI than to PrE or TE, resulting in ICM cells clustering with EPI cells; (2) PrE differentiates from EPI. More experiments are necessary to solve these hypotheses, but our study provides a framework; we have pinpointed the morphology associated with specific marker expression and provide novel markers informative of EPI/PrE specification, such as IFI16 and GATA4. In particular, IFI16 characterizes the transition between molecular states during EPI and PrE peri-implantation development. IFI16 expression suggests that IFNg signaling might be important for EPI specification. Furthermore, IFI16 has been shown to induce epigenetic silencing of viral promoters in immune cells (Roy et al., 2019). Therefore, one hypothesis is that IFI16 might inhibit the burst of transposable elements expressed at the morula stage (Giocanti-Auregan et al., 2016; Theunissen et al., 2016). Shutting down transposable elements might be necessary for EPI/PrE specification.

Transcriptomically, TE acquires a distinct expression profile at the transition from the B2 to the B3 stage, with cells progressively losing expression of pluripotency-associated genes, correlating with loss of plasticity of TE cells (De Paepe et al., 2013). We provide evidence showing that an EPI/TE molecular dialog could be involved in TE maturation. Interestingly, it is TE cells adjacent to the EPI, on the polar side, that typically initiate implantation prior to maturation of the remaining mural TE cells. However, in mouse embryos, secretion of Fgf4 and nodal by EPI contributes to the progression of polar and mural TE fates, and attachment is mediated by the mural, mature TE cells, highlighting differences between the two species (Guzman-Ayala et al., 2004; Yamagata and Yamazaki, 1991). It will be interesting to understand what triggers maturation of TE and whether NR2F2 plays a central role in this process in the mouse and humans.

Studies have demonstrated the importance of TE morphological quality for prediction of successful IVF (Ahlström et al., 2011; Chen et al., 2014; Hill et al., 2013; Thompson et al., 2013). Therefore, understanding this aspect of human pre-implantation development is of utmost importance to improve of IVF. We will now be able to focus on specific secreted markers associated with NR2F2⁺ cells that could inform clinicians about the implantation potential of the blastocyst before transfer. Indeed, secreted markers that correlate with expression of NR2F2 could be predictive of the implantation capacity of embryos. This discovery will support the much needed hypothesis regarding human implantation and complement knowledge resulting from study of murine reproduction (Aplin and Ruane, 2017).

Our study also provides key knowledge regarding modeling pre-implantation development with cellular models. Embryonic signature comparison with pluripotent stem cells residing in various states of pluripotency showed that the established hierarchy of pluripotent stem cells mimics EPI: naive pluripotent cells are closest to pre-implantation EPI (5–8 dpf), whereas primed pluripotent cells, commonly used, are closer to post-implantation EPI (after 10 dpf) (Castel et al., 2020; Kilens et al., 2018; Liu et al., 2017; Takashima et al., 2014; Theunissen et al., 2014). We and others also discovered that naive pluripotent stem cells can convert to human trophoblast stem cells (hTSCs), which is reminiscent of late specification in human blastocysts (Castel et al., 2020; Cinkornpumin et al., 2020; Dong et al., 2020; Guo et al., 2021). Recently, we proposed that human trophoblast stem cells correspond to human day 8 post-implantation cytotrophoblast (Castel et al., 2020). Our study highlights the importance of knowledge about human peri-implantation development to understand pluripotent and trophoblast stem cell biology.

Our study clarifies the timing of molecular events and signaling pathways involved in human pre-implantation development. Fine-tuning those pathways will lead to more efficient medium formulation for embryo culture during IVF procedures. Improvement of IVF procedures is necessary because the procedural average efficiency is below 27% (European Society of Human Reproduction and Embryology, 2015). Ultimately, our study contributes to understanding human pre-implantation, a gateway to improve IVF success rates.

Limitations of study

A current limitation of human embryo work is the variability of human developmental time *in vitro*, which impairs the reproducibility of experiments. Our study provides a molecular blueprint of human development coupled to time-lapse staging. We unveiled numerous hypotheses and interactions that remain to be validated. Positional information could be improved to discriminate between polar TE and ICM. Fate specification needs to be addressed with lineage tracing approaches, and the importance of specific transcription factors will need to be assessed with CRISPR-Cas9 strategies, which remain restricted in most countries.

STAR★METHODS

Detailed methods are provided in the online version of this paper and include the following:

- **KEY RESOURCES TABLE**
- **RESOURCE AVAILABILITY**
 - Lead contact
 - Materials availability
 - Data and code availability
- **EXPERIMENTAL MODEL AND SUBJECT DETAILS**
 - Human pre-implantation embryos
- **METHOD DETAILS**
 - Human pre-implantation embryos culture
 - Human embryo prolonged culture
 - Human embryo time-lapse imaging
 - Immunofluorescence of human embryos
 - Imaging
 - Single-cell isolation
- **QUANTIFICATION AND STATISTICAL ANALYSIS**
 - Single-cell RNA sequencing
 - Raw count table treatments
 - Computation of pseudotime
 - WGCNA
 - UMAP and cell clustering
 - Loess regressed expression by pseudotime
 - Subdivision of pseudotime branches
 - Data representation used in each figure
 - Mouse single-cell RNA-Seq analysis
 - RNA velocity
 - Enrichment analysis

SUPPLEMENTAL INFORMATION

Supplemental information can be found online at <https://doi.org/10.1016/j.stem.2021.04.027>.

ACKNOWLEDGMENTS

We thank our colleagues F. Lanner and K. Niakan for sharing data and providing feedback. We thank J. Jullien for critical review of the manuscript. D.M. is supported by FINOX, and MSD contributed to the project. We thank the core facilities BIRD, PFI-PSC, and MicroPicell. This work was supported by “Paris Scientifique region Pays de la Loire: HUMPLURI” and IHU CESTI.

AUTHOR CONTRIBUTIONS

T.F. and L.D. designed the study. D.M., A. Bruneau, S.L., and L.D. wrote the manuscript with input from all authors. S.L., A.R., J.F., J.L., and A. Bruneau performed embryo manipulation. P.H., S.N., S.L., A. Bruneau, A.R., and L.D. performed IF analyses. A.R. and S.K. prepared scRNA-seq samples. M.S. and T.M. performed scRNA-seq. D.M., V.F.-C., and Y.L. performed bioinformatics analyses under the supervision of A. Bihouée and J.B. and with input from B.B. and G.C. T.F. and P.B. supervised human embryo donation. All authors approved the final version of the manuscript.

DECLARATION OF INTERESTS

The authors declare no competing interests.

INCLUSION AND DIVERSITY

We worked to ensure gender balance in the recruitment of human subjects. We worked to ensure that the study questionnaires were prepared in an inclusive way. One or more of the authors of this paper self-identifies as a member of the LGBTQ+ community. The author list of this paper includes contributors from the location where the research was conducted who participated in the data collection, design, analysis, and/or interpretation of the work.

Received: August 6, 2019

Revised: July 16, 2020

Accepted: April 22, 2021

Published: May 17, 2021

REFERENCES

- Aberkane, A., Essahib, W., Spits, C., De Paepe, C., Sermon, K., Adriaenssens, T., Mackens, S., Tournaye, H., Brosens, J.J., and Van de Velde, H. (2018). Expression of adhesion and extracellular matrix genes in human blastocysts upon attachment in a 2D co-culture system. *Mol. Hum. Reprod.* **24**, 375–387.
- Acampora, D., Omodei, D., Petrosino, G., Garofalo, A., Savarese, M., Nigro, V., Di Giovannantonio, L.G., Mercadante, V., and Simeone, A. (2016). Loss of the Otx2-Binding Site in the Nanog Promoter Affects the Integrity of Embryonic Stem Cell Subtypes and Specification of Inner Cell Mass-Derived Epiblast. *Cell Rep.* **15**, 2651–2664.
- Ahlström, A., Westin, C., Reimer, E., Wikland, M., and Hardarson, T. (2011). Trophoctoderm morphology: an important parameter for predicting live birth after single blastocyst transfer. *Hum. Reprod.* **26**, 3289–3296.
- Allègre, N., Chauveau, S., Dennis, C., Renaud, Y., Estrella, L.V., Pouchin, P., Cohen-Tannoudji, M., and Chazaud, C. (2019). A Nanog-dependent gene cluster initiates the specification of the pluripotent epiblast. *bioRxiv*. <https://doi.org/10.1101/707679>.
- Alpha Scientists in Reproductive Medicine and ESHRE Special Interest Group of Embryology (2011). The Istanbul consensus workshop on embryo assessment: proceedings of an expert meeting. *Hum. Reprod.* **26**, 1270–1283.
- Anders, S., Pyl, P.T., and Huber, W. (2015). HTSeq—a Python framework to work with high-throughput sequencing data. *Bioinformatics* **31**, 166–169.
- Aplin, J.D., and Ruane, P.T. (2017). Embryo-epithelium interactions during implantation at a glance. *J. Cell Sci.* **130**, 15–22.
- Apter, S., Ebner, T., Freour, T., Guns, Y., Kovacic, B., Le Clef, N., Marques, M., Meseguer, M., Montjean, D., Sfontouris, I., et al. (2020). Good practice recommendations for the use of time-lapse technology(dagger). *Hum. Reprod. Open.* **2020**, hoaa008.
- Barcroft, L.C., Hay-Schmidt, A., Caveney, A., Gilfoyle, E., Overstrom, E.W., Hyttel, P., and Watson, A.J. (1998). Trophoctoderm differentiation in the bovine embryo: characterization of a polarized epithelium. *J. Reprod. Fertil.* **114**, 327–339.
- Barcroft, L.C., Offenberg, H., Thomsen, P., and Watson, A.J. (2003). Aquaporin proteins in murine trophoctoderm mediate transepithelial water movements during cavitation. *Dev. Biol.* **256**, 342–354.
- Bentin-Ley, U., Horn, T., Sjögren, A., Sorensen, S., Falck Larsen, J., and Hamberger, L. (2000). Ultrastructure of human blastocyst-endometrial interactions in vitro. *J. Reprod. Fertil.* **120**, 337–350.
- Blakeley, P., Fogarty, N.M.E., del Valle, I., Wamaita, S.E., Hu, T.X., Elder, K., Snell, P., Christie, L., Robson, P., and Niakan, K.K. (2015). Defining the three cell lineages of the human blastocyst by single-cell RNA-seq. *Development* **142**, 3151–3165.
- Boroviak, T., Stirparo, G.G., Dietmann, S., Hernando-Herraez, I., Mohammed, H., Reik, W., Smith, A., Sasaki, E., Nichols, J., and Bertone, P. (2018). Single cell transcriptome analysis of human, marmoset and mouse embryos reveals common and divergent features of preimplantation development. *Development* **145**, dev167833.
- Buecker, C., Srinivasan, R., Wu, Z., Calo, E., Acampora, D., Faial, T., Simeone, A., Tan, M., Swigut, T., and Wysocka, J. (2014). Reorganization of enhancer patterns in transition from naive to primed pluripotency. *Cell Stem Cell* **14**, 838–853.
- Castel, G., Meistermann, D., Bretin, B., Firmin, J., Blin, J., Loubersac, S., Bruneau, A., Chevolleau, S., Kilens, S., Chariau, C., et al. (2020). Induction of Human Trophoblast Stem Cells from Somatic Cells and Pluripotent Stem Cells. *Cell Rep.* **33**, 108419.
- Chan, C.J., Costanzo, M., Ruiz-Herrero, T., Mönke, G., Petrie, R.J., Bergert, M., Diz-Muñoz, A., Mahadevan, L., and Hiiragi, T. (2019). Hydraulic control of mammalian embryo size and cell fate. *Nature* **571**, 112–116.

- Chazaud, C., and Yamanaka, Y. (2016). Lineage specification in the mouse preimplantation embryo. *Development* *143*, 1063–1074.
- Chazaud, C., Yamanaka, Y., Pawson, T., and Rossant, J. (2006). Early lineage segregation between epiblast and primitive endoderm in mouse blastocysts through the Grb2-MAPK pathway. *Dev. Cell* *10*, 615–624.
- Chen, X., Zhang, J., Wu, X., Cao, S., Zhou, L., Wang, Y., Chen, X., Lu, J., Zhao, C., Chen, M., and Ling, X. (2014). Trophoctoderm morphology predicts outcomes of pregnancy in vitrified-warmed single-blastocyst transfer cycle in a Chinese population. *J. Assist. Reprod. Genet.* *31*, 1475–1481.
- Cinkornpumin, J.K., Kwon, S.Y., Guo, Y., Hossain, I., Sirois, J., Russett, C.S., Tseng, H.W., Okae, H., Arima, T., Duchaine, T.F., et al. (2020). Naive Human Embryonic Stem Cells Can Give Rise to Cells with a Trophoblast-like Transcriptome and Methyloome. *Stem Cell Reports* *15*, 198–213.
- Ciray, H.N., Campbell, A., Agerholm, I.E., Aguilar, J., Chamayou, S., Esbert, M., and Sayed, S.; Time-Lapse User Group (2014). Proposed guidelines on the nomenclature and annotation of dynamic human embryo monitoring by a time-lapse user group. *Hum. Reprod.* *29*, 2650–2660.
- De Mot, L., Gonze, D., Bessonard, S., Chazaud, C., Goldbeter, A., and Dupont, G. (2016). Cell Fate Specification Based on Tristability in the Inner Cell Mass of Mouse Blastocysts. *Biophys. J.* *110*, 710–722.
- De Paepe, C., Cauffman, G., Verloes, A., Sterckx, J., Devroey, P., Tournaye, H., Liebaers, I., and Van de Velde, H. (2013). Human trophoctoderm cells are not yet committed. *Hum. Reprod.* *28*, 740–749.
- De Paepe, C., Aberkane, A., Dewandre, D., Essahib, W., Sermon, K., Geens, M., Verheyen, G., Tournaye, H., and Van de Velde, H. (2019). BMP4 plays a role in apoptosis during human preimplantation development. *Mol. Reprod. Dev.* *86*, 53–62.
- Deglincerti, A., Croft, G.F., Pietila, L.N., Zernicka-Goetz, M., Siggia, E.D., and Brivanlou, A.H. (2016). Self-organization of the in vitro attached human embryo. *Nature* *533*, 251–254.
- Dong, C., Beltcheva, M., Gontarz, P., Zhang, B., Popli, P., Fischer, L.A., Khan, S.A., Park, K.M., Yoon, E.J., Xing, X., et al. (2020). Derivation of trophoblast stem cells from naïve human pluripotent stem cells. *eLife* *9*, e52504.
- Dumortier, J.G., Le Verge-Serandour, M., Tortorelli, A.F., Mielke, A., de Plater, L., Turlier, H., and Maltre, J.L. (2019). Hydraulic fracturing and active coarsening position the lumen of the mouse blastocyst. *Science* *365*, 465–468.
- Ester, M., Kriegel, H.P., Sander, J., and Xu, X. (1996). A density-based algorithm for discovering clusters in large spatial databases with noise. In *Proceedings of the Second International Conference on Knowledge Discovery and Data Mining*, pp. 226–231.
- European Society of Human Reproduction and Embryology (2015). *Data collection and research*. <https://www.eshre.eu/>.
- Feyeux, M., Reignier, A., Mocaer, M., Lammers, J., Meistermann, D., Barrière, P., Paul-Gilloteaux, P., David, L., and Fréour, T. (2020). Development of automated annotation software for human embryo morphokinetics. *Hum. Reprod.* *35*, 557–564.
- Fogarty, N.M.E., McCarthy, A., Snijders, K.E., Powell, B.E., Kubikova, N., Blakeley, P., Lea, R., Elder, K., Wamaitha, S.E., Kim, D., et al. (2017). Genome editing reveals a role for OCT4 in human embryogenesis. *Nature* *550*, 67–73.
- Frum, T., Murphy, T.M., and Ralston, A. (2018). HIPPO signaling resolves embryonic cell fate conflicts during establishment of pluripotency in vivo. *eLife* *7*, e42298.
- Gardner, D.K., Lane, M., Stevens, J., Schlenker, T., and Schoolcraft, W.B. (2000). Blastocyst score affects implantation and pregnancy outcome: towards a single blastocyst transfer. *Fertil. Steril.* *73*, 1155–1158.
- Gerri, C., McCarthy, A., Alanis-Lobato, G., Demtschenko, A., Bruneau, A., Loubersac, S., Fogarty, N.M.E., Hampshire, D., Elder, K., Snell, P., et al. (2020). Initiation of a conserved trophoctoderm program in human, cow and mouse embryos. *Nature* *587*, 443–447.
- Giacomini, G., Tabibzadeh, S.S., Satyaswaroop, P.G., Bonsi, L., Vitale, L., Bagnara, G.P., Strippoli, P., and Jasonni, V.M. (1995). Epithelial cells are the major source of biologically active granulocyte macrophage colony-stimulating factor in human endometrium. *Hum. Reprod.* *10*, 3259–3263.
- Giocanti-Auregan, A., Vacca, O., Bénard, R., Cao, S., Siqueiros, L., Montañez, C., Paques, M., Sahel, J.A., Sennlaub, F., Guillonnet, X., et al. (2016). Altered astrocyte morphology and vascular development in dystrophin-Dp71-null mice. *Glia* *64*, 716–729.
- Grabarek, J.B., Zzyńska, K., Saiz, N., Piliszek, A., Frankenberg, S., Nichols, J., Hadjantonakis, A.K., and Plusa, B. (2012). Differential plasticity of epiblast and primitive endoderm precursors within the ICM of the early mouse embryo. *Development* *139*, 129–139.
- Graham, S.J., and Zernicka-Goetz, M. (2016). The Acquisition of Cell Fate in Mouse Development: How Do Cells First Become Heterogeneous? *Curr. Top. Dev. Biol.* *117*, 671–695.
- Greenberg, M.V.C., and Bourc'his, D. (2019). The diverse roles of DNA methylation in mammalian development and disease. *Nat. Rev. Mol. Cell Biol.* *20*, 590–607.
- Grewal, S., Carver, J.G., Ridley, A.J., and Mardon, H.J. (2008). Implantation of the human embryo requires Rac1-dependent endometrial stromal cell migration. *Proc. Natl. Acad. Sci. USA* *105*, 16189–16194.
- Gu, Z., Eils, R., and Schlesner, M. (2016). Complex heatmaps reveal patterns and correlations in multidimensional genomic data. *Bioinformatics* *32*, 2847–2849.
- Guo, G., Stirparo, G.G., Strawbridge, S.E., Spindlow, D., Yang, J., Clarke, J., Dattani, A., Yanagida, A., Li, M.A., Myers, S., et al. (2021). Human naïve epiblast cells possess unrestricted lineage potential. *Cell Stem Cell*.
- Guzman-Ayala, M., Ben-Haim, N., Beck, S., and Constam, D.B. (2004). Nodal protein processing and fibroblast growth factor 4 synergize to maintain a trophoblast stem cell microenvironment. *Proc. Natl. Acad. Sci. USA* *101*, 15656–15660.
- Handyside, A.H. (1978). Time of commitment of inside cells isolated from pre-implantation mouse embryos. *J. Embryol. Exp. Morphol.* *45*, 37–53.
- Hannan, N.J., Paiva, P., Dimitriadis, E., and Salamonsen, L.A. (2010). Models for study of human embryo implantation: choice of cell lines? *Biol. Reprod.* *82*, 235–245.
- Hill, M.J., Richter, K.S., Heitmann, R.J., Graham, J.R., Tucker, M.J., DeCherney, A.H., Browne, P.E., and Levens, E.D. (2013). Trophoctoderm grade predicts outcomes of single-blastocyst transfers. *Fertil. Steril.* *99*, 1283–1289.e1.
- Hirate, Y., Hirahara, S., Inoue, K., Suzuki, A., Alarcon, V.B., Akimoto, K., Hirai, T., Hara, T., Adachi, M., Chida, K., et al. (2013). Polarity-dependent distribution of angiomin localizes Hippo signaling in preimplantation embryos. *Curr. Biol.* *23*, 1181–1194.
- Jedrusik, A., Parfitt, D.E., Guo, G., Skamagki, M., Grabarek, J.B., Johnson, M.H., Robson, P., and Zernicka-Goetz, M. (2008). Role of Cdx2 and cell polarity in cell allocation and specification of trophoctoderm and inner cell mass in the mouse embryo. *Genes Dev.* *22*, 2692–2706.
- Kilens, S., Meistermann, D., Moreno, D., Chariau, C., Gaignerie, A., Reignier, A., Lelièvre, Y., Casanova, M., Vallot, C., Nedellec, S., et al.; Milieu Intérieur Consortium (2018). Parallel derivation of isogenic human primed and naïve induced pluripotent stem cells. *Nat. Commun.* *9*, 360.
- Kimmelman, J., Heslop, H.E., Sugarman, J., Studer, L., Benvenisty, N., Caulfield, T., Hyun, I., Murry, C.E., Sipp, D., and Daley, G.Q. (2016). New ISSCR guidelines: clinical translation of stem cell research. *Lancet* *387*, 1979–1981.
- Korotkevich, G., Sukhov, V., and Sergushichev, A. (2019). Fast gene set enrichment analysis. *bioRxiv*. <https://doi.org/10.1101/060012>.
- Kuijk, E.W., van Tol, L.T., Van de Velde, H., Wubbolts, R., Welling, M., Geijssen, N., and Roelen, B.A. (2012). The roles of FGF and MAP kinase signaling in the segregation of the epiblast and hypoblast cell lineages in bovine and human embryos. *Development* *139*, 871–882.
- La Manno, G., Soldatov, R., Zeisel, A., Braun, E., Hochgerner, H., Petukhov, V., Lidschreiber, K., Kastrioti, M.E., Lönnerberg, P., Furlan, A., et al. (2018). RNA velocity of single cells. *Nature* *560*, 494–498.
- Langfelder, P., and Horvath, S. (2008). WGCNA: an R package for weighted correlation network analysis. *BMC Bioinformatics* *9*, 559.

- Lindenberg, S. (1991). Experimental studies on the initial trophoblast endometrial interaction. *Dan. Med. Bull.* **38**, 371–380.
- Liu, Z.P., Wu, C., Miao, H., and Wu, H. (2015). RegNetwork: an integrated database of transcriptional and post-transcriptional regulatory networks in human and mouse. *Database* **2015**, bav095.
- Liu, X., Nefzger, C.M., Rossello, F.J., Chen, J., Knaupp, A.S., Firas, J., Ford, E., Pflueger, J., Paynter, J.M., Chy, H.S., et al. (2017). Comprehensive characterization of distinct states of human naive pluripotency generated by reprogramming. *Nat. Methods* **14**, 1055–1062.
- Lun, A.T., McCarthy, D.J., and Marioni, J.C. (2016). A step-by-step workflow for low-level analysis of single-cell RNA-seq data with Bioconductor. *F1000Res.* **5**, 2122.
- McInnes, L., Healy, J., and Melville, J. (2018). UMAP: Uniform Manifold Approximation and Projection for Dimension Reduction. *arXiv*, 1802.03426, [arXiv. https://arxiv.org/abs/1802.03426](https://arxiv.org/abs/1802.03426).
- Niakan, K.K., and Eggan, K. (2013). Analysis of human embryos from zygote to blastocyst reveals distinct gene expression patterns relative to the mouse. *Dev. Biol.* **375**, 54–64.
- Petropoulos, S., Edsgård, D., Reinius, B., Deng, Q., Panula, S.P., Codeluppi, S., Plaza Reyes, A., Linnarsson, S., Sandberg, R., and Lanner, F. (2016). Single-Cell RNA-Seq Reveals Lineage and X Chromosome Dynamics in Human Preimplantation Embryos. *Cell* **165**, 1012–1026.
- Posfai, E., Petropoulos, S., de Barros, F.R.O., Schell, J.P., Jurisica, I., Sandberg, R., Lanner, F., and Rossant, J. (2017). Position- and Hippo signaling-dependent plasticity during lineage segregation in the early mouse embryo. *eLife* **6**, e22906.
- Qiu, X., Mao, Q., Tang, Y., Wang, L., Chawla, R., Pliner, H.A., and Trapnell, C. (2017). Reversed graph embedding resolves complex single-cell trajectories. *Nat. Methods* **14**, 979–982.
- Ramos-Ibeas, P., Sang, F., Zhu, Q., Tang, W.W.C., Withey, S., Klisch, D., Wood, L., Loose, M., Surani, M.A., and Alberio, R. (2019). Pluripotency and X chromosome dynamics revealed in pig pre-gastrulating embryos by single cell analysis. *Nat. Commun.* **10**, 500.
- Reijo Pera, R.A., and Prezzoto, L. (2016). Species-Specific Variation Among Mammals. *Curr. Top. Dev. Biol.* **120**, 401–420.
- Rivron, N.C., Frias-Aldeguer, J., Vrij, E.J., Boisset, J.C., Korving, J., Viví, J., Truckenmüller, R.K., van Oudenaarden, A., van Blitterswijk, C.A., and Geijsen, N. (2018). Blastocyst-like structures generated solely from stem cells. *Nature* **557**, 106–111.
- Roode, M., Blair, K., Snell, P., Elder, K., Marchant, S., Smith, A., and Nichols, J. (2012). Human hypoblast formation is not dependent on FGF signalling. *Dev. Biol.* **367**, 358–363.
- Rossant, J., and Lis, W.T. (1979). Potential of isolated mouse inner cell masses to form trophoblast derivatives in vivo. *Dev. Biol.* **70**, 255–261.
- Roy, A., Ghosh, A., Kumar, B., and Chandran, B. (2019). IFI16, a nuclear innate immune DNA sensor, mediates epigenetic silencing of herpesvirus genomes by its association with H3K9 methyltransferases SUV39H1 and GLP. *eLife* **8**, e49500.
- Sergushichev, A.A. (2016). An algorithm for fast preranked gene set enrichment analysis using cumulative statistic calculation. *bioRxiv*. <https://doi.org/10.1101/060012>.
- Shahbazi, M.N., Jedrusik, A., Vuoristo, S., Recher, G., Hupalowska, A., Bolton, V., Fogarty, N.N.M., Campbell, A., Devito, L., Ilic, D., et al. (2016). Self-organization of the human embryo in the absence of maternal tissues. *Nat. Cell Biol.* **18**, 700–708.
- Shahbazi, M.N., Scialdone, A., Skorupska, N., Weberling, A., Recher, G., Zhu, M., Jedrusik, A., Devito, L.G., Noli, L., Macaulay, I.C., et al. (2017). Pluripotent state transitions coordinate morphogenesis in mouse and human embryos. *Nature* **552**, 239–243.
- Shoukir, Y., Chardonens, D., Campana, A., Bischof, P., and Sakkas, D. (1998). The rate of development and time of transfer play different roles in influencing the viability of human blastocysts. *Hum. Reprod.* **13**, 676–681.
- Singh, M., Widmann, T.J., Bansal, V., Cortes, J.L., Schumann, G.G., Wunderlich, S., Martin, U., Garcia-Canadas, M., Garcia-Perez, J.L., Hurst, L.D., and Izsvak, Z. (2019). The selection arena in early human blastocysts resolves the pluripotent inner cell mass. *BioRxiv* **318329**.
- Stirparo, G.G., Boroviak, T., Guo, G., Nichols, J., Smith, A., and Bertone, P. (2018). Integrated analysis of single-cell embryo data yields a unified transcriptome signature for the human pre-implantation epiblast. *Development* **145**, dev158501.
- Takashima, Y., Guo, G., Loos, R., Nichols, J., Ficiz, G., Krueger, F., Oxley, D., Santos, F., Clarke, J., Mansfield, W., et al. (2014). Resetting transcription factor control circuitry toward ground-state pluripotency in human. *Cell* **158**, 1254–1269.
- Theunissen, T.W., Powell, B.E., Wang, H., Mitalipova, M., Faddah, D.A., Reddy, J., Fan, Z.P., Maetzel, D., Ganz, K., Shi, L., et al. (2014). Systematic identification of culture conditions for induction and maintenance of naive human pluripotency. *Cell Stem Cell* **15**, 471–487.
- Theunissen, T.W., Friedli, M., He, Y., Planet, E., O’Neil, R.C., Markoulaki, S., Pontis, J., Wang, H., Iouranova, A., Imbeault, M., et al. (2016). Molecular Criteria for Defining the Naive Human Pluripotent State. *Cell Stem Cell* **19**, 502–515.
- Thompson, S.M., Onwubalili, N., Brown, K., Jindal, S.K., and McGovern, P.G. (2013). Blastocyst expansion score and trophoblast morphology strongly predict successful clinical pregnancy and live birth following elective single embryo blastocyst transfer (eSET): a national study. *J. Assist. Reprod. Genet.* **30**, 1577–1581.
- Tiegs, A.W., Sun, L., Patounakis, G., and Scott, R.T. (2019). Worth the wait? Day 7 blastocysts have lower euploidy rates but similar sustained implantation rates as Day 5 and Day 6 blastocysts. *Hum. Reprod.* **34**, 1632–1639.
- Trombetta, J.J., Gennert, D., Lu, D., Satija, R., Shalek, A.K., and Regev, A. (2014). Preparation of Single-Cell RNA-Seq Libraries for Next Generation Sequencing. *Curr. Protoc. Mol. Biol.* **107**, 4.22.1–17.
- White, M.D., Zenker, J., Bissiere, S., and Plachta, N. (2018). Instructions for Assembling the Early Mammalian Embryo. *Dev. Cell* **45**, 667–679.
- Xiang, L., Yin, Y., Zheng, Y., Ma, Y., Li, Y., Zhao, Z., Guo, J., Ai, Z., Niu, Y., Duan, K., et al. (2020). A developmental landscape of 3D-cultured human pre-gastrulation embryos. *Nature* **577**, 537–542.
- Xiong, Y., Tan, Y.J., Xiong, Y.M., Huang, Y.T., Hu, X.L., Lu, Y.C., Ye, Y.H., Wang, T.T., Zhang, D., Jin, F., et al. (2013). Expression of aquaporins in human embryos and potential role of AQP3 and AQP7 in preimplantation mouse embryo development. *Cell. Physiol. Biochem.* **31**, 649–658.
- Yamagata, T., and Yamazaki, K. (1991). Implanting mouse embryo stain with a LNF-I bearing fluorescent probe at their mural trophoblast side. *Biochem. Biophys. Res. Commun.* **181**, 1004–1009.
- Yan, L., Yang, M., Guo, H., Yang, L., Wu, J., Li, R., Liu, P., Lian, Y., Zheng, X., Yan, J., et al. (2013). Single-cell RNA-Seq profiling of human preimplantation embryos and embryonic stem cells. *Nat. Struct. Mol. Biol.* **20**, 1131–1139.
- Zhou, F., Wang, R., Yuan, P., Ren, Y., Mao, Y., Li, R., Lian, Y., Li, J., Wen, L., Yan, L., et al. (2019). Reconstituting the transcriptome and DNA methylome landscapes of human implantation. *Nature* **572**, 660–664.
- Ziebe, S., Loft, A., Povlsen, B.B., Erb, K., Agerholm, I., Aasted, M., Gabrielsen, A., Hnida, C., Zobel, D.P., Munding, B., et al. (2013). A randomized clinical trial to evaluate the effect of granulocyte-macrophage colony-stimulating factor (GM-CSF) in embryo culture medium for in vitro fertilization. *Fertil. Steril.* **99**, 1600–1609.

STAR★METHODS

KEY RESOURCES TABLE

REAGENT or RESOURCE	SOURCE	IDENTIFIER
Antibodies		
IFI16	Novusbio	Cat# NBP1-83118; RRID:AB_11041205
AQP3	Antibodies-online	Cat# ABIN863208
NR2F2	Abcam	Cat# ab211776
GATA2	Sigma	Cat# WH0002624M1; RRID:AB_1841726
CDH1	Abcam	Cat# ab1416; RRID:AB_300946
GATA3	R&D systems	Cat# AF2605; RRID:AB_2108571
NANOG	R&D systems	Cat# AF1997; RRID:AB_355097
SOX17	R&D systems	Cat# AF1924; RRID:AB_355060
ZO1	Invitrogen	Cat# 40-2200; RRID:AB_2533456
NANOG	ThermoFisher	Cat# PA1-097; RRID:AB_2539867
GATA4	Invitrogen	Cat# 14-9980-82; RRID:AB_763541
IFI16	Abcam	Cat# ab55328; RRID:AB_943797
OTX2	R&D	Cat# AF1979; RRID:AB_2157172
Donkey anti rabbit Alexa Fluor 488	Life Technologies	Cat#A21206; RRID:AB_2535792
Donkey anti mouse Alexa Fluor 488	Life Technologies	Cat#A21202; RRID:AB_141607
Donkey anti rabbit Alexa Fluor 568	Life Technologies	Cat#A10042; RRID:AB_2534017
Donkey anti mouse Alexa Fluor 568	Life Technologies	Cat#A10037; RRID:AB_2534013
Donkey anti goat Alexa Fluor 568	Life Technologies	Cat#A11057; RRID:AB_2534104
Donkey anti goat Alexa Fluor 647	Life Technologies	Cat#A21447; RRID:AB_2535864
Donkey anti rat DyLight 550	ThermoFisher	Cat#SA5-10027; RRID:AB_2556607
Donkey anti mouse Alexa Fluor Plus 647	Life Technologies	Cat#A32787; RRID:AB_2762830
Biological samples		
Human pre-implantation embryos from 8 cells to B5 stage	Assisted Reproductive Technology unit of the University Hospital of Nantes	Authorized project: RE13-010 and RE18-010
Chemicals, peptides, and recombinant proteins		
RapidWarmBlast	Vitrolife	10120
RapidWarCleave	Vitrolife	10118
G2 plus	Vitrolife	10132
HSA solution	Vitrolife	10064
G-PGD	Vitrolife	10074
GTL	Vitrolife	10145
IVC1 medium	Cell guidance systems	M11-6
IVC2 medium	Cell guidance systems	M12-6
Deposited data		
scRNA-seq original data	This paper; ENA	https://www.ebi.ac.uk/ena/browser/view/PRJEB30442
scRNA-Seq alignment pipeline	This paper; GitLab	https://gitlab.univ-nantes.fr/E114424Z/SingleCell_Align
scRNA-Seq preprocessing and normalization	This paper; GitLab	https://gitlab.univ-nantes.fr/E114424Z/singlecellnormalize
WGCNA workflow	This paper; GitLab	https://gitlab.univ-nantes.fr/E114424Z/WGCNA
Monocle2 workflow, UMAP and cell clustering	This paper; GitLab	https://gitlab.univ-nantes.fr/E114424Z/monocle2_workflow

(Continued on next page)

Continued

REAGENT or RESOURCE	SOURCE	IDENTIFIER
Pseudotime User Interface source code	This paper; GitLab	https://gitlab.univ-nantes.fr/E114424Z/ptuihost
Software and algorithms		
Volocity	Quorum technologies	V6.3
Fiji	ImageJ	V1.53c
R	Bioconductor	v 4.0.3

RESOURCE AVAILABILITY

Lead contact

Further information and requests should be directed to the Lead Contact, Laurent DAVID (laurent.david@univ-nantes.fr)

Materials availability

This study did not generate new unique reagents

Data and code availability

The accession number for the original scRNA-seq data reported in this paper is ENA: PRJEB30442.

The source code can be retrieved by following the links below.
scRNaseq alignment pipeline:

https://gitlab.univ-nantes.fr/E114424Z/SingleCell_Align

scRNaseq preprocessing and normalization:

<https://gitlab.univ-nantes.fr/E114424Z/singlecellnormalize>

WGCNA workflow:

<https://gitlab.univ-nantes.fr/E114424Z/WGCNA>

Monocle2 workflow, UMAP and cell clustering:

https://gitlab.univ-nantes.fr/E114424Z/monocle2_workflow

Pseudotime User Interface source code:

<https://gitlab.univ-nantes.fr/E114424Z/ptuihost>

All other parts of the code are available upon request

EXPERIMENTAL MODEL AND SUBJECT DETAILS

Human pre-implantation embryos

The use of human embryo donated to research as surplus of IVF treatment was allowed by the French embryo research oversight committee: Agence de la Biomédecine, under approval number RE13-010 and RE18-010. All human pre-implantation embryos used in this study were obtained from and cultured at the Assisted Reproductive Technology unit of the University Hospital of Nantes, France, which are authorized to collect embryos for research under approval number AG110126AMP of the Agence de la Biomédecine. Embryos used were initially created in the context of an assisted reproductive cycle with a clear reproductive aim and then voluntarily donated for research once the patients have fulfilled their reproductive needs or tested positive for the presence of monogenic diseases. Informed written consent was obtained from both parents of all couples that donated spare embryos following IVF treatment. Before giving consent, people donating embryos were provided with all of the necessary information about the research project and opportunity to receive counselling. No financial inducements are offered for donation. Molecular analysis of the embryos was performed in compliance with the embryo research oversight committee and The International Society for Stem Cell Research (ISSCR) guidelines (Kimmelman et al., 2016).

METHOD DETAILS

Human pre-implantation embryos culture

Human embryos were thawed following the manufacturer's instructions (Cook Medical: Sydney IVF Thawing kit for slow freezing and Vitrolife: RapidWarmCleave or RapidWarmBlast for vitrification). Human embryos frozen at 8-cell stage were loaded in a 12-well dish

(Vitrolife: Embryoslide Ividi) with non-sequential culture media (Vitrolife G2 plus) under mineral oil (Origio: Liquid Paraffin), at 37°C, in 5% O₂/6% CO₂.

Human embryo prolonged culture

Embryos cultured for 5 days (11xB3 and 5xB4 blastocysts) were thawed as described above. The *zona pellucida* (ZP) of each embryo was removed by brief laser impulse followed by manual extrusion or aspiration of the embryo. *Zona pellucida* free embryos were washed in GTL medium and immediately transferred in 8-well IbiTreat μ -plates (IB-80826; Ividi GmbH) with 300 μ L IVC1 medium (M11-6, Cell Guidance systems) (Deglincerti et al., 2016) and cultured at 37°C, in 21% O₂/5% CO₂. After 48h of *in vitro* culture (day 2), 250 μ L of IVC1 was replaced with 250 μ L of IVC2 medium (M12-6, Cell Guidance systems). At B3 or B4 + 72h *in vitro* culture, 11/16 embryos (69%) were attached, 3 (19%) were floating and 2 (12%) disaggregated.

Human embryo time-lapse imaging

Embryos were loaded into the Embryoscope® (Vitrolife®), a tri-gas incubator with a built-in microscope allowing time-lapse monitoring of embryo development. Images were captured on seven focal plans every 15-min intervals using Hoffman modulation contrast (HMC) optical setup¹ and a 635 nm LED as light source as provided in the Embryoscope®. The resolution of the camera is 1280x1024 pixels. The development of each embryo was prospectively annotated as described by Ciray et al., by two trained embryologists undergoing regular internal quality control in order to keep inter-operator variability as low as possible (Ciray et al., 2014). ZP thickness was measured by our analysis pipeline (Feyeux et al., 2020). The term tM refers to a fully compacted morula. At the blastocyst stage, tSB is used to describe the onset of a cavity formation, tB is used for full blastocyst i.e the last frame before the ZP starts to thin, tEB for expanded blastocyst, i.e., when the ZP is 50% thinned. Blastocyst contractions and the beginning of herniation were also recorded.

Immunofluorescence of human embryos

Embryos were fixed at the morula, B1, B2, B3, B4, B5 or B6 stages according to the grading system proposed by Gardner and Schoolcraft (Gardner et al., 2000) or at B3 or B4 + 72h *in vitro* culture. Embryos were fixed with 4% paraformaldehyde for 5 min at room temperature and washed in PBS/BSA. Embryos were permeabilized and blocked in IF Buffer (PBS–0.2% Triton, 10% FBS) at room temperature for 60 min. Samples were incubated with primary antibodies over-night at 4°C. Incubation with secondary antibodies was performed for 2 hours at room temperature along with DAPI counterstaining. Primary and secondary antibodies with dilutions used in this study are listed in Table S4.

Imaging

Confocal immunofluorescence pictures were taken with a Nikon confocal microscope and a 20 × Mim objective. Optical sections of 1 μ m-thick were collected. The images were processed using Fiji (<https://fiji.sc/>) and Volocity 6.3 visualization softwares. Volocity software was used to detect and count nuclei. Two experienced operators graded nuclei signal for each IF channel. Grading was performed independently and counts were then averaged. A nucleus is considered positive for staining if signal is clearly higher than background. “High” or “low” positive staining is up to each operator according to the general signal intensity for each channel. Several embryos were photobleached in order to restrain it (Figure 6C; Figures S6A and S6B). Under Nikon A1 confocal, lasers at 568nm and 647nm were set to 100% power for 10min. The NR2F2 (Rabbit / 488) – SOX17 (Goat / 647) – IFI16 (Mouse / 568) stained embryos were restained with NR2F2 (Rabbit / 488) – GATA4 (Rat / 568) – IFI16 (Mouse / 647). Scale of Figure S1E was estimated with the diameter of the STRIPPER® tip.

Single-cell isolation

PGD-trained people performed brief laser impulses to separate the polar TE and ICM and mural TE of blastocysts. Embryos were then incubated 10min in G-PGD/HSA (Vitrolife®) and transferred in accutase. Embryos were triturated with gentle pipette flush under binocular magnifier for 3-4min. Single-cells/clumps were washed in GTL (Vitrolife®) and triturated again if necessary. Single-cells were picked one by one with IVF-lab capillaries.

QUANTIFICATION AND STATISTICAL ANALYSIS

Single-cell RNA sequencing

Single-cell isolation and overall dataset are presented in Figure S1 and Tables S1 and S5. Single-cell RNA-seq libraries were prepared according to the SmartSeq2 protocol with some modifications (Trombetta et al., 2014). Briefly, total RNA was purified using RNA-SPRI beads. Poly(A)⁺ mRNA was reverse-transcribed to cDNA which was then amplified. cDNA was subject to transposon-based fragmentation that used dual-indexing to barcode each fragment of each converted transcript with a combination of barcodes specific to each sample. In the case of single cell sequencing, each cell was given its own combination of barcodes. Barcoded cDNA fragments were then pooled prior to sequencing. Sequencing was carried out as paired end 2x25bp with an additional 8 cycles for each index. The FASTQ files were mapped with Hisat2 on GRChH38 genome version, downloaded from ensembl.org. HTSeq (Anders et al., 2015) was used to generate raw counts tables from BAM files, using the matching GTF for the reference genome.

Raw count table treatments

Samples were filtered with the use of the R function *isOutlier* from SCRAN (Lun et al., 2016) library. This function tags samples as outliers with a threshold based on median derivation away from the median of the metric. We filtered samples with two metrics: the number of expressed genes with a threshold of 2 median away derivation from median, and the total number of counts in the sample with a threshold of 3 median away derivation from median. Both metrics were used to discard samples in a two-sided way, below and above the median. This two-sided filter was applied to remove samples carrying too little (93876 counts – 5558 genes) or too much (80431229 counts – 18711 genes) information. Indeed, these are considered as potential doublet events. Genes that were expressed in less than two cells and with an average expression less than 0.1 were removed.

The four datasets were then normalized together using the *computeSumFactor* function from SCRAN. Logged and non-logged data were collected using the *normalize* function from scater R library. To compute batch effect free expression, we normalized the data as described above but per dataset. We used mutual nearest neighbors correction implemented by the function *mnnCorrect* to achieve the batch correction from the log-normalized data. The reference dataset that were used for *mnnCorrect* is from Petropoulos et al. (2016).

Computation of pseudotime

Monocle2 needs a subset of genes to make the dimensionality reduction and pseudotimes trajectories. To choose the best set of ordering genes we took samples that passed the quality control from Petropoulos et al. (2016) to avoid batch effects. We used SCRAN for processing size factors (normalization factor). We then created an R object with the *newCellDataSet* object used by Monocle2 with the raw expression and the expressionFamily parameter set as “negbinomial.size()”. Size factors were attributed according to the SCRAN results. The next step consisted of estimating empirical dispersion of each gene in the negative binomial model with the *estimateDispersions* function. We used the dispersion table function to gather the empirical dispersion and the fitted theoretical dispersion for each gene. We made a ratio of empirical dispersion on the theoretical dispersion for each gene. This ratio describes an over-dispersion score.

For a given gene i the over-dispersion score S_i is calculated as follows: $S_i = \frac{\sigma_{amp,i}^2}{\sigma_{theo,\mu_i}^2}$

Genes with an average log expression < 0.5 across samples were filtered out. Remaining genes were ranked based on their over-dispersion score.

Pseudotimes were generated using a range of top ranked ordering genes from the top 500 to the top 5500. This led to 5000 pseudotimes. For each pseudotime, A new R object was created with the *newCellDataSet* function, with the batch corrected expression from the four datasets as input and the expressionFamily parameter set as “gaussianff()”. Selected ordering genes were then set as input of Monocle2 algorithm, with the number of resulting dimensions set to three dimensions. An automatic classification of pseudotimes was set up following three criteria based on their topology:

- Number of branches populated by mural TE cells.
- Succession of developmental stage.
- Position and number of branching points.

The most common topologies were: (i) all mural TE cells within one branch, (ii) developmental stages succeeding one other, i.e., morula between 8-cell and blastocysts, (iii) two branching points, (iv) first branching point at E5. The chosen pseudotime belonged systematically to the most abundant topologies and is calculated from 4484 ordering genes. The resulting 3-dimension pseudotime was rotated to obtain a 2-dimensional projection.

WGCNA

WGCNA (Langfelder and Horvath, 2008) was performed on batch corrected data using a soft power of 10 with signed Pearson correlation. Resulting module were manually curated to choose a set of 8 modules that were well represented in data and that have distinct behaviors. For each module we use the module eigengene metric that is given by WGCNA to infer the global module expression across the samples. A loess regression of eigengene by pseudotime was used for Figure S4C. Gene list for each module can be found in Table S3.

UMAP and cell clustering

UMAP was computed with the R library uwot. Module eigengenes from the 8 studied WGCNA modules were used as features for the UMAP algorithm. The *n_neighbors* parameter was set to 1751 (size of the dataset) and *min_dist* = 0.01. Density clustering of cells was performed with *dbSCAN* with *eps* = 0.21 and *minPts* = 5. 52 outliers were attributed manually to existing clusters. An additional *kmeans* ($k = 2$) was performed on the main TE cluster from NR2F2 and GATA2 module eigengenes to separate the medium and the late TE (Korotkevich et al., 2019; Sergushichev, 2016).

Loess regressed expression by pseudotime

We used a Locally Weighted Regression (LOESS) to fit expression in the pseudotime by cell fate with a neighbor impact of 0.75. Expression profiles of common segments were fitted to extract global tendencies. A last LOESS was computed with a low neighbor impact to merge segments to obtain continuous expression curves.

Subdivision of pseudotime branches

The original pseudotime was constituted by five states, as Monocle2 separates states only by branching point. We subdivided pre-specification and trophectoderm branch samples by using WGCNA module eigengene. For both branches, WGCNA modules with a Pearson correlation higher than 0.75 with the pseudotime were selected. A loess regression of these module eigengene by pseudotime was performed, followed by a hierarchical clustering of regressed module eigengenes. The clustering was then partitioned. For each branch the best partition was determined at three clusters with the greatest relative loss of inertia method.

Data representation used in each figure

Raw expression:

- estimation of gene dispersion and select ordering genes

Normalized expression:

- projection of gene expression on pseudotime or UMAP (Figures 1C and 1E; Figure S3B)
- Heatmap (Figure 2C)
- Pseudotime User Interface (Figure S4E)

Loess regressed expression by pseudotime:

- expression profile curves (Figure S7)

Batch corrected logged expression:

- computation of pseudotime
- computation of WGCNA modules

ComplexHeatmap (Gu et al., 2016), ggplot2 and d3.js. were used for graphical representation. Hierarchical clustering was done using the Ward criteria and from a correlation distance for the gene/pathway eigengenes, or from the euclidean distance for other metrics.

Mouse single-cell RNA-Seq analysis

Mouse dataset were analyzed in a similar way to human datasets, without batch correction. Alignment step was done from the mm10 version of the genome. Timing of blastulation is corroborated by time-lapse. Cell annotations can be found in Table S2.

RNA velocity

RNA velocity was performed from BAM of samples that have passed all quality control in the final counts table. First, we used velocity.py using the command `velocity run`, with the parameter `-logic` as “SmartSeq2,” and the parameter `-m` (RepeatMasker annotations) as a GTF downloaded from the UCSC genome browser. The global GTF was the same that were used for the computation of raw counts table. Resulting loom files were merged using `loompy.combine` from `loompy` python package. We used `velocity.R` for computing Velocity matrix. Loom files were read with the function `read.loom.matrices`. Then we separated spliced reads matrix, unspliced reads matrix and spanning reads matrix. For each of the matrices gene filtering was performed with the function `filter.genes.by.cluster.expression`. The `min.max.cluster.average` parameters were set for the corresponding matrix as:

- spliced reads matrix: 5
- unspliced reads matrix: 1
- spanning reads matrix: 0.5

Then RNA velocity was estimated using `gene.relative.velocity.estimate`, with the following parameters: `fit.quantile = 0.05`, `deltaT = 1`, `kCells = 5`.

PCA of Figures 3D and 3E were calculated with the function `pca.velocity.plot`.

RNA velocity vectors were projected on an isometric representation of the UMAP (Figures 3F, 3G, 5G, and 5H) with the function `show.velocity.on.embedding.cor`. Only the cells from the Petrolooulos et al. dataset are projected to avoid batch effects during the computation of RNA velocities.

In the Figures 3F and 3G, the limit between the sector of early TE and EPI is the bisector of the angle formed by the cluster centroid of EPI, B1 & B2 and early TE in the UMAP.

In the Figures 5G and 5H, the sector of the circular diagram was oriented to face the centroid of the PrE cluster from the centroid of the EPI.PrE cluster.

Enrichment analysis

Module enrichment analysis was performed with FGSEA ([Sergushichev, 2016](#)). Ranking metric for fGSEA was set as WGCNA gene module membership ([Korotkevich et al., 2019](#)). This score is processed by Pearson correlation of module eigengene and gene expression. Enrichment was made on five databases: Gene ontology (Cellular Component, Molecular Function and Biological Process), Reactom and KEGG. All retained terms were enriched below an adjusted Benjamini-Hochberg p value of 0.05. A list of transcriptional factors (TF) was downloaded from the RegNetwork database ([Liu et al., 2015](#)). Pathway eigengene metric ([Figure S4D](#)) was processed by taking the first component of a principal component analysis of genes from each enriched term.

Human blastoids model blastocyst development and implantation


<https://doi.org/10.1038/s41586-021-04267-8>

Received: 12 February 2021

Accepted: 18 November 2021

Published online: 2 December 2021

Open access

 Check for updates

Harunobu Kagawa^{1,7}, Alok Javali^{1,7}, Heidar Heidari Khoei^{1,7}, Theresa Maria Sommer¹, Giovanni Sestini¹, Maria Novatchkova^{1,2}, Yvonne Scholte op Reimer¹, Gaël Castel³, Alexandre Bruneau³, Nina Maenhoudt⁴, Jenna Lammers^{3,5}, Sophie Loubersac^{3,5}, Thomas Freour^{3,5}, Hugo Vankelecom⁴, Laurent David^{3,6} & Nicolas Rivron^{1,✉}

One week after fertilization, human embryos implant into the uterus. This event requires the embryo to form a blastocyst consisting of a sphere encircling a cavity lodging the embryo proper. Stem cells can form a blastocyst model that we called a blastoid¹. Here we show that naive human pluripotent stem cells cultured in PXGL medium² and triply inhibited for the Hippo, TGF- β and ERK pathways efficiently (with more than 70% efficiency) form blastoids generating blastocyst-stage analogues of the three founding lineages (more than 97% trophoderm, epiblast and primitive endoderm) according to the sequence and timing of blastocyst development. Blastoids spontaneously form the first axis, and we observe that the epiblast induces the local maturation of the polar trophoderm, thereby endowing blastoids with the capacity to directionally attach to hormonally stimulated endometrial cells, as during implantation. Thus, we propose that such a human blastoid is a faithful, scalable and ethical model for investigating human implantation and development^{3,4}.

A model of the human blastocyst would support scientific and medical progress. Its ability to predict human development will, however, depend on its ability to reproduce the sequences of blastocyst cellular determination and morphogenesis effectively, faithfully, and according to the developmental sequence and pace. Such modelling would ensure the formation of cells that reflect the blastocyst stage as a starting point to recapitulate aspects of subsequent developmental steps, including implantation. During this year, diverse ways of forming models of the human blastocyst have been proposed^{5–9}. However, the cells generated often do not match those of the blastocyst^{5,7–9} (at 5–7 days post fertilization (dpf)) and have been proposed to rather reflect later developmental stages, including gastrulation (E14) and germ layers (mesoderm and endoderm) stages¹⁰. Here we form a model of the human blastocyst that specifically generates and spatially patterns cellular analogues of the blastocyst stage with similar developmental sequence and pace, which enables the model to mimic aspects of implantation.

Inhibition of Hippo, ERK and TGF β pathways

At 4 dpf, the conceptus forms a morula that initiates cavitation to make a blastocyst. Blastocyst development (at 5–7 dpf) supports the generation of the three founding lineages¹¹: the epiblast (EPI), which is embryonic; trophoderm (TE), which is extraembryonic; and primitive endoderm (PrE), which is extraembryonic (Fig. 1a). Peripheral cells become TE through inhibition of the Hippo pathway^{12,13}. Naive human pluripotent stem cells (PSCs) cultured in PXGL² efficiently form TE analogues upon inhibition of TGF β and ERK pathways^{14–16}. We aggregated naive PSCs in

non-adherent hydrogel microwells and inhibited these three pathways (Fig. 1b, Extended Data Fig. 1ac). Upon exposure to lysophosphatidic acid (LPA) (a Hippo pathway inhibitor), A83-01 (an inhibitor of TGF β family receptors) and PD0325901 (an ERK inhibitor) in a chemically defined medium containing the STAT activator leukaemia inhibitory factor (LIF) and Y-27632 (a ROCK inhibitor), blastocyst-like structures formed efficiently (Fig. 1c–e, Supplementary Videos 1, 2; more than 70% efficiency, diameters 150–250 μ m; full morphometric criteria are presented in Methods) and consistently (Extended Data Fig. 1d, more than 20 passages). LPA was essential for this high efficiency (Extended Data Fig. 1b–d). Within 4 days, the cell number (47 ± 9 to 129 ± 27) and overall size (65–200 μ m) had increased (Extended Data Fig. 1e, f) to ranges similar to those for 5–7 dpf blastocysts¹⁷ (stages B3 to B6). TE cell analogues¹¹ (identified as GATA2⁺GATA3⁺CDX2⁺TROP2⁺) formed, proliferated (Fig. 1f–h, Extended Data Fig. 1g–i), and established adherens junctions (marked by epithelial cadherin (CDH1)), apical–basal polarity (indicated by atypical PKC (aPKC) localization) and tight junctions (marked by ZO-1; Fig. 1i, Extended Data Fig. 1m) while undergoing cycles of inflations and deflations¹⁸ (Extended Data Fig. 1n, Supplementary Video 2). Of note, all blastocyst-like structures set apart a unique inner cell cluster reflecting the EPI (OCT4⁺; 27 ± 13 cells; 26% of total cells) and PrE (GATA4⁺SOX17⁺PDGFRa⁺; 7 ± 5 cells; 7% of total cells) (Fig. 1f–h, Extended Data Fig. 1i, j, l). Multiple lines of naive human embryonic stem (ES) cells (Shef6, H9 and HNES1) and human naive induced PSCs (niPSC 16.2.b and cR-NCRM2) formed similar structures with comparably high efficiency (Fig. 1e, Extended Data Fig. 1o), whereas primed PSCs that reflect the post-implantation EPI did not (Extended Data Fig. 1p).

¹Institute of Molecular Biotechnology of the Austrian Academy of Sciences (IMBA), Vienna BioCenter (VBC), Vienna, Austria. ²Institute of Molecular Pathology (IMP), Vienna Biocenter, Vienna, Austria. ³Université de Nantes, CHU Nantes, INSERM, Centre de Recherche en Transplantation et Immunologie, UMR 1064, ITUN, Nantes, France. ⁴Unit of Stem Cell Research, Cluster of Stem Cell and Developmental Biology, Department of Development and Regeneration, KU Leuven, (University of Leuven), Leuven, Belgium. ⁵CHU Nantes, Service de Biologie de la Reproduction, Nantes, France. ⁶Université de Nantes, CHU Nantes, INSERM, CNRS, SFR Santé, FED 4203, INSERM UMS 016, CNRS UMS 3556, Nantes, France. ⁷These authors contributed equally: Harunobu Kagawa, Alok Javali, Heidar Heidari Khoei. ✉e-mail: nicolas.rivron@imba.oew.ac.at

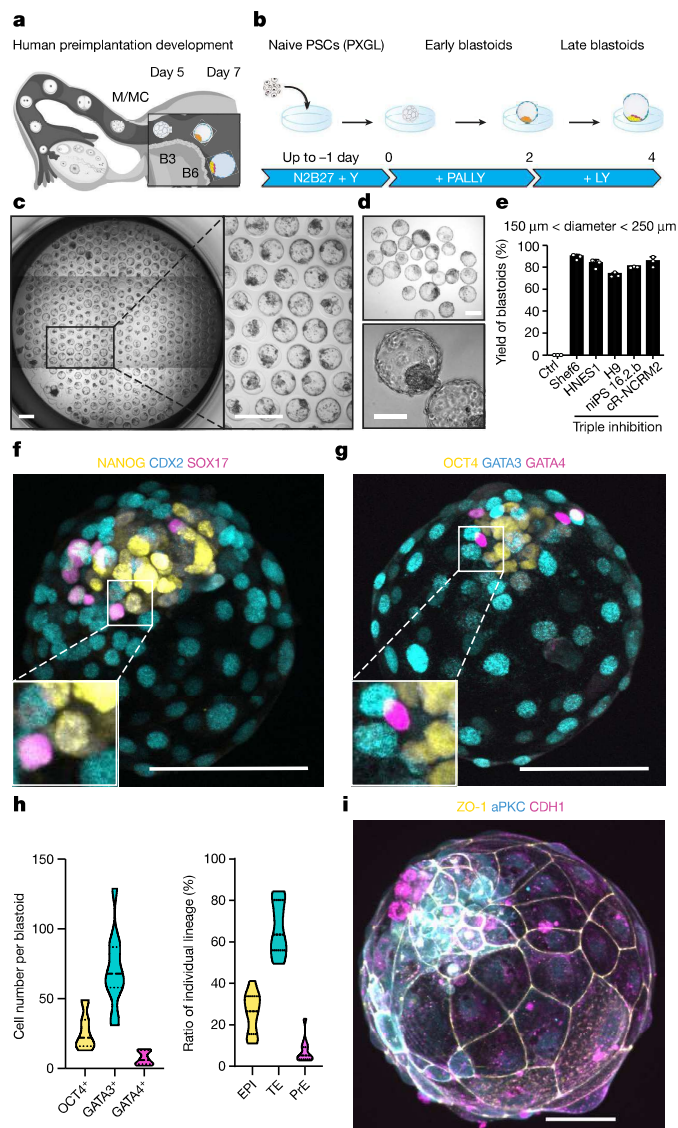


Fig. 1 | Triply inhibited naive PSCs efficiently form human blastocyst-like structures comprising analogues of the three founding lineages.

a, A schematic of the time window of human peri-implantation development modelled by blastoids (days 5–7). M/MC, morula/morula compacted; B, blastocyst. **b**, One-step protocol of human blastocyst-like structure formation. N2B27, serum-free medium; PALLY, PD0325901 + A83-01 + LPA + hLIF + Y-27632. **c**, Phase-contrast image of human blastocyst-like structures formed on a non-adherent hydrogel microwell array after 96 h. Each microwell is 200 μm in diameter. Scale bars, 400 μm . **d**, Phase-contrast images of representative human blastocyst-like structures harvested from microwells. Scale bars, 200 μm (top) and 100 μm (bottom). **e**, Percentages of microwells including a human blastocyst-like structure for different naive PSC lines cultured in the PALLY condition with optimized LPA concentration compared with a H9 control (Ctrl) deprived of the three inhibitors. The morphometric definition of blastocyst-like structures is provided in Methods. $n = 3$ microwell arrays; mean \pm s.d. **f, g**, Immunofluorescence of the epiblast (EPI) markers NANOG (yellow) (**f**) and OCT4 (yellow) (**g**), the TE markers CDX2 (cyan) (**f**) and GATA3 (cyan) (**g**), and the PrE markers SOX17 (magenta) (**f**) and GATA4 (magenta) (**g**) in human blastocyst-like structures. Scale bars, 100 μm . **h**, Absolute number of cells positive for OCT4, GATA3 and GATA4 (left) and ratios of cells belonging to individual lineages represented as percentage of total number of cells (right) in blastocyst-like structures (96 h) based on immunofluorescence. **i**, Representative immunofluorescence of the tight junction molecule ZO-1 (yellow), the adherence junction molecule CDH1 (magenta) and the apical domain molecule aPKC (cyan) in a representative human blastocyst-like structure. Scale bar, 50 μm .

Formation of blastocyst-stage analogues

Single-cell transcriptomics analysis showed that blastocyst-like structures formed only three distinct transcriptomic states (Fig. 2a, b, Extended Data Fig. 2a) marked by genes specific to the three founding lineages, including *GATA2* and *GATA3* (TE), *POU5F1* and *KLF17* (EPI), and *GATA4* and *SOX17* (PrE) (Fig. 2c, d, Extended Data Fig. 2b). Comparison with cells from blastocysts, in vitro cultured blastocysts and a gastrulation-stage embryo indicated that the cells in the blastocyst-like structures were transcriptionally similar to the blastocyst stage and distinct from post-implantation stages (Fig. 2e, f, Extended Data Fig. 2c–g). A higher-resolution clustering analysis (from resolution 0.02 to resolution 1) isolated one cluster of non-blastocyst-like cells with a gene-expression pattern reminiscent of post-implantation tissues¹⁵ (*GABRP*, *ISL1*, *APLN*R and *CRABP2*) (Extended Data Fig. 3a–c) that also appeared transcriptionally similar to amnion (annotated as non-neural ectoderm) and extra-embryonic mesoderm (Extended Data Fig. 3d–j). This sub-population constituted less than 3% of all sequenced cells (Extended Data Fig. 3i). Of note, we found that naive PSC culture also contained 5–6% similarly differentiated cells¹⁹ (Extended Data Fig. 3i). Bulk RNA-sequencing (RNA-seq) analysis showed that isolated trophoblast analogues (TROP2⁺) had an intermediate transcriptome between those of naive PSCs and post-implantation-like trophoblasts (TSCs) (Extended Data Fig. 4a). Furthermore, trophoblasts were enriched in blastocyst-stage TE transcripts¹¹ (*ESRRB*, *GRHL1*, *OVOL1*, *GATA2*, *GATA3*, *TBX3*, *KRT19*, *CGA*, *CGB5* and *CGB7*) but not in some post-implantation trophoblast markers¹¹ (*SIGLEC6* and *DPP4*) (Extended Data Fig. 4b, c). The transcriptome of isolated EPI analogues (TROP2⁺PDGFRa⁻) resembled that of naive PSCs (Extended Data Fig. 4a), was enriched in markers specific for blastocyst-stage EPI²¹ (*KLF17*, *ATG2A*, *SUSD2*, *TFCP2L1*, *DPPA2* and *PRDM14*), and differed from the transcriptome of primed PSCs (Extended Data Fig. 4a, d). Finally, isolated PrE analogues (PDGFRa⁺) had an intermediate transcriptome between those of naive PSCs and extra-embryonic endoderm cell lines²² (nEND cells) (Extended Data Fig. 4a). PrE analogues were enriched in blastocyst-stage PrE markers (early blastocyst: *GATA6*, *MSX2* and *HNF4A*; late blastocyst: *PDGFRA*, *GATA4*, *SOX17*, *HNF1B* and *FOXA2*) and downregulated in EPI genes (*ARGFX*, *PRDM14*, *SOX2*, *NANOG*, *DPPA2* and *POU5F1*), similar to during blastocyst development²¹ (Extended Data Fig. 4e). Blastocysts have the ability to establish stem cell lines²; similarly, blastocyst-like structures enabled de novo derivation of naive PSCs² (*NANOG*⁺*SOX2*⁺*OCT4*⁺*KLF17*⁺) (Extended Data Fig. 5a) that could form second-generation blastocyst-like structures (Extended Data Fig. 5b, c) and of TSCs²⁰ (*CDX2*⁺*GATA3*⁺*CK7*⁺) (Extended Data Fig. 5d) endowed with the capacity for rapid differentiation into syncytiotrophoblasts (SCT) and extravillous trophoblasts (EVT) (over 3–6 days; Extended Data Fig. 5e–j). Of note, derivation of PrE cell lines from human blastocysts has not been reported. Thus, blastocyst-like structures formed blastocyst-stage cellular analogues (accounting for more than 97% of the cells sequenced).

Hippo inhibition is essential

Knowledge about human blastocyst lineage segregation is limited (Fig. 3a). However, inhibition of the Hippo pathway is known to occur in peripheral cells upon acquisition of an apical domain, and is required to initiate TE specification¹² (Extended Data Fig. 6a). We tested whether blastocyst-like structures co-opted this mechanism. Of note, aPKC and F-actin expression domains appeared co-aligned in outer cells that also accumulated the Hippo downstream effector YAP1 in nuclei (Extended Data Fig. 6b, c). YAP1 nuclear location correlated with *GATA2* and *GATA3* expression, contrasted with *NANOG* expression, and became restricted to TE analogues¹² (Fig. 3b, Extended Data Fig. 6d, e). An aPKC inhibitor (CRT0103390)¹² largely prevented YAP1 nuclear accumulation, decreased the number of *GATA3*⁺ cells

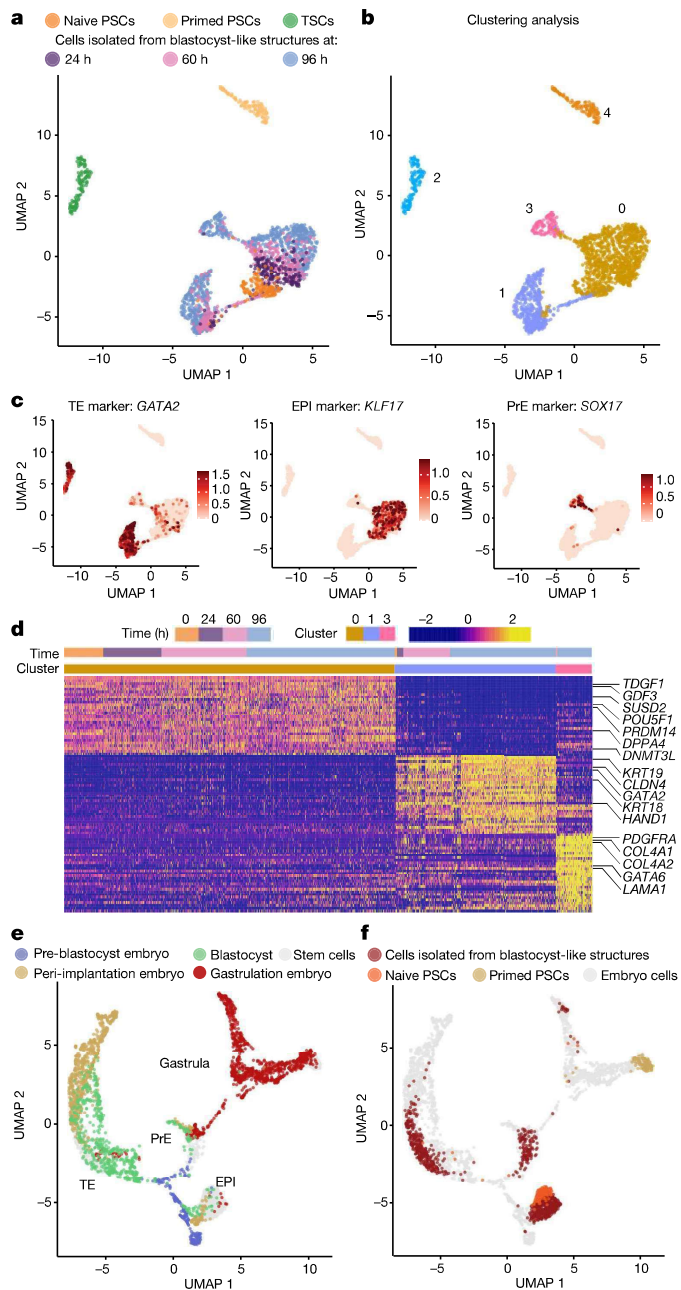


Fig. 2 | Human blastocyst-like structures for analogues of the three pre-implantation lineages. **a, b**, Uniform manifold approximation and projection (UMAP) of the transcriptome of single cells originating from blastocyst-like structures (at 24, 60 and 96 h), naive PSCs, primed PSCs and TSCs (representing post-implantation cytotrophoblasts); individual cells are coloured on the basis of their origin (**a**) or their unsupervised cluster affiliation (**b**). **c**, Expression level of markers of each blastocyst lineage. **d**, Unsupervised distance map generated using the top 30 genes that are enriched in clusters 0, 1 and 3 (defined in the UMAP in **b**). Note that this list includes epiblast markers specific to the blastocyst stage (for example, *SUSD2*, *KLF17* and *PRDM14*). **e, f**, UMAP of single-cell transcriptome of cells from blastocyst-like structures, naive PSCs and primed PSCs integrated with published datasets from human embryos at pre-implantation, peri-implantation (in vitro cultured blastocysts) and gastrulation (Carnegie stage 7, that is, between embryonic days 16 and 19) stages. Individual cells are coloured on the basis of their origin in human embryos (**e**) or blastocyst-like structures or stem cells (**f**).

and prevented the formation of blastocyst-like structures (Extended Data Fig. 6f–h). Conversely, ligands of LPA receptors (LPA and NAEPA) that can inhibit the Hippo pathway enhanced the formation of

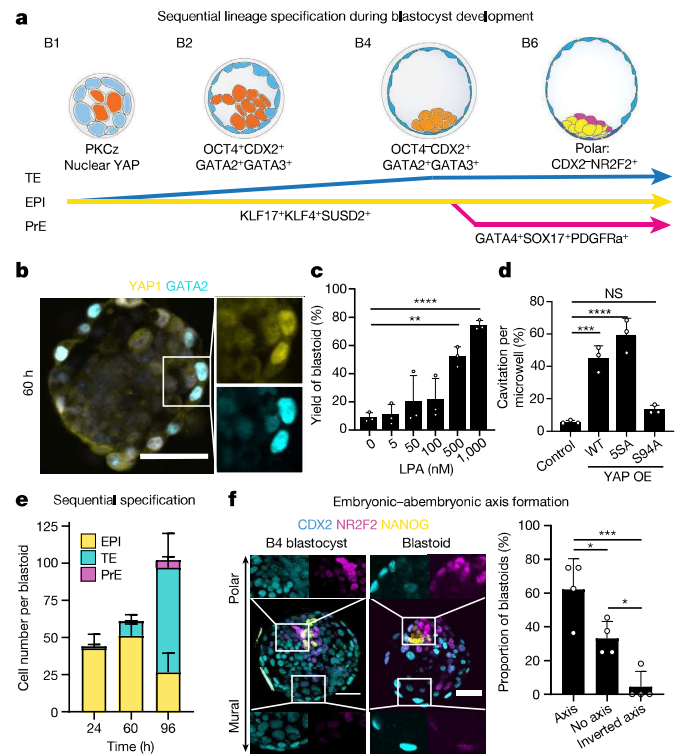


Fig. 3 | The three lineages form according to the sequence and time of blastocyst development. **a**, Schematic depicting the sequential lineage specification of human blastocysts. **b**, Immunofluorescence of YAP1 (yellow) and GATA2 (cyan) in aggregates of naive PSCs cultured in PALLY medium for 60 h. Scale bar, 50 μ m. **c**, Dose-dependent effect of LPA on the yield of blastocyst-like structures. $n = 3$ independent microwell arrays; mean \pm s.d.; one-way analysis of variance (ANOVA) and Dunnett’s multiple comparisons test. $**P = 0.0016$, $****P < 0.0001$. **d**, Effect of the overexpression of different variants of YAP1 on cavitation events in early blastocyst-like structures. $n = 3$ experiments; mean \pm s.d.; one-way ANOVA and Tukey’s multiple comparisons test. NS, not significant; $***P = 0.0004$, $****P = 0.00004$. **e**, Total cell numbers per lineage developing blastocyst-like structures at three time points of development (24, 60 and 96 h). Mean \pm s.d. EPI: $n = 11$ blastocyst-like structures at 24, 68 and 96 h; TE: $n = 8$ (24 h), $n = 14$ (48 h) and $n = 15$ (96 h) blastocyst-like structures; PrE: $n = 9$ (24 h), $n = 37$ (48 h) and $n = 9$ (96 h) blastocyst-like structures. **f**, Immunofluorescence of CDX2 (cyan), NR2F2 (magenta) and NANOG (yellow) in representative B4-stage human blastocyst (left) and blastocyst-like structures (middle). Quantification of the proportion of blastocyst-like structures with a preferentially polar NR2F2 expression pattern (axis) compared with a preferentially mural NR2F2 expression pattern (inverted axis) (right). $n = 4$ independent experiments with 4–12 blastocyst-like structures in each experiment; mean \pm s.d.; one-way ANOVA and Tukey’s multiple comparisons test. $*P < 0.05$, $***P < 0.001$. Scale bar, 50 μ m.

blastocyst-like structures (Fig. 3c, Extended Data Fig. 6i). Because Hippo pathway inhibition frees YAP1 to enter the nucleus, we tested whether genetically engineered levels and functions of YAP1 could affect morphogenesis. Overexpression of wild-type or constitutively active forms of YAP1 (5SA) accelerated cavitation (Fig. 3d). The interaction between YAP1 and TEAD transcription factors is necessary for downstream gene regulation. Accordingly, over-expression of YAP1 with a mutation in the TEAD binding site (S94A) did not affect cavitation (Fig. 3d, Extended Data Fig. 6j), and verteporfin—which disrupts the YAP1–TEAD interaction—prevented the formation of blastocyst-like structures (Extended Data Fig. 6k). Cavity morphogenesis occurred through the apparent coalescence of multiple fluid-filled cavities²³ (Extended Data Fig. 6l). Aquaporin 3 (AQP3), the water transporter most highly expressed in human blastocysts¹¹, was initially visible in all cells (36 h) and was then restricted to TE analogues (96 h) (Extended

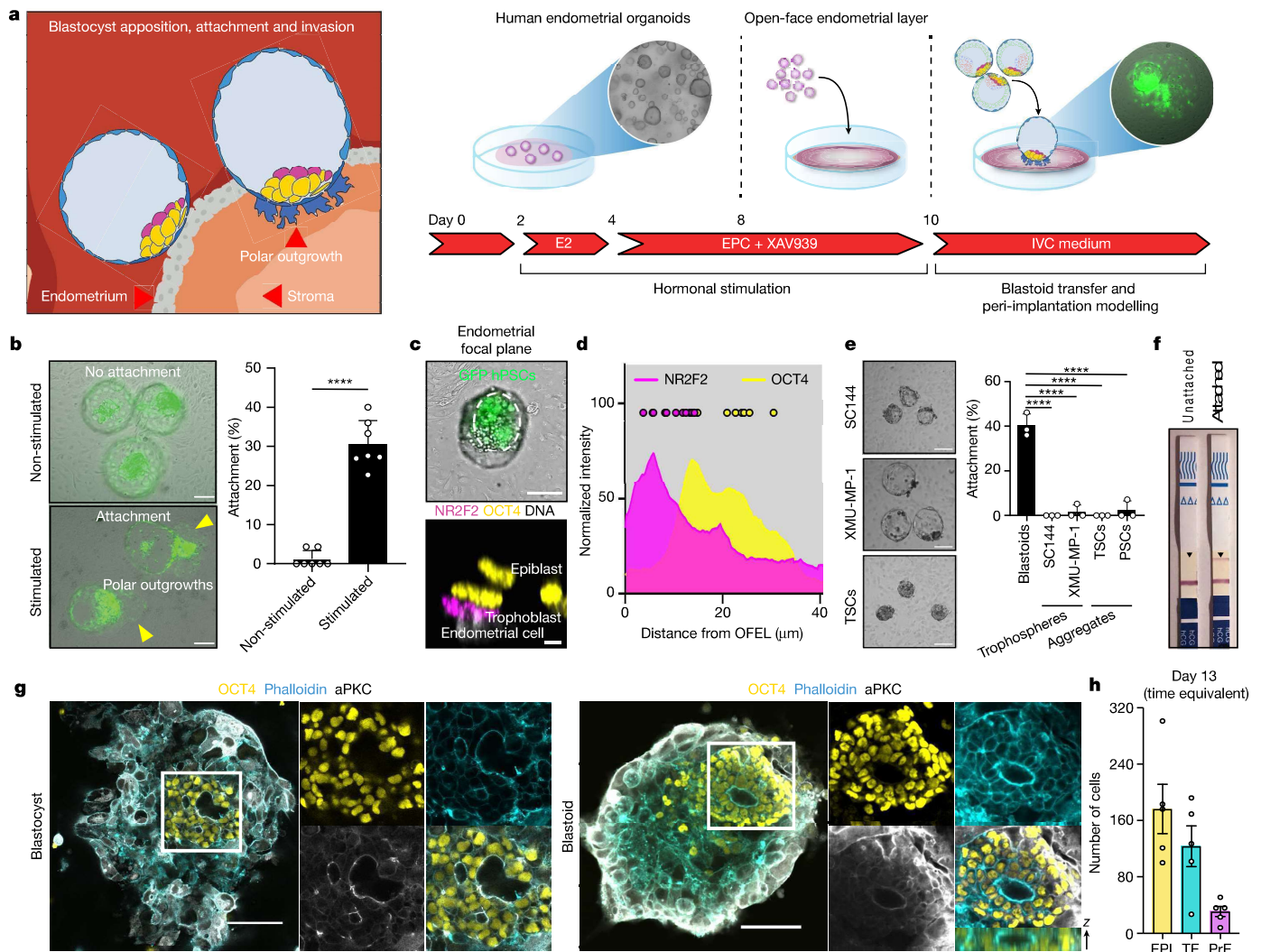


Fig. 4 | Human blastoids recapitulate aspects of implantation. **a**, Left, schematic of the modelled implantation process. Right, OFEL priming assay using EPC/XAV939. E2, β-oestradiol; EPC, E2 + progesterone + cAMP. **b**, Representative phase-contrast images of blastoids (GFP⁺) 24 h after deposition onto non-stimulated (top left) or stimulated (bottom left) OFELs. Scale bar, 100 μm. Attachment efficiency of human blastoids (right). *n* = 7 independent experiments from 3 different donors; mean ± s.d.; unpaired two-tailed *t*-test. *****P* = 4.5×10^{-8} . **c**, Representative images of recently attached human blastoids (12 ± 4 h). Top, the dashed delineates the inner cluster of blastoids formed from GFP⁺ naive PSCs (also see Supplementary Video 3). Scale bar, 100 μm. Bottom, x-z plane of NR2F2 (magenta) and OCT4 (yellow) immunofluorescence in blastoids immediately after attachment. Scale bar, 5 μm. **d**, Intensity profile of immunofluorescence of NR2F2 and OCT4 in blastoids immediately after attachment. *n* = 10. **e**, Left, representative

phase-contrast images of trophospheres formed using 3 μM SC144 (top) or 2 μM XMU-MP-1 (middle), and aggregates of TSCs (bottom) deposited onto stimulated OFELs. Scale bar, 100 μm. Right, attachment efficiency. *n* = 3 independent experiments; mean ± s.d.; one-way ANOVA and Dunnett's multiple comparisons test. *****P* < 0.0001. **f**, Pregnancy test strips detecting secretion of CGβ into the medium of unstimulated OFELs with unattached blastoids and stimulated OFELs with attached blastoids (48 h on OFEL; see ELISA assay in Extended Data Fig. 10b). **g**, Immunofluorescence of OCT4 (yellow) and aPKC (grey) in human blastocysts (left) or blastoids (right) grown in post-implantation culture condition for 4 days, counterstained with phalloidin marking F-actin (cyan). Scale bars, 100 μm. **h**, Number of cells positive for OCT4, GATA3 and GATA4 in blastoids grown in post-implantation culture for 6 days (time equivalent, day 13). *n* = 5. mean ± s.d.

Data Fig. 6m). Thus, similar to human blastocysts¹², TE specification and morphogenesis within these structures depends on aPKC, inhibition of the Hippo pathway, nuclear translocation of YAP1 and the ability of YAP1 to bind TEAD transcription factors.

Adequate developmental sequence

In blastocysts, TE (GATA2⁺DAB2⁺) and EPI (KLF17⁺NANOG⁺) cells appear first^{11,21} (5–6 dpf) and PrE cells (GATA6⁺ADM⁺) and polar TE cells (pTE) (CDX2⁺NR2F2⁺) appear last²¹ (6–7 dpf). This sequence is recapitulated in the blastocyst-like structures. Trophoblasts (DAB2⁺, CDX2⁺, GATA2⁺, GATA3⁺) formed first (within 24 h

(Fig. 3e, Extended Data Fig. 7a), and changed the levels of transcripts related to PKC and Hippo signalling (*AKAP12*, *CAPZB*, *ULK4*, *MOB1A*, *AMOT*, *AMOTL2*, *LATS2* and *TEAD1*) (Supplementary Table 1). At protein level, early TE-like cells were first YAP1^{nuclear}GATA2⁺ (at 24 h) and then CDX2⁺GATA3⁺, while maintaining expression of KLF17 and OCT4, but not NANOG (at 60 h) (Extended Data Fig. 7b–d). Subsequently, OCT4 became undetectable¹¹ (Fig. 1g, Extended Data Fig. 1i). Genes associated with SMAD, ERK, Notch and Wnt signaling pathways were regulated during this process (Extended Data Fig. 7e, f, Supplementary Table 1). Finally, pTE analogues matured as marked by expression of *OVOL1*, *GREM2*, *CCR7*, *SP6* and *NR2F2* (Extended Data Fig. 7g–j), upregulation of NR2F2 and CCR7¹¹ and downregulation of CDX2 (Fig. 3f, Extended Data Fig. 7h, j).

Article

The transcriptome of EPI analogues maintained core blastocyst markers (*POUSF1*, *NANOG*, *KLF17*, *SUSD2*, *KLF4*, *ARGFX* and *GDF3*) (Fig. 3e, Extended Data Fig. 7k, l, Supplementary Table 1), while undergoing a progression characterized by regulation of Nodal (*NODAL*, *LEFTY1* and *LEFTY2*) and mTOR (*LAMTOR1*, *LAMTOR4*, *LAMTOR5*, *XBPI1* (*XBPI*, also known as *SEC13* and *MLST8*) signalling-related genes, and of the X chromosome activation-related gene *XACT* (Extended Data Fig. 7k–m, Supplementary Table 1, cluster 4 versus cluster 0). At the protein level, EPI analogues were marked by *KLF17* and *SUSD2*, which are specifically highly expressed at the blastocyst stage (Extended Data Fig. 7l). PrE analogues appeared within 60 h and *GATA4*, *OTX2* and *SOX17* were detected¹¹ within 72 h (Fig. 3e, Extended Data Fig. 7n–p). Early PrE marker genes²¹ (*GATA6*, *LBH*, *ADM* and *LAMA1*) were uniformly expressed among the PrE analogues, while some late PrE marker genes (*CTSE*, *APOA1*, *PITX2* and *SLCO2A1*) were expressed only in a subpopulation of cells, suggesting a progression toward the late blastocyst stage¹¹ (Extended Data Fig. 7q). By 96 h, mature PrE analogues had regulated SMAD (*NODAL*, *BMP2*, *BMP6*, *GDF3*, *ID1* and *ID2*) and Wnt signalling-related transcripts (*WNT3*, *RSPO3* and *LBH*) and were enriched in transcripts controlling extracellular matrix organization (*LAMA1*, *LAMB1*, *LAMC1*, *COL4A1* and *COL4A2*), and endodermal and epithelial differentiation (Extended Data Fig. 7q, r, Supplementary Table 1, cluster 6 versus cluster 8). Because this model morphologically resembles the human blastocyst (see criteria in Methods), efficiently generates analogues of the three lineages with transcriptomes matching the blastocyst stage, and forms these analogues according to the sequence and approximate pace of blastocyst development, we refer to it as a human blastoid.

Distinct attachment to endometrial cells

At 7 dpf, the human blastocyst initiates implantation in utero through the attachment of its TE to a receptive endometrium (Fig. 4a, left). We tested whether blastoids could model this interaction by seeding endometrial organoids²⁴ in 2D to form an open-faced endometrial layer (OFEL) to facilitate the deposition of blastoids (Fig. 4a, right). Subpopulations of the OFEL were positive for acetylated α -tubulin, marking ciliated epithelial cells²⁴ (Extended Data Fig. 8a), and *FOXA2*, marking glandular epithelial cells (Extended Data Fig. 8b). The window of implantation is the period during which the uterus becomes receptive for blastocyst implantation. It opens upon exposure to oestrogen (E2) and progesterone (P4), and correlates with regulation of Wnt signalling²⁵. Accordingly, OFELs responded to E2, P4, cAMP and XAV939 by upregulating the expression of genes that mark the mid-secretory-phase endometrium (Extended Data Fig. 8c–e) and decreasing proliferation, which are hallmarks of receptivity²⁵ (Extended Data Fig. 8e, f). Notably, blastoids deposited onto non-stimulated OFELs did not attach; however, they did attach to and repel the endometrial cells of stimulated OFELs, as occurs in utero (Fig. 4b, Extended Data Fig. 8g, h). The contraceptive levonorgestrel impaired blastoid attachment (Extended Data Fig. 8i). We concluded that human blastoids are capable of interacting specifically with endometrial cells that have been made receptive.

Epiblast signals gatekeep trophoderm attachment

Human blastocysts attach to the endometrium via the pTE, which is defined by its contact with the EPI. Similarly, blastoids reproducibly initiated attachment through this region (Fig 4c, d, Extended Data Fig. 9a–c, Supplementary Videos 3, 4). We tested the role of the pTE–EPI interface by forming trophospheres devoid of EPI. IL-6 is highly expressed in the pTE and transcripts for its receptor (*IL6R* and *IL6ST* (also known as *GPI30*)) and effector (*STAT3*) are present at high levels in the EPI (Extended Data Fig. 9d). Consistent with a role for STAT signalling in the EPI, the efficiency of blastoid formation increased with LIF concentration (Extended Data Fig. 9e), whereas the addition of a GPI30 inhibitor (SC144) yielded trophospheres (Fig. 4e, Extended Data

Fig. 9f). The presence of a potent inhibitor of the Hippo kinases MST1 and MST2 (XMU-MP-1) also yielded trophospheres (Fig. 4e, Extended Data Fig. 9g). The transcriptomes of these trophospheres reflected early and late blastocyst-stage TE (Extended Data Fig. 9h, i). Neither type of trophosphere attached to OFELs (Fig. 4e), and nor did aggregates of TSCs²⁰ that reflect post-implantation cytotrophoblasts²⁶ (*CDX2*^{CK7}) or aggregates of naive PSCs (Fig. 4e, Extended Data Fig. 9j, k). We thus conclude that signals from the EPI induce pTE maturation and endow it with the potential to interact with endometrial cells. This potential appears lost in TSCs reflecting a post-implantation stage. On the basis of transcriptome analysis and in utero data²⁵, we propose several pairs of molecules whose transcripts became more abundant upon endometrial cell stimulation and pTE analogue maturation (Extended Data Fig. 9l) that might mediate the first contact between blastocyst and uterus. Overall, we conclude that a polar-like TE state, whose maturation depends on EPI inductions, gatekeeps the interaction of the blastocyst with the endometrium. This interaction and subsequent maturation create a window of opportunity for blastocyst implantation.

Modelling post-stages on day 13

The blastoid morphology was stable for two days in peri-implantation culture conditions^{27,28} (Extended Data Fig. 10a). Clinical pregnancy is characterized by the detection of chorionic gonadotropin- β hormone (CG β). Accordingly, upon attachment, blastoids formed trophoblasts expressing CG β at levels detectable using standard pregnancy tests and ELISA (Fig. 4f, Extended Data Fig. 10b). NR2F2⁺ pTE analogues proliferated and decreased *CDX2* expression while upregulating the peri-implantation gene cyokeratin 7 (*KRT7* (a.k.a. *CK7*)) (Extended Data Fig. 10c, d). Some trophoblasts further differentiated into SCT and EVT expressing CG β and HLA-G, respectively (Extended Data Fig. 10e, f). EPI analogues maintained expression of *OCT4* and *SOX2*, upregulated the primed pluripotency marker *CD24* (Fig. 4g, Extended Data Fig. 10g) and patterned cortical F-actin as during post-implantation EPI epithelization, and some blastoids cultured in vitro for 4 days past the equivalent of the blastocyst stage (day 7) formed pro-amniotic-like cavities enriched with F-actin, *PODXL* and *aPKC* (Fig. 4g, Extended Data Fig. 10h). A subpopulation in the periphery of the EPI analogue expressed *CDX2* along with *SOX2* or *TFAP2C*, suggestive of early amnion analogues (Extended Data Fig. 10i, j). Extra-embryonic endoderm analogues were characterized by restricted expression of *OTX2*¹¹ (Extended Data Figs. 7o, 10k). Upon prolonged culture (up to 6 days), the three lineages consistently expanded (Fig. 4h, Extended Data Fig. 10l, m) until a time equivalent of day 13, although, similar to blastocysts, their organization did not reflect that developmental stage.

Discussion

Human blastoids morphologically resemble the human blastocyst (criteria described in Methods), efficiently generate analogues of its three lineages with transcriptomes matching the human blastocyst stage, and form these analogues according to the sequence (TE and EPI, then pTE and PrE) and approximate pace (4 days) of blastocyst development. We therefore propose that this model is relevant for the study of human blastocyst development and implantation. Some initial parameters and end-point criteria that are useful to form and define these models^{5–9} are summarized in Supplementary Table 2. Mimicking the interaction between the epiblast and trophectoderm revealed that the epiblast induces the local maturation of polar trophectoderm and subsequently endows it with the capacity to attach onto stimulated endometrial cells. In future, human blastoids may be used to help identify therapeutic targets and contribute to preclinical modelling (for example, in vitro fertilization medium complements such as LPA and NAEPA or contraceptives such as SC144 (ref.³)). Considering the proportionality

(balancing the benefits and harms) and subsidiarity (pursuing goals using the morally least problematic means) of human embryology, blastoids represent an ethical opportunity to complement research using embryos⁴.

Online content

Any methods, additional references, Nature Research reporting summaries, source data, extended data, supplementary information, acknowledgements, peer review information; details of author contributions and competing interests; and statements of data and code availability are available at <https://doi.org/10.1038/s41586-021-04267-8>.

1. Rivron, N. C. et al. Blastocyst-like structures generated solely from stem cells. *Nature* **557**, 106–111 (2018).
2. Guo, G. et al. Naive pluripotent stem cells derived directly from isolated cells of the human inner cell mass. *Stem Cell Rep.* **6**, 437–446 (2016).
3. Rivron, N. et al. Debate ethics of embryo models from stem cells. *Nature* **564**, 183–185 (2018).
4. Clark, A. T. et al. Human embryo research, stem cell-derived embryo models and in vitro gametogenesis: Considerations leading to the revised ISSCR guidelines. *Stem Cell Rep.* **16**, 1416–1424 (2021).
5. Liu, X. et al. Modelling human blastocysts by reprogramming fibroblasts into iBlastoids. *Nature* **591**, 627–632 (2021).
6. Yanagida, A. et al. Naive stem cell blastocyst model captures human embryo lineage segregation. *Cell Stem Cell* **28**, 1016–1022 (2021).
7. Yu, L. et al. Blastocyst-like structures generated from human pluripotent stem cells. *Nature* **591**, 620–626 (2021).
8. Sozen, B. et al. Reconstructing aspects of human embryogenesis with pluripotent stem cells. *Nat. Commun.* **12**, 5550 (2021).
9. Fan, Y. et al. Generation of human blastocyst-like structures from pluripotent stem cells. *Cell Discov.* **7**, 81 (2021).
10. Zhao, C. et al. Reprogrammed iBlastoids contain amnion-like cells but not trophectoderm. Preprint at <https://doi.org/10.1101/2021.05.07.442980> (2021).
11. Meistermann, D. et al. Integrated pseudotime analysis of human pre-implantation embryo single-cell transcriptomes reveals the dynamics of lineage specification. *Cell Stem Cell* **28**, 1625–1640.e6 (2021).
12. Gerri, C. et al. Initiation of a conserved trophectoderm program in human, cow and mouse embryos. *Nature* **587**, 443–447 (2020).
13. Rossant, J. Making the mouse blastocyst: past, present, and future. *Curr. Top. Dev. Biol.* **117**, 275–288 (2016).
14. Amita, M. et al. Complete and unidirectional conversion of human embryonic stem cells to trophoblast by BMP4. *Proc. Natl. Acad. Sci. USA* **110**, E1212–E1221 (2013).
15. Jo, S. et al. Capturing human trophoblast development with naive pluripotent stem cells in vitro. *Cell Stem Cell* **28**, 1023–1039.e13 (2021).
16. Guo, G. et al. Human naive epiblast cells possess unrestricted lineage potential. *Cell Stem Cell* **28**, 1040–1056.e6 (2021).
17. Hardy, K., Handyside, A. H. & Winston, R. M. The human blastocyst: cell number, death and allocation during late preimplantation development in vitro. *Development* **107**, 597–604 (1989).
18. Lewis, W. H. & Gregory, P. W. Cinematographs of living developing rabbit-eggs. *Science* **69**, 226–229 (1929).
19. Messmer, T. et al. Transcriptional heterogeneity in naive and primed human pluripotent stem cells at single-cell resolution. *Cell Rep.* **26**, 815–824.e4 (2019).
20. Okae, H. et al. Derivation of human trophoblast stem cells. *Cell Stem Cell* **22**, 50–63.e6 (2018).
21. Stirparo, G. G. et al. Integrated analysis of single-cell embryo data yields a unified transcriptome signature for the human pre-implantation epiblast. *Development* **146**, dev158501 (2018).
22. Linneberg-Agerholm, M. et al. Naive human pluripotent stem cells respond to Wnt, Nodal, and LIF signalling to produce expandable naive extra-embryonic endoderm. *Development* **146**, dev180620 (2019).
23. Dumortier, J. G. et al. Hydraulic fracturing and active coarsening position the lumen of the mouse blastocyst. *Science* **365**, 465–468 (2019).
24. Boretto, M. et al. Development of organoids from mouse and human endometrium showing endometrial epithelium physiology and long-term expandability. *Development* **144**, 1775–1786 (2017).
25. Wang, W. et al. Single-cell transcriptomic atlas of the human endometrium during the menstrual cycle. *Nat. Med.* **26**, 1644–1653 (2020).
26. Castel, G. et al. Induction of human trophoblast stem cells from somatic cells and pluripotent stem cells. *Cell Rep.* **33**, 108419 (2020).
27. Ma, H. et al. In vitro culture of cynomolgus monkey embryos beyond early gastrulation. *Science* **366**, eaax7890 (2019).
28. Xiang, L. et al. A developmental landscape of 3D-cultured human pre-gastrulation embryos. *Nature* **577**, 537–542 (2020).

Publisher's note Springer Nature remains neutral with regard to jurisdictional claims in published maps and institutional affiliations.



Open Access This article is licensed under a Creative Commons Attribution 4.0 International License, which permits use, sharing, adaptation, distribution and reproduction in any medium or format, as long as you give appropriate credit to the original author(s) and the source, provide a link to the Creative Commons license, and indicate if changes were made. The images or other third party material in this article are included in the article's Creative Commons license, unless indicated otherwise in a credit line to the material. If material is not included in the article's Creative Commons license and your intended use is not permitted by statutory regulation or exceeds the permitted use, you will need to obtain permission directly from the copyright holder. To view a copy of this license, visit <http://creativecommons.org/licenses/by/4.0/>.

© The Author(s) 2021

Article

Methods

Ethical approvals

The use of human embryos donated to research as surplus of IVF treatment was allowed by the French embryo research oversight committee (Agence de la Biomédecine) under approval number RE13-010 and RE18-010. All human pre-implantation embryos used in this study were obtained following informed consent from the couples who donated embryos and cultured at the Assisted Reproductive Technology unit of the University Hospital of Nantes, France, which are authorized to collect embryos for research under approval number AG110126AMP of the Agence de la Biomédecine. Human endometrium samples were obtained from patients who signed an informed consent form and protocols approved by the Ethics Committee of Royan Institute (IR.ACECR.ROYAN.REC.1397.93) and of Shahid Beheshti University of Medical Sciences (IR.SBMU.MSP.REC.1396.25). The Wicell line H9 was used under the agreement 20-WO-341 for a research program entitled 'Modeling early human development: Establishing a stem cell based 3D in vitro model of human blastocyst (blastoids)'. Blastoid generation was approved by the Commission for Science Ethics of the Austrian Academy of Sciences. This work did not exceed a developmental stage normally associated with 14 consecutive days in culture after fertilization even though this is not forbidden by the ISSCR Guidelines as far as embryo models are concerned. All experiments complied with all relevant guidelines and regulations, including the 2021 ISSCR guidelines that forbid the transfer of human blastoids into any uterus⁴.

Culture of human naive pluripotent stem cells

Experiments were done using the following PSC lines; human ES cell lines: H9, Shef6 and HNES1. Induced pluripotent stem cell (iPSC) lines: cR-NCRM2 and niPSC.16.2.b. The H9 and H9-GFP lines reset to the naive state were provided by the laboratory of Y. Takashima. Other naive human ES cells and iPSCs were provided by the laboratory of A. Smith. Naive PSCs were cultured on gelatin-coated plates including a feeder layer of gamma-irradiated mouse embryonic fibroblasts (MEFs) in PXGL medium, as previously reported²⁹. PXGL medium is prepared using N2B27 basal medium supplemented with PD0325901 (1 μ M, MedChemExpress, HY-10254), XAV-939 (1 μ M, MedChemExpress, HY-15147), Gö 6983 (2 μ M, MedChemExpress, HY-13689) and human leukemia inhibitory factor (hLIF, 10 ng ml⁻¹, in-house made) as previously reported²⁹. N2B27 basal medium contained DMEM/F12 (50%, in house made), neurobasal medium (50%, in-house made), N-2 supplement (Thermo Fisher Science, 17502048), B-27 supplement (Thermo Fisher Science, 17504044), GultaMAX supplement (Thermo Fisher Science, 35050-038), non-essential amino acid, 2-mercaptoethanol (100 μ M, Thermo Fisher Science, 31350010), and bovine serum albumin solution (0.45%, Sigma-Aldrich, A7979-50ML). Cells were routinely cultured in hypoxic chambers (5% CO₂, 5% O₂) and passaged as single cells every three to four days. All cell lines had routinely tested negative for mycoplasma.

Culture of primed pluripotent embryonic stem cells

Primed H9 cells were cultured on Vitronectin XF (STEMCELL Technologies, 07180) coated plates (1.0 μ g cm⁻²) using Essential 8 medium (prepared in-house).

Microwell arrays

Microwell arrays comprising microwells of 200 μ m diameter were imprinted into 96-well plates as previously described^{30,31}.

Induction of blastoids and trophospheres

Naive PSCs were treated with Accutase (Biozym, B423201) at 37 °C for 5 min, followed by gentle mechanical dissociation with a pipette. After centrifugation, the cell pellet was resuspended in PXGL medium, supplemented with Y-27632 (10 μ M, MedChemExpress, HY-10583). To exclude

MEFs, the cell suspension was transferred onto gelatin-coated plates and incubated at 37 °C for 70 min. After MEF exclusion, the cell number was determined using a Countess automated cell counter (Thermo Fisher Scientific) and trypan blue staining to assess cell viability. The cells were then resuspended in N2B27 medium containing 10 μ M Y-27632 (aggregation medium) and 3.0×10^4 cells were seeded onto a microwell array included into a well of a 96-well plate and placed in a hypoxic chamber (5% CO₂, 5% O₂) for the whole period of blastoid or trophosphere formation. The cells were allowed to form aggregates inside the microwell for a period ranging from 0 to 24 h depending on the cell lines and based on their propensity for aggregation. Subsequently, the aggregation medium was replaced with PALLY medium (N2B27 supplemented with PD0325901 (1 μ M), A 83-01 (1 μ M, MedChemExpress, HY-10432), 1-oleoyl lysophosphatidic acid sodium salt (LPA)³² (500 nM, Tocris, 3854), hLIF (10 ng ml⁻¹) and Y-27632 (10 μ M)). The PALLY medium was refreshed every 24 h. After 48 h, the PALLY medium was replaced with N2B27 medium containing 500 nM LPA and 10 μ M Y-27632. At 96 h, a blastoid is defined based (1) on morphological similarities to B6 staged human blastocyst, as a structure composed of a monolayered cyst with an overall diameter of 150–250 μ m comprising one inner cell cluster, and (2) on similarities to the molecular dynamic of human development as a structure that forms analogues of the three blastocyst cell lineages in the sequential and timely manner of a blastocyst. For example, >90% of morphologically adequate structures generated from the lines analysed formed >97% of analogues of three blastocyst-stage lineages (see Fig. 1h and Extended Data Fig. 3i). An exception is the line Shef6, which efficiently formed morphologically correct structures but appeared less efficient at forming PrE analogues. See also Supplementary Table 2. Blastoids reproducibly formed at high efficiency and we did not observe differences based on the number of passages after resetting in PXGL culture conditions. The effect of LPA, NAEPA (Sigma-Aldrich, N0912) and Verteporfin (Selleck Chemicals Llc, S1786) on the yield of blastoid formation was assessed by culturing naive PSC aggregates in PALLY medium (without LPA) complemented with molecules added every day from 0 to 96 h. The Verteporfin treatment was executed without exposure to the light. The effect of the aPKC inhibitor CRT0103390 (a gift from the laboratory of K. Niakan) was assessed by culturing naive PSC aggregates in PALLY medium complemented with 2 μ M CRT0103390 every day from 0 to 96 h. The formation of trophospheres was induced by culturing naive PSC aggregates in PALLY medium complemented with 2 μ M XMU-MP-1 (Med Chem Express, HY-100526) or 3 μ M SC-144 (Axon, 2324) every day from 0 to 96 h. The BSA concentration was titrated within the range of 0–0.3% for individual cell lines used for the formation of the blastoids and trophospheres. A step-by-step protocol is available on Protocol Exchange (<https://doi.org/10.21203/rs.3.pex-1639/v1>).

Derivation of cell lines from human blastoids

Derivation experiments were performed with blastoids cultured for 96 h as described in the previous section. Blastoids were individually transferred on gelatin-coated 96-well plates with feeder layers of gamma-irradiated MEFs. Naive PSCs were derived in PXGL medium². TSCs were derived in human TSC medium²⁰. After 24 h of culture on feeders, blastoids attached and, within one week, colonies were formed. Derivation was considered successful after three passages after blastoid transfer. For immunofluorescence assays, naive PSCs were transferred onto Geltrex (0.5 μ l cm⁻²)-coated coverslips, and TSCs were transferred onto fibronectin-coated coverslips (5 μ g ml⁻¹, Sigma Aldrich, 08012).

Trophoblast organoid formation

Organoid formation was performed with blastoid-derived TSC lines. Organoids were cultured as previously described³³ with some modifications. Colonies of TSCs were dissociated into single cells using 1 \times trypsin at 37 °C for 5 min. After centrifugation, 200,000 cells were resuspended in 150 μ l Matrigel (Corning, 356231). Droplets of 20 μ l were

placed into a prewarmed 48-well cell culture plate and placed upside down into the incubator for 20 min. Organoids were cultured in 250 μ l TOM medium (Advanced DMEM-F12, N2 supplement, B27 supplement minus vitamin A, PenStrep, *N*-acetyl-L-cysteine (1.25 mM), L-glutamine (2 mM), A83-01 (500 nM), CHIR99021 (1.5 μ M), recombinant human EGF (50 ng ml⁻¹), 10% R-spondin 1 conditioned medium, recombinant human FGF2 (100 ng ml⁻¹), recombinant human HGF (50 ng ml⁻¹), PGE2 (2.5 μ M). Medium was refreshed every other day. For SCT formation organoids were maintained in TOM medium until day 7.

2D trophoblast differentiations

The differentiation of blastoid derived TSCs was performed as described previously²⁰ with some modifications. TSC lines were adapted to Fibronectin coating (5 μ g ml⁻¹, Sigma Aldrich, 08012) for at least three passages prior to the experiments. For EVT and SCT differentiation, cells were dissociated with TrypLE for 5 min at 37 °C and cells were seeded at a density of 55,000 cells per well onto 12-well plates. For SCT differentiation, the plates were pre-coated with 10 μ g ml⁻¹ fibronectin and cultured in SCT medium (DMEM/F12, supplemented with 0.1 mM 2-mercaptoethanol, 0.5% penicillin-streptomycin, 1% ITS-X supplement, 7.5 mM A83-01, 2.5 mM Y27632, 4% KnockOut Serum Replacement and 2 mM forskolin) for 3 days. For EVT differentiation, plates were pre-coated with Matrigel and cells were cultured in EVT medium (DMEM/F12, supplemented with 0.1 mM 2-mercaptoethanol, 0.5% penicillin-streptomycin, 1% ITS-X supplement, 2% Matrigel, 7.5 mM A83-01, 2.5 mM Y27632, 4% KnockOut Serum Replacement and 100 ng ml⁻¹ NRG1). After three days, the medium was changed to EVT medium with 0.5% Matrigel and without NRG1. Cells were cultured until day 6.

Human pre-implantation embryos culture

Human embryos were thawed following the manufacturer's instructions (Cook Medical: Sydney IVF Thawing kit for slow freezing and Vitrolife: RapidWarmCleave or RapidWarmBlast for vitrification). Human embryos frozen at the 8-cell stage were loaded into a 12-well dish (Vitrolife: Embryoslide I bidi) with non-sequential culture medium (Vitrolife G2 plus) under mineral oil (Origio: Liquid Paraffin) at 37 °C in 5% O₂/6% CO₂.

Plasmid construction

The cDNA sequence of hYAP1, hYAP1(5SA) and hYAP1(5SA + S94A) were amplified from the pQCXIH-Myc-YAP, pQCXIH-Myc-YAP-5SA and pQCXIH-Myc-YAP-S94A plasmids, respectively. These YAP plasmids³⁴ were gifts from K. Guan (Addgene #33091, #33093 and #33094). The individual cDNA sequences were cloned into pDONR211, followed by cloning into PB-TAC-ERP2 using Gateway (Invitrogen) cloning strategy. PB-TAC-ERP2³⁵ was a gift from K. Woltjen (Addgene plasmid #80478). Complete sequences of the resulting plasmids are available upon request.

Cell transfection in human naive PSCs

pCAG-PBase (5 μ g) and PB-TAC-YAP1-ERP (5 μ g) were transfected by NEPA21 electroporation (Nepa Gene) into 5×10^4 cells in single-cell suspension. Electroporated naive PSCs were plated on Geltrex (0.5 μ l cm⁻², Thermo Fisher Science, A1413302)-coated 6-well plates with PXGL medium containing Y-27632 (10 μ M). Puromycin (0.5 μ g ml⁻¹, Sigma-aldrich, P7255) was added to PXGL medium from day 1 to day 3–4 to select transformed cells. pCAG-PBase was a gift from K. Woltjen.

YAP overexpression in naive PSC aggregates

The naive PSC aggregates were formed from naive H9 cell lines integrated with the doxycycline inducible cassette as described in the section above. The aggregates were cultured in PALLY medium with reduced LPA concentration (5 nM) from 0 h to 48 h along with

100 ng ml⁻¹ doxycycline. Higher LPA concentrations masked the effects of the genetic overexpression of the YAP1 variants. The number of caviated aggregates was counted at 72 h.

Single-cell RNA-seq library preparation and sequencing

To avoid over-representation of TE cells, blastoids were collected, dissociated and the cell suspension was stained using antibodies against TROP2 and PDGFRa that mark trophoblasts and primitive endoderm, respectively. For the 96 h time point, blastoids were selectively picked up from the microwell arrays before the dissociation, according to the morphological criteria described above. On the contrary, for the 24 and 65 h time points, all structures, including the ones that will not develop into a blastoid, were included. Accordingly, this non-selective picking correlated with the presence of more off-target cells. Cells were FACS-sorted into 384-well-plates containing the lysis buffer for Smart-seq2 and immediately frozen. The antibody staining was exploited in order to harvest specific numbers of TROP2⁺, PDGFRa⁺ and double-negative cells. The abutted FACS gates (DiVa 9.0.1) covered the whole spectrum and no blastoid cells were excluded. The H9 naive cells cultured on MEF were stained using an antibody against SUSD2, then FACS-sorted. Dead cells were excluded by DAPI staining. Smart-seq2 libraries were generated as described previously with minor optimization³⁶. Maxima H Minus reverse transcriptase (3 U per reaction, Thermo Fisher Science, EP0751) was used for the cDNA synthesis. The prepared libraries were sequenced on the S1 or SP flow cell using an Illumina Novaseq instrument in 50-bp paired-end mode.

Single-cell RNA-seq data analysis

Smart-Seq transcriptome sequencing experiments were analysed using genome sequence and gene annotation from Ensembl GRCh38 release 103 as reference. For gene-expression quantification RNA-seq reads were first trimmed using trim-galore v0.6.6 and thereafter aligned to the human genome using hisat2 v2.2.1. Uniquely mapping reads in genes were quantified using htseq-count v0.13.5 with parameter -s no. TPM estimates were obtained using RSEM v1.3.3 with parameter -single-cell-prior. Further analysis was performed in R v4.0.3 with Seurat v4.0.1. Based on initial evaluation of per-cell quality control metrics and outlier identification using the median absolute deviation algorithm, cells with $\leq 2,000$ detected genes or $\geq 12.5\%$ mitochondrial gene percentage were filtered out. Only genes detected in at least five cells were retained. Count-data were log-normalized, top 3,000 highly variable were selected, and standardization of per-gene expression values across cells was performed using NormalizeData, FindVariableFeatures and ScaleData data functions in Seurat. Principal component analysis (PCA) based on the standardized highly variable features was used for linear dimension reduction, a shared nearest neighbor (SNN) graph was constructed on the dimensionally reduced data, and the graph was partitioned using a SNN modularity optimization-based clustering algorithm at a range of resolutions using RunPCA, FindNeighbors and FindClusters from Seurat with default settings. Cluster marker and marker genes between identity groups were determined with the Wilcox likelihood-ratio test (two-sided) using the FindAllMarker and FindMarkers functions with *P*-value adjustment using Bonferroni correction and followed by filtering at a adjusted *P* value cut-off of 0.05. UMAP was used for visualization.

For integration of Smart-seq experiments from multiple sources we followed the previously described procedure¹⁰. Published data from E-MTAB-3929 (human preimplantation embryos³⁷ ranging from embryonic day 3 to 7), GSE109555 (in vitro cultured blastocysts³⁸) were downloaded, and data from Carnegie stage 7 embryo were kindly provided by the authors of the study³⁹. All the data was preprocessed to obtain per gene read counts using the same protocol as described for blastoid cells, in the case of GSE109555 including adaptations to

Article

accommodate UMI and CB information following the authors' instructions (https://github.com/WRui/Post_Implantation). For GSE109555 we used 1,000 cells randomly subsampled from the 3,184 high-quality single cells described in the original publication. Similar to ref.¹⁰, we excluded cells belonging to haemogenic endothelial progenitors and erythroblasts. After evaluation of per-cell quality control metrics, and as in ref.¹⁰, cells with >2,000 detected genes and <12.5% mitochondrial gene percentage were retained. Genes detected in at least five cells in any dataset were retained. log-normalization was performed using `computeSumFactors` in `scran` package v1.18.7, per-batch scaling normalization using `multiBatchNorm` in `batchelor` v1.6.3. Datasets were aligned using the `fastMNN` approach via `SeuratWrappers` v0.3.0 using the log-normalized batch-adjusted expression values. MNN low-dimensional coordinates were then used for clustering and visualization by UMAP. The data processing and analysis pipelines are publicly available at https://github.com/RivronLab/Human_Blastoid_Kagawa_et_al-

Bulk RNA-seq library preparation and sequencing

Bulk RNA-seq libraries were prepared using Smart-Seq2 protocol as previously described³⁶. For each sample, 50 cells were pooled together and prepared for sequencing. The libraries were then sequenced using an Illumina Novaseq 6000 with 50-bp paired end mode. For each sample, approximately 10 million reads were obtained.

Bulk RNA-seq data analysis

RNA-seq reads were first trimmed using `trimgalore` v0.5.0 and reads mapping to abundant sequences included in the iGenomes Ensembl GRCh38 bundle (rDNA, mitochondrial chromosome, phiX174 genome, adapter) were removed using `bowtie2` v2.3.4.1 alignment. Remaining reads were analyzed using genome and gene annotation for the GRCh38/hg38 assembly obtained from Ensembl release 94. Reads were aligned to the genome using `star` v2.6.0c and reads in genes were counted with `featureCounts` (subread v1.6.2) and parameter `-s 0`. Differential gene-expression analysis on raw counts and variance-stabilized transformation of count data for heatmap visualization were performed using `DESeq2` v1.18.1.

Culture of human trophoblast stem cells and aggregate formation

Experiments were performed using the human blastocyst-derived TSC line bTSS provided by the laboratory of T. Arima. Cells were cultured on Laminin 511 (5 $\mu\text{g ml}^{-1}$, BioLamina, LN511) coated plates in TSC medium as previously described²⁰. Aggregates of TSCs were formed as follows. Colonies were dissociated into single cells using `Accutase` at 37 °C for 5 min. The cells were resuspended into TSC medium containing 10 μM Y-27632, and 3.0×10^4 cells were seeded onto a microwell array imprinted into a well of a 96-well plate. The same medium²⁰ was refreshed daily. After 72 h, the aggregates were used for both characterization and implantation experiments.

Endometrial organoid culture

Cryopreserved human endometrial organoids were provided by the H. Baharvand laboratory (Royan Institute) within the framework of collaboration agreements. Human endometrial organoids were established from healthy human donors following the protocol described previously^{24,40} with some modifications. In brief, organoids were cultured in human endometrial expansion medium composed of 10% R-spondin 1 conditioned medium (in-house made) and 10% noggin-Fc-conditioned medium⁴¹ (in-house made), supplemented with 1 \times N2 supplement, 1 \times B27 supplement, 1 \times insulin-transferrin-selenium (in-house), Glutamax (1 μM), *N*-acetylcysteine (1.25 mM, Sigma-Aldrich, A7250), nicotinamide (2.5 mM, Sigma-Aldrich, 72340), EGF (50 ng ml^{-1} , Peprotech, 100-47), bFGF (2 ng ml^{-1} , Peprotech, 100-18B), HGF (10 ng ml^{-1} , Peprotech, 315-23), FGF10 (10 ng ml^{-1} , Peprotech, 100-26),

A83-01 (500 nM) and SB202190 (10 μM , Tocris, 1264). Y-27632 (10 μM) was used in the first 2 days after passaging to prevent apoptosis. The medium was changed every 2 days and the organoids were passaged with TrypLE followed by mechanical dissociation every 7–9 days.

Hormonal stimulation of endometrial organoids and OFEL culture

Endometrial organoids were passaged as described in the previous section. The dissociated cells were resuspended in Matrigel supplemented with Y-27632 (10 μM), cell suspension was deposited in 48-well plates and were cultured in endometrial expansion medium for 2 days. The organoids were stimulated first with E2 (10 nM, Sigma-Aldrich, E2758) for 2 days, followed by the mixture of E2 (10 nM), P4 (1 μM , Sigma-Aldrich, P8783), and cAMP (250 μM , Biolog, B 007) with or without XAV939 (10 μM) (EPC or EPCX respectively) for 4 days. For OFEL culture, organoids were recovered from the matrigel droplets with ice-cold DMEM/F12 and mechanical pipetting. The organoids were dissociated using TrypLE and mechanically triturated to generate single cells and seeded at a density of $3\text{--}3.5 \times 10^4$ cells per well into a 96-well glass bottom plate (Cellvis, P96-1.5H-N) and cultured for 2–3 days with stimulation. For contraceptive treatment, levonorgestrel⁴² (LNG) (10 μM , Sigma-Aldrich, PHR1850) was added every day to the medium after hormonal stimulation and continued until the end of the experiment.

In vitro implantation assay

Confluent OFELs were prepared for the implantation assay at least 2 h prior to the deposition of blastoids, trophospheres, naive PSCs or TSCs aggregates by washing the OFEL two times with DMEM/F12 and adding mIVC1 medium²⁸. Structures were then transferred onto the OFELs using a mouth pipette under an inverted microscope. After 24–48 h, the medium was removed, the well was washed with PBS, fixed using 4% formaldehyde for 30 min at room temperature and subsequently processed for immunofluorescence staining. The percentage of attached structures was reported as the percentage of total transferred structures.

In vitro culture of human blastoids in post implantation conditions

Human blastoids were selected using a mouth pipette, washed with CMRL1066 medium and transferred into suspension culture plates or 96-well plates coated with Matrigel containing pre-equilibrated media adapted from monkey blastocyst culture²⁷ with minor modifications as followed. For the first day, the culture medium was CMRL1066 supplemented with 10% (v/v) FBS, 1 mM L-glutamine (Gibco), 1 \times N2 supplement, 1 \times B27 supplement, 1 mM sodium pyruvate (Sigma) and 10 μM Y27632. After 24 h, half of the medium was replaced with a new medium including 5% Matrigel. After 48h, 50% of medium was replaced with a new medium supplemented with 20% (v/v) FBS and 5% Matrigel. After 72 h, half of the medium was replaced with a new medium supplemented with 30% (v/v) KSR and 5% Matrigel. Then, half of the medium was replaced every day and blastoids were cultured for up to 6 days. Cultures were fixed for staining after 4 and 6 days of in vitro culture with 4% PFA as mentioned above.

Human pre-implantation embryos

The use of human embryos donated to research as surplus of IVF treatment was allowed by the French embryo research oversight committee: Agence de la Biomédecine, under approval numbers RE13-010 and RE18-010. All human pre-implantation embryos used in this study were obtained from and cultured at the Assisted Reproductive Technology unit of the University Hospital of Nantes, France, which is authorized to collect embryos for research under approval number AG110126AMP of the Agence de la Biomédecine. Embryos used were initially created

in the context of an assisted reproductive cycle with a clear reproductive aim and then voluntarily donated for research once the patients had fulfilled their reproductive needs or the embryos had tested positive for the presence of monogenic diseases. Informed written consent was obtained from both parents of all couples that donated spare embryos following IVF treatment. Before giving consent, people donating embryos were provided with all of the necessary information about the research project and the opportunity to receive counselling. No financial inducements were offered for donation. Molecular analysis of the embryos was performed in compliance with the guidelines of the embryo research oversight committee and The International Society for Stem Cell Research (ISSCR)⁴³.

RNA extraction, cDNA synthesis and RT-qPCR

RNA was extracted using the RNeasy mini kit (Qiagen, 74106) and cDNA synthesis was performed using the Superscript III (Invitrogen, 18080093) enzyme. qPCR reactions were performed using GoTaq qPCR Master Mix (Promega, A6001) on CFX384 Touch Real-Time PCR Detection System (Bio-rad). Quantification was performed using Microsoft Office Excel by applying the comparative cycle threshold (C_t) method. Relative expression levels were normalized to GAPDH. The primers used for the qPCR analysis are listed in Supplementary Table 3.

ELISA assay for CG β detection

Medium from wells containing unattached or attached blastoids was collected and centrifuged to remove debris and stored at -80°C until use. The supernatant was subject to CG β ELISA (Abcam, ab178633), according to the manufacturer's instructions, alongside CG β standards.

Ligand-receptor analysis

The Cellinker web-platform was used to predict putative receptor-ligand interactions between polar TE and endometrial epithelial cells. Enriched genes in polar TE along with upregulated genes in stimulated OFELs were used as the query to search ligands and receptors in the database.

Immunohistochemistry

The samples were fixed with 4% formaldehyde for 30 min at room temperature. Post fixation, formaldehyde solution was removed and the samples were washed at least three times with PBS. The samples were then permeabilized and blocked using 0.3% Triton X-100 and 10% normal donkey serum in PBS for at least 60 min. The samples were then incubated overnight at 4°C with primary antibodies diluted in fresh blocking/permeabilization solution. The samples were washed with PBS containing 0.1% Triton X-100 (PBST) at least three times for 10 min each. The washing buffer was then replaced with Alexafluor tagged secondary antibodies (Abcam or ThermoFisher scientific) along with a nuclear dye Hoechst-33342 (1:500 or 1:300 for 2D or 3D samples respectively, Life Technologies, H3570) diluted in PBST for 30 min in dark at room temperature. The samples were then washed with PBST three times for 10 min each. For human blastocysts, the samples were fixed at the B4 or B6 stage according to the grading system proposed by Gardner and Schoolcraft⁴⁴ or at B3 or B4 +72 h in vitro culture. Embryos were fixed with 4% paraformaldehyde for 10 min at room temperature and washed in PBS/BSA. Embryos were permeabilized and blocked in PBS containing 0.2% Triton-x100 and 10% FBS at room temperature for 60 min. Samples were incubated with primary antibodies overnight at 4°C . Incubation with secondary antibodies was performed for 2 h at room temperature along with Hoechst counterstaining. The samples were mounted for imaging in PBS in the wells of glass bottom micro slides (Ibidi, 81507). The details of antibodies and their dilutions along with stainings previously performed on human blastocysts (other studies) are provided in the Supplementary Tables 4, 5. EdU staining was done using Click-iT EdU Alexa Fluor 647 Imaging Kit (Thermo Scientific, C10640) following the manufacturer's instructions.

Microscopy and image analysis

The phase-contrast images were acquired using Thermo Fisher scientific EVOS cell imaging system and inverted wide-field microscope Axio VertA1. The number of blastoids or cavitated structures were counted manually for each well. After 96 h, a blastoid is defined based on the morphological parameters as described in previous sections. The fluorescent images and time-lapse images were acquired using Olympus IX83 microscope with Yokogawa W1 spinning disk (Software: CellSense 2.3; camera: Hamamatsu Orca Flash 4.0) or Nikon Eclipse Ti E inverted microscope, equipped with a Yokogawa W1 spinning disc (Software: Visiview 4.5.0.7 ; camera: Andor Ixon Ultra 888 EMCCD). The confocal images were analysed and display images were exported using Fiji 1.53k or Bitplane Imaris 9.7.0 softwares. For cell counting, Bitplane Imaris software was used. Cell count parameters were set for size and fluorescence strength of voxels and then overall cell count data was obtained for each image using the Imaris spot function. Note that large cavities in blastoids increase the depth of the imaging field and cause poor signal from deeply located cells. Therefore, our counting data in Figs. 1h, 3g could be underrepresented values, particularly in the case of trophoctoderm cells. The quantification of the percentage of blastoids forming the NR2F2 axis was done manually. To do so, blastoids stained to detect NR2F2 expression were imaged using a confocal spinning disk microscope. The images were projected using a 3D-project function in Fiji. The blastoid was classified to have an axis when NR2F2 expression was restricted to its polar half with no expression or lower level of expression in the mural half. The inverted pattern of NR2F2 expression was classified as an invert axis. The blastoids with NR2F2 expression on their both polar and mural halves were classified to have no axis. Confocal immunofluorescence images of human blastocysts were acquired with a Nikon confocal microscope and a $20\times$ mim or $25\times$ silicon objective. Optical sections of $1\ \mu\text{m}$ -thick were collected. The images were processed using Fiji (<http://fiji.sc>) and Volocity 6.3 visualization softwares. Volocity software was used to detect and count nuclei.

Statistics and reproducibility

All the experiments were performed at least in three biological replicates unless specifically described in the Methods and the figure legends. Statistical analyses were performed using Graphpad prism 8.1.1 (330).

Reporting summary

Further information on research design is available in the Nature Research Reporting Summary linked to this paper.

Data availability

Single-cell RNA-seq and bulk RNA-seq data for human blastoids used in this study were deposited at the Gene Expression Omnibus under the accession number GSE177689. Source data are provided with this paper.

- Guo, G. et al. Epigenetic resetting of human pluripotency. *Development* **144**, 2748–2763 (2017).
- Rivron, N. C. et al. Tissue deformation spatially modulates VEGF signaling and angiogenesis. *Proc. Natl. Acad. Sci. USA* **109**, 6886–6891 (2012).
- Vrij, E. J. et al. 3D high throughput screening and profiling of embryoid bodies in thermoformed microwell plates. *Lab Chip* **16**, 734–742 (2016).
- Yu, F.-X. et al. Regulation of the Hippo-YAP pathway by G-protein-coupled receptor signaling. *Cell* **150**, 780–791 (2012).
- Turco, M. Y. et al. Trophoblast organoids as a model for maternal-fetal interactions during human placentation. *Nature* **564**, 263–267 (2018).
- Zhao, B. et al. Inactivation of YAP oncoprotein by the Hippo pathway is involved in cell contact inhibition and tissue growth control. *Genes Dev.* **21**, 2747–2761 (2007).
- Kim, S.-I. et al. Inducible transgene expression in human iPS cells using versatile all-in-one piggyBac transposons. *Methods Mol. Biol.* **1357**, 111–131 (2016).
- Picelli, S. et al. Full-length RNA-seq from single cells using Smart-seq2. *Nat. Protoc.* **9**, 171–181 (2014).

Article

37. Petropoulos, S. et al. Single-cell RNA-seq reveals lineage and X chromosome dynamics in human preimplantation embryos. *Cell* **165**, 1012–1026 (2016).
 38. Zhou, F. et al. Reconstituting the transcriptome and DNA methylome landscapes of human implantation. *Nature* **572**, 660–664 (2019).
 39. Tyser, R. C. V. et al. Single-cell transcriptomic characterization of a gastrulating human embryo. *Nature* **600**, 285–289 (2021).
 40. Turco, M. Y. et al. Long-term, hormone-responsive organoid cultures of human endometrium in a chemically defined medium. *Nat. Cell Biol.* **19**, 568–577 (2017).
 41. Heijmans, J. et al. ER stress causes rapid loss of intestinal epithelial stemness through activation of the unfolded protein response. *Cell Rep.* **3**, 1128–1139 (2013).
 42. Matsuo, M. et al. Levonorgestrel inhibits embryo attachment by eliminating uterine induction of leukemia inhibitory factor. *Endocrinology* **161**, bqz005 (2020).
 43. Kimmelman, J. et al. New ISSCR guidelines: clinical translation of stem cell research. *Lancet* **387**, 1979–1981 (2016).
 44. Gardner, D. K., Lane, M., Stevens, J., Schlenker, T. & Schoolcraft, W. B. Blastocyst score affects implantation and pregnancy outcome: towards a single blastocyst transfer. *Fertil. Steril.* **73**, 1155–1158 (2000).
 45. Mischler, A. et al. Two distinct trophectoderm lineage stem cells from human pluripotent stem cells. *J. Biol. Chem.* **296**, 100386 (2021).
 46. Jeschke, U. et al. The human endometrium expresses the glycoprotein mucin-1 and shows positive correlation for Thomsen–Friedenreich epitope expression and galectin-1 binding. *J. Histochem. Cytochem.* **57**, 871–881 (2009).
 47. Zhang, Y. et al. Cellinker: a platform of ligand–receptor interactions for intercellular communication analysis. *Bioinformatics* **37**, 2025–2032 (2021).
- and H9-GFP cell lines; A. Smith, P. Andrews and G. Guo for sharing the HNES1, Shef6, niPSC 16.2b and cR-NCRM2 cell lines; H. Baharvand for sharing the endometrial organoids; K. Woltjen for sharing the PB-TAC-ERP2 and pCAG-PBase plasmids; K. Guan for sharing pQCXIH-Myc-YAP, pQCXIH-Myc-YAP-5SA, pQCXIH-Myc-YAP-S94A plasmids; J. M. Brickman for sharing the RNA isolated from PrE differentiated cells and nEND cells; S. Srinivas for sharing the single-cell RNA-seq data of peri-gastrulation embryo; A. Bykov and L. Cochella for technical assistance for SMARTSeq2 library preparation; and the NGS, Biooptic and Stem Cell facility at IMBA for critical assistance.

Author contributions H.K., A.J., H.H.K. and N.R. conceived the study; N.R. supervised the project; H.K., A.J., H.H.K., T.M.S. and N.R. designed the blastoid experiments; H.K., A.J., H.H.K., T.M.S. and Y.S.o.R. performed blastoid experiments; G.S., G.C. and M.N. performed the bioinformatic analysis of single-cell RNA-seq datasets; J.L., S.L. and T.F. managed human embryos donated for research in Nantes; A.B., J.L., S.L. and G.C. performed experiments on human embryos in Nantes; L.D. supervised experiments on human embryos in Nantes; H.H.K., N.M., H.V. and N.R. designed the experiments with endometrial organoids; N.R. hosted N.M. and G.C. in his laboratory; H.K., A.J., H.H.K., T.M.S., Y.S.o.R., G.C., A.B., N.M. and N.R. analysed data; N.R. wrote the manuscript with help from all of the authors.

Competing interests The Institute for Molecular Biotechnology, Austrian Academy of Sciences has filed patent application EP21151455.9 describing the protocols for human blastoid formation and for the blastoid–endometrium interaction assay. H.K., A.J., H.H.K. and N.R. are the inventors on this patent. All other authors declare no competing interests.

Additional information

Supplementary information The online version contains supplementary material available at <https://doi.org/10.1038/s41586-021-04267-8>.

Correspondence and requests for materials should be addressed to Nicolas Rivron.

Peer review information *Nature* thanks Jan Brosens, Jianping Fu, Insoo Hyun and the other, anonymous, reviewer(s) for their contribution to the peer review of this work.

Reprints and permissions information is available at <http://www.nature.com/reprints>.

Acknowledgements This project has received funding from the European Research Council (ERC) under the European Union's Horizon 2020 research and innovation programme (ERC-Co grant agreement no.101002317 'BLASTOID: a discovery platform for early human embryogenesis'). H.H.K. is supported by the Austrian Science Fund (FWF), Lise Meitner Programme M3131-B. This project has also received funding from the ANR 'BOOSTIVF'. L.D. thanks the iPSCDTC and MicroPICell core facilities. We thank Y. Takashima for sharing the H9

BIBLIOGRAPHIE

- Aberkane, A., W. Essahib, C. Spits, C. De Paepe, K. Sermon, T. Adriaenssens, S. Mackens, H. Tournaye, J. J. Brosens, et H. Van de Velde. 2018. « Expression of Adhesion and Extracellular Matrix Genes in Human Blastocysts upon Attachment in a 2D Co-Culture System ». *Molecular Human Reproduction* 24 (7): 375-87. <https://doi.org/10.1093/molehr/gay024>.
- Aghajani, Shahrzad, Ali Salehzadeh, Fatemeh Ghasemian, Marziyeh Mehrafza, et Ahmad Hosseini. 2022. « TEfect of Single Embryo Blastomere Biopsy from Human Frozen Embryos on Assisted Reproductive Outcomes ». *Cell Journal* 24 (10): 628-36. <https://doi.org/10.22074/cellj.2022.8328>.
- Alghobary, Moheiddin, et Taymour Mostafa. 2022. « Addiction and Human Male Fertility: A Systematic Review and a Critical Appraisal ». *Andrology* 10 (6): 1073-95. <https://doi.org/10.1111/andr.13196>.
- American College of Obstetricians and Gynecologists Committee on Gynecologic Practice and Practice Committee. 2014. « Female Age-Related Fertility Decline. Committee Opinion No. 589 ». *Fertility and Sterility* 101 (3): 633-34. <https://doi.org/10.1016/j.fertnstert.2013.12.032>.
- Amir, Hadar, Shiri Barbash-Hazan, Yael Kalma, Tsvia Frumkin, Mira Malcov, Nivin Samara, Joseph Hasson, Adi Reches, Foad Azem, et Dalit Ben-Yosef. 2019. « Time-Lapse Imaging Reveals Delayed Development of Embryos Carrying Unbalanced Chromosomal Translocations ». *Journal of Assisted Reproduction and Genetics* 36 (2): 315-24. <https://doi.org/10.1007/s10815-018-1361-8>.
- Auger, J., et P. Jouannet. 2005. « Age and Male Fertility: Biological Factors ». *Revue D'épidemiologie Et De Sante Publique* 53 Spec No 2 (novembre): 2S25-35.
- Bamford, Thomas, Amy Barrie, Sue Montgomery, Rima Dhillon-Smith, Alison Campbell, Christina Easter, et Arri Coomarasamy. 2022. « Morphological and Morphokinetic Associations with Aneuploidy: A Systematic Review and Meta-Analysis ». *Human Reproduction Update* 28 (5): 656-86. <https://doi.org/10.1093/humupd/dmac022>.
- Barberet, J., C. Biquet, M. Guilleman, A. Doukani, C. Choux, C. Bruno, A. Bourredjem, et al. 2021. « Do Assisted Reproductive Technologies and in Vitro Embryo Culture Influence the Epigenetic Control of Imprinted Genes and Transposable Elements in Children? ». *Human Reproduction (Oxford, England)* 36 (2): 479-92. <https://doi.org/10.1093/humrep/deaa310>.
- Bellver, José, et Jacques Donnez. 2019. « Introduction: Infertility Etiology and Offspring Health ». *Fertility and Sterility* 111 (6): 1033-35. <https://doi.org/10.1016/j.fertnstert.2019.04.043>.
- Berntsen, Sine, Viveca Söderström-Anttila, Ulla-Britt Wennerholm, Hannele Laivuori, Anne Loft, Nan B. Oldereid, Liv Bente Romundstad, Christina Bergh, et Anja Pinborg. 2019. « The Health of Children Conceived by ART: "The Chicken or the Egg?" ». *Human Reproduction Update* 25 (2): 137-58. <https://doi.org/10.1093/humupd/dmz001>.
- Blakeley, Paul, Norah M. E. Fogarty, Ignacio del Valle, Sissy E. Wamaitha, Tim Xiaoming Hu, Kay Elder, Philip Snell, Leila Christie, Paul Robson, et Kathy K. Niakan. 2015. « Defining the Three Cell Lineages of the Human Blastocyst by Single-Cell RNA-Seq ». *Development (Cambridge, England)* 142 (18): 3151-65. <https://doi.org/10.1242/dev.123547>.
- Bracewell-Milnes, Timothy, Srdjan Saso, Hossam Abdalla, Dimitrios Nikolau, Julian Norman-Taylor, Mark Johnson, Elaine Holmes, et Meen-Yau Thum. 2017. « Metabolomics as a Tool to Identify Biomarkers to Predict and Improve Outcomes in Reproductive Medicine: A Systematic Review ». *Human Reproduction Update* 23 (6): 723-36. <https://doi.org/10.1093/humupd/dmx023>.
- Brodie, D., C. E. Beyer, E. Osborne, V. Kravetski, S. Rasi, et T. Osianlis. 2012. « Preimplantation Genetic Diagnosis for Chromosome Rearrangements - One Blastomere Biopsy versus Two Blastomere Biopsy ». *Journal of Assisted Reproduction and Genetics* 29 (8): 821-27. <https://doi.org/10.1007/s10815-012-9782-2>.
- Brouillet, Sophie, Guillaume Martinez, Charles Coutton, et Samir Hamamah. 2020. « Is Cell-Free DNA in Spent Embryo Culture Medium an Alternative to Embryo Biopsy for Preimplantation Genetic Testing? A Systematic Review ». *Reproductive Biomedicine Online* 40 (6): 779-96. <https://doi.org/10.1016/j.rbmo.2020.02.002>.
- Budani, Maria Cristina, et Gian Mario Tiboni. 2017. « Ovotoxicity of Cigarette Smoke: A Systematic Review of the Literature ». *Reproductive Toxicology (Elmsford, N.Y.)* 72 (septembre): 164-81. <https://doi.org/10.1016/j.reprotox.2017.06.184>.
- Buran, Ali, Pinar Tulay, Nurten Dayıoğlu, Mustafa Emre Bakircioglu, Mustafa Bahceci, et Tulay İrez. 2019. « Evaluation of the Morphokinetic Parameters and Development of Pre-Implantation Embryos Obtained

- by Testicular, Epididymal and Ejaculate Spermatozoa Using Time-Lapse Imaging System ». *Andrologia* 51 (4): e13217. <https://doi.org/10.1111/and.13217>.
- Capalbo, Antonio, Graham Wright, Thomas Elliott, Filippo Maria Ubaldi, Laura Rienzi, et Zsolt Peter Nagy. 2013. « FISH Reanalysis of Inner Cell Mass and Trophectoderm Samples of Previously Array-CGH Screened Blastocysts Shows High Accuracy of Diagnosis and No Major Diagnostic Impact of Mosaicism at the Blastocyst Stage ». *Human Reproduction* 28 (8): 2298-2307. <https://doi.org/10.1093/humrep/det245>.
- Carles, Manon, Charlotte Sonigo, Olivier Binois, Laetitia Hesters, Julie Steffann, Serge Romana, Nelly Frydman, et Anne Mayeur. 2022. « Second Biopsy for Embryos with Inconclusive Results after Preimplantation Genetic Testing: Impact on Pregnancy Outcomes ». *Journal of Gynecology Obstetrics and Human Reproduction* 51 (8): 102436. <https://doi.org/10.1016/j.jogoh.2022.102436>.
- Castel, Gaël, et Laurent David. 2022. « Induction of Human Trophectoderm Stem Cells ». *Nature Protocols* 17 (12): 2760-83. <https://doi.org/10.1038/s41596-022-00744-0>.
- Castel, Gaël, Dimitri Meistermann, Betty Bretin, Julie Firmin, Justine Blin, Sophie Loubersac, Alexandre Bruneau, et al. 2020. « Induction of Human Trophectoderm Stem Cells from Somatic Cells and Pluripotent Stem Cells ». *Cell Reports* 33 (8): 108419. <https://doi.org/10.1016/j.celrep.2020.108419>.
- Charlesworth, Carsten T., et Hiromitsu Nakauchi. 2022. « An Optimized Sendai Viral Vector Platform for Reprogramming to Naive Pluripotency ». *Cell Reports Methods* 2 (11): 100349. <https://doi.org/10.1016/j.crmeth.2022.100349>.
- Chavez-Badiola, Alejandro, Adolfo Flores-Saiffe-Farías, Gerardo Mendizabal-Ruiz, Andrew J. Drakeley, et Jacques Cohen. 2020. « Embryo Ranking Intelligent Classification Algorithm (ERICA): Artificial Intelligence Clinical Assistant Predicting Embryo Ploidy and Implantation ». *Reproductive Biomedicine Online* 41 (4): 585-93. <https://doi.org/10.1016/j.rbmo.2020.07.003>.
- Checa Vizcaíno, Miguel A., Mireia González-Comadran, et Benedicte Jacquemin. 2016. « Outdoor Air Pollution and Human Infertility: A Systematic Review ». *Fertility and Sterility* 106 (4): 897-904.e1. <https://doi.org/10.1016/j.fertnstert.2016.07.1110>.
- Chen, Tsung-Jui, Wei-Lin Zheng, Chun-Hsin Liu, Ian Huang, Hsing-Hua Lai, et Mark Liu. 2019. « Using Deep Learning with Large Dataset of Microscope Images to Develop an Automated Embryo Grading System ». *Fertility & Reproduction* 01 (01): 51-56. <https://doi.org/10.1142/S2661318219500051>.
- Cimadomo, Danilo, Anabella Marconetto, Samuele Trio, Viviana Chiappetta, Federica Innocenti, Laura Albricci, Itay Erlich, et al. 2022. « Human Blastocyst Spontaneous Collapse Is Associated with Worse Morphological Quality and Higher Degeneration and Aneuploidy Rates: A Comprehensive Analysis Standardized through Artificial Intelligence ». *Human Reproduction (Oxford, England)* 37 (10): 2291-2306. <https://doi.org/10.1093/humrep/deac175>.
- Cimadomo, Danilo, Laura Rienzi, Antonio Capalbo, Carmen Rubio, Federica Innocenti, Carmen María García-Pascual, Filippo Maria Ubaldi, et Alan Handyside. 2020. « The Dawn of the Future: 30 Years from the First Biopsy of a Human Embryo. The Detailed History of an Ongoing Revolution ». *Human Reproduction Update* 26 (4): 453-73. <https://doi.org/10.1093/humupd/dmaa019>.
- Deglincerti, Alessia, Fred Etoc, M. Cecilia Guerra, Iain Martyn, Jakob Metzger, Albert Ruzo, Mijo Simunovic, et al. 2016. « Self-Organization of Human Embryonic Stem Cells on Micropatterns ». *Nature Protocols* 11 (11): 2223-32. <https://doi.org/10.1038/nprot.2016.131>.
- Desai, Nina, Pavinder Gill, Nicholas N. Tadros, Jeffrey M. Goldberg, Edmund Sabanegh, et Tommaso Falcone. 2018. « Azoospermia and Embryo Morphokinetics: Testicular Sperm-Derived Embryos Exhibit Delays in Early Cell Cycle Events and Increased Arrest Prior to Compaction ». *Journal of Assisted Reproduction and Genetics* 35 (7): 1339-48. <https://doi.org/10.1007/s10815-018-1183-8>.
- Desai, Nina, Jeffrey M. Goldberg, Cynthia Austin, et Tommaso Falcone. 2018. « Are Cleavage Anomalies, Multinucleation, or Specific Cell Cycle Kinetics Observed with Time-Lapse Imaging Predictive of Embryo Developmental Capacity or Ploidy? ». *Fertility and Sterility* 109 (4): 665-74. <https://doi.org/10.1016/j.fertnstert.2017.12.025>.
- Diakiw, S. M., J. M. M. Hall, M. D. VerMilyea, J. Amin, J. Aizpurua, L. Giardini, Y. G. Briones, et al. 2022. « Development of an Artificial Intelligence Model for Predicting the Likelihood of Human Embryo Euploidy Based on Blastocyst Images from Multiple Imaging Systems during IVF ». *Human Reproduction (Oxford, England)* 37 (8): 1746-59. <https://doi.org/10.1093/humrep/deac131>.
- Domínguez, Francisco, Blanca Gadea, Francisco J. Esteban, Jose Antonio Horcajadas, Antonio Pellicer, et Carlos Simón. 2008. « Comparative Protein-Profile Analysis of Implanted versus Non-Implanted Human Blastocysts ». *Human Reproduction (Oxford, England)* 23 (9): 1993-2000. <https://doi.org/10.1093/humrep/den205>.

- Dominguez, Francisco, Marcos Meseguer, Belen Aparicio-Ruiz, Paloma Piqueras, Alicia Quiñonero, et Carlos Simón. 2015. « New Strategy for Diagnosing Embryo Implantation Potential by Combining Proteomics and Time-Lapse Technologies ». *Fertility and Sterility* 104 (4): 908-14. <https://doi.org/10.1016/j.fertnstert.2015.06.032>.
- Eastick, Jessica, Christos Venetis, Simon Cooke, Ashleigh Storr, Daisy Susetio, et Michael Chapman. 2017. « Is Early Embryo Development as Observed by Time-Lapse Microscopy Dependent on Whether Fresh or Frozen Sperm Was Used for ICSI? A Cohort Study ». *Journal of Assisted Reproduction and Genetics* 34 (6): 733-40. <https://doi.org/10.1007/s10815-017-0928-0>.
- Edwards, R. G., B. D. Bavister, et P. C. Steptoe. 1969. « Early Stages of Fertilization in Vitro of Human Oocytes Matured in Vitro ». *Nature* 221 (5181): 632-35. <https://doi.org/10.1038/221632a0>.
- ESHRE Group on good practice in IVF lab. 2015. « Revised Guidelines for Good Practice in IVF Laboratories ».
- ESHRE Special Interest Group of Embryology et Alpha Scientists in Reproductive Medicine. 2017. « The Vienna Consensus: Report of an Expert Meeting on the Development of Art Laboratory Performance Indicators†‡ ». *Human Reproduction Open* 2017 (2): hox011. <https://doi.org/10.1093/hropen/hox011>.
- European IVF Monitoring Consortium (EIM), for the European Society of Human Reproduction and Embryology (ESHRE), C. Wyns, C. De Geyter, C. Calhaz-Jorge, M. S. Kupka, T. Motrenko, J. Smeenk, et al. 2022. « ART in Europe, 2018: Results Generated from European Registries by ESHRE ». *Human Reproduction Open* 2022 (3): hoac022. <https://doi.org/10.1093/hropen/hoac022>.
- Ezoe, Kenji, Tsubasa Takahashi, Kiyoe Shimazaki, Tetsuya Miki, Yuko Tanimura, Ayumi Amagai, Ayano Sawado, et al. 2022. « Human 1PN and 3PN Zygotes Recapitulate All Morphokinetic Events of Normal Fertilization but Reveal Novel Developmental Errors ». *Human Reproduction (Oxford, England)* 37 (10): 2307-19. <https://doi.org/10.1093/humrep/deac177>.
- Fishel, Simon B., Jacques Cohen, Carole Fehilly, Jean M. Purdy, D. Eurof Walters, et Robert G. Edwards. 1985. « Factors Influencing Human Embryonic Development in Vitro ». *Annals of the New York Academy of Sciences* 442 (1 In Vitro Fert): 342-56. <https://doi.org/10.1111/j.1749-6632.1985.tb37539.x>.
- Fogarty, Norah M. E., Afshan McCarthy, Kirsten E. Snijders, Benjamin E. Powell, Nada Kubikova, Paul Blakeley, Rebecca Lea, et al. 2017. « Genome Editing Reveals a Role for OCT4 in Human Embryogenesis ». *Nature* 550 (7674): 67-73. <https://doi.org/10.1038/nature24033>.
- Freour, T, J Lammers, C Spingart, M Jean, et P Barrière. 2012. « L'observation en continu du développement embryonnaire en FIV (time lapse) à l'aide de l'Embryoscope® : un an d'expérience au CHU de Nantes ».
- Gardner, D. K., et W. B. Schoolcraft. 1999. « Culture and Transfer of Human Blastocysts ». *Current Opinion in Obstetrics & Gynecology* 11 (3): 307-11. <https://doi.org/10.1097/00001703-199906000-00013>.
- Gardner, David K., Michelle Lane, et William B. Schoolcraft. 2002. « Physiology and Culture of the Human Blastocyst ». *Journal of Reproductive Immunology* 55 (1-2): 85-100. [https://doi.org/10.1016/s0165-0378\(01\)00136-x](https://doi.org/10.1016/s0165-0378(01)00136-x).
- Gazzo, Eduardo, Fernando Peña, Federico Valdéz, Arturo Chung, Marcelo Velit, Mario Ascenzo, et Ernesto Escudero. 2020. « Blastocyst Contractions Are Strongly Related with Aneuploidy, Lower Implantation Rates, and Slow-Cleaving Embryos: A Time Lapse Study ». *JBRA Assisted Reproduction* 24 (1): 77-81. <https://doi.org/10.5935/1518-0557.20190053>.
- Grau, Noelia, Laura Escrich, Yolanda Galiana, Marcos Meseguer, Sandra García-Herrero, José Remohí, et María-José Escribá. 2015. « Morphokinetics as a Predictor of Self-Correction to Diploidy in Trippronucleated Intracytoplasmic Sperm Injection-Derived Human Embryos ». *Fertility and Sterility* 104 (3): 728-35. <https://doi.org/10.1016/j.fertnstert.2015.05.024>.
- Guerif, F., A. Le Gouge, B. Giraudeau, J. Poindron, R. Bidault, O. Gasnier, et D. Royere. 2007. « Limited Value of Morphological Assessment at Days 1 and 2 to Predict Blastocyst Development Potential: A Prospective Study Based on 4042 Embryos ». *Human Reproduction (Oxford, England)* 22 (7): 1973-81. <https://doi.org/10.1093/humrep/dem100>.
- Guo, Hongshan, Ping Zhu, Liying Yan, Rong Li, Boqiang Hu, Ying Lian, Jie Yan, et al. 2014. « The DNA Methylation Landscape of Human Early Embryos ». *Nature* 511 (7511): 606-10. <https://doi.org/10.1038/nature13544>.
- Hart, R. J., et L. A. Wijs. 2022. « The Longer-Term Effects of IVF on Offspring from Childhood to Adolescence ». *Frontiers in Reproductive Health* 4: 1045762. <https://doi.org/10.3389/frph.2022.1045762>.
- Hassan, Md Rafiul, Sadiq Al-Insaf, M. Imtiaz Hossain, et Joarder Kamruzzaman. 2020. « A Machine Learning Approach for Prediction of Pregnancy Outcome Following IVF Treatment ». *Neural Computing and Applications* 32 (7): 2283-97. <https://doi.org/10.1007/s00521-018-3693-9>.

- Hernández-Vargas, Purificación, Manuel Muñoz, et Francisco Domínguez. 2020. « Identifying Biomarkers for Predicting Successful Embryo Implantation: Applying Single to Multi-OMICS to Improve Reproductive Outcomes ». *Human Reproduction Update* 26 (2): 264-301. <https://doi.org/10.1093/humupd/dmz042>.
- Huang, Thomas TF, David H Huang, Hyeong J Ahn, Christina Arnett, et Christopher TF Huang. 2019. « Early Blastocyst Expansion in Euploid and Aneuploid Human Embryos: Evidence for a Non-Invasive and Quantitative Marker for Embryo Selection ». *Reproductive BioMedicine Online* 39 (1): 27-39. <https://doi.org/10.1016/j.rbmo.2019.01.010>.
- Hur, Christine, Vaani Nanavaty, Meng Yao, et Nina Desai. 2023. « The Presence of Partial Compaction Patterns Is Associated with Lower Rates of Blastocyst Formation, Sub-Optimal Morphokinetic Parameters and Poorer Morphologic Grade ». *Reproductive Biology and Endocrinology: RB&E* 21 (1): 12. <https://doi.org/10.1186/s12958-023-01059-9>.
- Kagawa, Harunobu, Alok Javali, Heidar Heidari Khoei, Theresa Maria Sommer, Giovanni Sestini, Maria Novatchkova, Yvonne Scholte op Reimer, et al. 2022. « Human Blastoids Model Blastocyst Development and Implantation ». *Nature* 601 (7894): 600-605. <https://doi.org/10.1038/s41586-021-04267-8>.
- Karavani, Gilad, Yoav Kan-Tor, Natali Schachter-Safrai, Eliahu Levitas, Yuval Or, Assaf Ben-Meir, Amnon Buxboim, et Iris Har-Vardi. 2021. « Does Sperm Origin-Ejaculated or Testicular-Affect Embryo Morphokinetic Parameters? » *Andrology* 9 (2): 632-39. <https://doi.org/10.1111/andr.12952>.
- Kieslinger, D. C., C. G. Vergouw, L. Ramos, B. Arends, M. H. J. M. Curfs, E. Slappendel, E. H. Kosteljik, et al. 2023. « Clinical Outcomes of Uninterrupted Embryo Culture with or without Time-Lapse-Based Embryo Selection versus Interrupted Standard Culture (SELECTIMO): A Three-Armed, Multicentre, Double-Blind, Randomised Controlled Trial ». *Lancet (London, England)*, mars, S0140-6736(23)00168-X. [https://doi.org/10.1016/S0140-6736\(23\)00168-X](https://doi.org/10.1016/S0140-6736(23)00168-X).
- Kilens, Stéphanie, Dimitri Meistermann, Diego Moreno, Caroline Chariou, Anne Gaignerie, Arnaud Reignier, Johann Lelièvre, et al. 2018. « Parallel Derivation of Isogenic Human Primed and Naive Induced Pluripotent Stem Cells ». *Nature Communications* 9 (1): 360. <https://doi.org/10.1038/s41467-017-02107-w>.
- Kimelman, Dana, Rafael Confino, Ijeoma Okeigwe, Jaclyn Lambe-Steinmiller, Edmond Confino, Lee P. Shulman, John X. Zhang, et Mary Ellen Pavone. 2019. « Assessing the Impact of Delayed Blastulation Using Time Lapse Morphokinetics and Preimplantation Genetic Testing in an IVF Patient Population ». *Journal of Assisted Reproduction and Genetics* 36 (8): 1561-69. <https://doi.org/10.1007/s10815-019-01501-1>.
- Koeck, Rebekka M., Florence Busato, Jorg Tost, Heleen Zandstra, Sylvie Remy, Sabine Langie, Marij Gielen, et al. 2022. « At Age 9, the Methylome of Assisted Reproductive Technology Children That Underwent Embryo Culture in Different Media Is Not Significantly Different on a Genome-Wide Scale ». *Human Reproduction (Oxford, England)* 37 (11): 2709-21. <https://doi.org/10.1093/humrep/deac213>.
- Kokkali, G., J. Traeger-Synodinos, C. Vrettou, D. Stavrou, G. M. Jones, D. S. Cram, E. Makrakis, A. O. Trounson, E. Kanavakis, et K. Pantos. 2007. « Blastocyst Biopsy versus Cleavage Stage Biopsy and Blastocyst Transfer for Preimplantation Genetic Diagnosis of Beta-Thalassaemia: A Pilot Study ». *Human Reproduction (Oxford, England)* 22 (5): 1443-49. <https://doi.org/10.1093/humrep/del506>.
- Kunitomi, Akira, Ryoko Hirohata, Vanessa Arreola, Mitsujiro Osawa, Tomoaki M. Kato, Masaki Nomura, Jitsutaro Kawaguchi, et al. 2022. « Improved Sendai Viral System for Reprogramming to Naive Pluripotency ». *Cell Reports Methods* 2 (11): 100317. <https://doi.org/10.1016/j.crmeth.2022.100317>.
- La Rochebrochard, Élise de. 2018. « 1 enfant sur 30 conçu par assistance médicale à la procréation en France ». *Population & Sociétés* N° 556 (6): 1-4. <https://doi.org/10.3917/popsoc.556.0001>.
- Leaver, Megan, et Dagan Wells. 2020. « Non-Invasive Preimplantation Genetic Testing (NiPGT): The next Revolution in Reproductive Genetics? » *Human Reproduction Update* 26 (1): 16-42. <https://doi.org/10.1093/humupd/dmz033>.
- Lee, Chun-I., Yan-Ru Su, Chien-Hong Chen, T. Arthur Chang, Esther En-Shu Kuo, Wei-Lin Zheng, Wen-Ting Hsieh, Chun-Chia Huang, Maw-Sheng Lee, et Mark Liu. 2021. « End-to-End Deep Learning for Recognition of Ploidy Status Using Time-Lapse Videos ». *Journal of Assisted Reproduction and Genetics* 38 (7): 1655-63. <https://doi.org/10.1007/s10815-021-02228-8>.
- Leisegang, Kristian, et Sulagna Dutta. 2021. « Do Lifestyle Practices Impede Male Fertility? » *Andrologia* 53 (1): e13595. <https://doi.org/10.1111/and.13595>.
- Li, Lin, Fan Guo, Yun Gao, Yixin Ren, Peng Yuan, Liying Yan, Rong Li, et al. 2018. « Single-Cell Multi-Omics Sequencing of Human Early Embryos ». *Nature Cell Biology* 20 (7): 847-58. <https://doi.org/10.1038/s41556-018-0123-2>.

- Lindgren, Karin E., Fatma Gülen Yaldir, Julius Hreinsson, Jan Holte, Karin Kårehed, Inger Sundström-Poromaa, Helena Kaihola, et Helena Åkerud. 2018. « Differences in Secretome in Culture Media When Comparing Blastocysts and Arrested Embryos Using Multiplex Proximity Assay ». *Upsala Journal of Medical Sciences* 123 (3): 143-52. <https://doi.org/10.1080/03009734.2018.1490830>.
- Luke, Barbara, Morton B. Brown, Ethan Wantman, Nina E. Forestieri, Marilyn L. Browne, Sarah C. Fisher, Mahsa M. Yazdy, et al. 2021. « The Risk of Birth Defects with Conception by ART ». *Human Reproduction (Oxford, England)* 36 (1): 116-29. <https://doi.org/10.1093/humrep/deaa272>.
- Lundin, K., C. Bergh, et T. Hardarson. 2001. « Early Embryo Cleavage Is a Strong Indicator of Embryo Quality in Human IVF ». *Human Reproduction* 16 (12): 2652-57. <https://doi.org/10.1093/humrep/16.12.2652>.
- Mateo, Silvia, Francesca Vidal, Beatriz Carrasco, Ignacio Rodríguez, Buenaventura Coroleu, Anna Veiga, et Montserrat Boada. 2020. « Morphokinetics and in Vitro Developmental Potential of Monopronucleated ICSI Zygotes until the Blastocyst Stage ». *Zygote (Cambridge, England)* 28 (3): 217-22. <https://doi.org/10.1017/S0967199420000027>.
- Meistermann, Dimitri, Alexandre Bruneau, Sophie Loubersac, Arnaud Reignier, Julie Firmin, Valentin François-Campion, Stéphanie Kilens, et al. 2021. « Integrated Pseudotime Analysis of Human Pre-Implantation Embryo Single-Cell Transcriptomes Reveals the Dynamics of Lineage Specification ». *Cell Stem Cell* 28 (9): 1625-1640.e6. <https://doi.org/10.1016/j.stem.2021.04.027>.
- Moya-Jódar, Marta, Asier Ullate-Agote, Paula Barlabé, Juan Roberto Rodríguez-Madoz, Gloria Abizanda, Carolina Barreda, Xonia Carvajal-Vergara, et al. 2023. « Revealing Cell Populations Catching the Early Stages of Human Embryo Development in Naive Pluripotent Stem Cell Cultures ». *Stem Cell Reports* 18 (1): 64-80. <https://doi.org/10.1016/j.stemcr.2022.11.015>.
- Munné, Santiago, Brian Kaplan, John L. Frattarelli, Tim Child, Gary Nakhuda, F. Nicholas Shamma, Kaylen Silverberg, et al. 2019. « Preimplantation Genetic Testing for Aneuploidy versus Morphology as Selection Criteria for Single Frozen-Thawed Embryo Transfer in Good-Prognosis Patients: A Multicenter Randomized Clinical Trial ». *Fertility and Sterility* 112 (6): 1071-1079.e7. <https://doi.org/10.1016/j.fertnstert.2019.07.1346>.
- Niakan, Kathy K., et Kevin Eggan. 2013. « Analysis of Human Embryos from Zygote to Blastocyst Reveals Distinct Gene Expression Patterns Relative to the Mouse ». *Developmental Biology* 375 (1): 54-64. <https://doi.org/10.1016/j.ydbio.2012.12.008>.
- Niederberger, Craig, Antonio Pellicer, Jacques Cohen, David K. Gardner, Gianpiero D. Palermo, Claire L. O'Neill, Stephen Chow, et al. 2018. « Forty Years of IVF ». *Fertility and Sterility* 110 (2): 185-324.e5. <https://doi.org/10.1016/j.fertnstert.2018.06.005>.
- Okae, Hiroaki, Hidehiro Toh, Tetsuya Sato, Hitoshi Hiura, Sota Takahashi, Kenjiro Shirane, Yuka Kabayama, Mikita Suyama, Hiroyuki Sasaki, et Takahiro Arima. 2018. « Derivation of Human Trophoblast Stem Cells ». *Cell Stem Cell* 22 (1): 50-63.e6. <https://doi.org/10.1016/j.stem.2017.11.004>.
- OMS. 2023. « Selon l'OMS, dans le monde, une personne sur six est touchée par l'infertilité », avril 2023. <https://www.who.int/fr/news/item/04-04-2023-1-in-6-people-globally-affected-by-infertility>.
- Onfray, Constance, Jia Ping Tan, Stéphanie Kilens, Xiaodong Liu, Jose Polo, et Laurent David. 2022. « Induction of Human Naïve Pluripotent Stem Cells from Somatic Cells ». *Methods in Molecular Biology (Clifton, N.J.)* 2416: 39-51. https://doi.org/10.1007/978-1-0716-1908-7_4.
- Petropoulos, S., S. P. Panula, J. P. Schell, et F. Lanner. 2016. « Single-Cell RNA Sequencing: Revealing Human Pre-Implantation Development, Pluripotency and Germline Development ». *Journal of Internal Medicine* 280 (3): 252-64. <https://doi.org/10.1111/joim.12493>.
- Reignier, Arnaud, Julie Firmin, Jenna Lammers, Paul Barriere, et Thomas Freour. 2019. « Le time-lapse : bilan et perspectives en 2019 ».
- Rivron, Nicolas C., Javier Frias-Aldeguer, Erik J. Vrij, Jean-Charles Boisset, Jeroen Korving, Judith Vivié, Roman K. Truckenmüller, Alexander van Oudenaarden, Clemens A. van Blitterswijk, et Niels Geijsen. 2018. « Blastocyst-like Structures Generated Solely from Stem Cells ». *Nature* 557 (7703): 106-11. <https://doi.org/10.1038/s41586-018-0051-0>.
- Roode, Mila, Kathryn Blair, Philip Snell, Kay Elder, Sally Marchant, Austin Smith, et Jennifer Nichols. 2012. « Human Hypoblast Formation Is Not Dependent on FGF Signalling ». *Developmental Biology* 361 (2): 358-63. <https://doi.org/10.1016/j.ydbio.2011.10.030>.
- Rubio, Carmen, Luis Navarro-Sánchez, Carmen M. García-Pascual, Olcay Ocali, Danilo Cimadomo, William Venier, Gerardo Barroso, et al. 2020. « Multicenter Prospective Study of Concordance between Embryonic Cell-Free DNA and Trophoctoderm Biopsies from 1301 Human Blastocysts ». *American Journal of Obstetrics and Gynecology* 223 (5): 751.e1-751.e13. <https://doi.org/10.1016/j.ajog.2020.04.035>.

- Scarselli, Filomena, Valentina Casciani, Elisabetta Cursio, Saverio Muzzi, Alessandro Colasante, Simona Gatti, Maria Chiara Greco, Pierfrancesco Greco, Maria Giulia Minasi, et Ermanno Greco. 2018. « Influence of Human Sperm Origin, Testicular or Ejaculated, on Embryo Morphokinetic Development ». *Andrologia* 50 (8): e13061. <https://doi.org/10.1111/and.13061>.
- Seli, Emre, Denny Sakkas, Richard Scott, Shing C. Kwok, Scott M. Rosendahl, et David H. Burns. 2007. « Noninvasive Metabolomic Profiling of Embryo Culture Media Using Raman and Near-Infrared Spectroscopy Correlates with Reproductive Potential of Embryos in Women Undergoing in Vitro Fertilization ». *Fertility and Sterility* 88 (5): 1350-57. <https://doi.org/10.1016/j.fertnstert.2007.07.1390>.
- Shahbazi, Marta N., Agnieszka Jedrusik, Sanna Vuoristo, Gaele Recher, Anna Hupalowska, Virginia Bolton, Norah N. M. Fogarty, et al. 2016. « Self-Organization of the Human Embryo in the Absence of Maternal Tissues ». *Nature Cell Biology* 18 (6): 700-708. <https://doi.org/10.1038/ncb3347>.
- Simopoulou, Mara, Konstantinos Sfakianoudis, Evangelos Maziotis, Petroula Tsioulou, Sokratis Grigoriadis, Anna Rapani, Polina Giannelou, et al. 2021. « PGT-A: Who and When? A Systematic Review and Network Meta-Analysis of RCTs ». *Journal of Assisted Reproduction and Genetics* 38 (8): 1939-57. <https://doi.org/10.1007/s10815-021-02227-9>.
- Steer, C. V., C. L. Mills, S. L. Tan, S. Campbell, et R. G. Edwards. 1992. « The Cumulative Embryo Score: A Predictive Embryo Scoring Technique to Select the Optimal Number of Embryos to Transfer in an in-Vitro Fertilization and Embryo Transfer Programme ». *Human Reproduction (Oxford, England)* 7 (1): 117-19. <https://doi.org/10.1093/oxfordjournals.humrep.a137542>.
- Steptoe, P. C., R. G. Edwards, et J. M. Purdy. 1971. « Human Blastocysts Grown in Culture ». *Nature* 229 (5280): 133-34. <https://doi.org/10.1038/229133a0>.
- Sunderam, Saswati, Dmitry M Kissin, Yujia Zhang, Amy Jewett, Sheree L Boulet, Lee Warner, Charlan D Kroelinger, et Wanda D Barfield. 2022. « Assisted Reproductive Technology Surveillance — United States, 2018 » 71 (4).
- Szamatowicz, Marian, et Jacek Szamatowicz. 2020. « Proven and Unproven Methods for Diagnosis and Treatment of Infertility ». *Advances in Medical Sciences* 65 (1): 93-96. <https://doi.org/10.1016/j.advms.2019.12.008>.
- Takahashi, Kazutoshi, Koji Tanabe, Mari Ohnuki, Megumi Narita, Tomoko Ichisaka, Kiichiro Tomoda, et Shinya Yamanaka. 2007. « Induction of Pluripotent Stem Cells from Adult Human Fibroblasts by Defined Factors ». *Cell* 131 (5): 861-72. <https://doi.org/10.1016/j.cell.2007.11.019>.
- Teperek, Marta, Angela Simeone, Vincent Gaggioli, Kei Miyamoto, George E. Allen, Serap Erkek, Taejoon Kwon, et al. 2016. « Sperm Is Epigenetically Programmed to Regulate Gene Transcription in Embryos ». *Genome Research* 26 (8): 1034-46. <https://doi.org/10.1101/gr.201541.115>.
- Thomson, J. A., J. Itskovitz-Eldor, S. S. Shapiro, M. A. Waknitz, J. J. Swiergiel, V. S. Marshall, et J. M. Jones. 1998. « Embryonic Stem Cell Lines Derived from Human Blastocysts ». *Science (New York, N.Y.)* 282 (5391): 1145-47. <https://doi.org/10.1126/science.282.5391.1145>.
- Troude, Pénélope, Sophie Ancelet, Juliette Guibert, Jean-Luc Pouly, Jean Bouyer, et Elise de La Rochebrochard. 2012. « Joint Modeling of Success and Treatment Discontinuation in in Vitro Fertilization Programs: A Retrospective Cohort Study ». *BMC Pregnancy and Childbirth* 12 (août): 77. <https://doi.org/10.1186/1471-2393-12-77>.
- Troude, Pénélope, Gaëlle Santin, Juliette Guibert, Jean Bouyer, et Elise de La Rochebrochard. 2016. « Seven out of 10 Couples Treated by IVF Achieve Parenthood Following Either Treatment, Natural Conception or Adoption ». *Reproductive BioMedicine Online* 33 (5): 560-67. <https://doi.org/10.1016/j.rbmo.2016.08.010>.
- Uyar, Asli, et Emre Seli. 2014. « Metabolomic Assessment of Embryo Viability ». *Seminars in Reproductive Medicine* 32 (2): 141-52. <https://doi.org/10.1055/s-0033-1363556>.
- Ventimiglia, Eugenio, Edoardo Pozzi, Paolo Capogrosso, Luca Boeri, Massimo Alfano, Walter Cazzaniga, Rayan Matloob, et al. 2021. « Extensive Assessment of Underlying Etiological Factors in Primary Infertile Men Reduces the Proportion of Men With Idiopathic Infertility ». *Frontiers in Endocrinology* 12: 801125. <https://doi.org/10.3389/fendo.2021.801125>.
- Venturas, Marta, Xingbo Yang, Denny Sakkas, et Dan Needleman. 2023. « Noninvasive Metabolic Profiling of Cumulus Cells, Oocytes, and Embryos via Fluorescence Lifetime Imaging Microscopy: A Mini-Review ». *Human Reproduction (Oxford, England)* 38 (5): 799-810. <https://doi.org/10.1093/humrep/dead063>.
- VerMilyea, M., J. M. M. Hall, S. M. Diakiw, A. Johnston, T. Nguyen, D. Perugini, A. Miller, A. Picou, A. P. Murphy, et M. Perugini. 2020. « Development of an Artificial Intelligence-Based Assessment Model for Prediction

- of Embryo Viability Using Static Images Captured by Optical Light Microscopy during IVF ». *Human Reproduction (Oxford, England)* 35 (4): 770-84. <https://doi.org/10.1093/humrep/deaa013>.
- Vlajkovic, Tijana, Mihaela Grigore, Rik van Eekelen, et Lucian Puscasiu. 2022. « Day 5 versus Day 3 Embryo Biopsy for Preimplantation Genetic Testing for Monogenic/Single Gene Defects ». *The Cochrane Database of Systematic Reviews* 11 (11): CD013233. <https://doi.org/10.1002/14651858.CD013233.pub2>.
- Webster, Alexandre, et Melina Schuh. 2017. « Mechanisms of Aneuploidy in Human Eggs ». *Trends in Cell Biology* 27 (1): 55-68. <https://doi.org/10.1016/j.tcb.2016.09.002>.
- Whitelaw, Natalie, Siladitya Bhattacharya, Gwen Hoad, Graham W. Horgan, Mark Hamilton, et Paul Haggarty. 2014. « Epigenetic Status in the Offspring of Spontaneous and Assisted Conception ». *Human Reproduction (Oxford, England)* 29 (7): 1452-58. <https://doi.org/10.1093/humrep/deu094>.
- Xiang, Lifeng, Yu Yin, Yun Zheng, Yanping Ma, Yonggang Li, Zhigang Zhao, Junqiang Guo, et al. 2020. « A Developmental Landscape of 3D-Cultured Human Pre-Gastrulation Embryos ». *Nature* 577 (7791): 537-42. <https://doi.org/10.1038/s41586-019-1875-y>.
- Xu, Jian, Yan Li, Yanwen Xu, Chenhui Ding, Tao Li, et Canquan Zhou. 2014. « A Simple and Effective Method for the Isolation of Inner Cell Mass Samples from Human Blastocysts for Gene Expression Analysis ». *In Vitro Cellular & Developmental Biology - Animal* 50 (3): 232-36. <https://doi.org/10.1007/s11626-013-9713-2>.
- Xu, Kangpu, et Markus Montag. 2012. « New Perspectives on Embryo Biopsy: Not How, but When and Why? » *Seminars in Reproductive Medicine* 30 (4): 259-66. <https://doi.org/10.1055/s-0032-1313905>.
- Yan, Liying, Mingyu Yang, Hongshan Guo, Lu Yang, Jun Wu, Rong Li, Ping Liu, et al. 2013. « Single-Cell RNA-Seq Profiling of Human Preimplantation Embryos and Embryonic Stem Cells ». *Nature Structural & Molecular Biology* 20 (9): 1131-39. <https://doi.org/10.1038/nsmb.2660>.
- Yanagida, Ayaka, Daniel Spindlow, Jennifer Nichols, Anish Dattani, Austin Smith, et Ge Guo. 2021. « Naive Stem Cell Blastocyst Model Captures Human Embryo Lineage Segregation ». *Cell Stem Cell* 28 (6): 1016-1022.e4. <https://doi.org/10.1016/j.stem.2021.04.031>.
- Yu, Leqian, Yulei Wei, Jialei Duan, Daniel A. Schmitz, Masahiro Sakurai, Lei Wang, Kunhua Wang, Shuhua Zhao, Gary C. Hon, et Jun Wu. 2021. « Blastocyst-like Structures Generated from Human Pluripotent Stem Cells ». *Nature* 591 (7851): 620-26. <https://doi.org/10.1038/s41586-021-03356-y>.
- Zhang, Yue, Junhui Zhang, Jun Zhao, Xiang Hong, Hongguang Zhang, Qiaoyun Dai, Yuanyuan Wang, et al. 2020. « Couples' Prepregnancy Body Mass Index and Time to Pregnancy among Those Attempting to Conceive Their First Pregnancy ». *Fertility and Sterility* 114 (5): 1067-75. <https://doi.org/10.1016/j.fertnstert.2020.05.041>.
- Zou, Yaoyu, Yingxia Pan, Naidong Ge, Yan Xu, Ruihuan Gu, Zhichao Li, Jing Fu, Junhui Gao, Xiaoxi Sun, et Yijuan Sun. 2022. « Can the Combination of Time-Lapse Parameters and Clinical Features Predict Embryonic Ploidy Status or Implantation? » *Reproductive Biomedicine Online* 45 (4): 643-51. <https://doi.org/10.1016/j.rbmo.2022.06.007>.

Titre : Synergie entre biologie du développement et techniques d'assistance médicale à la procréation pour l'étude de l'embryon humain préimplantatoire.

Mots clés : AMP, embryons, time-lapse, développement

Résumé : Depuis les débuts de l'Assistance Médicale à la Procréation (AMP), les technologies permettant la culture et l'observation embryonnaire ont beaucoup évolué. Les incubateurs de type time-lapse ont notamment permis aux embryologistes d'avoir accès à l'ensemble du développement préimplantatoire. Dans le cadre de la partie clinique de ce travail, j'ai étudié l'apport des paramètres morphocinétiques pour l'évaluation de la qualité embryonnaire en AMP. En parallèle à ces avancées technologiques en AMP clinique, les connaissances fondamentales en biologie du développement humain préimplantatoire restent largement incomplètes.

La mise en place d'outils Omics de plus en plus performants, tels que l'analyse transcriptomique ou protéomique, ainsi que les modèles animaux, ont permis de faire progresser la connaissance. Cependant, il est indispensable de connaître très précisément le stade de développement et la localisation de chaque compartiment cellulaire / cellule pour comprendre les mécanismes de destin cellulaire. Dans le cadre de ce travail de recherche, j'ai pu tout d'abord mettre à profit mon expertise en time-lapse pour annoter précisément les embryons analysés. J'ai pu également appliquer mon expertise en micro-manipulation embryonnaire pour mettre au point une dissection embryonnaire permettant de séparer les cellules constituant les différents compartiments embryonnaires.

Title : Synergy between developmental biology and assisted reproductive technologies for the study of human preimplantation embryo development.

Keywords : ART, embryo, development, time-lapse

Abstract : Since the beginning of Assisted Reproductive Technologies (ART) in the 80's, techniques allowing embryo development and observation were optimized. Among them, Time-lapse incubators gave embryologists access to all embryo preimplantation development parameters. In the clinical part of this work, I focused on the contribution of morphokinetic parameters for the evaluation of embryo quality in ART. In parallel with these technological advances, fundamental knowledge concerning biology of pre-implantation human development remains largely incomplete.

Omics tools, such as transcriptomics and proteomics, allowing high throughput and indepth analysis, as well as animal models, have helped to advance knowledge in developmental biology. However, it is essential to identify very precisely the stage of development and the location of each cell to decipher the mechanisms of cellular specification in human morula and blastocyst. As part of this research, I was first able to use my time-lapse expertise to accurately annotate the analyzed embryos. I was also able to use my skills in embryonic micro-manipulation to set up and implement human embryo dissection to separate the cells of different embryonic compartments.